UNIVERSITÉ DU QUÉBEC

MÉMOIRE

PRÉSENTÉ À

L'UNIVERSITÉ DU QUÉBEC À CHICOUTIMI

COMME EXIGENCE PARTIELLE

DU DOCTORAT EN RESOURCES MINÉRALS

PAR

TAFADZWA SHARON GOMWE

BSc MSc

FORMATION DES ZONES RICHES EN PALLADIUM DE ROBY, TWILIGHT ET « HIGH-GRADE » DU COMPLEXE LAC DES ILES, ONTARIO

THE FORMATION OF THE PALLADIUM-RICH ROBY, TWILIGHT AND HIGH-GRADE ZONES OF THE LAC DES ILES COMPLEX, ONTARIO

Septembre 2008

Bibliothèque
Paul-Émile-Boulet

UQAC
Université du Québec
à Chicoutimi

Mise en garde/Advice

Afin de rendre accessible au plus grand nombre le résultat des travaux de recherche menés par ses étudiants gradués et dans l'esprit des règles qui régissent le dépôt et la diffusion des mémoires et thèses produits dans cette Institution, **l'Université du Québec à Chicoutimi (UQAC)** est fière de rendre accessible une version complète et gratuite de cette œuvre.

Motivated by a desire to make the results of its graduate students' research accessible to all, and in accordance with the rules governing the acceptation and diffusion of dissertations and theses in this Institution, the **Université du Québec à Chicoutimi (UQAC)** is proud to make a complete version of this work available at no cost to the reader.

L'auteur conserve néanmoins la propriété du droit d'auteur qui protège ce mémoire ou cette thèse. Ni le mémoire ou la thèse ni des extraits substantiels de ceux-ci ne peuvent être imprimés ou autrement reproduits sans son autorisation.

The author retains ownership of the copyright of this dissertation or thesis. Neither the dissertation or thesis, nor substantial extracts from it, may be printed or otherwise reproduced without the author's permission.

ABSTRACT

The Lac des Îles Complex contains the Roby, Twilight and High-grade Zones, which make up Canada's only primary platinum-group element (PGE) ore deposit. These Zones have remarkably high Pd/Pt ratios, averaging 7 in the Roby and Twilight Zones and 14 in the High-grade Zone. In contrast, most PGE dominated deposits have Pd/Pt ratios of 0.5 – 3. The Roby and Twilight Zones consist of gabbronorite magmatic breccia, which contains pegmatoidal and varitextured patches. Many of the rocks from these zones are metagabbronorites and consist of chlorite plus actinolite psuedomorphs after the magmatic minerals. Between the breccia of the Roby Zone and the homogeneous East Gabbro is an actinolite chlorite ± talc schist, which contains the highest grades found at Lac des Îles (the High-grade Zone).

Microstructures show that the plagioclase has undergone high temperature deformation and there is very little intercumulate material present in the fresh or metamorphosed gabbronorites. Most of the rocks regardless of the zone, the texture, or the degree of metamorphism have very low incompatible element contents, confirming the petrographic observation that there is very little trapped liquid component. Furthermore, they have similar incompatible element ratios indicating that they all are co-magmatic. Therefore, the process of breccia formation is interpreted as to have occurred when one batch of magma from a feeder chamber was injected into a superior partially consolidated magma chamber. The chamber was being deformed at the time of intrusion and fractionated liquid was squeezed out of the breccia zone. The formation of pegmatite and varitextured rocks could have occurred when the magma became saturated in aqueous fluid and this fluid infiltrated the partially consolidated gabbronorite causing recrystallization. However, the composition of the varitextured and pegmatoidal rocks is similar to that of the other rocks and thus the fluid did not appreciably change the composition of the recrystallized rocks. About half of the rocks in the High-grade Zone are of gabbronorite composition, similar to the Roby and Twilight Zones, however, the other half are more

mafic than the Twilight and Roby Zones and are olivine gabbronorites, regardless they appear to be co-magmatic as they have similar incompatible element ratios. The High-grade Zone appears to represent deformed and metamorphosed breccia similar to the Twilight and Roby Zones with the addition of some olivine gabbronorite.

The mineral trace element chemistry of plagioclase and orthopyroxene grains show an overall depletion in High Field Strength Elements (HFSE) and enrichment in Large Ion Lithophile Elements (LILE). The parental magma signature was calculated by inverting of the trace element concentrations within plagioclase and orthopyroxene. The calculated magma is comparable to island-arc calc-andesites, suggesting a destructive plate boundary setting with the possibility of contamination from the tonalitic country rock.

Processes that have been considered for forming the ores include: collection by sulphides from a silicate magma, zone refining of the sulphides during repeated injection of magmas, and collection of the metals by deuteric or hydrothermal fluids. For samples from the Twilight and Roby Zones and half the samples from the High-grade Zone there is a strong correlation between S, Cu and, PGE indicating that PGE are associated with sulphides. However the high Pd/Pt ratio of the ores suggests that they cannot simply have segregated from a primary mantle-derived mafic magma. The fractionation of Pd may have occurred in a feeder chamber by partial dissolution of primary sulphides forming a monosulphide solid solution rich in IPGE, an Fe-Pt alloy, and a liquid-rich in Cu, Pd, and S. This liquid was then injected into the Lac des Îles magma chamber and Pd-rich sulphides segregated from it. The liquid that dissolved the primary sulphides in the feeder chamber could have been either an S-undersaturated silicate magma or high temperature fluid. In about half of the High-grade Zone samples Pd and Pt do not correlate with S, but Cu and Ir do. In these samples Pd-grades are high and the Pd/Pt ratios are even higher (20) than in Roby and Twilight Zone samples. The correlation of Cu and Ir with S suggests that S has not been lost from the system. Furthermore, these samples are richer in Sb and As than the other samples. This suggests that a low temperature Pd-rich fluid introduced the final step

of mineralisation in the High-grade zone. This fluid may have come from the underlying feeder chamber and was focussed in the shear zone between the East Gabbro and the Roby Zone because most of the Lac des Îles Intrusion had solidified at this point.

RESUMÉ

Le Complexe du Lac-des-Îles est l'hôte des zones minéralisées Roby, Twilight et 'High-grade', et représente le seul gisement primaire d'éléments du groupe du platine (EGP). Ces zones montrent un rapport Pd/Pt remarquablement riche autour de 7 pour Roby et Twilight et de 14 pour High–grade. Par comparaison, la plupart des dépôts de EGP importants possèdent un ratio Pd/Pt autour de 0.5 – 3. Les zones Roby et Twilight comprennent des brèches magmatiques gabbronoritiques qui contiennent des amas pegmatoïdes de textures variées (varitextured). Plusieurs des roches de ces zones sont des métagabbronorites et comprennent de la chlorite et de l'actinote qui pseudomorphosent les minéraux primaires magmatiques. Entre la brèche de la zone Roby et le Gabbro Est homogène, se retrouve un schiste à actinote et chlorite ± talc qui contient les valeurs les plus fortes du Complexe du Lac-des-Îles (zone High-grade).

Les microstructures montrent que le plagioclase a subi une déformation de haute température et qu'il y a peu de matériel intercumulat présent dans les portions fraîches ou métagabbronoritiques. La plupart des roches, indépendamment de la zone, de la texture et du degré de métamorphisme, montrent un contenu faible en éléments incompatibles confirmant ainsi les observations pétrographiques à l'effet qu'il n'y a qu'une faible composante de liquide piégé. De plus, les ratios d'éléments incompatibles indiquent que ces roches sont comagmatiques. Par ailleurs, le processus responsable de la formation de la brèche est considéré comme étant actif lorsqu'une partie du magma ascendant s'est introduit dans un magma partiellement consolidé de la chambre d'alimentation. La déformation affectant la chambre au moment de l'injection serait responsable de l'expulsion d'un liquide fractionnée hors de la brèche. La formation de pegmatite et de roches à textures variées peut s'être opérée lorsque le magma est devenu saturé en fluide et que ce fluide s'est infiltré dans le gabbronorite partiellement consolidé causant ainsi la recristallisation. Comme le magma a évolué, il est devenu enrichi en eau favorisant ainsi la cristallisation de l'orthopyroxène plutôt que du clinopyroxène. Cependant, la composition

des roches à textures variées et pegmatoides est similaire à celles des autres roches et donc le fluide n'a pas modifié significativement la composition des roches recristallisées. Environ la moitié des roches de la zone High-grade a une composition gabbronoritique similaire aux zones Roby et Twilight. Cependant, bien que l'autre moitié montre des compositions plus mafiques, étant des gabbronorites à olivine, ils affichent des ratios similaires en éléments incompatibles et sont donc comagmatiques. Il est suggéré que la Zone High-grade est constituée d'une brèche déformée et métamorphisée similaire à celles des zones Twilight et Roby ainsi que de gabbronorite à olivine.

Les processus qui ont été considérés comme responsables de la minéralisation sont : la concentration des sulfures à partir d'un magma silicaté, l'enrichissement des sulfures par des injections répétées de magma, et une concentration des métaux par les fluides hydrothermaux et deutéritiques. Pour les échantillons des zones Twilight et Roby, et pour la moitié des échantillons de la zone High-grade, il y a une forte corrélation entre S, Cu et les EGP indiquant un contrôle des sulfures sur les EGP. Cependant, le ratio élevé Pd/Pt de la minéralisation suggère qu'elle ne peut provenir uniquement d'une ségrégation du liquide primaire. Il est suggéré que le fractionnement du Pd provient d'une chambre d'alimentation à partir d'une dissolution partielle de sulfures primaires formant une solution riche en lEGP, un alliage Fe-Pt et un liquide riche en Cu, Pd et S. Ce liquide a été injecté au sein de la chambre du Lac-des-Îles et les sulfures riches en Pd viennent d'une ségrégation de ce liquide. Le liquide qui a dissous les sulfures primaires de la chambre d'alimentation peut être soit un magma silicaté sous-saturé en soufre ou un fluide de haute température. Dans environ la moitié des échantillons de la zone High-grade, le Pd et Pt ne montrent pas de corrélation avec le S mais par contre Cu et Ir en montre. Dans ces échantillons, la concentration en Pd est élevée et le ratio Pd/Pt est également plus élevé (20) que dans les zones Roby et Twilight. La corrélation du Cu et Ir avec S suggère que le soufre n'a pas été perdu dans le système. De plus, ces échantillons sont plus riches en Sb et As que les autres échantillons. Ceci suggère que les fluides riches en Pd se sont introduits à l'étape finale de la minéralisation dans la zone High-grade. Il est possible que ces fluides

proviennent d'une chambre magmatique sous-jacente et se sont introduit par l'entremise de zones de cisaillement entre le Gabbro Est et la Zone Roby parce que la majeure partie de l'intrusion du Lac-des-Iles était consolidée à cet endroit.

ACKNOWLEDGEMENTS

Funding for this project was provided by the NSERC Discovery Grant Program held at l'Université du Québec à Chicoutimi (UQAC) by Prof. Sarah-Jane Barnes, the bursaries Lucien Bouchard and CONSOREM awarded to the author by UQAC.

My sincerest appreciation to Prof. Sarah-Jane Barnes for her supervision, support, advice and assistance during the course of this study, my understanding of sulphide and PGE geochemistry has been greatly increased through our discussions. Thank you also to my committee for their useful advice and suggestions.

I appreciate and thank North American Palladium Mine and M. Lavigne for their logistical support in the field and permission for the use of the mine data. Many thanks go to P. Bedard, R. Cox and D. Savard for their assistance in the laboratory at UQAC. Thank-you to R. Cox for his valued assistance with the LA-ICP-MS analyses and the discussions with regards to deciphering the data. Thank-you to R. Daigneaut and D. Gaboury for their assistance in the translation of sections of the manuscript. Special thanks to W.D. Maier for his helpful comments and corrections on parts of this thesis.

I would like to thank my parents, including those adopted in Chicoutimi for believing in me and always being there. To my friends and family for giving me the moral support needed to finish this project.

TABLE OF CONTENTS

LIST OF FIGURES

LIST OF TABLES

1.
INTRODUCTION

Most nickel–copper and platinum-group element (PGE) deposits are associated with mafic and ultramafic rocks. These deposits may be divided into two groups (Naldrett 1981). One group is typically sulphide-rich with >10% sulphide minerals and the main products are Ni and Cu with PGE's as by-products (e.g., Sudbury, Noril'sk, and Voisey's Bay). The second group is typically sulphide-poor with <5% sulphide minerals. Platinum-group elements are the main product whereas Ni and Cu are by-products (e.g., the Merensky Reef of the Bushveld Complex, South Africa and the J-M reef of the Stillwater Complex, Montana). The PGE-dominant group may be further divided into three groups. The first and economically most important comprises stratiform mineralisation represented by the Merensky Reef and the Upper-Group (UG-2) chromite layer of the Bushveld Complex in South Africa (Naldrett et al. 1986; Von Gruenewaldt et al. 1986), the J-M reef of the Stillwater Complex (Zientek et al. 2002), the reefs of the Penikat and Munni Munni layered intrusions (Alapieti and Lahtinen 1986; Barnes and Hoatson 1994), and the Platinova reef of the Skaergaard Complex (Nielsen 2001). The second group consists of mineralisation associated with breccia, for example, the Roby Zone of the Lac des Îles Complex (LDIC) and the Legris Lake Complex (Pettigrew and Hattori 2001). The third group comprises concentrically zoned Alaskan-type intrusions, for example the Tulameen Complex in British Columbia (Findlay 1969; Nixon et al. 1990).

The topic of this thesis is the Pd mineralization of the LDIC (Fig. 1). The Pd mineralisation occurs in serveral zones including the Roby, Twilight, High-grade, Baker, Creek and Moore Zones (Lavigne and Michaud 2001). Three of these are mined; the Roby, Twilight and High-grade Zones. The current estimate of the resources in these three zones are: indicated and measured 28.03 M tonnes at Pd 1.318 g/tonne for the open pit and an indicated and inferred for the underground mine 17.37 M tonnes at 5.47 g/tonne (North American Palladium Annual Report 2006). The Roby and Twilight Zones are ellipsoidal-shaped zones (100 to 500 m in diameter) of magmatic breccia. The High-grade Zone is defined by Pd grade rather than rock type; it is a Pd-rich layer 15-25 m thick between the Roby Zone and East Gabbro (Fig. 1).

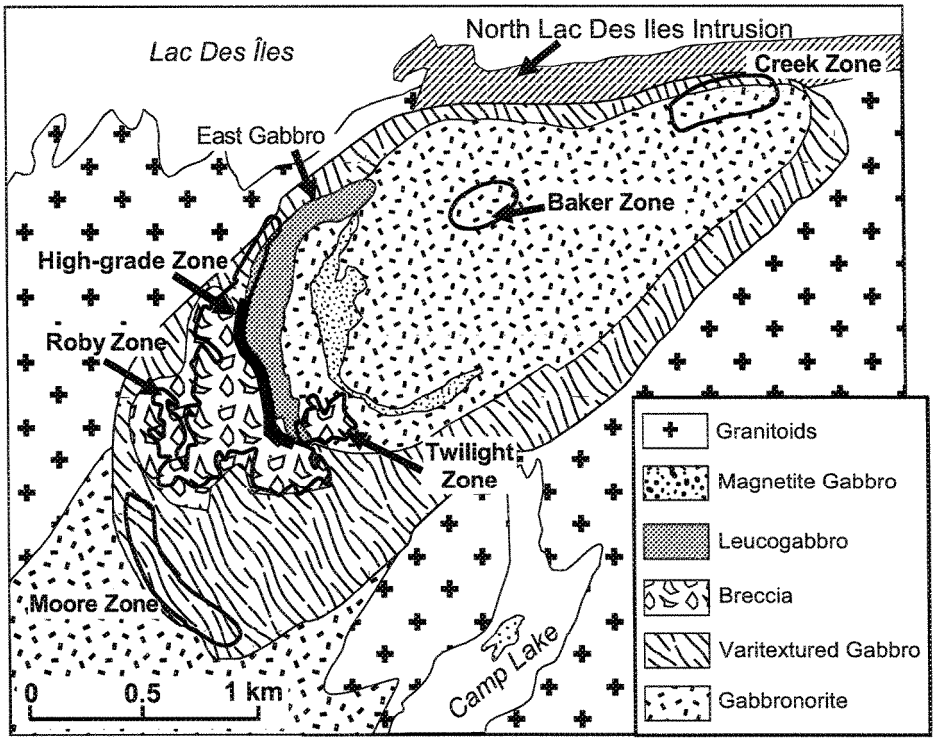

Figure 1. Simplified geological map showing part of the LDIC highlighting the zones and the High-grade Zone. Modified from Watkinson et al. (2002).

1.1. Previous Work

The presence of breccia, pegmatites, and varitextured gabbros along with the extensive amphibolitization suggests to many authors that fluids have a role to paly in the formation of the deposits. Watkinson and Dunning (1979) suggested that mineralization was due to mixing of two magmas to form the breccia followed by hydrothermal action to concentrate the Pd. Talkington and Watkinson (1984a) noted the occurrence of Te^{-}, As^{-}, Bi^{-} containing PGMs together with hydrous minerals and suggested that the PGE were

precipated as PGM from the fluid that caused the amphibolitization. Watkinson and Lavigne (2002) suggested that the fluid was deuteric, that it caused alteration of the pyroxene to amphibole, and that it mobilized and aided the concentration of Pd at Lac Des Îles.

Macdonald (1988) noted that the clasts (i.e. fragments) within the breccia of the Roby Zone represent all lithologies in the varitextured gabbro that surround the breccia ore, suggesting that the fragments in the breccia were derived locally by the injection of a new magma. Macdonald et al. (1989) divided the mineralization in the Roby Zone into three groups; a) low-grade (<1 ppm) hosted by the breccia; b) high-grade (up to 15 ppm) hosted by pyroxenitic dykes; c) highest grade (up to 37 ppm) hosted by gabbro pegmatitic dykes. They suggested that Pd was introduced into the Roby Zone by the pyroxenitic dykes and that this Pd mineralization was upgraded by interaction between the resident fractionated gabbro melt and deuteric fluid that redistributed the Pd into the pegmatites.

Brügmann et al. (1989) suggested a different mechanism for Pd concentration: zone refining. They suggested that Pd, Pt, and Au were introduced by a magma that formed by partial melting of the gabbro surrounding the Roby and Twilight Zones. The reason the gabbro surrounding the Roby and Twilight Zones melted is that the underlying magma had become saturated in volatiles. These volatiles rose and caused partial melting of the gabbro. If this melt was sulphide undersaturated it would have dissolved any sulphides present, releasing Pd, Pt, and Au into the melt. As this volatile-rich melt was injected into the Roby

and Twilight Zones and cooled a new base metal sulphide liquid segregated from the silicate magma and recollected the Pd, Pt and Au. In this model the rocks enclosing the Roby and Twilight Zones represent the residue and should be Pd-depleted and the pegmatitic leucocratic rocks in the Roby and Twilight Zones represent the partial melt which should be Pd-enriched.

The models prior to 2000 do not explicitly deal with the High-grade Zone, as it had not been defined and the sampling was confinded to a limited number of samples and surface exposures. Based on the larger data set available from mining and drill core Lavigne and Michaud (2001) and Michaud (1998) proposed a model whereby the proto Roby Zone was a partially consolidated gabbro. These zones were injected by a PGE–volatile-rich gabbroic magma. The magma became fluid satuated and brecciated the resident gabbroic rocks, producing Pd-rich pegmatites and hydrothermal alteration. In this model the matrix of the breccia is Pd-rich and the clasts are Pd-poor. As the temperature decreased fluid flow was focused between the impermeable East Gabbro and the now consolidated breccia. The fluid completely altered the rocks in this zone and Pd tellurides, antinomides, and arsenides percipiated from the fluid forming of the high-grade Pd mineralization.

Hinchey and Hattori (2005) and Hinchey et al. (2005) show that there is a correlation between S and Pd in the Roby Zone, indicating that Pd could have been collected by base metal sulphides, but that in the High-grade Zone there is no correlation,

indicating thatsome other process is required to form this zone. Hinchey and Hattori (2005) found that the matrix is richer in Pd than the fragments, as required by the Brugmann et al. (1989) model, but that Pd is concentrated in the MgO-rich rocks, rather than the leucocratic rocks. They suggested that there were three generations of magma: a) an early non-mineralized leucocratic gabbro; b) a middle mineralized melanocratic gabbro and, c) a late non-mineralized melanocratic gabbro. Although the rocks are extensively amphibolitized, they suggest that there is a difference in mineralogy between the three zones: that the Twilight Zone comprises norites, that the Roby Zone comprises gabbros and that the High-grade Zone comprises gabbros that are clinopyroxene enriched.

Brügmann et al. (1997) and Sutcliffe et al. (1989) proposed that the intrusion was derived from a parental magma of high-Al tholeiitic basalt composition. In the case of Brügmann et al. (1997) εNd(t) values ranging from 0 to +2 suggested to them that the magma was derived from a depleted mantle reservoir and assimilated continental crust, possibly the enclosing tonalite gneiss. These observations led Brügmann et al. (1997) to conclude that the LDIC displays similar characteristics to rock assemblages created at destructive plate boundaries, i.e. magmatic arcs or subduction zones. In contrast, based on whole rock and mineral compositions, Hinchley et al. (2005) calculated that the parental magma was picritic to komatiitic with E-MORB-like trace element contents, which suggests an oceanic environment.

1.2. Objectives of the Study

As outlined above there is no agreement on how the deposits at Lac des Îles formed. This is due in part to the unusual composition and textures of the rocks. For example, the Pd/Pt and Pd/Ir are unusually high (~10 and 6000 respectively) compared with other PGE-dominated deposits (Table 1), which tend to have Pd/Pt ratios of 0.5 – 2 and Pd/Ir ratios of 3 – 250, similar to primitive, mantle-derived magmas (Maier et al. 2004). Ore deposits formed by the collection of PGE by sulphide liquid fall as expected in this range. This is because the partition coefficients of all the PGE into sulphides are thought to be similar. Hence the sulphide liquid should inherit the Pd/Pt ratio of the silicate liquid from which it separated (Barnes and Maier 1999).

Table 1.1. Compilation of Pd/Pt and Pd/Ir ratios of stratiform PGE deposits.

Reef	Locality	Ir	Pt	Pd	Pd/Ir	Pd/Pt	Reference
Merensky	Bushveld Complex	60-139	3085-4616	1402-1968	14-23	0.35-0.64	(Barnes and Maier 2002)
UG-2	Bushveld Complex	20-350	2443-3920	920-3660	10-46	0.35-0.93	(Barnes and Maier 2002)
Plat Reef	Bushveld Complex	14-41	1078-1765	1328-2006	95-49	0.81-1.11	(Barnes and Maier 2002)
MSZ reef	Great Dyke	BD	2336	1730	-	0.74	(Prendergast and Keays 1989)
JM-reef	Stillwater	60	15600	54400	907	3.5	(Barnes and Naldrett 1985)
AP Reef	Penikat	15-63	975-3400	2960-11367	180-197	2.4-3.3	(Halkoaho et al. 1989a)
PV-reef	Penikat	77	3913	2317	30	0.59	(Huhtelin et al. 1989)
SJ-reef	Penikat	99	2667	2700	27	1.01	(Halkoaho et al. 1989b)
Platinova reef	Skaergaard	BD	0.15	1.9	-	12.7	(Nielsen 2001)
Subzone I	Munni Munni	12	525	1854	153	3.5	(Hoatson and Keays 1989)
LDI	Roby Zone	0.7	442	4586	6369	10.4	(Brügmann et al. 1989)

BD = Below Detection Limit

Much of the debate raised in previous studies has arisen because the rocks from the different zones and different textures have not been clearly separated and described. Also, while many broad statements have been made about the relationship between Pd mineralization, whole rock mineralogy, and composition, these have not explicitly been demonstated. To rectify this, the sampling for this study was designed to investigate three specific questions.

1. Is there a petrographic or compositional difference between the three ore zones?
2. Is there a petrographic or chemical difference between the fragments and the matrix?
3. Is there a correlation between the degree of alteration and mineralization?

Chapter 3 indicates that the petrography of the Roby and Twilight Zones are essentially the same, gabbronorite or metagabbronorite. The High-grade Zone consists of a micro breccia and chlorite-actinolite talc schist. Chapter 4 indicates that the whole-rock geochemistry of the Roby and the Twilight Zones are essentially similar in composition and most (73 out of 79) are orthopyroxene plagioclase adcumulates. The remaining 6 are orthopyroxene-clinopyroxene-plagioclase adcumulates. Most (10 out of 17) of the High-grade Zone samples are similar in composition to the Roby or Twilight Zones and are orthopyroxene-plagioclase adcumulates. The other High-grade Zone samples require the presence of cumulate olivine in addition to orthopyroxene and plagioclase (Chapter 4).

A number of previously-proposed models for the formation of the Breccia ore in the LDIC imply that the matrix represents a frozen liquid (Lavigne and Michaud 2001; Watkinson et al. 2002). In order to test such a hypothesis, this study investigates the fragments and the matrix of the breccia deposit of the Roby and Twilight Zones. Chapters 4 and 5 of this study show that the fragments and the matrix are plagioclase-orthopyroxene adcumulates and are similar both in mineral modal concentrations, major and trace element compositions. The matrix samples, on average, are more mafic than the fragment samples. Thus the overall low levels in incompatible elements (apart from LILE and U) indicate that there is very little trapped liquid component in both the fragments and matrix. The matrix material represents a finer-grained equivalent of the fragments and not a silicate liquid component. Chapter 6 of this study suggests a model that is based on the injection or exsolution of a volatile phase from the magma chamber brecciating a partially-consolidated gabbroic assemblage.

As mentioned above, some authors, (Brügmann et al. 1989; Brügmann et al. 1997; Lavigne and Michaud 2001; Watkinson et al. 2002) have suggested that Pd was introduced into the ore zone either by late magmatic fluids or high temperature redistribution of Pd by zone refining. However, this study demonstrates that there is no correlation between alteration and grade within the Roby and Twilight Zones (Chapter 5). However, for about half the High-grade Zone samples there is a high degree of alteration and deformation and these samples have the highest grade.

The Roby Zone, Twilight Zone and about half of the samples from the High-grade Zone show correlations between PGE and S suggesting that the PGE mineralization is associated with sulphides. The other half of the samples from the High-grade Zone show no correlation of Au, Pt, or Pd with S. Although the rocks in the High-grade Zone have undergone low temperature alteration, the lack of correlation with S cannot simply be a result of S loss during alteration. Palladium and Pt do show a correlation with Sb and As in the High-grade Zone, suggesting that these elements acted as fixing agents for Pd and Pt in the system.

The composition of the parental magma is determined using the composition of the silicate minerals plagioclase and orthopyroxene. The mineral chemistry in Chapter 4 suggests a parental magma composition similar to those produced in island-arc or back-arc settings.

2.
GENERAL GEOLOGY

The geology of the Lac des Îles area has been described by a number of authors (Sutcliffe 1987; Sheridan 1987; Sutcliffe et al. 1989; Brügmann et al. 1989; Brügmann et al. 1997; Lavigne and Michaud 2001; Dionne-Foster 2002; Hinchey et al. 2005). Their findings are summarised below. The LDIC is located within the western Superior Province, in the south-central Wabigoon Subprovince close to the north-western boundary of the Quetico Subprovince (Fig. 2.1) (Pye 1968; Dionne-Foster 2002). The Complex occurs within Archean granitoid rocks predominantly consisting of foliated gneissic tonalities that have been dated by U/Pb single zircon methods to range in age between 2775 and 2722 Ma (Stone et al. 2003). The Lac des Îles area also contains hornblende tonalite dated at 2727.8 ± 8 Ma and biotite tonalite dated at 2685 Ma (Stone et al. 2003). The LDIC has been dated by the U-Pb single zircon 2689 ±1 Ma (Stone et al. 2003). An internal Sm-Nd isochron on whole rock and mineral separates (plagioclase, clinopyroxene, and orthopyroxene) gave an intrusion age of 2736 ± 28 Ma (Brügmann et al. 1997). Late hydrothermal and post metamorphic episodes of the tonalite intrusions are constrained by U-Pb single titanite ages between 2670 and 2680 Ma (Davis et al. 1988).

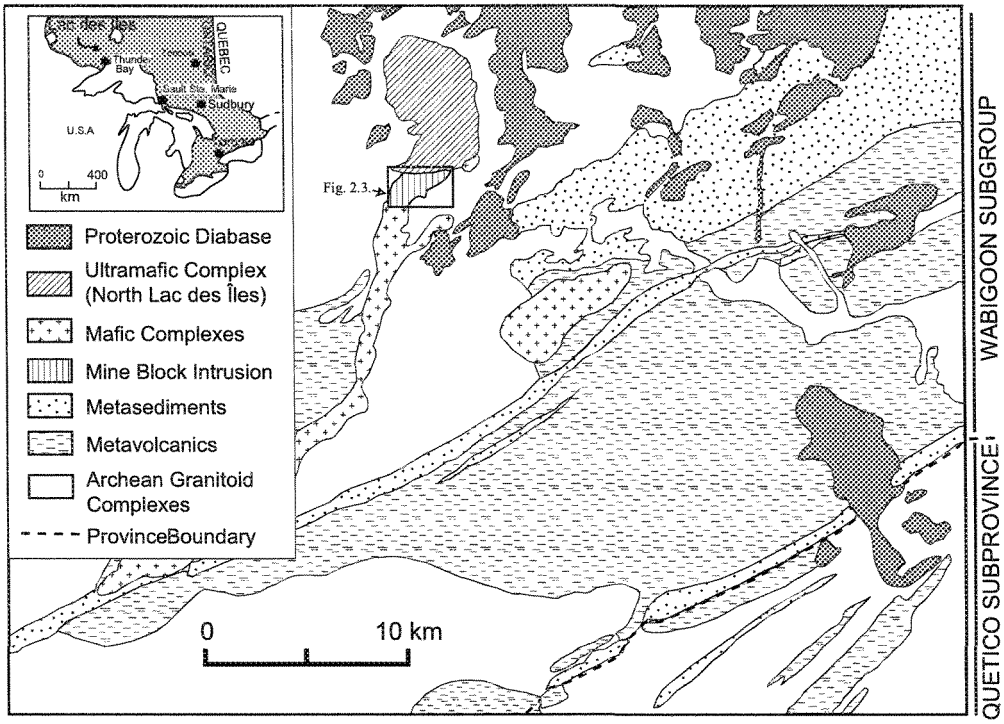

Figure 2.1. Simplified geological map of the Lac des Îles area, modified from Macdonald (1988) and Brügmann (1989). The Mine Block Intrusion is shown in detail in Figure 2.3.

The Wabigoon Subprovince is an Archean granite, gneiss-greenstone terrain. The central Wabigoon, where the LDIC is located, is granitoid-dominated terrain containing only small greenstone belts. The mineral assemblages in subcrustal and plutonic rocks suggests greenschist to lower amphibolite metamorphic conditions (Sage 1998). The Wabigoon Subprovince igneous rocks formed during several magmatic pulses: 1) 3014–2999 Ma mafic–felsic volcanic and tonalite complexes (Tomlinson et al. 2003), 2) 2750–2700 Ma mafic–felsic volcanic rocks, and 3) 2690 Ma monzodiorite–diorite and mafic–ultramafic suites (Sutcliffe 1989). The LDI appears to belong to the latter suite.

The Quetico Subprovince comprises metamorphosed greywackes, sedimentary siltstone units, and minor banded iron formations. The Quetico Subprovince has been interpreted as an accretionary wedge and the Wabigoon Subprovince as overlying a subduction zone (Percival and Williams 1989). Valli et al. (2004) identified three regional tectono-metamorphic stages that suggest up to four deformation stages. The first deformation stage occurred shortly after sedimentation and involved burial of sediments forming staurolite under medium pressure and temperature conditions. The second and third regional transpressive deformation, the peak metamorphic condition, formed a biotite-sillimanite-garnet assemblage along with hornblende-rich amphiboles. The fourth deformation occurred under retrograde greenschist metamorphism conditions at 2671-2667 Ma (U/Pb on monazite).

The Lac des Îles area consists of several coeval granitoid plutons intruded by the Lac des Îles Complex (Fig. 2.2) (Sutcliffe et al. 1989). The LDIC is divided into three intrusive units: the North LDIC, Mine Block, and Camp Lake intrusions. The North LDIC intrusion is centred on Lac des Îles, (Fig. 2.2) and comprises two intrusive phases based on mineralogical and chemical differences (Dunning 1979). One intrusive phase consists of wehrlite to clinopyroxenite and websterite to gabbronorite cumulates. The other intrusive phase comprises several cyclic units of peridotite, clinopyroxenite, websterite, and minor amounts of orthopyroxenite and gabbronorite cumulates (Brügmann et al. 1987; Brügmann et al. 1989). The most common rock type is clinopyroxenite, which forms thick layers (80 m) with gradational contacts with peridotite cumulates. The peridotites generally form thin

layers (up to 5 m), lenses or dyke-like bodies (Brügmann et al. 1989). The North LDIC contains uneconomic PGE-bearing sulphide mineralisation associated with pyrrhotite, chalcopyrite, and pentlandite (Brügmann et al. 1989).

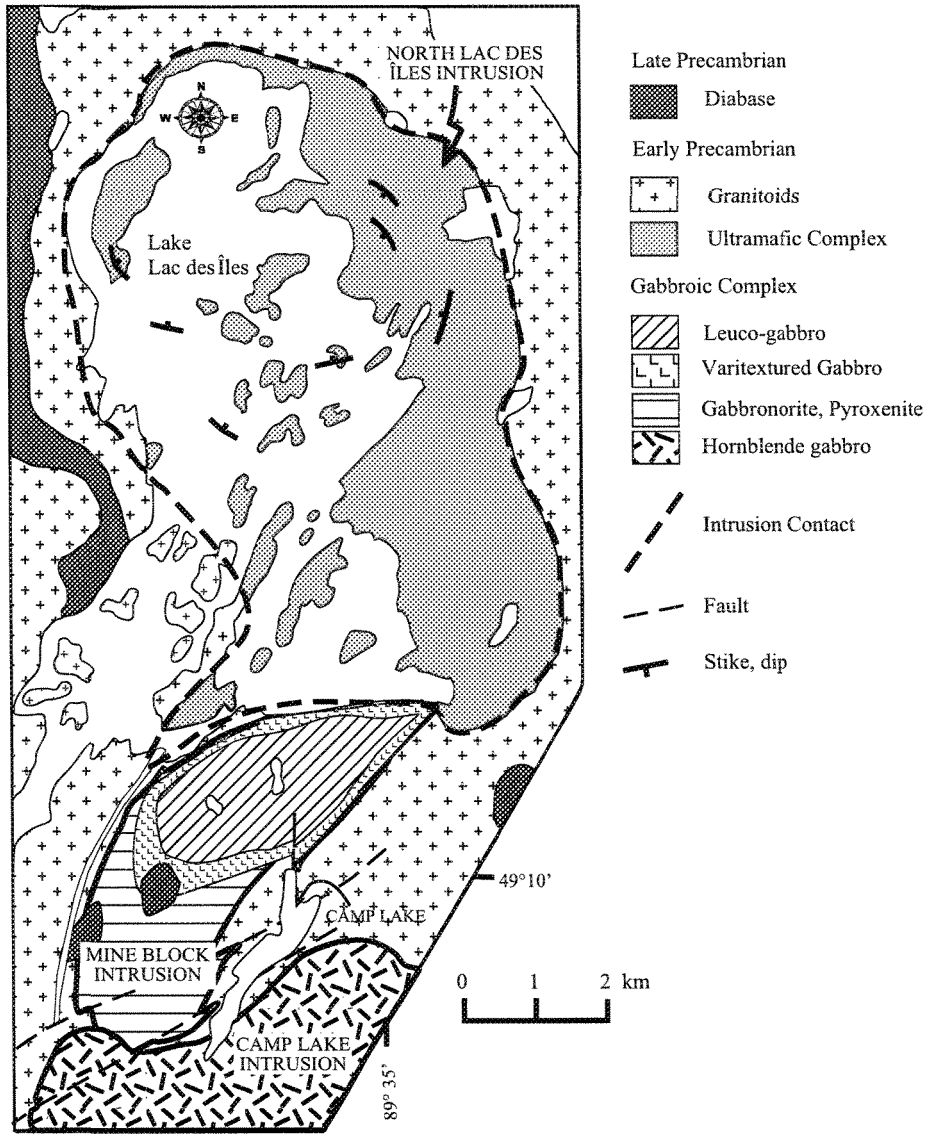

Figure 2.2. Simplified map of the Lac des Îles Complex, modified after Brügmann et al. (1989; 1997)

The Mine Block Intrusion (MBI) is predominantly gabbronorite breccia with varitextured and pegmatitic gabbronorite. The main unmineralized unit in the MBI is the East Gabbro, a massive, medium-grained oxide-rich, sulphide poor plagioclase-clinopyroxene cumulate (Fig. 2.3). The Mine Block intrusion hosts the Roby, High-grade and Twilight Zones Pd and Pt deposits and the Baker, Creek, and Moore Zone Pd and Pt occurrences (Fig. 2.3). The PGE mineralisation is associated with heterolithic gabbronorite breccia and an accompanying varitextured gabbro. Field and petrographic observations by the author revealed that the Breccia ore rock types range in composition from leucogabbronorite to melagabbronorite (Fig. 2.4). Larger fragments contain other fragments indicative of more than one intrusive phase during the emplacement of the MBI. Hinchey et al. (2005) suggest that the emplacement of the magma occurred in three main pulses based on field observations of the breccia mineralisation. Textures include equigranular fine- to coarse-grained, pegmatitic, varitextured (Fig. 2.5), and heterolithic gabbroic breccia (Fig. 2.4b). The breccia contains the economic Roby and Twilight Zones (Fig. 2.3). Alteration is moderate to strong, and is reflected by pervasive uralitization of pyroxene (Watkinson et al. 2002). Intense alteration typically occurs in isolated patches, and locally, narrow zones of mylonitization reduce the grain size of minerals. Sulphide mineralisation occurs as ubiquitous fine-grained disseminations, as irregular-shaped blebs interstitial to orthopyroxene and plagioclase grains, and as inclusions in mineral pseudomorphs such as anthophyllite after orthopyroxene (Lavigne and Michaud 2001).

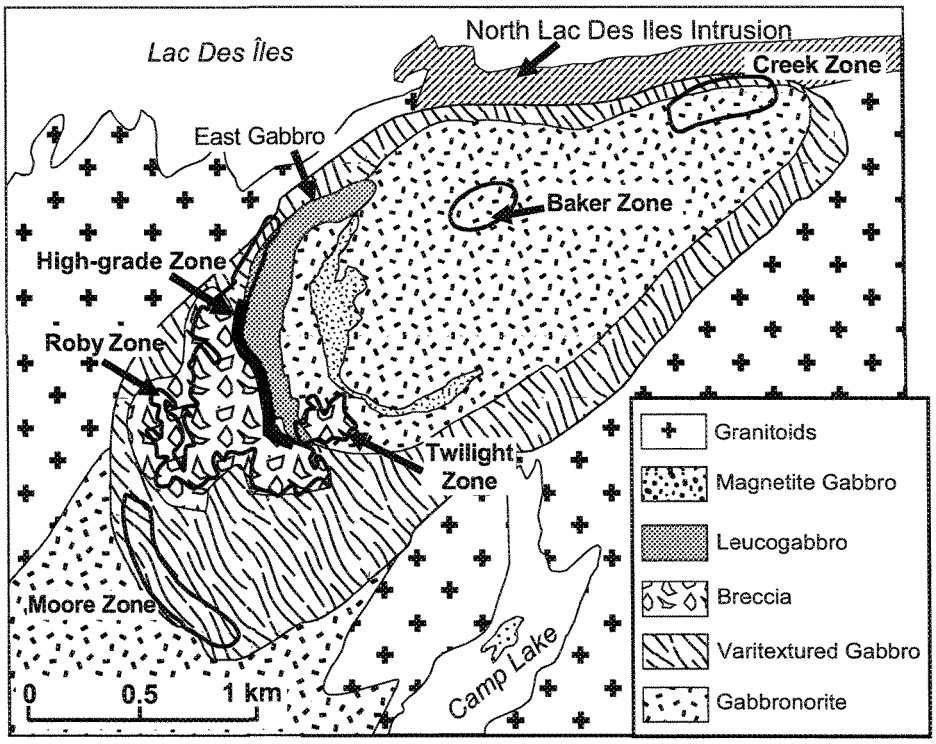

Figure 2.3. Simplified geological map of the Mine Block Intrusion, modified from Watkinson et al. (2002).

The Roby and Twilight Zones consist of breccia of similar lithology (Fig. 2.4). The Twilight Zone is separated from the Roby Zone by the East Gabbro to the west and by a barren gabbro dyke to the southeast (Fig. 2.2). The breccia is lithologically and texturally complex comprising rounded and angular fragments (Michaud 1998; Dionne-Foster 2002; Michaud and Lavigne 2003; Hinchey 2003). The matrix is leucogabbronorite and metagabbronorite, which in some places has been extensively amphibolitised, and the fragments are anorthosite, and gabbronorites (Dionne-Foster 2002).

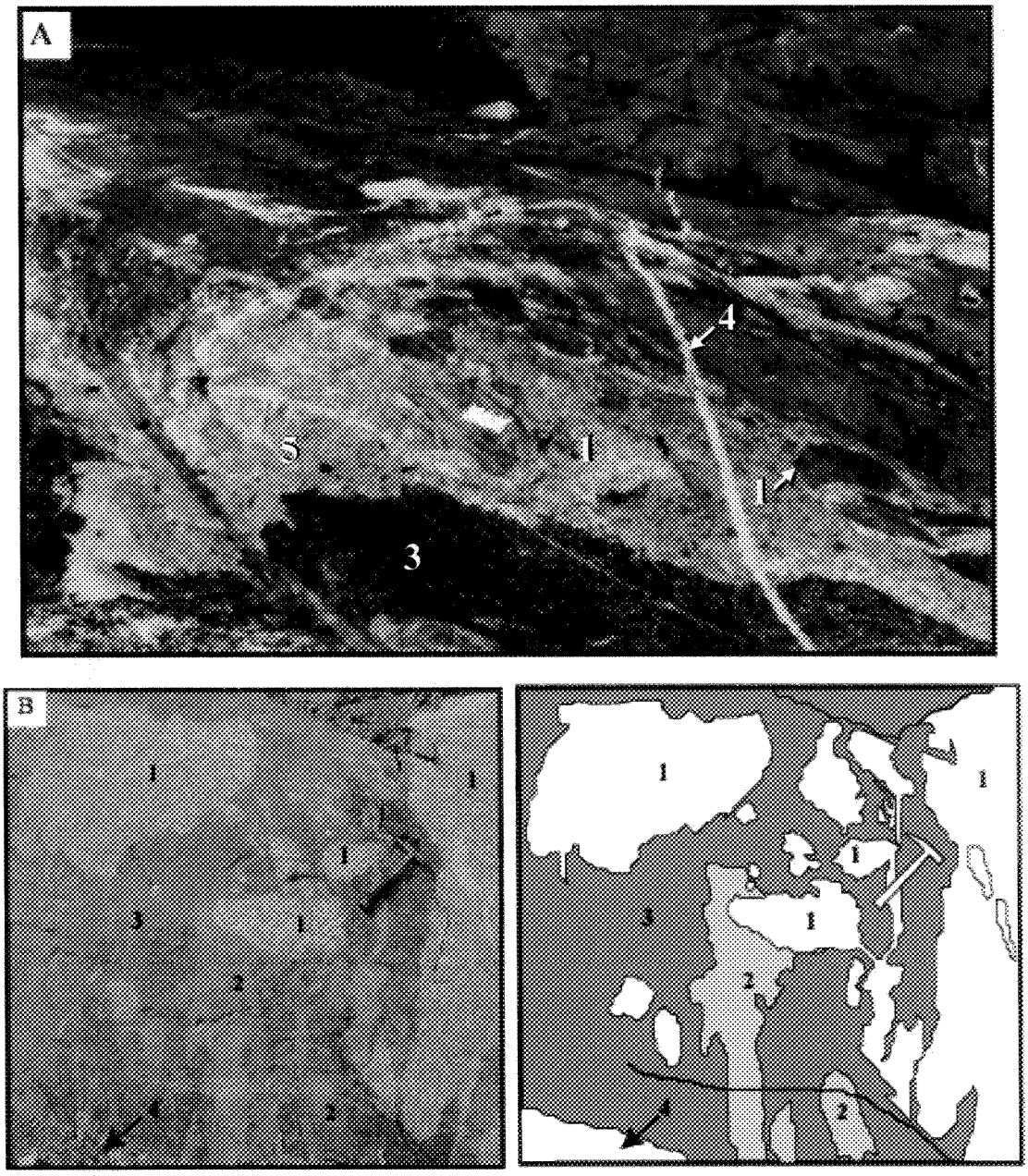

Figure 2.4. (a) Heterolithic breccia of the Roby Zone showing gabbronorite fragments (1) surrounded by a leucogabbronorite matrix (2), which is in turn surrounded by a melagabbronorite matrix (3). All three rock types are cut by a tonalite dyke (4). Also visible is a ductile shear (5) indicating that the rocks were sheared at high temperature. The Twilight Zone also shows similar structures. (b) Breccia of the Twilight Zone showing various sizes of medium-grained (1) and fine-grained (2) leucocratic fragments in melanocratic matrix (3) with pegmatitic patches (4).

The breccia is intruded by pegmatitic (Fig. 2.5a) and felsic dykes. The pegmatite dykes are gabbro, melagabbro, or gabbronorite in composition, the same as the host rock (Dionne-Foster 2002). The felsic dykes are later intrusions that cut through the fragments and matrix of the breccia (Fig. 2.4a). They trend east-west and are roughly parallel to each other. They are fine grained and granitic in composition with a mineral foliation parallel to the felsic dyke contact aureole.

The High-grade Zone is not a lithological unit. It is a 15-25m wide and 400m long Pd-rich shear zone between the Roby Zone and the barren East Gabbro (Fig. 2.3). At the level currently exposed most of the High-grade Zone is characterised by amphibole-chlorite-talc schist enriched in PGE, hosted by uniform medium- to coarse-grained metagabbronorite. Dunning (1979), Watkinson et al. (2002), and Lavigne and Michaud (2001) describe the High-grade Zone as a pyroxenite to melagabbro unit. The mineralisation is not stratabound, but is hosted by chlorite-talc schist and heterolithic breccia of the Roby Zone (Lavigne and Michaud 2001), as a result this Zone is defined by North American Palladium Limited as a zone with a mean concentration of 8 ppm Pd (Watkinson et al. 2002). Macdonald (1988), who studied surface exposures that no longer exist, described the High-grade Zone as consisting of several websterite dykes intrusive into anorthositic gabbro. The host rock may have been partially solidified and deformed in a ductile fashion during emplacement of the dykes (Macdonald 1988). The presence of gabbroic blocks in the dykes suggests that the dyke mixed with the margins of the East Gabbro.

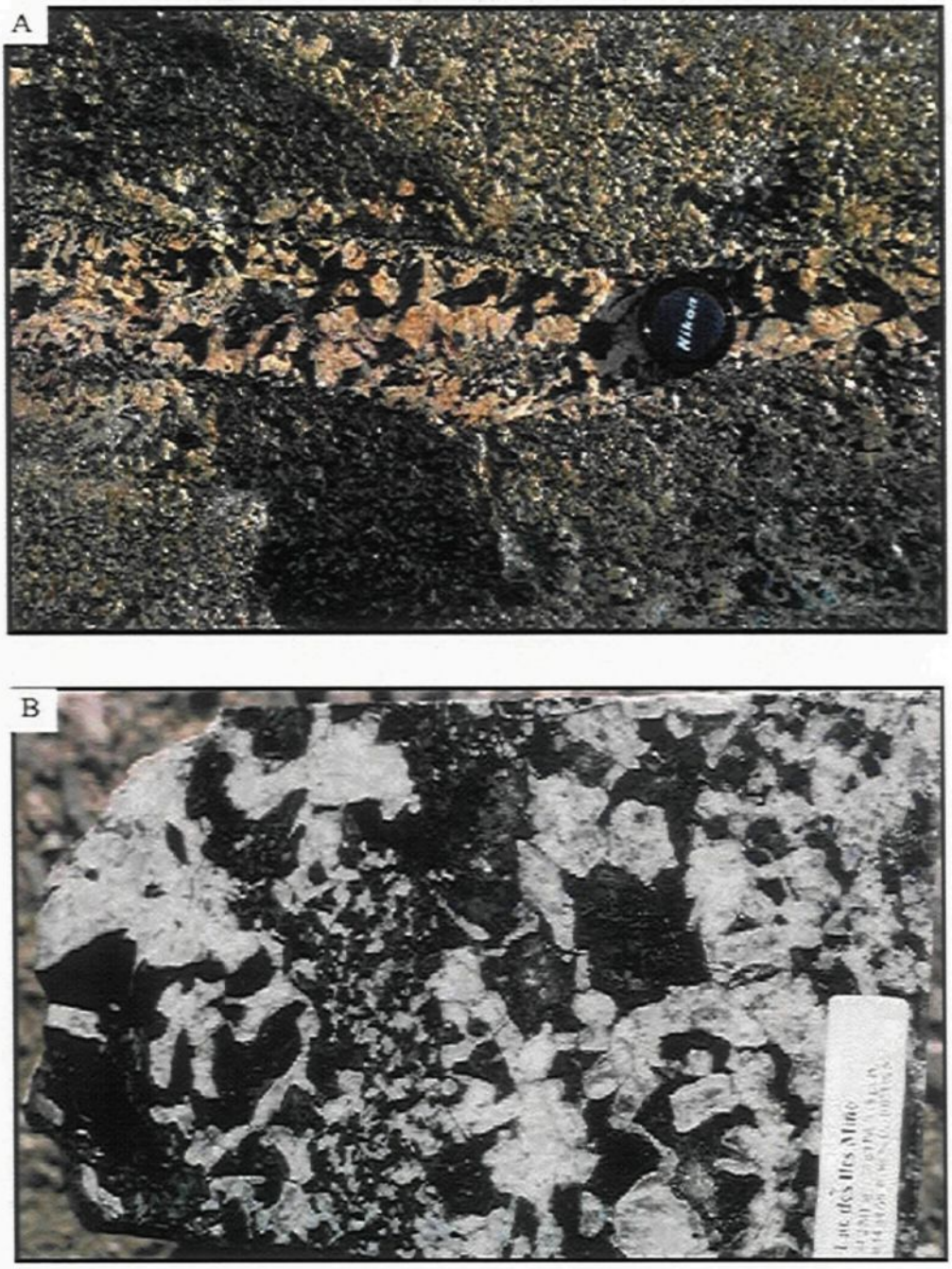

Figure 2.5. (a) Pegmatitic gabbro vein in the Roby Zone. The pegmatite and surrounding rock have the same gabbronorite rock composition (b) varitextured gabbronorite sample from the Roby Zone.

Well-developed foliation defines a C-S fabric that is interpreted to be a 15m-wide shear zone striking north-northwest and dipping steeply to the east (Michaud 1998). Hinchey and Hattori (2005) describe the High-grade Zone as an intensely-altered rock that underwent continuous alteration at various temperatures. Sulphide minerals are dominantly finely disseminated pyrrhotite, chalcopyrite, and pentlandite grains. Core samples collected for this study show microscopic evidence for both brittle and ductile deformation of moderate to highly altered gabbronorites. The transition from the High-grade Zone to the surrounding rock ranges from sharp to gradational; with the change in grade being much more abrupt than the change in rock type (Lavigne and Michaud 2001).

The Camp Lake intrusion comprises mainly hornblende gabbro (Brügmann et al. 1997). The intrusion also contains lesser amounts leucocratic and melanocratic breccia along with varitextured and porphyritic textures. This intrusion contains only minor PGE along the northern edge (Brügmann et al. 1997; Michaud and Lavigne 2003).

3.
PETROLOGY

3.1. Introduction

This study's sampling strategy was designed to consider three points, firstly to characterise the Roby, Twilight, and High-grade Zones, secondly to determine if there are differences between the fragments and the matrix, and thirdly to determine if deuteric and regional metamorphic alteration affects mineralisation.

Seventy-four samples identified as matrix and fragments were cut using a standard rock saw from the breccia-bearing outcrops of the Roby and Twilight Zones. Figure 3.1 shows the sample locations. The blocks measured on average 30 x 15 x 3cm in size. In addition to the samples collected by the author, the study made use of 29 rock samples from a previous study of the Twilight Zone (Dionne-Foster 2002). Samples showing a range in mineralogy from predominantly igneous to pervasively metamorphosed were collected to test the role of alteration in forming the Pd-enriched deposits. Furthermore, to consider the role of high temperature fluids, the pegmatoid and the varitextured rocks were also sampled. Finally to include the High-grade Zone, samples of drill core were collected. These samples were selected on the basis of assay values obtained from North American Palladium Ltd and on their definition of the High-grade Zone. Table 3.1 is a

Table 3.1. Simplified core log for samples collected from the High-grade Zone (North American Palladium Mine, 1999). Detailed descriptions and assays are in Appendix I.

SAMPLE NAME	Borehole	Depth Sampled (ft)	Mine Rock Type	FROM	TO	Pd (ppm)	Pd/Pt
Rz-1	99-052	120-121	VARITEXTURED GABBRO	62.35	72.35	3.2	13
Rz-2	99-096	646-650	VARITEXTURED GABBRO	639.80	649.60	0.1	-
Rz-9	99-096	637-639		649.60	659.40	0.1	-
Rz-3	98-012	107-112	PYROXENITE	107.00	112.00	16.6	80
Rz-5	99-068	519.8-516	PYROXENITE	504.70	509.30	1.8	20
Rz-8	98-068	509-512		509.30	513.80	11.2	21
Rz-10	99-068	505.9-509		513.80	519.20	11.3	18
Rz-4	99-075	227-230	PYROXENITE Shear ore type	217.10	221.90	5.3	14
Rz-6	99-075	217.7-219.7		221.90	226.90	0.5	19
Rz-13	99-075	220-226		226.90	231.70	4.3	16
Rz-7	99-092	501-505	PYROXENITE Shear ore type	498.30	502.90	2.8	13
				502.90	507.60	1.8	9
Rz-12	99-012	102-107	PYROXENITE	102.00	107.00	9.4	69
Rz-14	99-096	689-692	PYROXENITE	683.30	689.00	9.1	23
Rz-17	99-096	683-686		689.00	692.40	26.9	19
Rz-15	99-103	770-771	MELAGABBRONORITE (pyroxenite)	768.90	775.80	2.4	17
Rz-16	99-105	492.3-494	MELAGABBRO BRECCIA	492.10	499.50	2.0	6

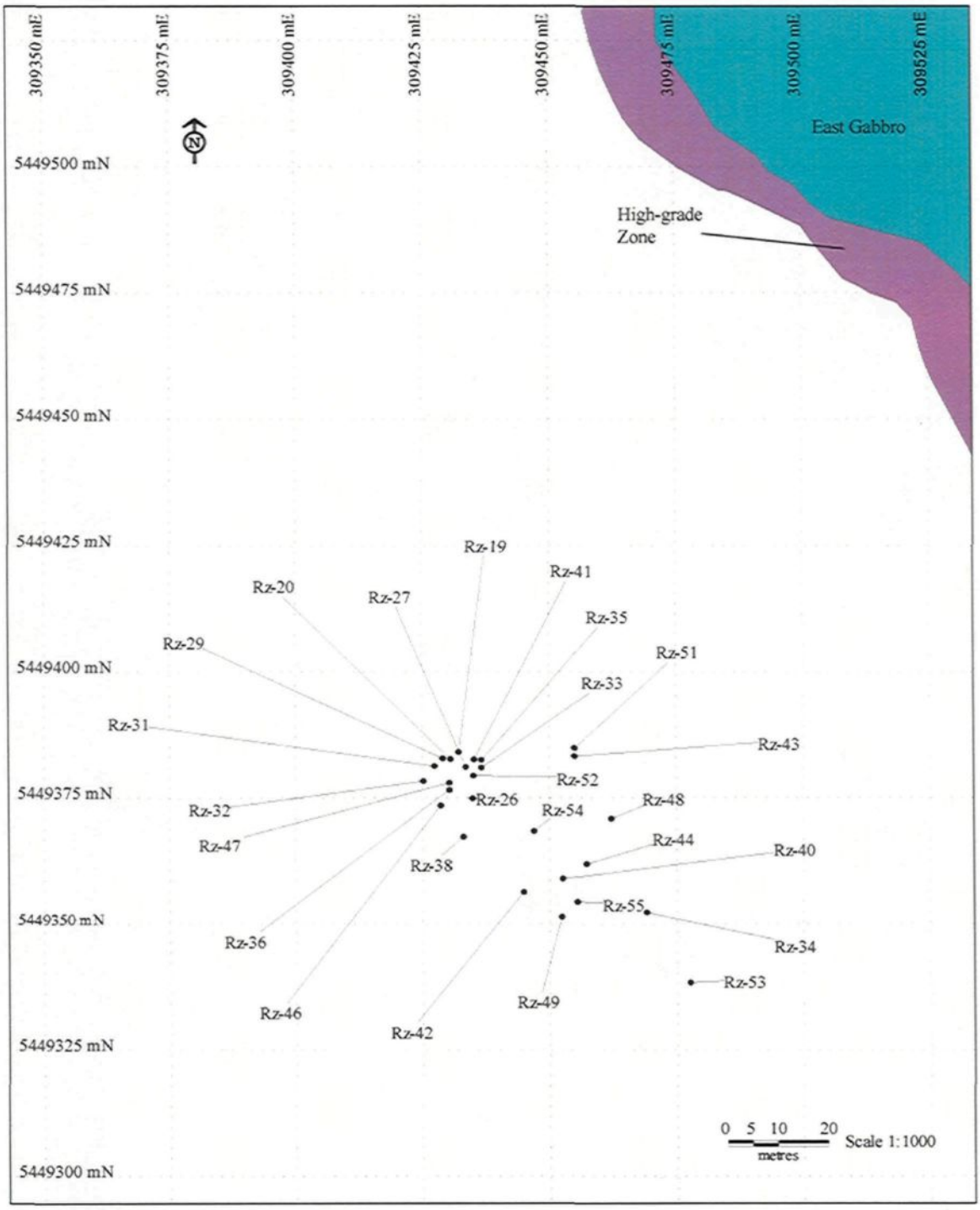

Figure 3.1(a) Sample location map for the Roby Zone. UTM coordinates are listed in Appendix I.

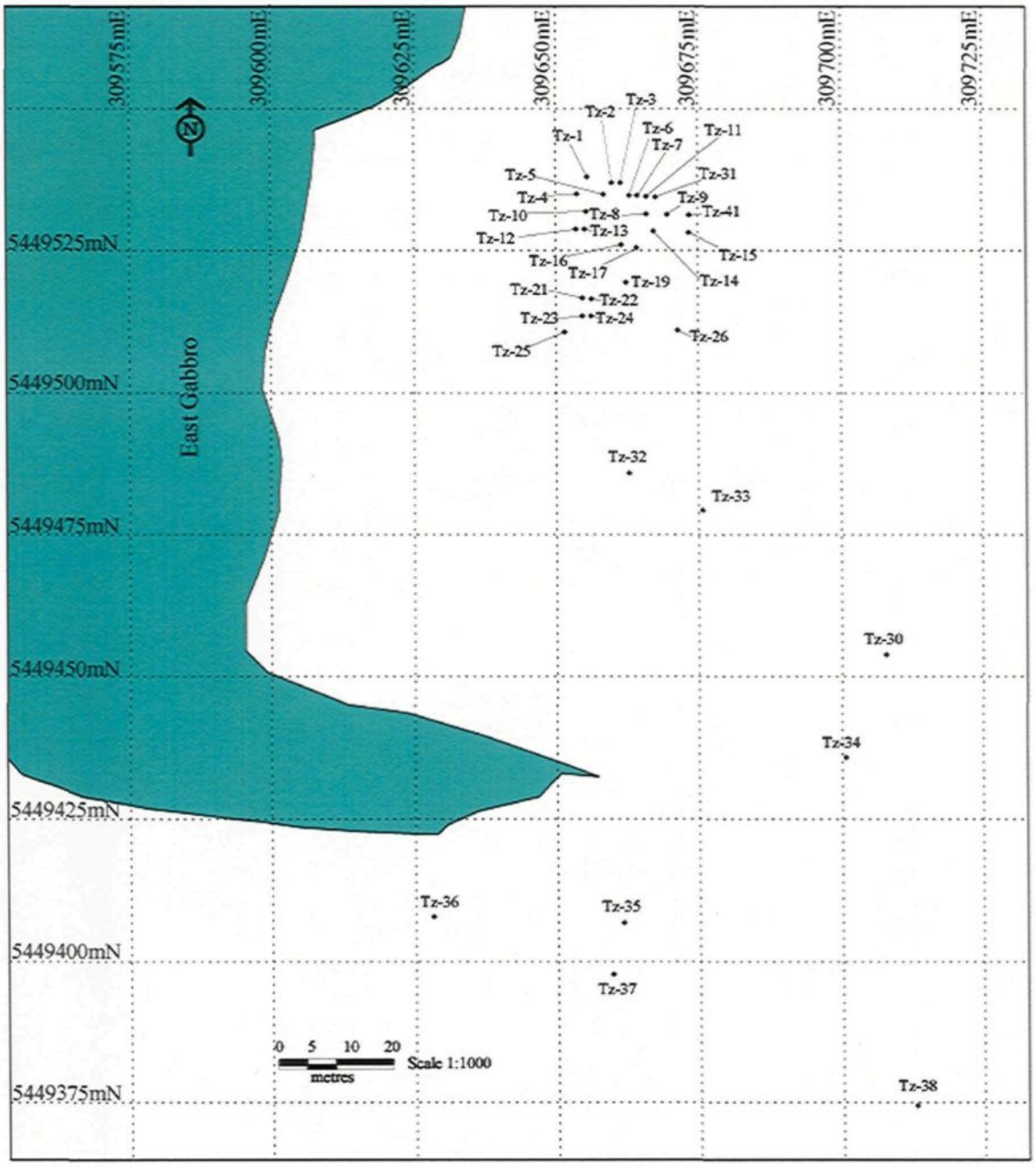

Figure 3.1(b). Sample location map for the Twilight Zone. UTM coordinates are listed in Appendix I.

summary of core logs of the samples collected from the High-grade Zone. Half-core sections 20 cm in length were selected on the basis of their high Pd concentrations (greater than 1 ppm) as representative samples of the high-grade ore type. Samples that represent the area adjacent to the high-grade ore type were also selected, their Pd concentrations fall below 1 ppm. These samples are considered as part of the High-grade Zone in this study and not high-grade ore type as per the definition by North American Palladium Ltd. Samples from the Roby and High-grade Zone were assigned the prefix Rz- and samples from the Twilight Zone, Tz. Samples from the High-grade Zone are from Rz1 to Rz17, inclusive.

Petrographic investigations were carried out on hand specimens and polished thin sections. Major element compositions of orthopyroxene, plagioclase and amphibole grains in representative samples from the Twilight, Roby and High-grade Zone were determined using a Cameca SX100 electron microprobe at Laval University, Québec. Operating conditions were 15.0 kV accelerating voltage, 20.0 nA beam current, and a beam diameter of 2–5 μm, with a counting time of 20 s and 10 s on peaks and backgrounds, respectively. Calibration standards were in Mineral Standard Mount MINM25-53 of Astimex Scientific Limited. The amphibole formula was determined using the method of Leake et al. (1997).

3.2. General Petrology

The majority of the rocks observed in the Roby and Twilight Zones are gabbronorites with minor anorthosite and felsic dykes. Most of gabbronorites have been altered and now consist largely of tremolite-actinolite and chlorite with some remnant plagioclase. These rocks do not have a preferred orientation of minerals and will be referred to as metagabbronorites. Most of the rocks in the High-grade Zone been have converted to chlorite-talc-actinolite schist; gabbronorite is confined to areas of less intense deformation.

Each rock type, except for the schist has a pegmatitic and varitextured textural equivalent. Much of the matrix material of the breccia is varitextured, but fragments of varitextured rocks are also present. Pegmatites form dyklets and isolated pods within the matrix both in the Roby and Twilight Zones (Fig. 1.5).

3.3. Gabbronorite

The majority of fragments in the breccia in the Twilight and Roby Zones are gabbronorites. Generally, these rocks have adcumulate textures and consist mainly of plagioclase (10 – 90%) and orthopyroxene (20 – 65%) (Fig. 3.2a). Trace to 5% clinopyroxene occurs mainly as exsolution lamellae in orthopyroxene (Fig. 3.2b). Hornblende, epidote, and sulphide minerals occur as minor interstitial phases. The

gabbronorites and leuco-gabbronorites are the least-altered rock types of the Roby and Twilight Zones. Alteration of the silicate minerals takes the form of slight uralitization of the orthopyroxene and sericitisation of the plagioclase (Fig. 3.3) to complete uralitization and sericitisation of orthopyroxene and plagioclase, respectively. Amphibole grains are interstitial and generally anhedral with straight edges. Electron probe microanalysis (EPMA) results range from tremolite-actinolite to hornblende in composition (Table 3.4). Fibrous interstitial grains observed in weakly altered grabbronorites are tremolite.

Overall, plagioclase makes up between 10 and 90 modal% of the gabbronorites. Most grains are moderately altered to sericite, chlorite, and epidote along fractures. Grains range in size from <1 mm to 4 mm, with subgrains <0.5 mm in size concentrated between plagioclase, orthopyroxene, and alteration minerals (Fig. 3.2). Plagioclase shows spindle twins and bending of the twin planes (Fig. 3.3) indicating high temperature deformation. The compositions of several plagioclase grains from Rz-9 (High-grade Zone), Rz-33 (Roby Zone fragment), Tz-7 (Twilight Zone fragment), and a pegmatite sample Tz-29 were determined by EPMA (Table 3.2). The An content of plagioclase varies from 54% (Tz-29, pegmatite) to about 65% (Rz-33, fragment).

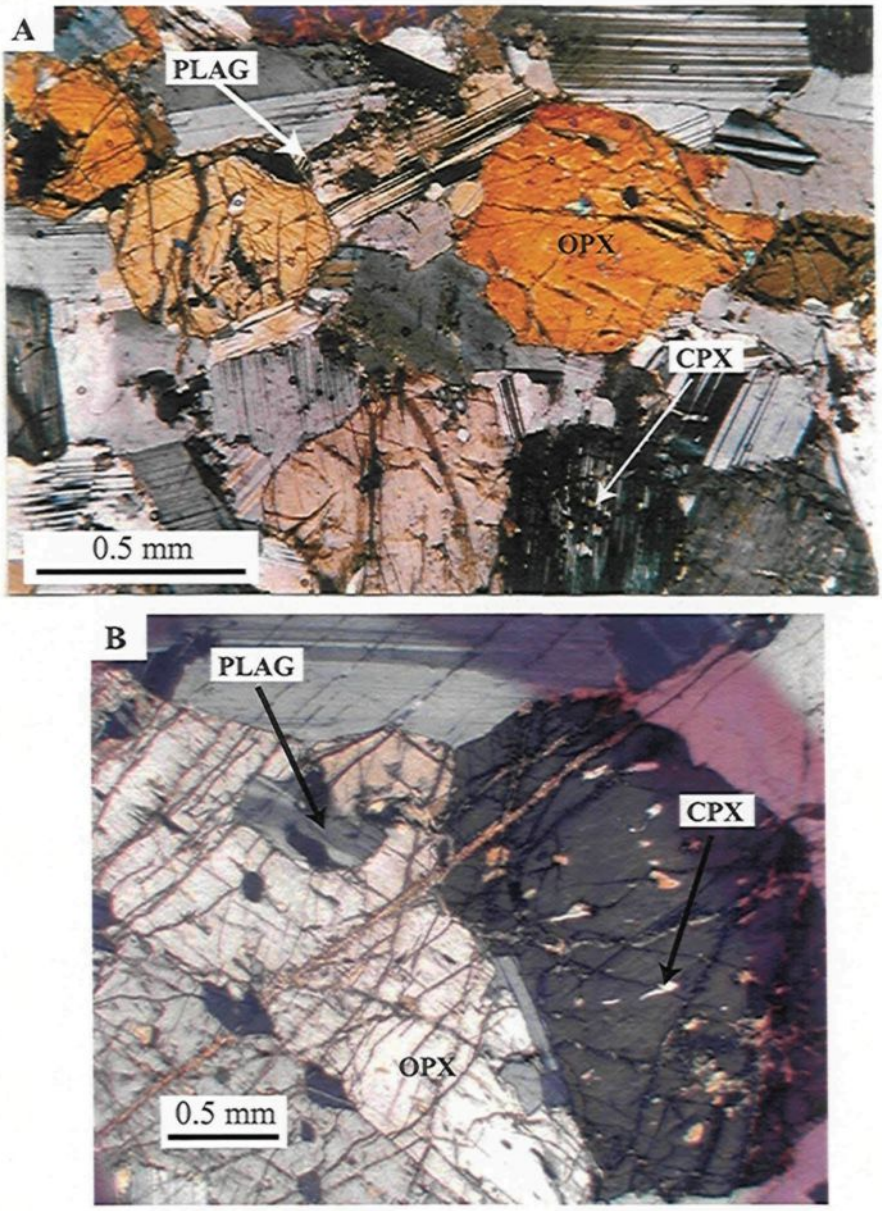

Figure 3.2. (a) Gabbronorite sample from the Twilight Zone, Tz-30 consisting of cumulate plagioclase and orthopyroxene. Clinopyroxene exsolution lamellae occur in orthopyroxene at the bottom right of image. Note, just off centre to the right the presence of small untwined subgrains of plagioclase between two orthopyroxene crystals. (b) Tz-10 Plagioclase occurs interstitial to as well as within orthopyroxene grains (left side of image). Clinopyroxene occurs mainly as exsolution lamellae in orthopyroxene to the right of image. Alteration occurs along fractures: tremolite-actinolite with epidote in opx and sericite assemblage along borders of some plagioclase grains.

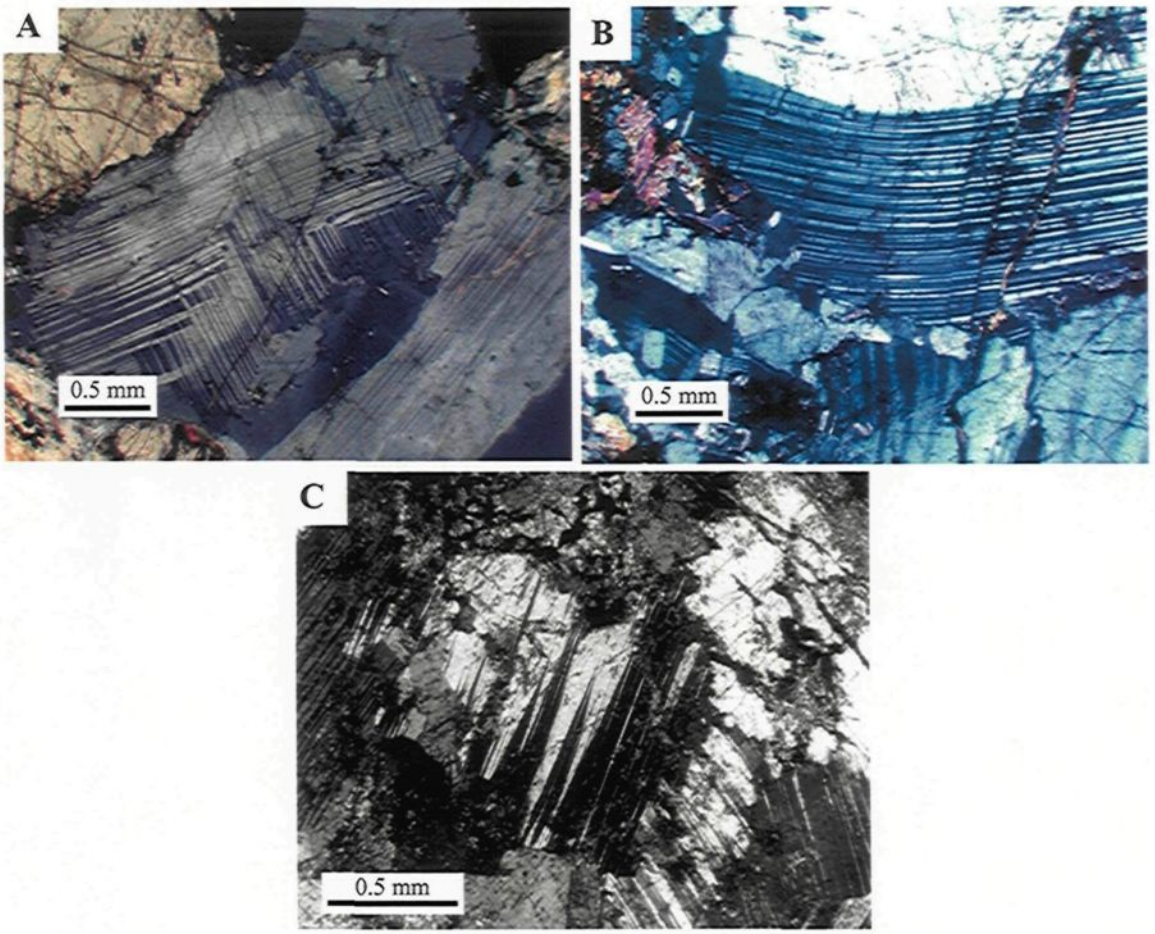

Figure 3.3. (a) Gabbronorite fragment (Tz-11) showing deformation lamellae at 90 degree angle intersections between different sets. (b) Plagioclase grain showing bent twin lamellae. Note smaller interstitial grains of plagioclase between larger deformed plagioclase grain. (c) Meta leucogabbro fragment (Rz-34) showing plagioclase grain in the centre with characteristic spindle twins indicating high temperature deformation.

Table 3.2. Average major element compositions of plagioclase from the Roby, Twilight and High-grade Zones. Individual analyses are in Appendix II.

Sample	**Rz9**	**Rz33**	**Tz7**	**Tz29**
Zone	**High-grade**	**Roby**	**Twilight**	**Twilight**
Occurence	Micro-breccia	Fragment	Fragment	Pegmatite
Lithology	Gabbro norite	Meta Leuco gabbronorite	Gabbro norite	Leuco gabbronorite
n	4	4	6	1
SiO_2 (wt%)	51.71	50.37	51.66	53.42
TiO_2	0.09	0.01	0.03	0.09
Al_2O_3	29.9	31.0	30.9	29.2
CaO	12.5	13.6	13.5	11.6
FeO	0.09	0.17	0.20	0.15
Na_2O	4.48	3.66	3.93	4.81
K_2O	0.03	0.11	0.09	0.06
Total	**98.84**	**99.17**	**100.59**	**99.68**
Si	3.02	3.61	3.02	4.8
Al	2.62	4.17	3.61	5.27
Ca	0.76	1.00	0.79	1.05
Fe	0.01	0.01	0.01	0.01
Na	0.52	0.52	0.46	0.87
K	<0.01	0.02	0.01	0.01
An	**60.02**	**65.11**	**62.72**	**54.45**

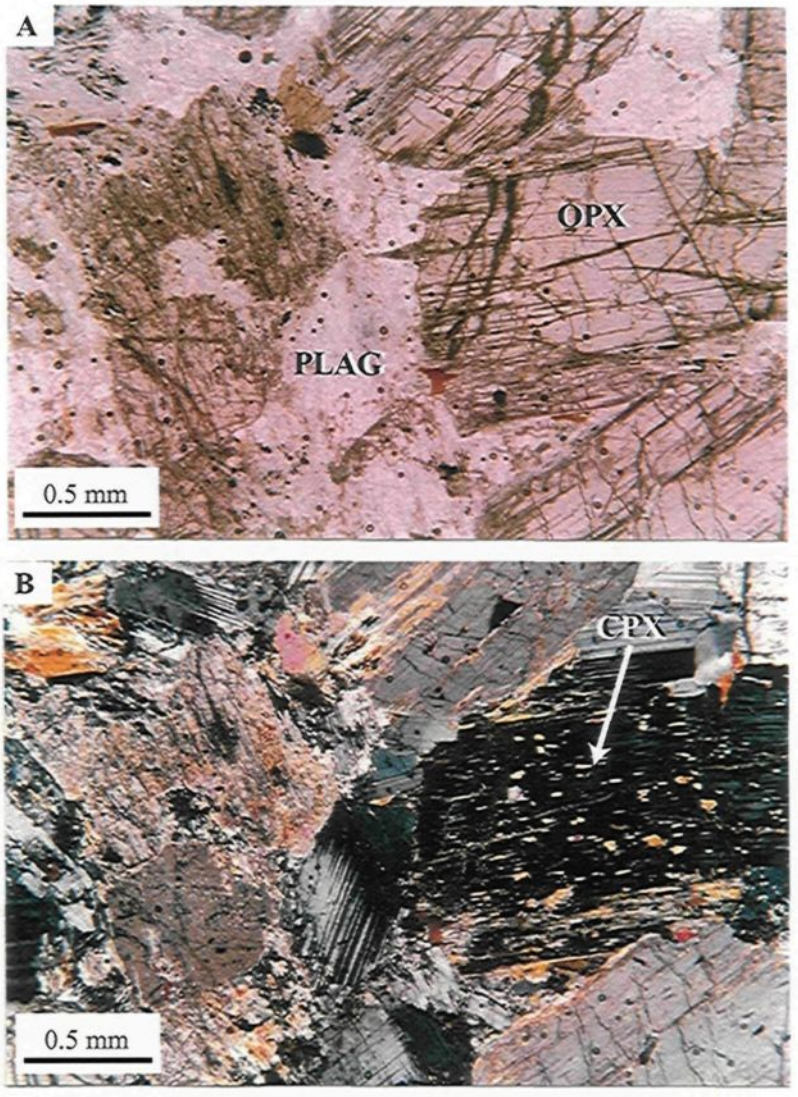

Figure 3.4. Alteration of gabbronorite (Tz-30). (a) In plane-polarised light most of the orthopyroxene is clear, but two grains to the left-of centre are cloudy or granular in texture due to alteration. Biotite is present interstitially along with minor epidote. Chlorite and amphibole are present as alteration material at the edge of the pyroxene grains. Plagioclase in this image is generally clear indicating low degree of alteration. The large orthopyroxene grain to the right of the image shows two distinct fractures traversing the grain at 10-20 degrees. (b) In cross-polarised light the cloudy pyroxene grains show moderate to intense alteration, the edges and most fractures of the other pyroxene grains are altered to tremolite-actinolite assemblage. The orthopyroxene grain dominating the right field displays clinopyroxene exsolution lamellae and as well as the deformation fractures. Note that primary igneous structures are still visible.

Orthopyroxene (1 mm – 3 mm) is generally subhedral, or rounded (Fig. 3.2) and makes up between 20 to 65 modal% of the rock. Alteration of orthopyroxene occurs along fractures and at the edges of clinopyroxene exsolution lamellae (Fig. 3.4(b)). On average orthopyroxene Mg number (Mg/(Mg + Fe) and hereafter abbreviated as Mg# is between 70 and 71 for the Roby and Twilight Zones matrix and fragment samples analysed (Table 3.3). There is a similarity in composition between the fragments and the matrix from both the Roby and Twilight Zones. Orthopyroxene grains from the Roby Zone matrix have an average composition of $Wo_3En_{68}Fs_{28}$ and the avergage fragment composition is $Wo_3En_{69}Fs_{28}$. Twilight Zone orthopyroxene in the matrix average $Wo_4En_{67}Fs_{29}$ and the fragments average $Wo_3En_{68}Fs_{29}$ (Table 3.3). These ranges are comparable to those determined by Michaud (1998). There is little variation in SiO_2, MgO, Al_2O_3, and TiO_2 in orthopyroxene composition, whether from fragment or matrix (Table 3.3).

Amphibole makes up up to 20 vol% of the rock. Major element contents of analysed amphiboles (Table 3.4) range between tremolite-actinolite and magnesiohornblende in composition (classification from Leake et al. 1997). Petrographic observations show that magnesiohornblende is generally less fibrous than actinolite. All amphibole analyses fall within the amphibolite metamorphic zone (TiO_2 <1.5 wt%) according to the classification by Ernst and Liu (1998). Magnesiohornblendes have higher TiO_2 concentrations than actinolites.

Biotite is present in minor amounts up to 1 modal%, occurs interstitial to plagioclase and orthopyroxene, and is associated with sulphide minerals and amphiboles. Minor amounts of epidote and trace amounts of amphibole and chlorite occur where there is alteration of orthopyroxene.

Total sulphide minerals vary in concentration from less than 1 modal% to about 2 modal%. The sulphides consist of blebs of pyrrhotite, pentlandite, and chalcopyrite with or without pyrite in approximately oval shapes (Fig. 3.5). The boundaries of the blebs against primary igneous minerals are curved and rational indicating equilibrium conditions. The boundaries with alteration minerals (amphibole, chlorite-actinolite) are interdigitated indicating disequilibrium conditions. In addition to its occurrence in the blebs the chalcopyrite occurs as finely disseminated grains associated with tremolite-actinolite indicating a redistribution of S and Cu. A small quantity of ilmenite and magnetite (up to 0.5 modal%) is associated with the sulphides. Interstitial minerals such as magnetite-ilmenite are associated with sulphides and alteration.

Table 3.3. Average pyroxene compositions from the Roby and Twilight Zones. Individual results can be found in Appendix II.

Sample	**Rz30**	**Rz33**	**Tz7**	**Tz2**	**Tz10**	**Tz8**	**Tz41**
Zone	**Roby**	**Roby**	**Twilight**	**Twilight**	**Twilight**	**Twilight**	**Twilight**
Occurence	Matrix	Fragment	Fragment	Fragment	Fragment	Matrix	Matrix
Lithology	Gabbro Norite	Meta Leuco gabbronorite	Gabbro norite	Leuco gabbro	Gabbro Norite	Gabbro norite	Gabbro norite
n	7	10	8	6	8	5	6
SiO_2 (wt%)	52.7	52.9	52.0	51.7	52.1	52.1	51.9
TiO_2	0.13	0.14	0.20	0.14	0.15	0.31	0.22
Al_2O_3	1.80	1.92	2.02	2.37	2.35	2.28	2.31
Cr_2O_3	0.08	0.06	0.08	0.13	0.13	0.13	0.13
FeO	17.6	17.8	19.0	17.8	17.4	17.9	17.8
MnO	0.35	0.34	0.36	0.31	0.30	0.32	0.32
MgO	24.2	24.6	23.3	24.8	24.5	22.6	23.6
CaO	1.44	1.34	1.74	1.40	1.85	3.22	2.32
Na_2O	0.02	0.02	0.04	0.02	0.03	0.07	0.06
K_2O	<0.01	<0.01	0.01	0.01	0.01	0.01	0.01
TOTAL	**98.43**	**99.32**	**98.88**	**98.73**	**98.82**	**99.09**	**98.82**
Mg#	0.71	0.71	0.69	0.71	0.72	0.69	0.70
Ca (atomic %)	1.03	0.96	1.24	1.00	1.32	2.30	1.66
Wo	3	3	4	3	4	6	5
En	68	69	66	69	68	64	66
Fs	28	28	32	28	28	29	29
Ac	0.1	0.1	0.1	0.1	0.1	0.3	0.2
Si	1.956	1.948	1.939	1.919	1.929	1.936	1.931
Ti	0.004	0.004	0.006	0.004	0.004	0.009	0.006
Al (IV)	0.043	0.052	0.061	0.073	0.070	0.064	0.069
Al (VI)	0.036	0.032	0.028	0.031	0.032	0.035	0.032
Cr	0.002	0.002	0.002	0.004	0.004	0.004	0.004
Fe(III)	0.041	0.024	0.036	0.072	0.045	0.022	0.038
Fe(II)	0.508	0.526	0.557	0.479	0.492	0.535	0.515
Mn	0.011	0.010	0.011	0.010	0.009	0.010	0.010
Mg	1.340	1.354	1.297	1.372	1.352	1.257	1.309
Ca	0.057	0.053	0.069	0.056	0.073	0.128	0.092
Na	0.002	0.002	0.003	0.001	0.002	0.005	0.004
TOTAL	**4.000**	**4.007**	**4.009**	**4.021**	**4.013**	**4.005**	**4.011**

Table 3.4. Average compositions for amphibole grains analysed from the Roby, Twilight and High-grade Zones. Recalculated using method of Leake et al. (1997). Individual analyses are in Appendix II.

Sample	Hornblende	Actinolite	Hornblende	Actinolite	Hornblende	Actinolite
Zone	High-grade	High-grade	Roby	Roby	Twilight	Twilight
n	27	24	22	26	11	6
SiO_2 (wt%)	48.3	52.8	49.5	53.5	48.3	53.4
TiO_2	0.74	0.18	0.51	0.12	0.87	0.11
Al_2O_3	7.31	2.80	6.08	2.55	6.30	2.19
Cr_2O_3	0.05	0.02	0.04	0.08	0.11	0.06
MgO	14.9	15.6	16.7	16.8	15.0	16.8
CaO	11.4	11.9	11.9	12.3	11.9	12.1
MnO	0.15	0.23	0.15	0.22	0.16	0.21
FeO (total)	11.5	11.5	10.1	10.8	12.5	11.2
Na_2O	0.85	0.25	0.72	0.29	0.77	0.26
K_2O	0.29	0.04	0.26	0.07	0.39	0.04
H_2O (measured)	2.01	2.07	2.03	2.07	2.00	2.04
F	0.05	0.02	0.04	0.02	0.04	0.04
Cl	0.03	0.03	0.04	0.02	0.06	0.05
TOTAL	**97.89**	**99.55**	**98.42**	**99.02**	**98.52**	**98.75**
Mg#	0.82	0.78	0.89	0.80	0.80	0.81
$Fe^{3+}/(Fe^{3+}+[6]A)$	0.72	0.72	0.86	0.83	0.84	0.92
Si	7.01	7.69	7.10	7.63	7.02	7.65
Al(IV)	0.98	0.31	0.90	0.36	0.97	0.34
Al(VI)	0.27	0.16	0.13	0.07	0.11	0.03
Fe(III)	0.71	0.35	0.75	0.41	0.69	0.48
Ti	0.08	0.02	0.05	0.01	0.09	0.01
Cr	0.01	0.00	0.01	0.01	0.01	0.01
Fe(ii)	0.72	0.97	0.48	0.88	0.84	0.87
Mn	0.02	0.03	0.02	0.03	0.02	0.03
Mg	3.22	3.47	3.59	3.59	3.25	3.58
Ca	1.78	1.84	1.83	1.88	1.85	1.87
Na	0.24	0.08	0.20	0.08	0.22	0.07
K	0.05	0.01	0.05	0.01	0.07	0.01
TOTAL	**15.09**	**14.92**	**15.10**	**14.97**	**15.15**	**14.95**

3.4. Metagabbronorite

Metagabbronorite is defined as a rock that displays magmatic textures but no longer contains pyroxene. Amphibole-rich metagabbronorite is the most common rock type found in the matrix of both the Roby and Twilight Zones. All samples contain plagioclase, chlorite, and amphibole. The metagabbronorite is generally medium- to fine-grained with the sporadic occurrence of very coarse-grained varieties with maximum grain sizes >2 cm. It is possible that previous authors (Lavigne and Michaud 2001; Hinchey et al. 2005) classified these rocks as pyroxenite or websterite due to the intense alteration assemblage.

Most tremolite-actinolite occurs as aggregates of acicular grains that pseudomorph pyroxene (Fig. 3.7 and Fig. 3.8(a)) or as intergranular fibrous aggregates associated with talc-carbonate, chlorite, and epidote alteration-assemblages. Tremolite-actinolite makes up between 25 and 70 modal% of the rock. The grains are bent and therefore deformed (Fig. 3.8(b)). In addition to pseudomorphs after pyroxenes, they also occur as randomly orientated grains and as aggregates of grains that radiate from a central point, creating a snowflake effect. Electron probe micro analyses show that most of the amphibole grains are tremolite (Table 3.4). Backscattered electron images of the grains show that they may represent multiple grain aggregates with significant variations in major element compositions (Mg# varies between 79% and 83%) between adjacent grains (Fig. 3.9(a) and (b)). This indicates disequilibrium conditions.

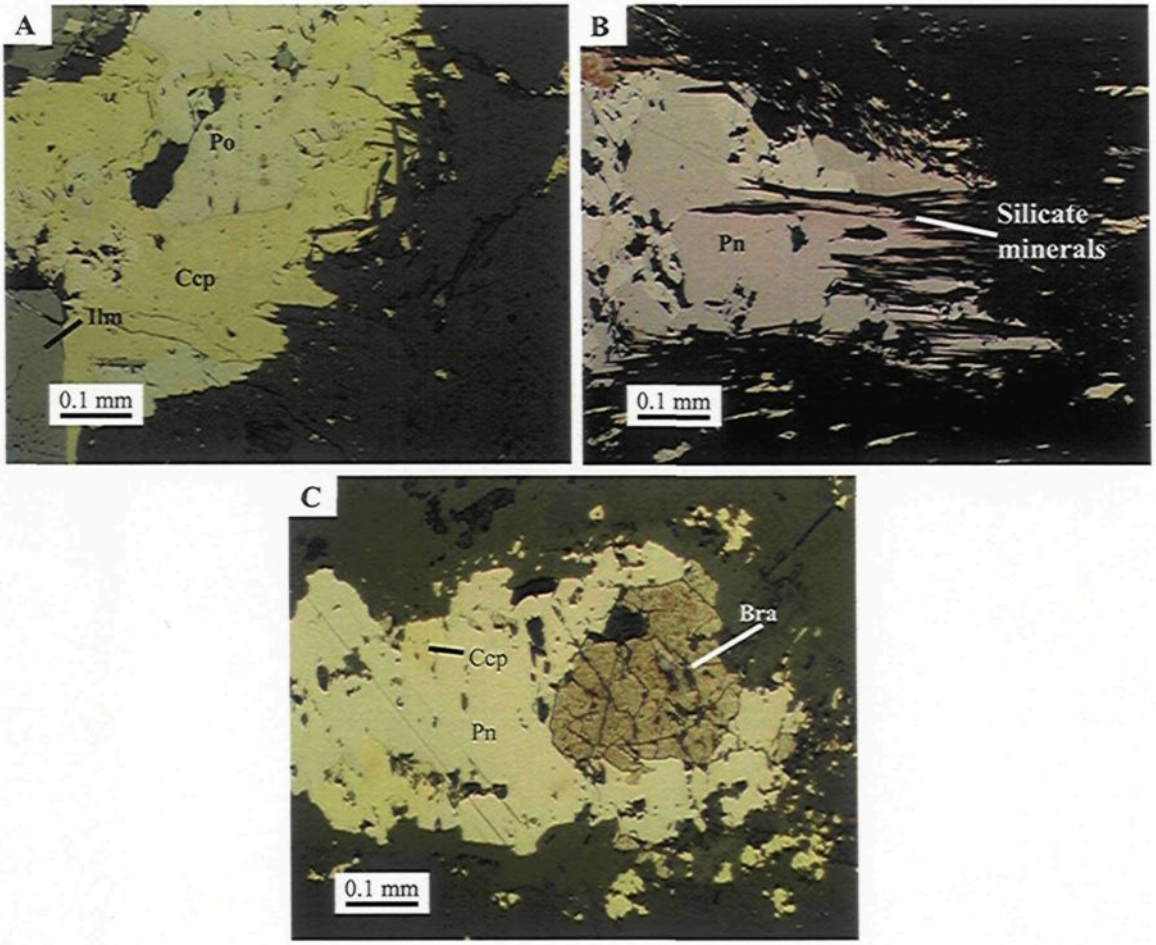

Figure 3.5. (a) Gabbronorite fragment sample (Tz-1) containing a bleb of chalcopyrite (Ccp), pyrrhotite (Po) with pentlandite (Pn) exsolution and ilmenite (Ilm - dark grey to the left of image). Chalcopyrite is intergrown with the silicate minerals. (b) Gabbronorite matrix sample (Rz-30) containing a jiggered bleb showing intergrowth of silicates (tremolite-actinolite) with sulphides (pentlandite-Pn). (c) Gabbronorite fragment sample (Tz-4) containing an irregular bleb of pentlandite, chalcopyrite, and bravoite (Bra) (alteration of pentlandite).

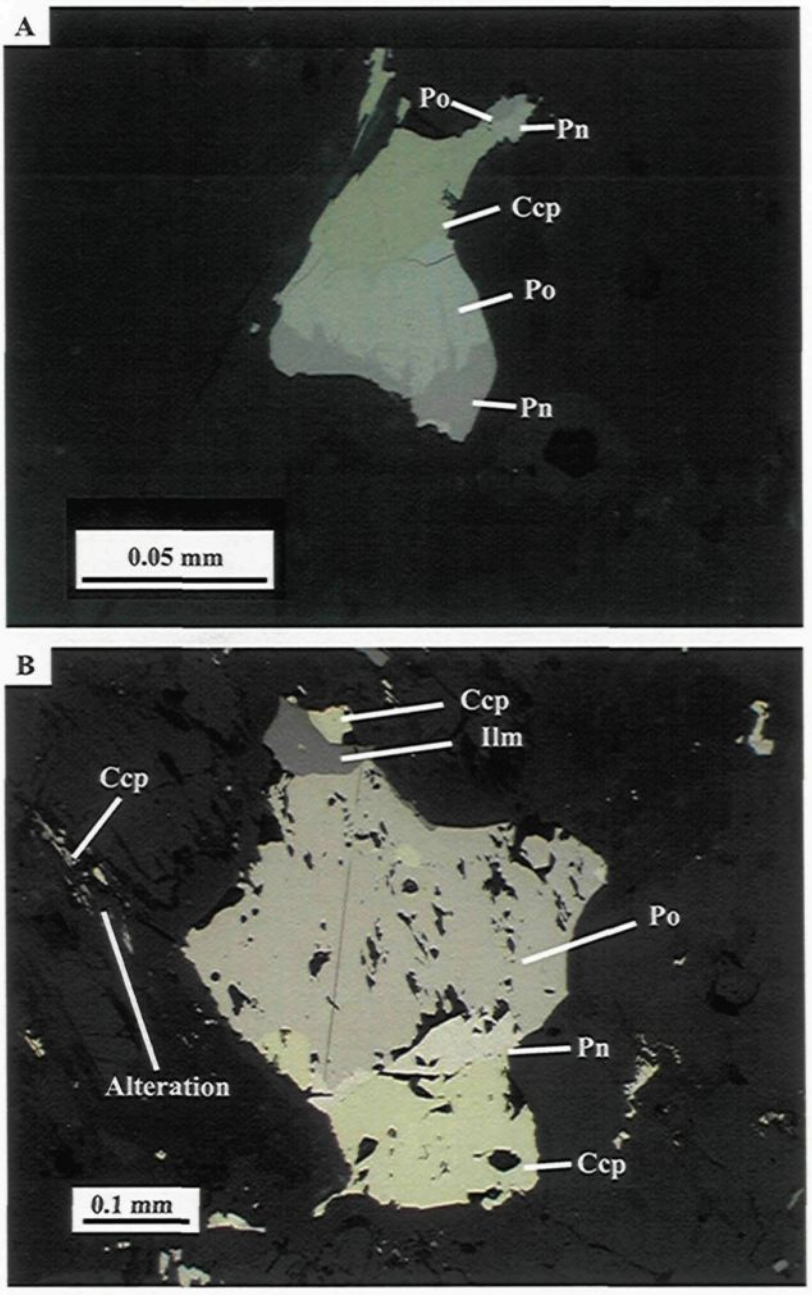

Figure 3.6. Sulphide mineralisation in gabbronorite matrix (Rz-30) showing (a) chalcopyrite (Ccp), pyrrhotite (Po) and pentlandite (Pn). Pentlandite forms fine intergrowths into pyrrhotite. (b) Ilmenite grain at the edge of pyrrhotite, bound with chalcopyrite. Note at left edge of grain alteration due to remobilised sulphides and this occurs as fine disseminated grains of chalcopyrite.

Plagioclase ranges in size from less than 1 mm to about 3 mm. It is present in low concentrations, between 5 and 35 modal%. The characteristics of plagioclase are similar to those found in the gabbronorite samples. Alteration of the plagioclase ranges from moderate to pervasive sericitisation. In plane polarised light, the altered plagioclase grains are cloudy to granular. Spindle twinning (Fig. 3.3(c)) and bending of the plagioclase grains due to deformation are common throughout the metagabbro samples. The cumulus plagioclase grains are generally subhedral and are usually surrounded by a dense fibrous halo of chlorite. The degree of alteration is high forming an agglomeration of alteration minerals around rare, isolated, anhedral, remnant igneous minerals (Fig. 3.7 and Fig. 3.8).

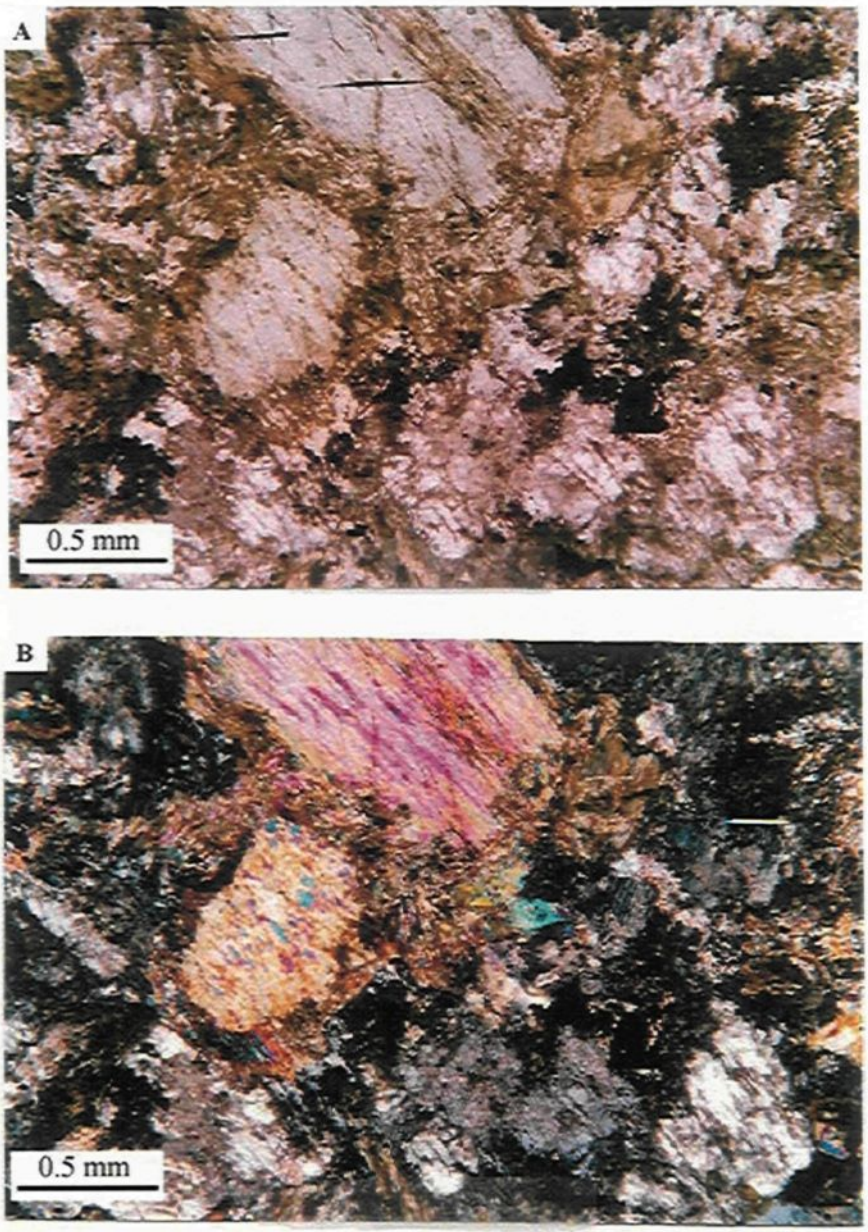

Figure 3.7. (a) Metagabbronorite fragment (Rz-26) in plane-polarised light showing pervasive chlorite, actinolite and epidote pseudomorph alteration of orthopyroxene and plagioclase. In cross-polarised light (b) pervasive alteration of the two prominent pyroxene grains is noted as complete pseudomorphism by tremolite-actinolite fibres.

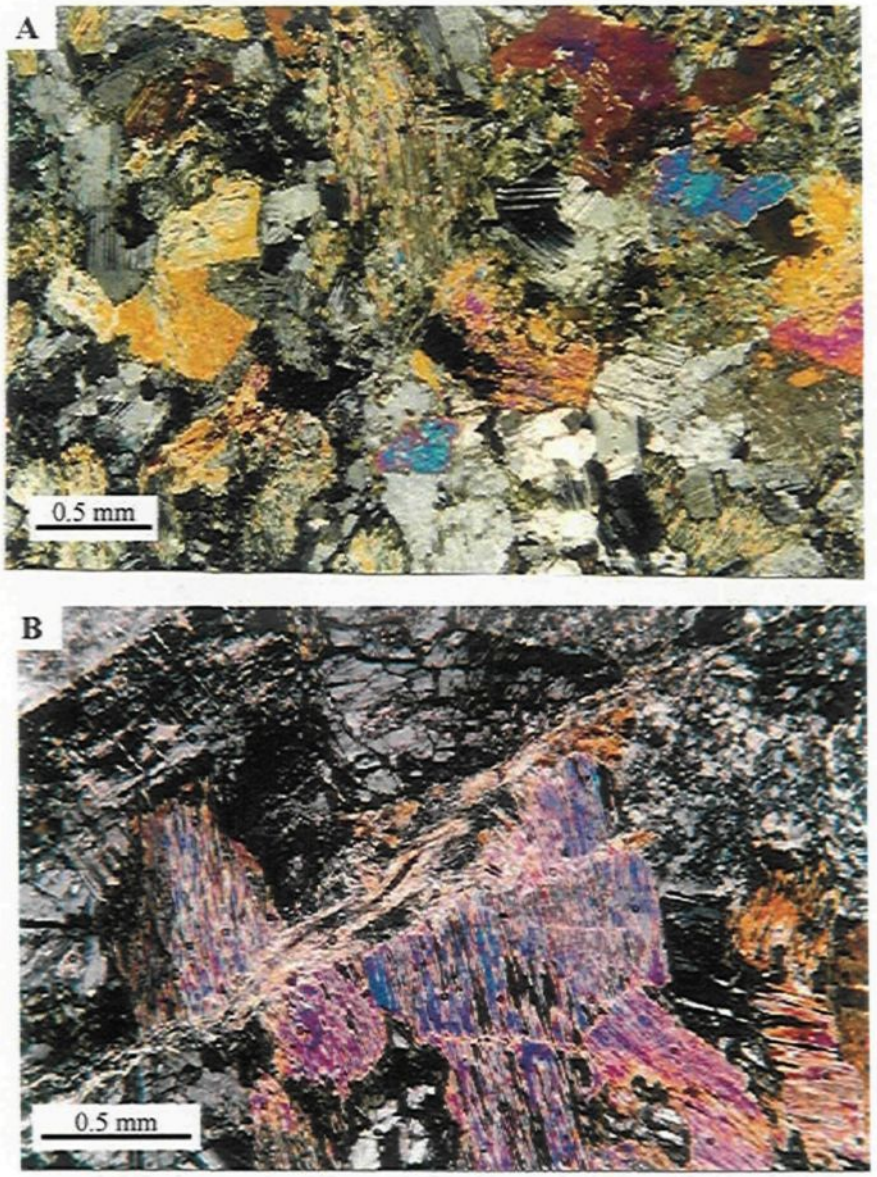

Figure 3.8. (a) Metagabbronorite sample (Tz-32) showing pervasive alteration of the orthopyroxene grains. Plagioclase grains are weakly to moderately altered. (b) A metagabbronorite matrix sample (Rz-5) in cross-polarised light the alteration is pervasive with complete replacement of the pyroxene grains by tremolite actinolite. Plagioclase grains at the top right corner of the image are fragmented by serictic alteration. A vein of tremolite-actinolite-chlorite-talc and epidote cuts through the field of view.

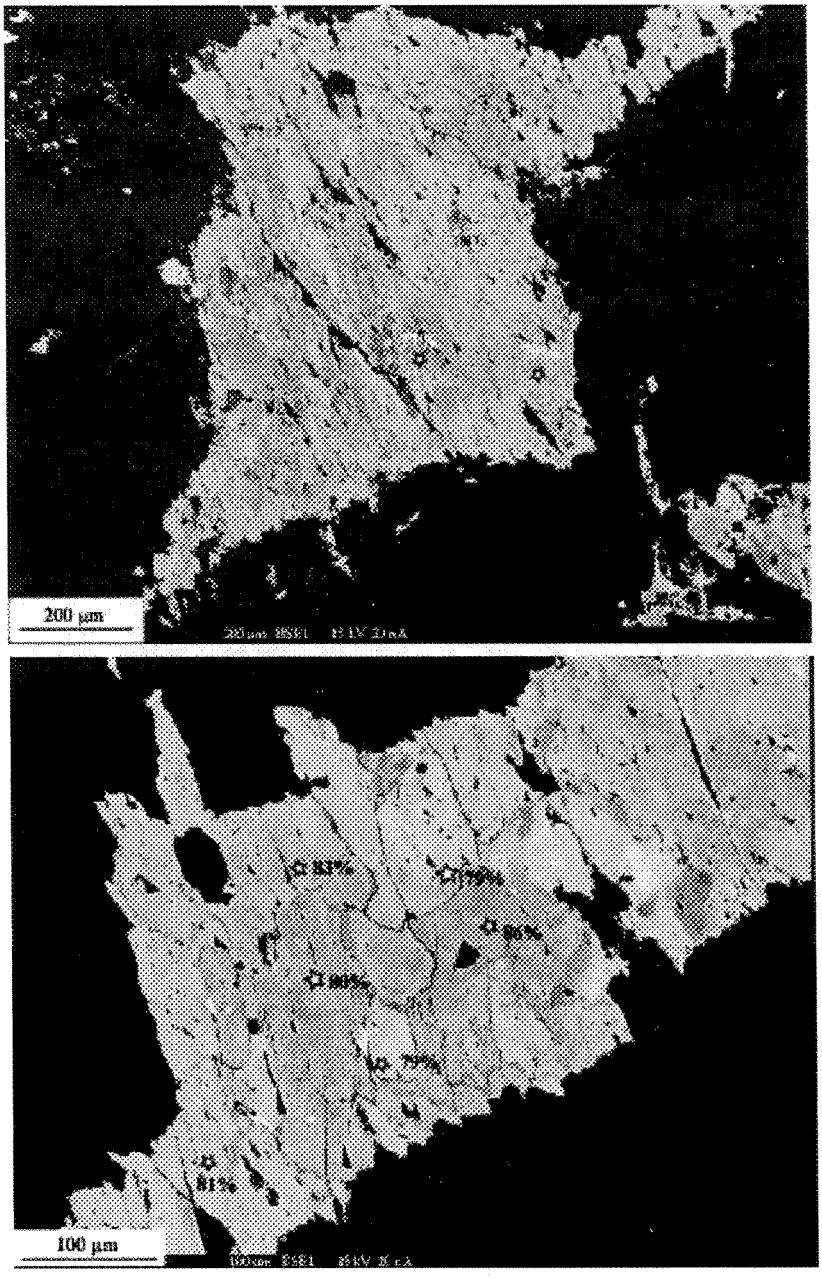

Figure 3.9. Backscatted electron images of an amphibole grain in a metagabbronorite fragment (Rz-28). The images show variations in intensity creating patches. The stars represent the magnesium number [Mg/(Mg+Fe)*100] determined by microprobe analysis. The major element analysis of the grains show considerable variation in composition indicating disequilibrium.

The percentage of sulphides varies greatly between 1 and 5 modal%. The size of the sulphide grains ranges from 0.5 mm to 2 cm (Sample Rz-33 from the Roby Zone contains the largest domain of sulphide at 2cm in size). The sulphide minerals are mainly chalcopyrite, pyrrhotite, pentlandite, and pyrite (Fig. 3. 10, Fig. 3. 11 and Fig 3.12). In the moderately to highly altered rocks the sulphides are located predominantly in the fractures and along the grain boundaries of altered orthopyroxene, as well as within fractures in plagioclase (Fig. 3. 10(a) and Fig. 3.12(a)). The disseminated grains are angular to rounded in form and appear to be fragments of larger grains. Where large grains are present, the chalcopyrite and, less commonly, the pyrrhotite at the periphery of the grains may be intergrown with the silicate minerals. Pyrite grains are most common in the grain aggregates (3. 10(b)). Trace amounts of magnetite and ilmenite occur in the gangue mineralisation as very finely disseminated grains or at boundaries between sulphide and silicate grains (Fig. 3. 12). Magnetite also contains exsolution lamellae of ilmenite and scattered inclusions of chalcopyrite (Fig. 3.11 and 3. 12).

Platinum-group minerals (PGM) occur in different locations within the gangue material or as inclusions in pyrite (Fig. 3.11(a)). In samples that are highly altered, the PGM are associated with the alteration minerals, with chalcopyrite, and with recrystallised pyrite grains (Fig. 3.11). The presence of pyrite is indicative of low temperatures within the system.

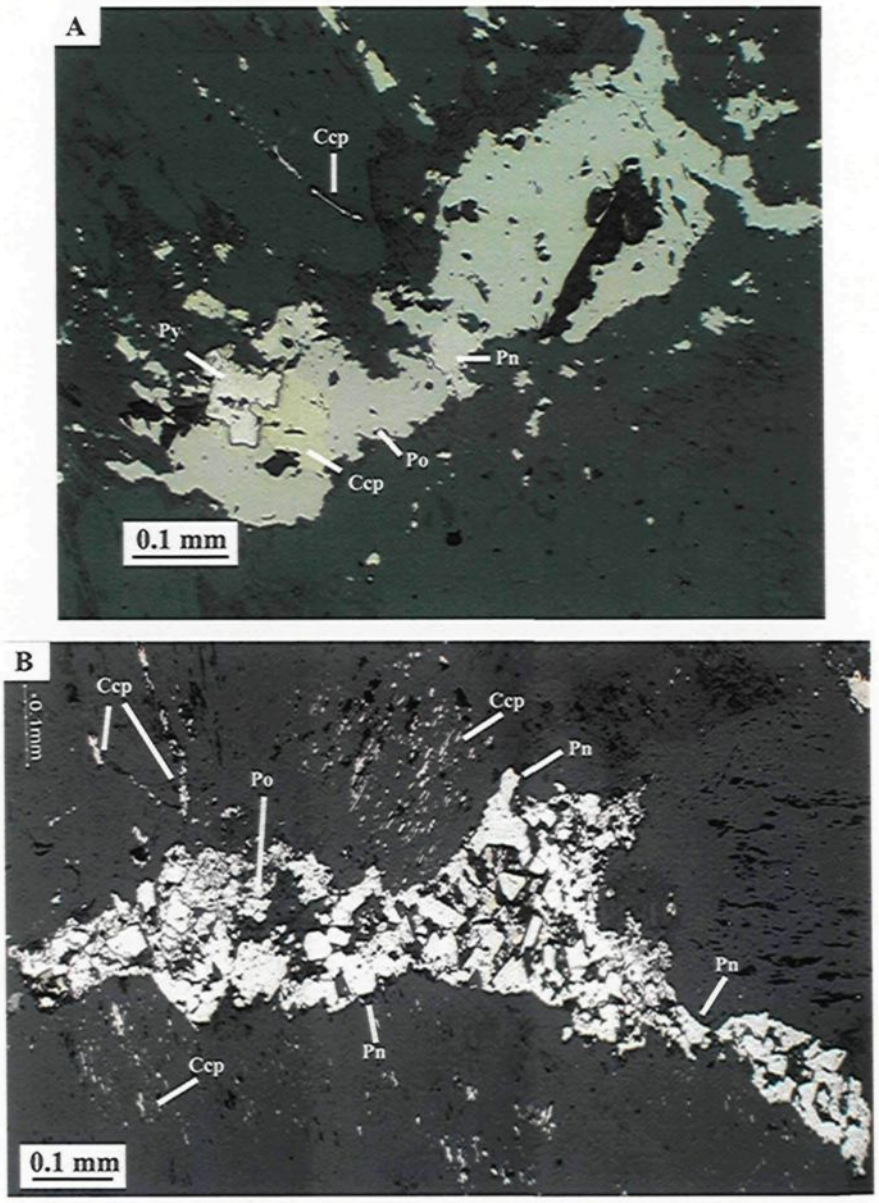

Figure 3.10. (a) Metagabbronorite matrix sample (Rz-45) showing the occurrence of pyrite (Py) with chalcopyrite (Ccp), pyrrhotite (Po) and pentlandite (Pn). Chalcopyrite is remobilised into the fractures of the silicate host mineralisation. (b) Metagabbronorite matrix (Rz-19) displaying pyrite grain aggregates (euhedral grains) with remnant sulphides mainly pyrrhotite with minor chalcopyrite. Chalcopyrite is the dominant sulphide in the small grains that surround the pyrite grains.

3.4.1. Microbreccia

Microbreccia makes up part of the High-grade Zone and is located within 2 m of the shear zone. Five samples from the High-grade Zone were collected from this rock type (Rz-2, 6, 9, 10, and 11). Microbreccia is defined as a breccia where the fragments are remnant minerals, mostly plagioclase and orthopyroxene, ranging in size from 0.5 to 1 mm in size. These fragments are hosted by a rock powder matrix comprised of an alteration assemblage of tremolite-actinolite, chlorite, talc and epidote (Fig 3.13).

Microbreccia have petrographic assemblages similar to those of the gabbronorites of the Roby and Twilight Zones, with higher amphibole contents at about 10 modal%. Plagioclase grains are between 0.1 mm and 3 mm in size, the smaller grains make up part of the local matrix material. Orthopyroxene, where preserved, contains some exsolution lamellae of clinopyroxene. The characteristics of alteration are the same as in the metagabbronorites.

Sulphide minerals generally occur as disseminated grains located in the matrix and they make up less than 1 modal% of the samples. The sulphides are similar in composition and texture to those located in the metagabbronorite with chalcopyrite more abundant than pentlandite.

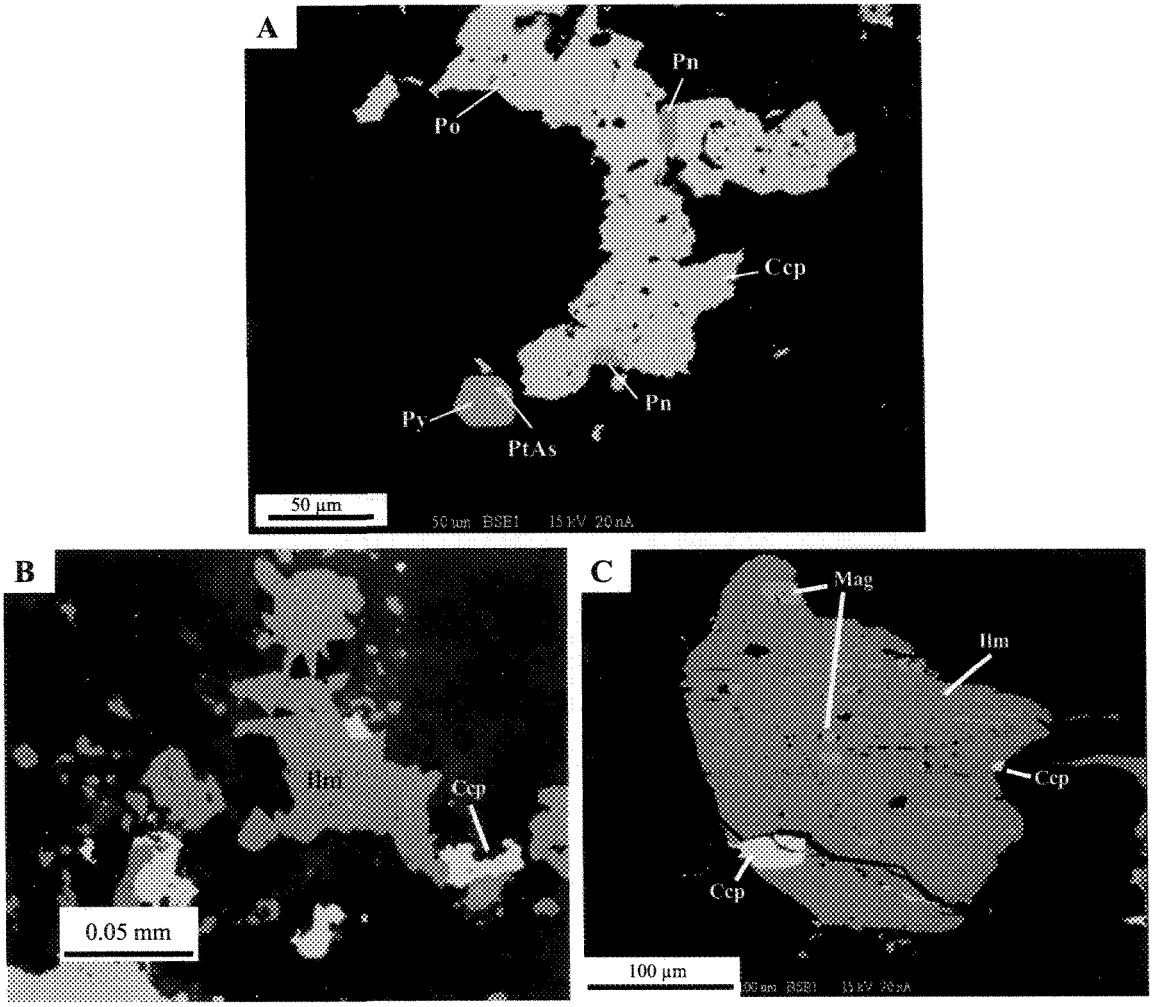

Figure 3.11. (a) Backscattered electron image of a sulphide grain from a meta-anorthosite fragment (Tz-25) showing pyrrhotite (Po), chalcopyrite (Ccp) and pentlandite (Pn). A pyrite (Py) grain contains a PtAs inclusion. Host material is tremolite-actinolite. (b) Reflected light microscope image from a meta-leucogabbro fragment (Rz-26) showing ilmenite (Ilm) grain with sulphides, mainly chalcopyrite, at the borders and as minute grains (sulphides and minor PGM) embedded within the ilmenite grain. (c) Backscattered electron image of an ilmenite grain from a leucogabbronorite pegmatite (Tz 27). This grain shows magnetite exsolution. Chalcopyrite (Ccp) is at the edges as blebs.

3.5. Pegmatite

Gabbronorites and metagabbronorites may locally form pegmatites. In such rocks, plagioclase ranges in size from 5 mm to 3 cm and crystals of orthopyroxene and actinolite may reach up to 4 cm (average 1 cm). Minor biotite and sulphide minerals may occur interstitially to the other phases. The mineral association is similar to that of all 15 gabbronorites and metagabbronorites examined in this study. Sulphides occur as small globular aggregates < 1 mm in size making up < 1 modal% of the samples; they consist mainly of pentlandite, chalcopyrite, and pyrrhotite. Ilmenite and magnetite occur interstitial to plagioclase and orthopyroxene; magnetite occurs mainly as inclusions within larger grains of ilmenite. Both oxides contain inclusions of sulphide minerals, most commonly chalcopyrite (Fig. 3.11(c))

3.6. Actinolite-Chlorite-Talc Schist

The gabbronorites become progressively more altered towards the interior of the shear zone of the High-grade Zone, essentially changing into actinolite-chlorite-talc schist. The degree of alteration is directly proportional to the deformation features, therefore the most altered rocks are confined to the shear zone of the High-grade Zone. The tremolite-actinolite grains range in size from millimetre to 5cm long aligned fibres. Chlorite occurs as stubby grain aggregates interstitial to talc. Epidote is rarely present with the chlorite and talc minerals.

Of all the rock types, the schist contains the lowest proportion of sulphide minerals (mostly <0.1 wt%). This observation is in agreement with observations made by Watkinson et al. (2002), Michaud and Lavigne (2003), and Hinchey and Hattori (2005). The sulphide fraction consists mainly of chalcopyrite, which is present as very finely disseminated grains (Fig. 3.12(a)). The association between grains of sulphide and tremolite-actinolite is similar to that observed in the metagabbro. Chalcopyrite grains are generally intergrown with silicate minerals. Small grains (> 1mm) of pyrrhotite, pentlandite and magnetite are also present. These grains are irregular to rounded in shape; magnetite generally occurs on the edges of pyrrhotite or pentlandite and is associated with chlorite and talc as an alteration product. Euhedral and anhedral pyrite grains are associated with the remnant pyrrhotite sulphide minerals.

The High-grade Zone samples contain the highest number of PGM grains. The PGM include Pd- or Pt-arsenides (PdSbAs, PtAs), bismuth-telurides (PdBiTe), and minor antinomides (PdSb). They range 1-10 microns in size, and in some cases these form composite grains up to 50 micronsin size (Fig. 3.14). The larger grains are usually composed of Pd-Sb-As with associated bravoite (PdS). Most examples contain chalcopyrite and pyrite grains within the gangue material (Fig. 3.14(d))

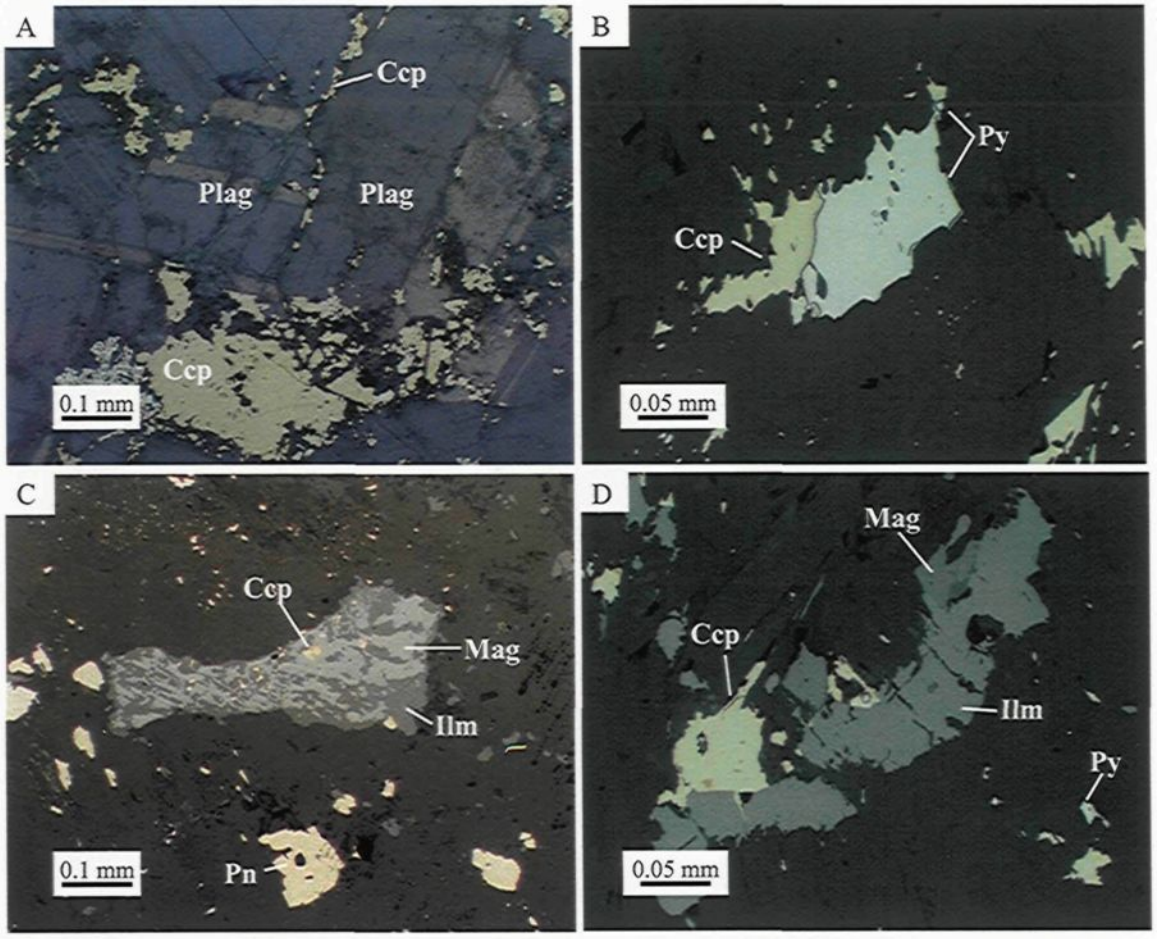

Figure 3.12. (a) Distribution of sulphides in gangue material in high-grade ore (Rz-17). Chalcopyrite (Ccp) occurs as 0.2 mm anhedral grain and as finer grains interstitial to and in altered fractures of plagioclase (Plag) grains. The darker grey shadows around the sulphides are the alteration products. (b) Pyrite and chalcopyrite within gangue material (Rz-6) (c) Rz-17 sample shows an ilmenite (Ilm) grain with magnetite (Mag) and chalcopyrite (Ccp) as inclusions. The grain is surrounded by crystals of pentlandite (Pn). (d) Rz-6 sample showing ilmenite grain with magnetite at the top edge associated with chalcopyrite. Chalcopyrite enters into fractures in the ilmenite grain.

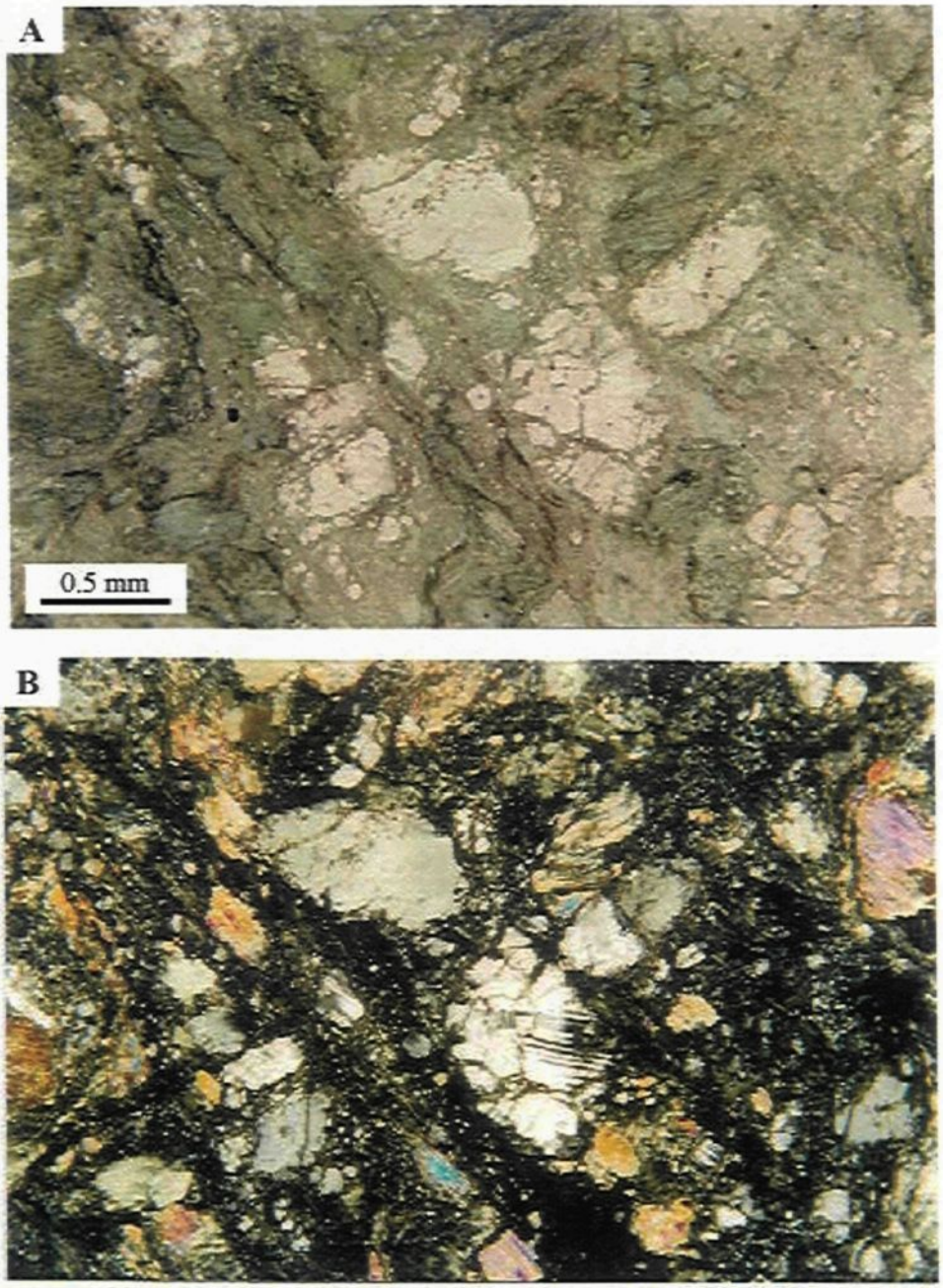

Figure 3.13. Microbreccia (Rz-2). (a) In plane-polarised light shows strong alteration, indicating tremolite-actinolite, chlorite, epidote and minor talc. Isolated grains of relatively unaltered plagioclase of varying sizes (mm to cm) are preserved. (b) In cross-polarised light the sample shows typical micro-breccia texture, fragments of plagioclase (clear minerals in plane-polarised light) and altered orthopyroxene grains, replaced by tremolite-actinolite within a matrix of alteration minerals.

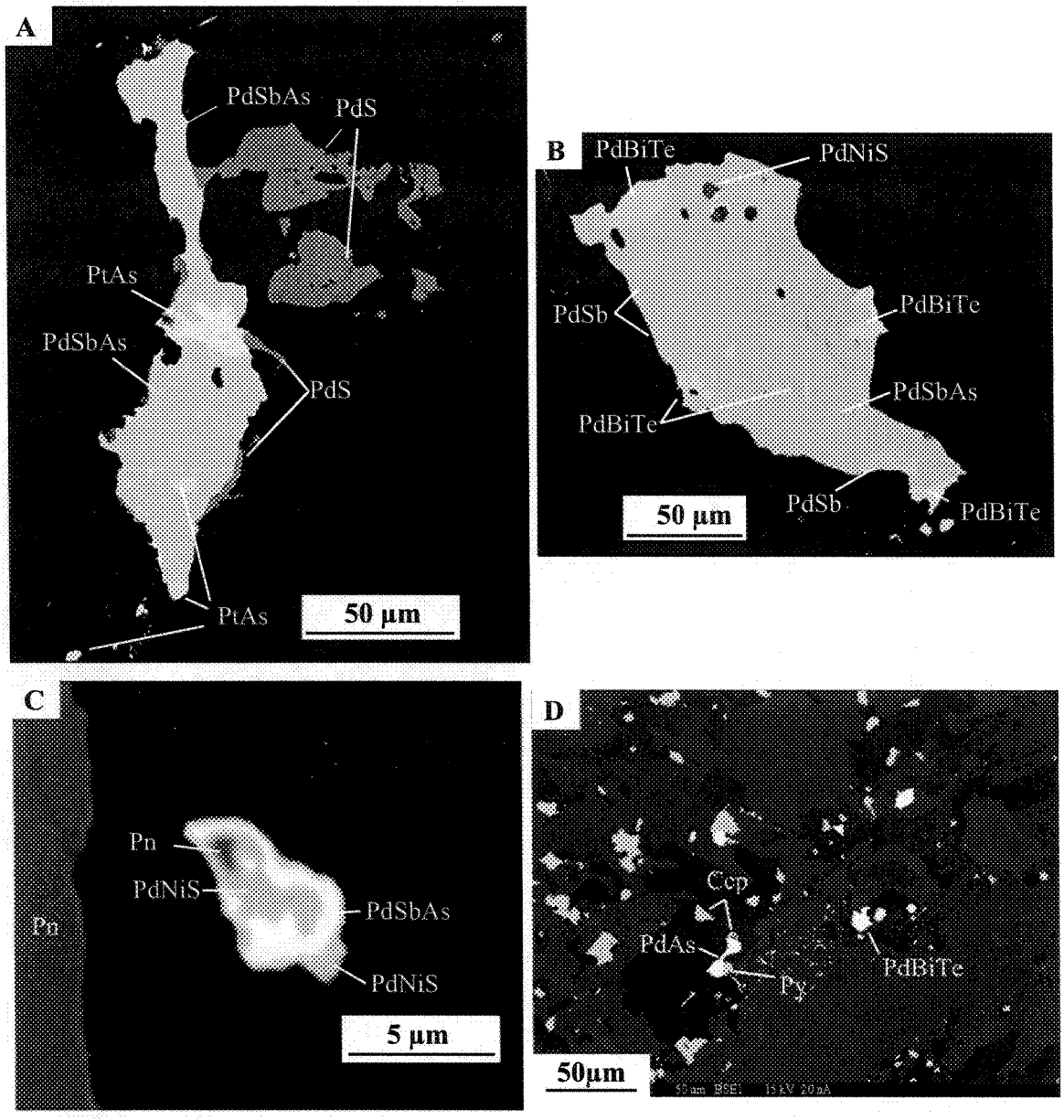

Figure 3.14. (a)-(c) Backscattered electron images showing representative mineralisation of Platinum-Group minerals in the High-grade Zone in an actinolite-chlorite-talc schist (Rz-3). The host material in each case is tremolite-actinolite with chlorite and talc. (d) An actinolite-chlorite-talc schist from the High-grade Zone (Rz-17) showing the presence of PGMs along with chalcopyrite (Ccp) and pyrite (Py).

3.7. Summary

The most common rock type is metagabbronorite followed by gabbronorite, chlorite-actinolite schist, pegmatite, varitextured, gabbronorite and microbreccia (Fig 3.15 (a, b and c)). Both the fragments and the matrix consist of these rock types, but the matrix is more commonly metagabbronorite, i.e. the matrix appears to be more altered than the fragments (Fig 3.15d and e). The Twilight and Roby Zones both consist primarily of gabbronorite and metagabbronorite (Fig 3.15 (a and b)). However, the Twilight Zone contains more gabbronorite than the Roby Zone (i.e., it is less altered). The High-grade Zone (Fig 3.15 (e)) consists of chlorite-actinolite schist and microbreccia of metagabbronorite.

In considering the objectives:

a) Characterising the three zones: there appears to be no difference between the rock types present (gabbronorite and metagabbronorite and pegmatite) in the Roby and Twilight Zones, although there is more metagabbronorite present in the Roby Zone. The High-grade Zone also contains metagabbronorite and chlorite-actinolite schist, but the latter appears to be altered gabbronorite.

b) The difference between the matrix and fragments: the rock types present in the matrix and the fragments are the same: namely gabbronorite and metagabbronorite. Varitextured lithologies and pegmatites are more common in the matrix.

c) The association between alteration and mineralization: The amount of sulphide mineralisation present in the metagabbronorite, chlorite-actinolite schist, and gabbronorite are similar, i.e., the altered samples do not contain more sulphides. The sulphide mineralization in the metagabbronorite is essentially igneous and in equilibrium with high-temperature minerals. The sulphide mineralization in the metagabbronorite and chlorite-actinolite schist has undergone recrystallisation and redistribution on the thin-section scale. Pyrite is more common and pyrrhotite is less common in the metagabbronorite and chlorite-actinolite schist. Although PGM were observed in all three rock types, more PGM grains were observed in the chlorite-actinolite schist.

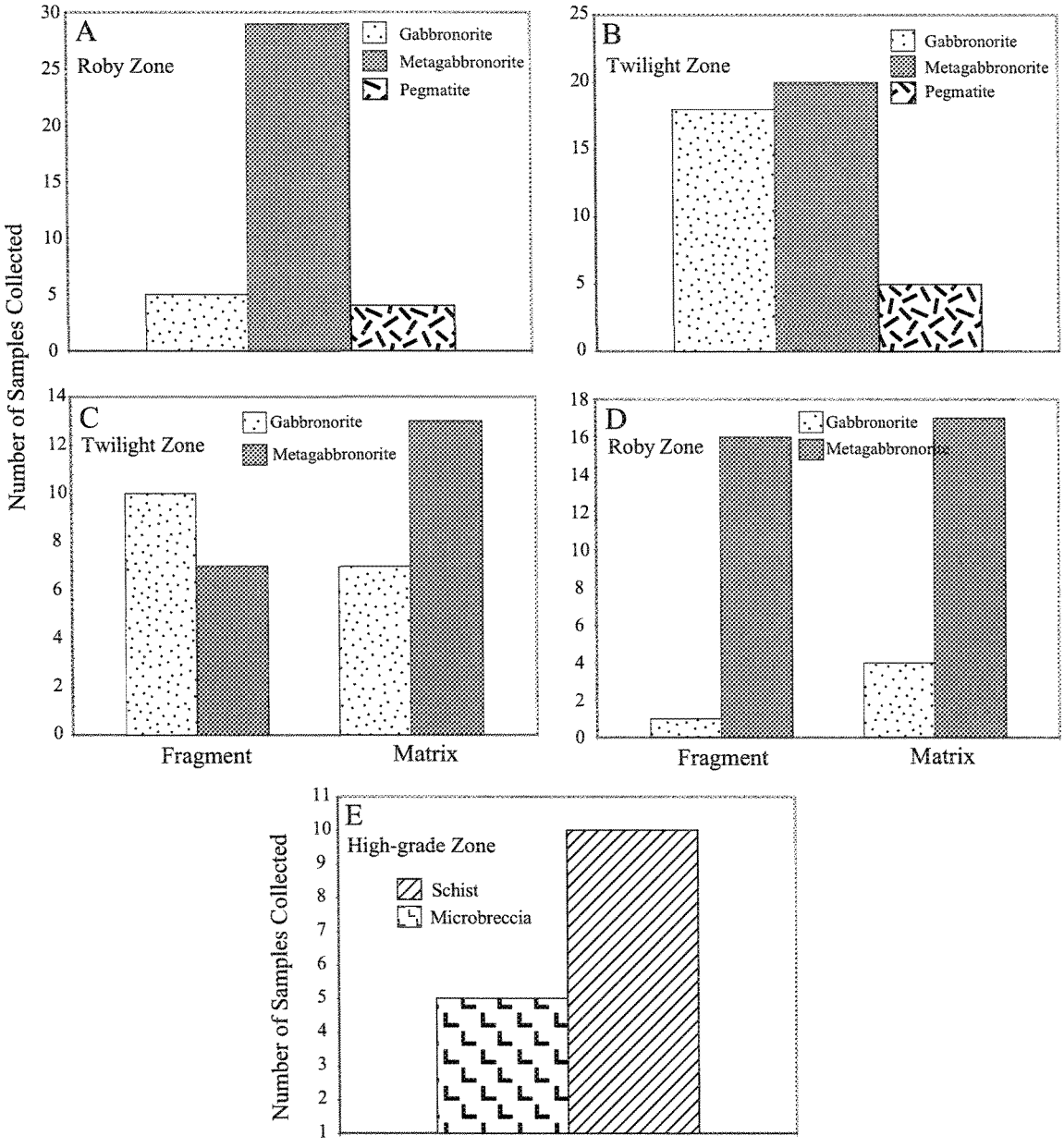

Figure 3.15. Histograms showing the distribution of the rock types within each zone, Twilight, Roby and High-grade. The rock types are described in the text.

4.
WHOLE-ROCK GEOCHEMISTRY

4.1. Analytical methods

Whole rock chemical analyses were carried out on all the samples collected. In the case of the samples collected from surface outcrops, the top 2 – 5 cm of the sample was removed prior to sample preparation to avoid the effects of weathering. Samples were crushed at the Université du Québec à Chicoutimi (UQAC) using a steel jaw crusher and were pulverised in an aluminina-ceramic mill. The alumina-ceramic mill was tested as a source of contaminantion by pulverizing 20g of quartz sand in the mill for 5 minutes. The results from the samples produce about 0.2 wt% Al_2O_3 contamination, but no other elements were detected.

Major element oxides were determined by X-ray fluorescence (XRF) at the Geoscience Laboratories in Sudbury, Ontario. Copper was determined on 1 g of rock powder by atomic absorption spectrometry at UQAC. Whole-rock sulphur was determined in duplicate using an infrared Horiba EMIA 220V sulphur and carbon analyser at UQAC, following the method described by Bedard et al. (in press). The relative standard deviation (RSD) is at ~2% for the standard LDI-2 (Bédard et al. in press). All other elements, except for the PGEs, were determined by instrumental neutron-activation analysis (INAA) on 2 g of rock powder using the method by Bedard and Barnes (2002). The Ontario Geological

Survey (OGS) has recently issued certified rock standards from the LDIC and one of these, LDI1, was used to monitor precision and accuracy of the analyses in this study (Table 4.1 a and b). Two in-house standards KPT1 and a Shale (SH-1) were also used to monitor the accuracy. The UQAC and OGS results agree within analytical error for all elements (Table 4.1 b).

In addition to the whole rock chemistry mineral composition of plagioclase, orthopyroxene, and the amphiboles in 15 polished 30 μm thick thin-sections were determined by electron microanalysis wavelength dispersive x-ray emission spectrometry using a Cameca SX100 at Laval University. The trace-elements in the minerals were determined for a subset of 8 of the 15 thin-sections (30 μm thick) using a New Wave Research Nd YAG 213 nm UV laser ablation system coupled to a Thermo X7 ICP-MS at UQAC. All analyses were performed using 40 μm laser-beam size with pulse energy of 0.18 or 0.5 mJ and a frequency of 20 Hz. Analyses were conducted using line traverses on thin-sections. Ablated material was carried into the ICP-MS using a flow of ~1 l/min of He in the laser cell. All elements were measured using a 10 ms dwell time. All measurements were made using Thermo Elemental PlasmaLab "time-resolved analysis" (TRA) data acquisition software allowing about 30 s for background followed by 70 s for laser ablation. NIST 612 (Pearce et al. 1997) glass was used for instrument calibration and NIST 610 was used as a secondary standard. NIST 612 values showed relative standard deviations between 2 and 10 for the 45 points analysed during data acquisition (Table 4.2). For the five NIST 610 samples the standard deviations are within the range of the standard values

(Table 4.2). Calcium was used as an internal standard to correct the ablation yield differences between and during individual analyses on both the samples and the standards. The Ca concentrations determined by EPMA were used to off-set analytical uncertainties that occur due to variations in the concentrations of the internal standards. Data processing was carried out using the PlasmaLab software. Typical detection limits are 1 – 20 ppm for Sc, V, Co, Cu, Zn, Ga, Rb and Ba.

Table 4.1(a). Standards LDI-1 and KPT 1 accepted major element values compared with results obtained at UQAC.

Standard	**LDI-1**		**LDI-1**		**KPT1**		**KPT1**
	Accepted (OGS)		**This Study**		**Working values (UQAC)**		**This Study**
n	n=36	σ	n=2	σ		σ	n=1
Element							
SiO_2 (wt%)	48.77	0.13	49.52	0.30	54.14	1.19	54.06
TiO_2	0.12	0.01	0.12	0.01	0.90	0.04	0.9
Al_2O_3	17.36	0.04	17.94	0.48	14.41	0.39	14.91
MgO	10.87	0.05	10.48	0.08	4.30	0.14	4.4
CaO	10.16	0.03	9.78	0.02	6.89	0.21	6.83
MnO	0.13	0.01	0.13	0.01	0.14	0.01	0.15
Fe_2O_3	7.69	0.01	7.45	0.21	12.2	0.34	12.5
Na_2O	1.89	0.01	1.62	0.20	2.61	0.09	2.57
K_2O	0.21	0.01	0.26	0.06	1.65	0.06	1.69
P_2O_5	ND	-	0.01	-	0.17	0.01	N/A
LOI	2.74	0.04	2.69	0.29	1.51	0.06	1.27
S (n=24)	0.12	0.01	0.13	0.05	1.03	0.34	N/A
Total	**99.94**	-	**99.97**	-	**97.47**	-	**99.43**

ND = Not Detected
N/A = Not analysed

Table 4.1(b). Standards LDI-1, KPT 1 and Shale accepted minor element values compared with results obtained at UQAC.

Standard	LDI-1 Accepted (OGS)		LDI-1 UQAC			KPT1 Accepted*		KPT1 UQAC			SHALE Accepted*		SHALE UQAC		
n	36	σ	1	σ	RSD		σ	1	σ	RSD		σ	3	σ	RSD
Element															
Ba	55	1	55	4.55	8.3	465	29	473	10	2.1	652	11 (n=100)	618	54	8.7
Ce	2.5	0.1	1.99	0.34	17.1	55.7	4.87	62.9	0.42	0.7	68	1.6 (n=24)	68.9	2.0	2.9
Cr	-	-	263	1	0.4	142	11	146	1	0.7	116	0.98 (n=101)	80.8	48.1	59.5
Cs	1.07	0.03	0.94	0.08	8.5	4.42	0,57	4.21	0.11	2.6	2.98	0.07 (n=100)	2.5	0.2	8.0
Cu	413	12	412	(n=1)		1112	102	N/A					N/A		
Eu	0.18	0.01	0.11	0.014	12.7	1.24	0.19	1.15	0.04	3.5	0.75	0.16 (n=24)	1.28	0.04	3.1
Hf	0.2	0.1	0.21	0.06	28.6	4.41	0.56	4.26	0.09	2.1	3.95	0.07 (n=97)	3.49	0.25	7.2
La	1.2	0.1	1.03	0.03	2.9	26.9	2.6	25.5	0.1	0.4	31.7	0.45 (n=101)	26.4	5.5	20.8
Lu	0.05	0.01	0.05	0.004	8.3	0.42	0.08	0.04	0.004	10.0	0.45	0.01 (n=101)	0.42	0.03	7.1
Nd	1.2	0.1	1.06	0.24	22.6	24.6	2.4	23.1	0.6	2.6	29.1	0.9 (n=101)	26.9	0.7	2.6
Ni	656	14	430	21	4.9	1093	71.7	N/A					N/A		
Rb	7.8	0.2	<3.3	-		61.5	5.3	58.1	2.1	3.6	133	1.5 (n=100)	124	4	3.2
Sc	24.5	1.7	25.7	0.04	0.2	24.8	2.5	24.0	0.03	0.1	19.6	0.19 (n=101)	18.2	0.2	1.1
Sm	0.28	0.02	0.28	0.002	0.7	4.90	0.62	4.96	0.01	0.2	5.5	0.08 (n=101)	4.95	1.09	22.0
Ta	<0.3	N/A	<.03	-		0.60	0.10	0.64	0.07	10.9	1.3	0.03 (n=99)	0.93	0.53	57.0
Tb	0.06	0.01	0.04	0.01	25.0	0.74	0.12	0.08	0.03	37.5	0.74	0.02 (n=100)	0.89	0.12	13.5
Th	0.12	0.01	0.1	0.02	20.0	7.27	0.86	7.72	0.06	0.8	9.2	0.11 (n=100)	9.30	0.40	4.3
U	0.04	0.01	<0.09	-		1.79	0.26	1.81	0.07	3.9	4.8	0.08 (n=100)	4.32	0.95	22.0
W	-	-	1.05	0.18	17.1	1.14	0.21	1.4	0.3	21.4	70	2 (n=99)	56.6	19.7	34.8
Yb	0.31	0.02	0.31	0.02	6.5	2.69	0.37	2.62	0.03	1.1	2.76	0.04 (n=101)	2.47	0.29	11.7

N/A = Not Analysed

* Working values UQAC

Table 4.2. Standards NIST 612 and 610 accepted values from (Pearce et al. 1997) with results obtained at UQAC.

Standard	**NIST610**		**NIST610**		**NIST612**		**NIST612**	
	UQAC		Accepted		UQAC		Accepted	
Element	n = 5	σ		σ	n = 45	σ		σ
^{65}Cu	259	37.4	430	23.6	37.7	3.98	36.7	3.07
^{85}Rb	252	26.6	431	11.4	32.6	3.05	31.6	0.59
^{88}Sr	409	15.1	497	18.3	76.4	4.52	76.1	2.29
^{89}Y	455	15.8	449	19.3	38.2	3.12	38.2	2.14
^{133}Cs	215	45.3	390	67.5	43.1	5.71	41.6	2.59
^{137}Ba	386	36.6	424	29.3	38.0	2.32	37.7	1.26
^{139}La	382	11.0	457	72.4	35.7	2.27	35.7	2.15
^{140}Ce	322	25.4	447	16.8	38.3	2.02	38.3	1.64
^{141}Pr	376	11.3	429	30.0	37.1	2.15	37.1	0.93
^{146}Nd	402	34.2	430	37.5	35.1	2.21	35.2	2.44
^{147}Sm	419	46.3	450	20.6	36.6	2.43	36.7	2.63
^{153}Eu	382	5.22	461	52.1	34.4	2.14	34.4	1.59
^{157}Gd	439	58.0	419	25.2	36.9	2.81	36.9	1.06
^{159}Tb	402	4.69	442	22.4	35.8	2.72	35.9	2.68
^{163}Dy	450	43.1	426	18.0	35.8	2.79	35.9	0.82
^{165}Ho	430	3.28	449	24.6	37.8	2.98	37.8	1.09
^{166}Er	437	38.9	426	23.9	37.3	2.95	37.4	1.50
^{169}Tm	430	8.11	420	19.2	37.4	3.02	37.5	1.25
^{172}Yb	486	54.1	461	30.6	39.9	3.08	39.9	2.86
^{175}Lu	427	8.21	434	31.0	37.5	3.09	37.7	1.95
^{181}Ta	445	44.3	376	77.6	39.8	2.83	39.7	2.15
^{208}Pb	245	11.0	413	15.4	37.3	2.08	38.9	1.84

4.2. Lithophile Chemistry

Brügmann et al. (1997) and Sutcliffe et al. (1989) presented a scenario for the magmatic evolution of the LDIC that involves the emplacement of multiple pulses of fractionated magma. Watkinson et al. (2002) also state that the breccia of the high-grade areas comprise heterolithic gabbroic breccia with gabbroic or melagabbroic matrix, implying that a magmatic mechanism formed the breccia ore. All these authors proposed a model that is based on the intrusion of a volatile-rich magma followed by the exsolution of a PGE-enriched deuteric fluid. This fluid, whilst still hot, migrated through the partially solidified magma promoting melting of the host rock which would crystallise to the pegmatitic and varitextured pods.

Brügmann et al. (1989) proposed 'constitutional zone refining' as the process that formed the mineralized zone, which involves migration of a volatile-rich magma, partially melting and crystallising cumulates *in situ* as it passes through previously crystallized cumulates. A mixture of the melanocratic and leucocratic components represents the residue and the partial melt. Macdonald (1988) observed that the clasts (fragments) within the breccia represent all the lithologies present in the varitextured gabbro that surround the breccia ore. This observation suggested to him that the fragments in the breccia were locally derived. The matrix is described as a mixed magmatic rock that intruded before the generation of the gabbro breccia.

Previous workers refer to the rocks of the High-grade Zone as websterite or pyroxenite (Brügmann et al. 1997; Lavigne and Michaud 2001; Hinchey et al. 2005). Several authors (Watkinson and Dunning 1979; Lavigne and Michaud 2001; Hinchey et al. 2005) mention clinopyroxenite and cumulus clinopyroxene in rocks from the High-grade and Roby Zones. No cumulate clinopyroxene was observed in the gabbronorite samples collected for this study (Chapter 3). Apart from a few exsolution lamellae of cpx in orthopyroxene very little clinopyroxene was observed. Estimating the original mineralogy and subsequently assigning an igneous rock name to the protolith rocks is made difficult by the pervasive alteration throughout the rocks. To investigate whether the metagabbronorites originally contained clinopyroxene that has now been replaced by actinolite and chlorite, CIPW norms were calculated for all the samples.

The CIPW norms for the samples were calculated after removing Fe present in sulphides and assuming an FeO / (Fe_2O_3 + FeO) ratio of 0.8. The CIPW norms confirm the petrographic observations that the majority of the rocks are gabbronorites containing less than 20 wt% clinopyroxene and consisting largely of plagioclase and orthopyroxene (Fig. 4.1 and APPENDIX I). No pyroxenite samples were observed. The samples range from melanogabbronorite to leucogabbronorite. Samples from the Roby and Twilight Zones cover all three subdivisions. In contrast, there are no samples from the High-grade Zone that fall in the leucogabbronorite field.

Most of the samples contain less than 20 % clinopyroxene. None of the samples were classified as pyroxenites. Because the CIPW norm attributes all Al_2O_3 to plagioclase, but in cases some of the Al_2O_3 is also present in pyroxene (~1-2%), so the CIPW norm tends to overestimate the amount of plagioclase. However, this would not lead to a reclassification of the samples (except Rz-27 – Fig. 4.1a) as in the most extreme cases for example a rock with 90% pyroxene where all the Al_2O_3 in the pyroxene is attributed to plagioclase in the norm, there is an overestimation of the plagioclase content by only 5%. Previous workers may have been misled by the extensive alteration in the High-grade Zone. This alteration resulted in a high percentage of actinolite and chlorite in the rocks and they interpreted this actinolite to have formed only from clinopyroxene. However, the reaction of orthopyroxene and plagioclase with H_2O will also produce actinolite and chlorite. Actinolite need not have formed from clinopyroxene, thus the modal amount of actinolite and chlorite in the rocks does not reflect the original amount of clinopyroxene in the rock. Some samples from the Twilight and Roby Zones shown in Figure 4.1a (ii) fall in the melagabbronorite zone and if they were to be completely altered they could also have been previously misclassified as pyroxenite. Figure 4.1b shows samples from Brügmann et al. (1989) and Hinchey et al. (2005). All samples were collected from the same area as this study and they all fall within the same field. (Hinchey et al. 2005) classified some samples as clinopyroxenites, but this plot does not show these samples to fall within the pyroxenite field.

According to Figure 4.1a (i) there are 4 Roby and 5 Twilight Zone samples that contain more than 20 % normative clinopyroxene (Fig. 4.1a and APPENDIX I), but none are from the High-grade Zone. As will be outlined below these samples show different trends on bivarient plots compared to the bulk of the samples.

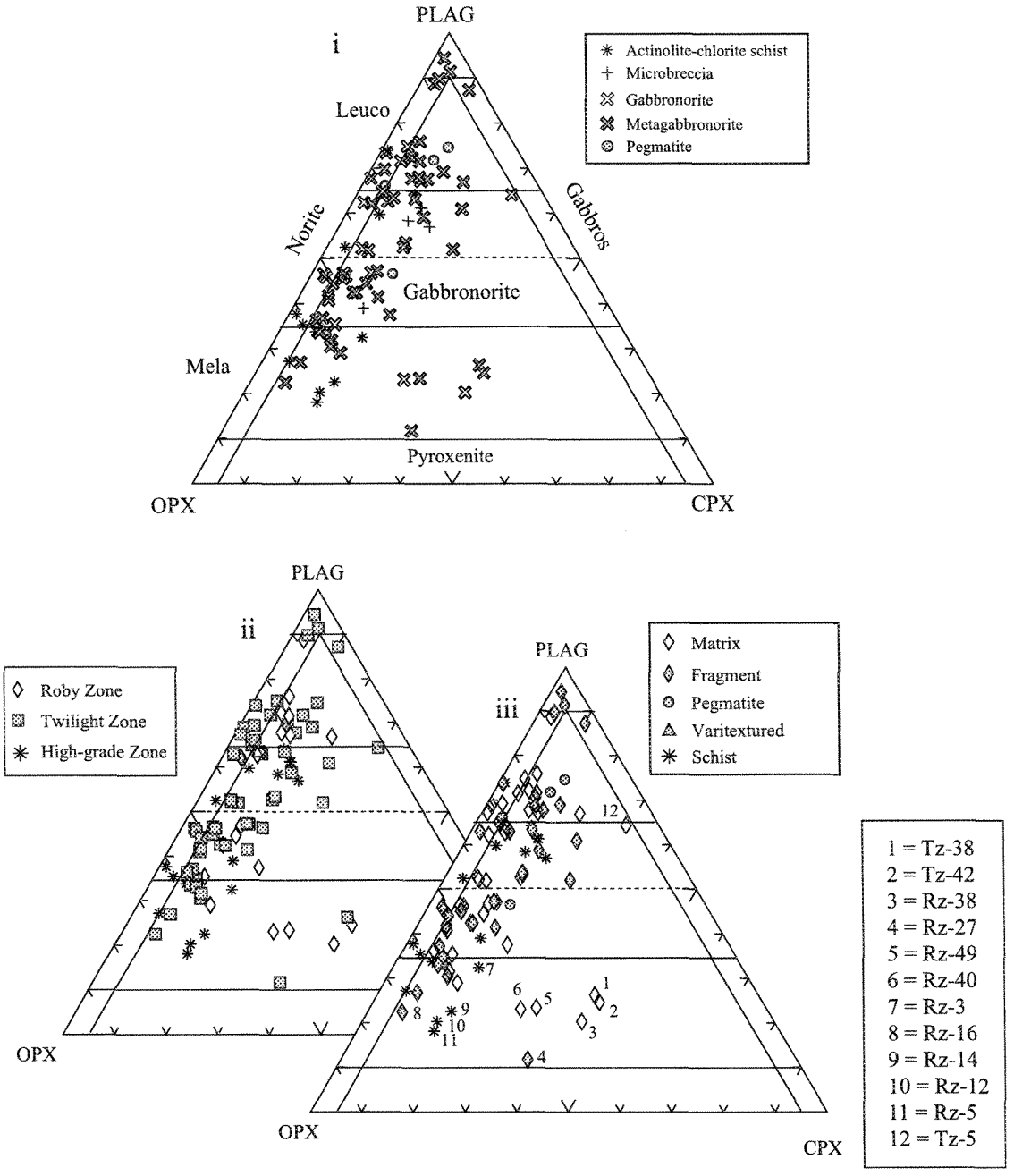

Figure 4.1a CIPW normative rock compositions for samples from the Roby and Twilight Zones, (i) The different rock types of the zones. Plagioclase (Plag) - pyroxene: clinopyroxene (Cpx) and orthopyroxene (Opx). (ii) The different zones and the fragment and matrix and (iii) the different textures. Note that the rocks from all three zones cover the same compositional range, also note that the dominant pyroxene is orthopyroxene. Nomenclature and divisions from Streckeisen (1975).

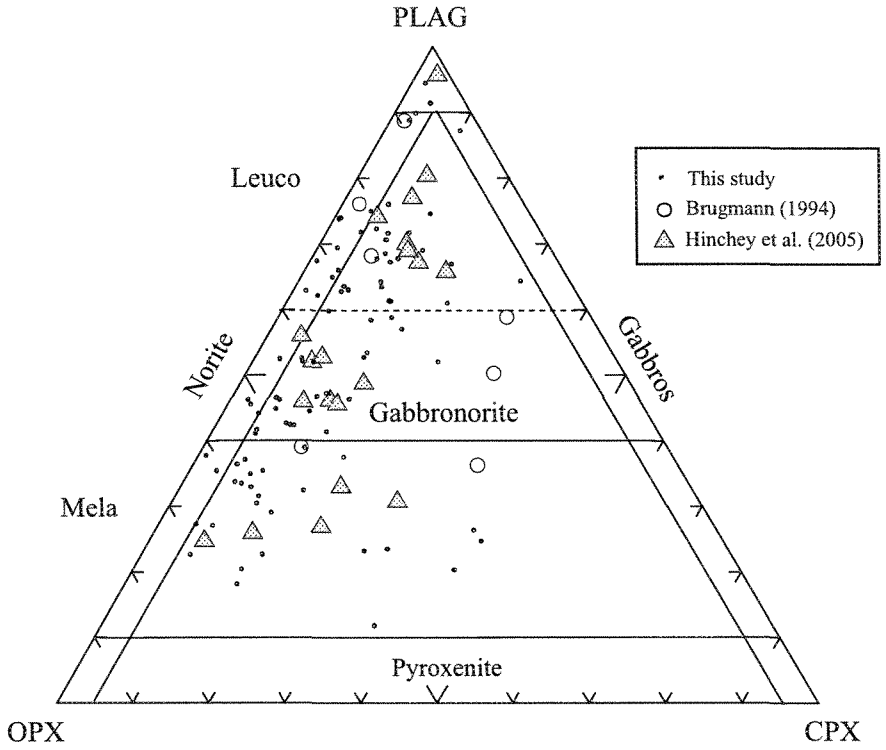

Figure 4.1b CIPW normative rock compositions for samples from this study and samples from (Brügmann et al. 1989) and (Hinchey et al. 2005). Nomenclature and divisions from Streckeisen (1975).

4.2.1. Major Elements

Hinchey et al. (2005) identify three magmatic events, an early felsic, middle melanocratic sulphide-bearing gabbro, and a late sulphide-free melanocratic gabbro event. In this model the matrix for the LDIC is sulphide-enriched melanogabbro. Hinchey et al. (2005) suggest that their geochemical data indicates a co-magmatic origin for most of the gabbroic rocks except for the clinopyroxenite. Clinopyroxenite according to Hinchey et al. (2005) is concentrated in the High-grade Zone. As discussed in section 4.2. this does not appear to be the case from the samples examined in this study.

Macdonald (1988), who studied surface exposures, described the High-grade Zone as consisting of several websterite dykes intruded into anorthositic gabbro. The host rock may have been partially consolidated and subsequently deformed in a ductile fashion during emplacement of the dykes (Macdonald 1988). Dunning (1979), Watkinson et al. (2002), Lavigne and Michaud (2001) and Hinchey and Hattori (2005) describe the high-grade ore as a 15 – 25 m thick pyroxenite to melagabbro unit.

The SiO_2 values of the rocks in this study range from 46 – 56 wt%, encompassing the compositional range from felsic to mafic (APPENDIX I). The average compositions (Table 4.3.) show that samples from the High-grade Zone are richer in mafic components (MgO and Cr) and poorer in felsic components (SiO_2, Al_2O_3, Na_2O, K_2O, Ba, Rb) than the average Roby and Twilight Zones. This correlates with the petrographic observations,

where the most felsic samples are from the Twilight and Roby Zones (Fig. 3.15). The average values of the Roby and Twilight Zones are similar, although the Twilight Zone contains slightly lower concentrations of Al_2O_3, SiO_2, and Na_2O. Although the average compositions of the individual zones are different it must be emphasized that there is overlap in compositions as can be seen on the bivarent plots of the major elements (Fig. 4.2).

The division of the samples collected into fragments, matrix, and pegmatite/varitextured rocks shows that the varitextured samples from the Roby Zone are the most leucocratic with the highest average SiO_2 value. The fragments from the Roby and Twilight Zones have the next highest SiO_2 values. The High-grade Zone along with the average matrix in the Roby and the Twilight are more mafic in composition (MgO values are higher than 12-15 wt% in comparison to 8.5 and 11 wt% for the fragments and pegmatoids) (Tables 4.3, 4.4 and 4.5). In order to consider the effects of alteration one can compare the gabbronorite, metagabbronorite, and high-grade samples. Most oxides are similar in the gabbronorite and metagabbronorite (Table 4.6). The metagabbronorite does, however, contain more H_2O, Na_2O and K_2O, possibly due to alteration. The chlorite-actinolite schist contains more H_2O.

Table 4.3. Average major and trace element compositions of the High-grade, Roby and Twilight Zones

Zone	High-grade		Roby		Twilight	
n	**17**	σ	**36**	σ	**40**	σ
SiO_2	48.6	1.63	49.6	1.46	48.8	0.84
TiO_2	0.17	0.09	0.14	0.10	0.22	0.07
Al_2O_3	12.4	4.84	16.0	5.66	14.1	4.52
Fe_2O_3 (Total)	10.1	2.72	8.74	2.91	11.3	3.23
Fe_2O_3	9.73	2.34	8.09	2.58	11.0	2.99
Fe(s)	0.30	0.59	0.26	0.38	0.35	0.40
MnO	0.17	0.05	0.15	0.04	0.17	0.04
MgO	15.0	5.64	11.0	4.39	12.3	3.72
CaO	7.79	1.99	9.21	1.46	8.14	1.86
Na_2O	1.25	0.85	2.10	0.87	1.37	0.66
K_2O	0.22	0.20	0.73	0.33	0.50	0.41
P_2O_5	0.00	0.02	0.01	0.00	0.01	0.01
LOI	3.90	1.50	2.60	0.56	2.25	1.11
Total	**99.9**	**0.76**	**100.2**	**0.85**	**99.8**	**0.55**
Mg#	0.74	0.07	0.72	0.03	0.70	0.06
Ba (ppm)	43	36	147	75	90	58
Ce	3.74	4.80	3.20	3.17	2.95	2.46
Cr	425	271	307	392	361	167
Cs	1.50	1.22	2.52	1.78	1.28	0.81
Eu	0.18	0.09	0.23	0.16	0.23	0.07
Hf	0.27	0.29	0.22	0.20	0.22	0.25
La	0.99	0.73	1.30	0.56	1.27	0.98
Lu	0.08	0.01	0.08	0.01	0.08	0.01
Nd	1.12	0.50	1.51	2.57	1.08	1.07
Rb	10.6	9.74	17.2	9.02	13.7	12.0
Sc	37.6	7.44	31.8	11.4	37.6	11.9
Sm	0.30	0.16	0.44	0.71	0.35	0.26
Ta	0.03	0.02	0.02	0.02	0.03	0.05
Tb	0.07	0.02	0.07	0.10	0.07	0.03
Th	0.16	0.17	0.12	0.09	0.19	0.46
U	0.10	0.06	0.09	0.03	0.10	0.11
W	2.90	1.15	2.36	3.47	1.82	2.50
Yb	0.33	0.14	0.30	0.18	0.39	0.15

Petrographic observations and the norm calculations indicate that plagioclase and orthopyroxene are the two main cumulate phases in the rock. Previous workers referred to these rocks as websterites, which would require the presence of clinopyroxene. In order to further establish which minerals were present as cumulate phases in the rocks prior to their metamorphism, various oxides were plotted versus MgO (Fig. 4.2). For elements that are essential to orthopyroxene or plagioclase (SiO_2, MnO, Al_2O_3, MgO, FeO, CaO and Na_2O), most of the samples fall along the plagioclase-orthopyroxene tie line suggesting that the magma was the same for all these samples and that plagioclase and orthopyroxene were on the liquidus. Elements incompatible in both plagioclase and orthopyroxene (e.g., TiO_2, P_2O_5, and K_2O) are present at very low levels and do not show any coherent trends on the bivariant plots.

Six samples from the High-grade Zone and seven from the Twilight and Roby zones plot above the plagioclase-orthopyroxene mixing line on the Al_2O_3 versus MgO graph (Fig. 4.2.) suggesting the presence of another MgO-rich phase (probably olivine) in these samples. On the CaO vs MgO plot the six samples with normative clinopyroxene >20% plot above the plagioclase-orthopyroxene tie line, showing the influence of cumulate clinopyroxene in these samples.

In order to differentiate between the influence of orthopyroxene and clinopyroxene, CaO was plotted against Al_2O_3 (Fig. 4.3(a)). Ninety of the 96 samples plot along the plagioclase-orthopyroxene mixing line, indicating that most of the samples are plagioclase-

orthopyroxene cumulates with <20% clinopyroxene component. This is consistent with the petrographic observations. Six of the samples plot off the trend towards clinopyroxene, but these are not from the High-grade Zone. The presence of olivine may be investigated by plotting Al_2O_3 versus FeO (Fig.4.3(b)). Twelve samples from both the zones may have contained olivine and/or clinopyroxene, (Rz-3, 8, 12 to 15, 27, 38, 40, 42, 49 and Tz-38). They come from all the three zones: 6 from the High-grade, 5 from the Roby Zone of which, one is a fragment (Rz-27), and one is a fragment from the Twilight Zone (Tz-38).

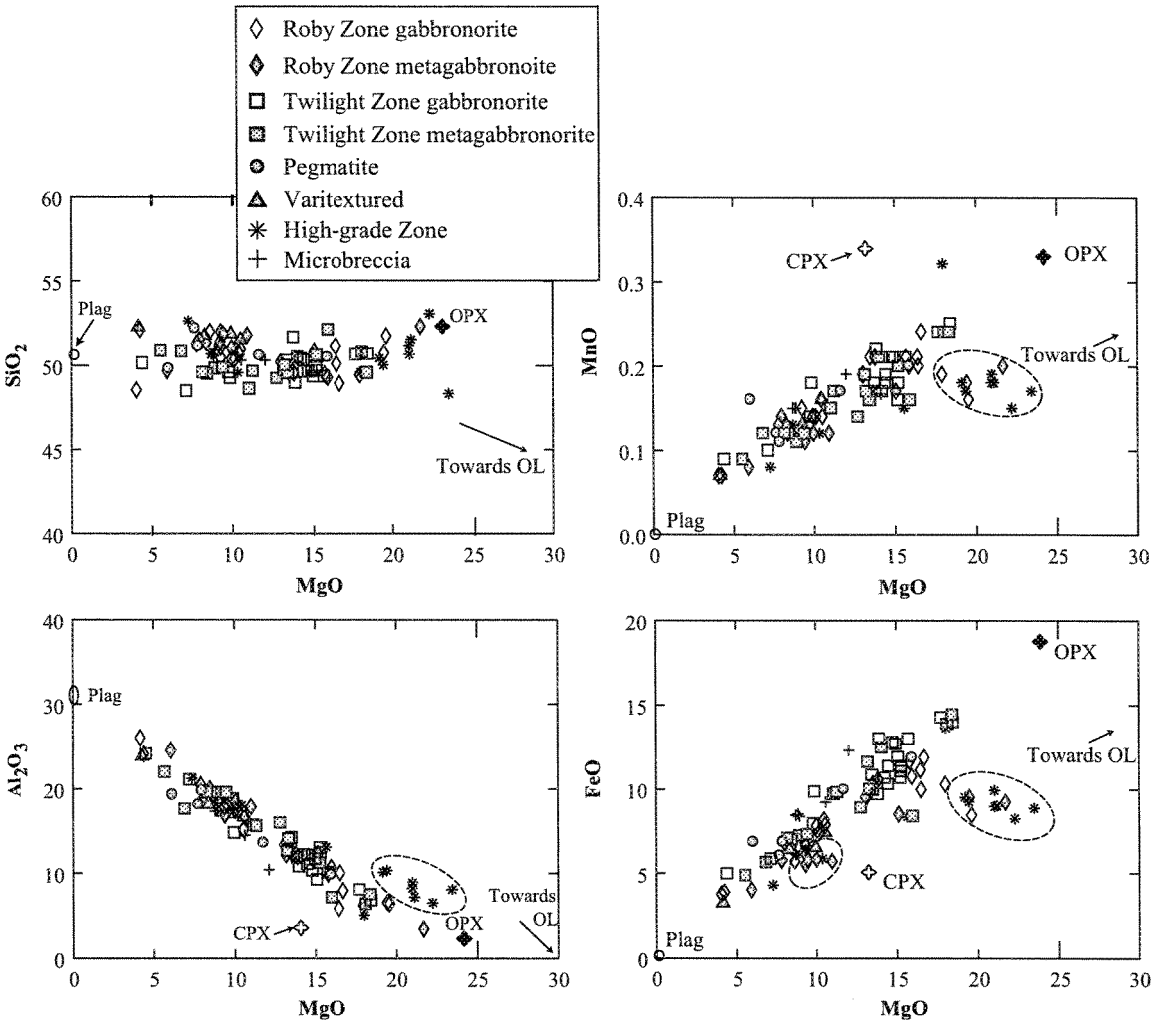

Figure 4.2(a). Variation diagrams of selected major element oxides versus MgO (wt%) showing composition of altered and unaltered samples from the Roby and Twilight Zones along with pegmatite, varitextured, and microbreccia. The High-grade Zone schist samples are also plotted. Compositions of plagioclase (Plag), and Opx (Orthopyroxene) are averages from EPMA data obtained in this study and clinopyroxene (Cpx) values are from Michaud (1998). Circled samples plot above the plagioclase-orthopyroxene (Plag-Opx) mixing line. Note that neither alteration, nor texture has an effect on the rock composition.

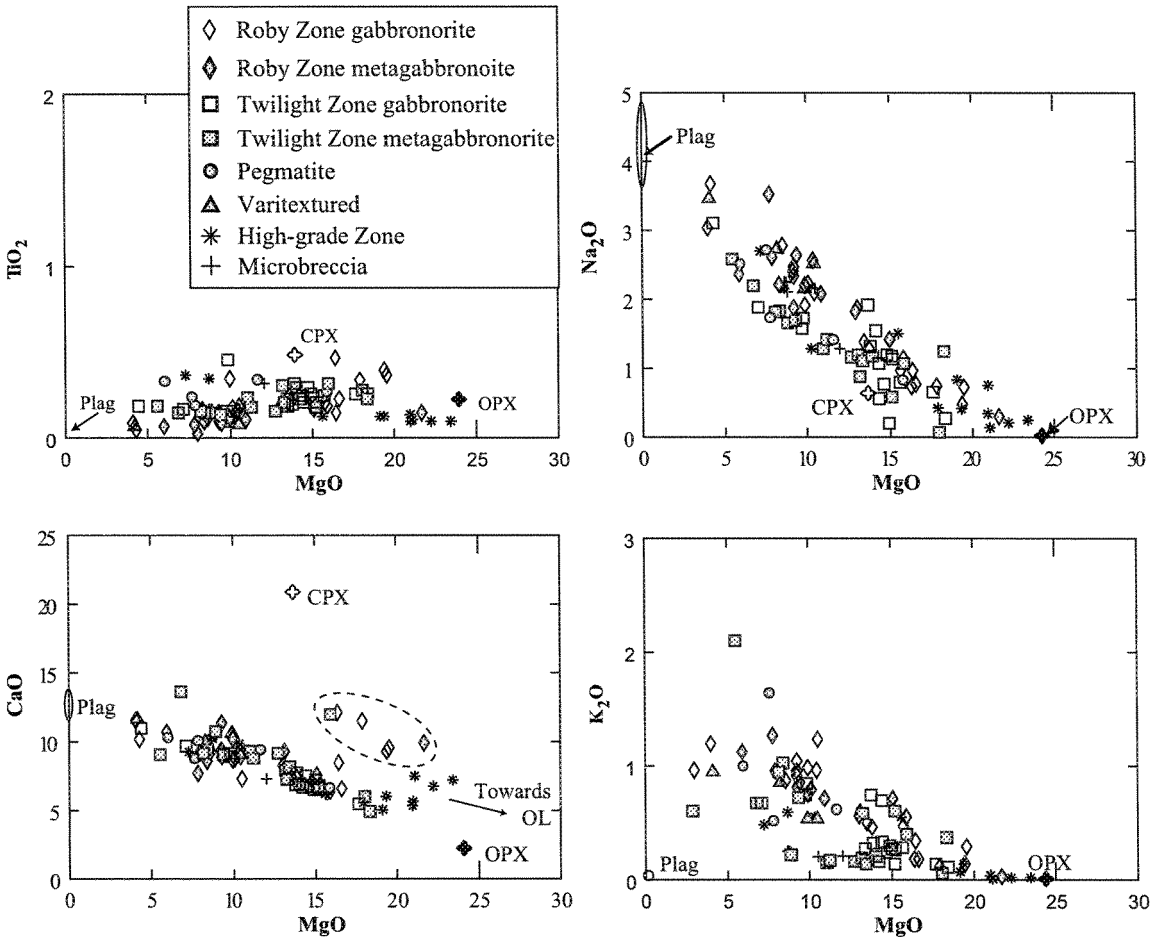

Figure 4.2(b). Variation diagrams of selected major element oxides versus MgO (wt%). Compositions of plagioclase (Plag), and Orthopyroxene (Opx) are averages from EMPA data obtained in this study and clinopyroxene (Cpx) values are from Michaud (1998). Note the trend in most of the plots show a mixing line of plagioclase and orthopyroxene with minor clinopyroxene. Other samples that do not follow the mixing line trend are highlighted in the CaO vs MgO graph (circled). See text for details.

4.2.2. Distribution of Trace Elements

The averages for the different zones, fragments, matrix, and pegmatoid/varitextured components are presented in Tables 4.3 to 4.6. As in the case of the major oxides the trace elements incompatible with plagioclase or orthopyroxene are present at very low concentrations. There is also no correlation between incompatible elements such as Hf, Ti and Sm (not shown) and Mg#, (Fig. 4.4). These very low levels indicate that there is very little trapped liquid component in these rocks, in agreement with the inference from petrographic observations. This is in contradiction to the model of Lavigne and Michaud (2001), which suggests that the matrix represents an injected volatile-rich gabbroic magma that brecciated the partially crystallized resident magma.

Elements compatible with orthopyroxene (Cr, Co, Ni) show a broad positive correlation with MgO (Fig. 4.5). On the MgO vs Co and Ni plots some samples plot above the general trend (Fig. 4.5). These samples contain sulphides and are therefore enriched in Ni and Co. The sulphide component of the MBI will be discussed in detail in the following chapter.

Cr is a major component of early crystallizing phases and preferentially partitions into pyroxenes. As shown in the previous sections the rocks grade from leucocratic to melanocratic in composition containing various concentrations of pyroxene mineralisation and rare chromite occurrences. Variation diagrams of Cr vs Mg# and CaO are shown in

Fig. 4.6 (a) and (b). Plagioclase rejects chromium almost completely giving plagioclase-rich gabbronorite rocks relatively low chromium concentrations. Therefore, samples with low Mg contents have the lowest Cr concentrations.

There are twelve samples on the Cr vs MgO and vs CaO diagrams that do not fall along the trend between orthopyroxene and plagioclase (Fig. 4.6). These samples comprise six High-grade Zone samples, five from the Roby Zone and one from the Twilight Zone. These are the samples which contain more normative olivine and clinopyroxene. The total pyroxene concentration in these samples reaches a maximum of 70 normative percent (see APPENDIX III). For example sample Rz-8 contains 6% normative clinopyroxene, 50% normative orthopyroxene and 10% normative olivine, and Rz-38 comprises 38% normative clinopyroxene, 4% normative olivine, and 28% normative orthopyroxene. These higher concentrations in clinopyroxene and olivine compared to the rest of the samples may account for these samples plotting away from the general mixing line of orthopyroxene and plagioclase. The samples that have the higher clinopyroxene and olivine concentrations could be similar to the samples that were mis-interpreted as pyroxenite by previous authors.

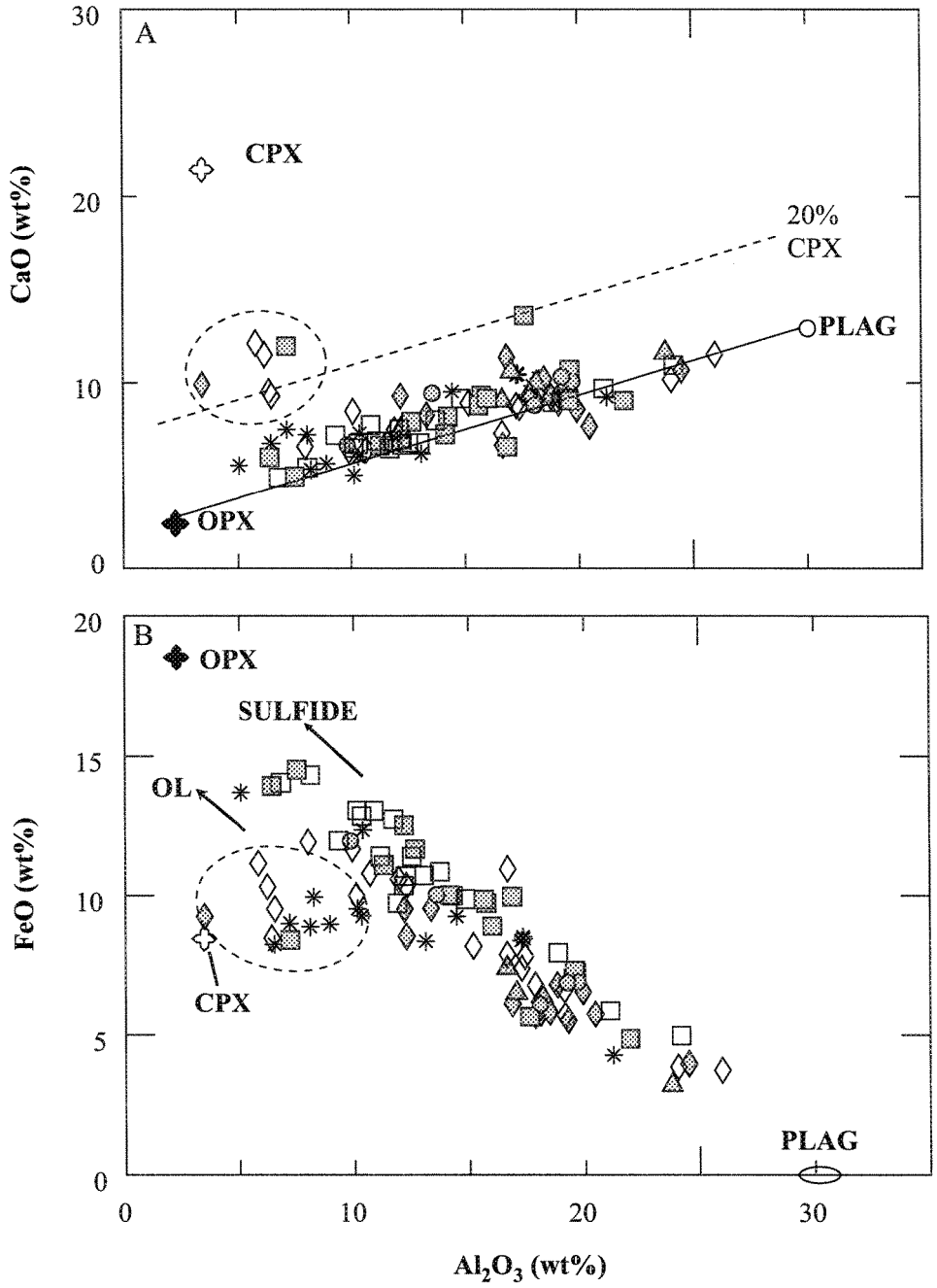

Figure 4.3. Variation diagrams of (a) CaO and (b) FeO (wt%) versus Al_2O_3 (wt%). Plagioclase (Plag) and orthopyroxene (Opx) averages are taken from this study, clinopyroxene (Cpx) values are from Michaud (1998). For the samples circled in (b) Cpx and/or olivine (OL) are present as cumulate phases.

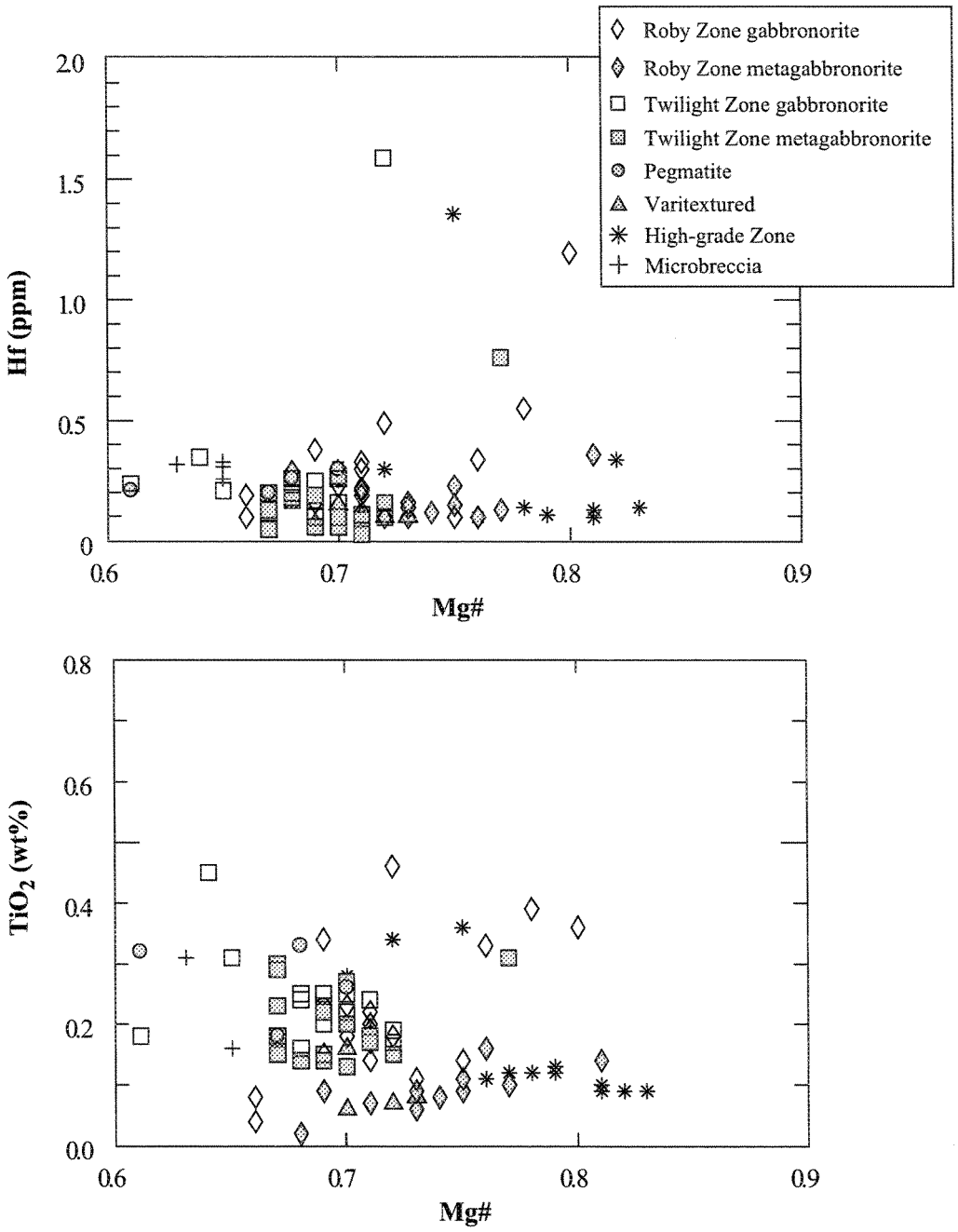

Figure 4.4. Variation diagrams of incompatible element Hf (ppm) and oxide TiO_2 (wt%) versus Mg#. Note the very low levels of the incompatible components.

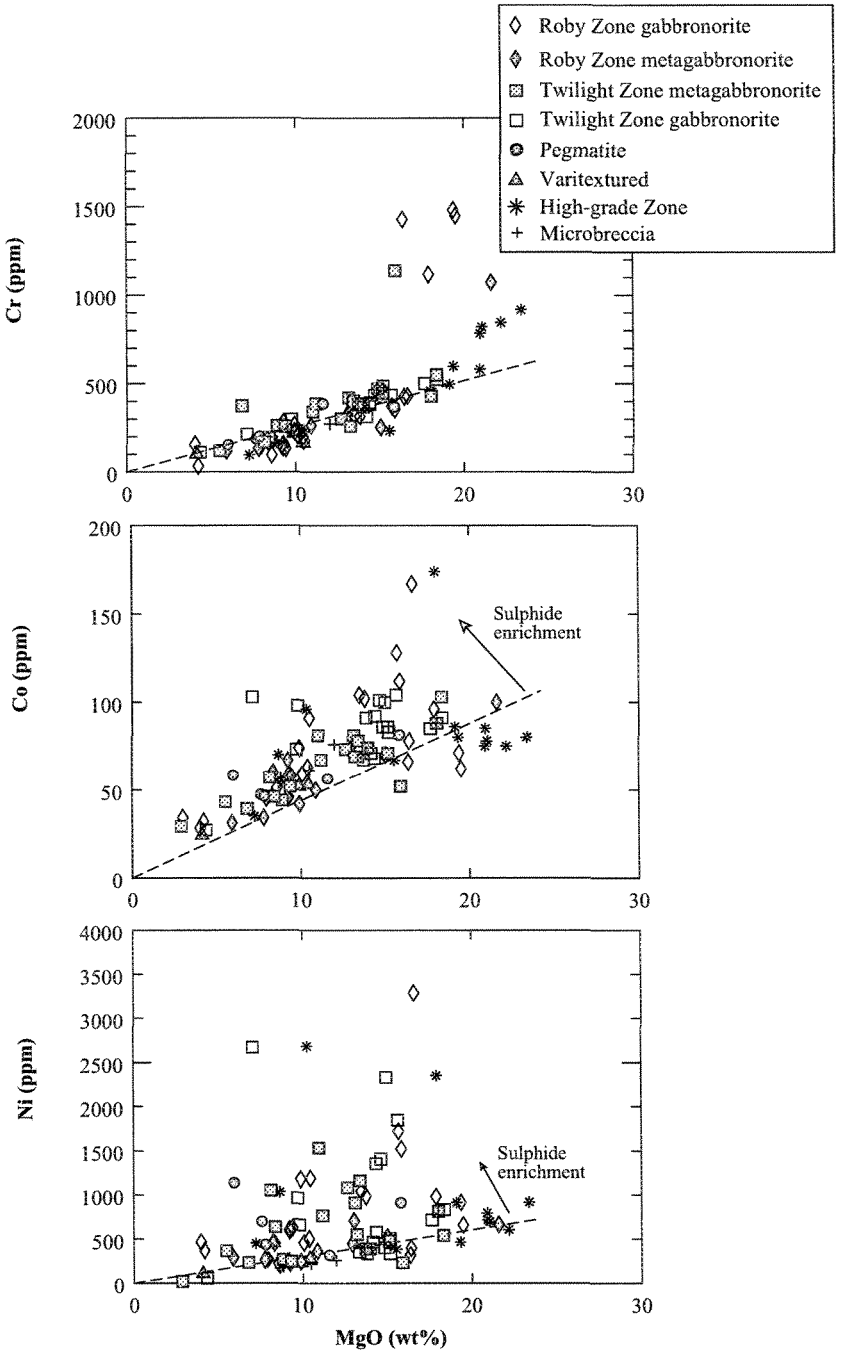

Figure 4.5. Variation diagrams of trace elements Cr, Co and Ni in ppm versus MgO (wt%). The dashed line represents the Opx-Plag tie-line. Plagioclase (Plag) and orthopyroxene (Opx) averages are from this study.

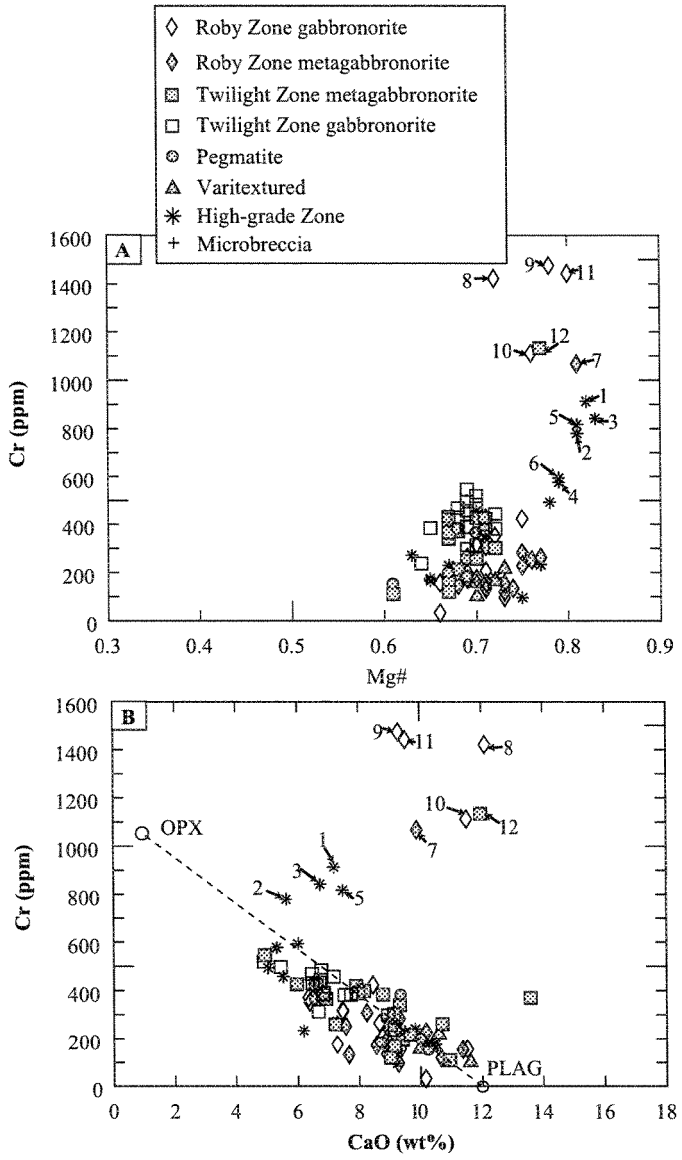

Figure 4.6. Variation diagrams showing Cr (ppm) versus (a) Mg# and (b) CaO. The two samples that have the lowest Mg# are Rz-46 and Tz-37 (Mg# 0.33 and 0.34 respectively). Most of the samples between 0.6 and 0.78 have Cr values below 600ppm. Above 0.77, 12 samples show elevated Cr values. (b) Shows that plagioclase (Plag) and orthopyroxene (Opx) are the main cumulate phases except for the following samples. 1 = Rz-3, 2 = Rz-8, 3 = Rz-12, 4 = Rz-13, 5 = Rz-14, 6 = Rz-15, 7 = Rz-27, 8 = Rz-38, 9 = Rz-40, 10 = Rz-42, 11 = Rz-49, 12 = Tz-38.

Table 4.4. Average compositions for major and trace element concentrations of the fragments and matrix from the Roby and Twilight Zones. Full data list is documented in the Appendix I

Zone	Roby		Roby		Twilight		Twilight	
Occurrence	Fragments		Matrix		Fragments		Matrix	
n	17	σ	19	σ	16	σ	19	σ
SiO_2	50.31	1.16	48.93	1.41	48.85	0.72	48.69	0.82
TiO_2	0.10	0.05	0.22	0.11	0.20	0.06	0.23	0.07
Al_2O_3	16.9	4.82	13.7	5.93	14.3	4.36	13.4	4.64
Fe_2O_3 (Total)	8.11	2.65	9.63	2.99	11.2	3.12	11.6	3.39
Fe_2O_3	7.34	1.99	9.51	2.66	10.7	2.76	11.7	3.07
Fe(s)	0.16	0.17	0.39	0.47	0.25	0.25	0.46	0.50
MnO	0.14	0.04	0.16	0.05	0.16	0.04	0.18	0.05
MgO	10.3	3.89	12.7	4.55	12.3	3.37	13.0	3.77
CaO	9.55	1.14	8.84	1.65	8.68	2.12	7.47	1.46
Na_2O	2.26	0.73	1.72	0.91	1.29	0.50	1.31	0.72
K_2O	0.76	0.28	0.62	0.36	0.41	0.30	0.49	0.45
P_2O_5	0.01	0.00	0.01	0.00	0.01	0.01	0.01	0.01
LOI	2.44	0.44	2.77	0.61	2.18	1.21	2.36	1.13
Total	**100.5**	**0.72**	**99.9**	**0.85**	**99.8**	**0.31**	**99.8**	**0.74**
Mg#	0.73	0.03	0.72	0.03	0.71	0.07	0.70	0.06
Ba (ppm)	141	64	137	84	83	35	87	66
Ce	2.43	1.21	4.71	3.92	2.94	3.36	2.94	1.60
Cr	252	221	477	473	390	213	365	118
Cs	2.54	1.37	2.12	2.08	1.26	0.84	1.08	0.59
Eu	0.19	0.05	0.31	0.20	0.24	0.08	0.22	0.07
Hf	0.16	0.07	0.30	0.24	0.18	0.16	0.25	0.32
La	1.15	0.52	1.48	0.56	1.43	1.43	1.13	0.46
Lu	0.08	0.00	0.08	0.02	0.08	0.02	0.08	0.01
Nd	0.93	0.59	2.43	3.34	1.18	1.46	0.97	0.67
Rb	19.0	8.75	14.1	8.80	13.9	14.1	11.3	9.22
Sc	32.3	11.9	33.3	11.0	36.0	12.4	39.4	10.4
Sm	0.28	0.11	0.76	0.91	0.37	0.35	0.33	0.17
Ta	0.02	0.02	0.02	0.02	0.04	0.06	0.03	0.04
Tb	0.05	0.03	0.11	0.12	0.07	0.04	0.07	0.03
Th	0.12	0.09	0.13	0.09	0.15	0.21	0.24	0.63
U	0.09	0.04	0.09	0.03	0.11	0.13	0.10	0.11
W	2.06	2.88	3.25	3.88	1.30	1.74	2.45	2.97
Yb	0.26	0.11	0.40	0.21	0.40	0.18	0.39	0.12

Table 4.5. Average compositions for major and trace element concentrations of the varitextured and pegmatite textures from the Roby and Twilight Zones. Full data list is documented in the Appendix I

Zone	**Roby**		**Twilight**	
Texture	**Varitextured**		**Pegmatites**	
n	**4**	**σ**	**5**	**σ**
SiO_2	51.34	0.54	49.62	0.88
TiO_2	0.09	0.04	0.26	0.06
Al_2O_3	18.9	2.88	16.1	3.80
Fe_2O_3 (Total)	7.06	1.77	10.9	2.48
Fe_2O_3	6.53	1.77	9.27	2.48
Fe(s)	0.07	0.03	0.24	0.20
MnO	0.13	0.03	0.15	0.03
MgO	8.20	2.48	9.82	3.54
CaO	10.3	0.94	8.99	1.32
Na_2O	2.73	0.48	1.85	0.70
K_2O	0.71	0.19	0.83	0.45
P_2O_5	<0.01	<0.01	0.03	0.01
LOI	1.90	0.21	2.04	0.55
Total	**100.9**	**0.33**	**99.6**	**0.19**
Mg#	0.71	0.01	0.70	0.40
Ba (ppm)	146	40	128	67
Ce	2.73	1.54	3.02	1.60
Cr	158	41	254	97
Cs	2.26	0.82	2.10	0.88
Eu	0.20	0.04	0.23	0.06
Hf	0.13	0.03	0.23	0.04
La	1.36	0.75	1.28	0.45
Lu	0.08	0.00	0.07	0.01
Nd	0.85	0.51	1.20	0.69
Rb	27.7	6.06	22.0	12.4
Sc	30.0	5.67	36.1	14.5
Sm	0.28	0.11	0.38	0.19
Ta	0.03	0.03	0.05	0.05
Tb	0.05	0.02	0.08	0.03
Th	0.18	0.13	0.09	0.03
U	0.09	0.03	0.07	0.03
W	1.60	0.88	0.43	0.40
Yb	0.21	0.07	0.34	0.15

Table 4.6. Average compositions for major element concentrations of the gabbronorite and metagabbronorite samples from the Roby and Twilight Zones. Full data list is documented in the Appendix I

Lithology	**Gabbronorite**			**Meta-gabbronorite**		
n	**21**	**σ**	**RSD**	**50**	**σ**	**RSD**
SiO_2	48.90	0.87	1.78	49.30	1.35	2.74
TiO_2	0.22	0.09	40.9	0.18	0.09	50
Al_2O_3	14.2	4.15	29.1	14.7	5.56	37.7
Fe_2O_3 (Total)	11.1	3.36	30.2	9.76	3.27	33.5
Fe_2O_3	10.8	2.43	22.5	9.47	3.28	34.6
Fe(s)	0.41	0.44	107	0.29	0.38	131
MnO	0.17	0.04	23.5	0.16	0.05	31.2
MgO	12.5	3.25	25.9	11.9	4.35	36.3
CaO	8.62	1.83	21.2	8.58	1.76	20.5
Na_2O	1.33	0.44	33.0	1.77	0.92	51.9
K_2O	0.37	0.28	75.6	0.66	0.38	57.5
P_2O_5	0.01	0.01	100	0.01	0.00	0.0
LOI	1.77	0.83	46.8	2.73	0.81	29.6
Total	**99.8**	**0.59**	**0.59**	**100.1**	**0.79**	**0.79**
Mg#	0.71	0.06	8.45	0.72	0.05	6.94
Ba (ppm)	78	51	66	129	74	57
Ce	3.09	2.66	86.0	3.37	3.00	89.0
Cr	453	333	73.6	339	283	83.4
Cs	1.26	0.82	65.0	1.95	1.64	84.1
Eu	0.28	0.16	57.1	0.23	0.11	47.8
Hf	0.19	0.12	63.1	0.24	0.26	108
La	1.19	0.43	36.1	1.34	0.94	70.1
Lu	0.08	0.01	12.5	0.08	0.01	12.5
Nd	1.44	1.54	106	1.38	2.18	157
Rb	13.2	12.5	95.0	15.1	9.71	64.3
Sc	33.9	8.87	26.1	35.6	12.8	35.9
Sm	0.47	0.59	125	0.43	0.52	120
Ta	0.04	0.06	150	0.02	0.03	150
Tb	0.08	0.08	100	0.08	0.07	87.5
Th	0.11	0.07	63.6	0.19	0.41	215
U	0.10	0.11	110	0.10	0.07	70
W	2.62	2.68	102	2.20	3.22	146
Yb	0.39	0.17	43.5	0.35	0.17	48.5

Elements compatible to slightly compatible with plagioclase (Eu, Sr, Ba, K, Cs and La) were plotted versus Al (Fig. 4.7). Although there is a crude positive correlation between these elements and Al_2O_3, most of the samples plot above the orthopyroxene-plagioclase tie line (Fig. 4.7). This indicates that another Al_2O_3-bearing phase is controlling these elements. There is a good correlation between K_2O and Cs, Rb, Ba and Eu (Fig. 4.8.), which suggests that these elements are controlled by either K-feldspar or K_2O-white mica, probably sericite. There is very little K-feldspar within the samples, and there is no correlation between SiO_2 and K_2O (Fig. 4.8.). There is however, extensive sericitisation of most of the plagioclase within the altered samples, which could also accommodate Cs, Rb, Ba and Eu in its structure. Sericite averages 49 wt% SiO_2, 9 wt% K_2O and 32 wt% Al_2O_3 (Eberl et al. 1987), which would account for the scatter of samples toward high K_2O on the SiO_2 and K_2O plot (Fig. 4.8.).

The multi-element primitive mantle normalized diagrams (spidergrams) for all three zones and textures show similar characteristics (Fig. 4.9). All are enriched (3 –200ca times primitive mantle) in LILE (Cs, Rb, Ba, K) relative to the high field strength elements and REE (0.1 – 8 times primitive mantle). In addition, there are positive anomalies at U and Eu and may be attributed to the presence of sericite alteration assemblage, and to a lesser degree, to the presence of cumulate plagioclase. The Twilight and High-grade Zones have average Eu/Eu* ratios of 3 and 4 respectively (where Eu* value is interpolated from adjacent elements), whereas the Roby Zone has a higher average Eu/Eu* ratios of 5. The fragments from the Roby Zone have the highest Eu anomaly average of 8, whereas the

fragment and matrix samples from the Roby and Twilight Zones have Eu/Eu* ratios averaging 4. This correlates with the more leucocratic nature of the fragments compared to the matrix from the Roby and Twilight Zones. Apart from the Eu anomalies the incompatible elements are essentially flat from the HREE to Ta [$La/Lu_{[n]}$ between 1 and 3]. The enrichment in LILE and U could be the product of alteration during greenschist facies metamorphism (consistent with the regional metamorphism) it may indicate that the rocks formed in an island arc or back-arc setting, or it may indicate that the magma was contaminated by upper continental crust. This would be consistent with the tectonic setting close to the Quetico volcanic and sedimentary units (Stone et al. 2003).

The samples were plotted to evaluate trends with respect to alteration (Fig. 4.10) and different textures of the zones (Fig. 4.11). The samples from the gabbronorite and metagabbronorite of the Roby and Twilight Zones and the actinolite-chlorite schist and microbreccia from the High-grade Zone have similar REE distributions. The characteristic enrichment in LILE (Cs, Rb, Ba, and K) and positive Eu anomalies are highlighted in these plots. Although the highest average Eu anomalies are from the gabbro (average Eu/Eu* = 5), the difference from the metagabbro is minimal (average Eu/Eu* = 4). The similarity in the pattern between the altered and unaltered samples from the Roby, Twilight, and High-grade Zones suggest that alteration did not significantly affect the REE concentrations. Table 4.6 shows the relative standard deviation (RSD) between the gabbronorite and metagabbronorite samples. For the mobile elements Cs, Rb, Ba, and K, the metagabbronorite shows more variation than the gabbronorite samples. The relatively

immobile elements such as Hf, Ti, Yb, and Lu also have higher RSD values in the metagabbronorite than in the gabbronorite samples. This higher variability in the altered samples may be an indication of the effects of alteration on the geochemical signature within the LDIC. The varitextured gabbros and pegmatites from the Roby and Twilight Zones also show similar patterns with enrichment in LILE and flat REE patterns [$La/Lu_{[n]}$ = 2 for both] with positive Eu anomalies. The pegmatite and varitextured samples also have similar patterns to samples from the Roby and Twilight Zones (Fig. 4.10 and Fig. 4.11).

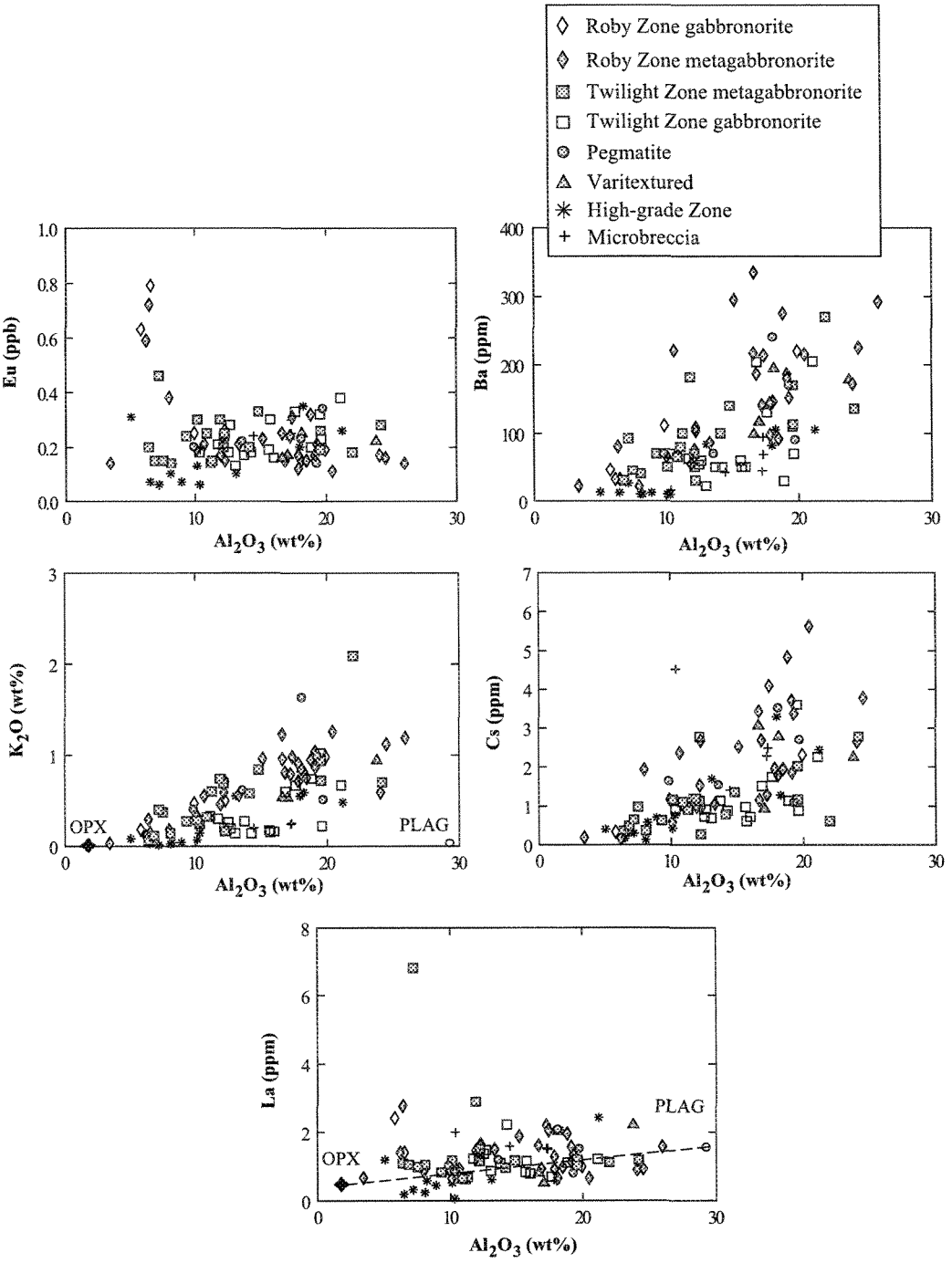

Figure 4.7. Variation diagrams of trace elements and K_2O (wt%) versus Al_2O_3 (wt%). Trace elements such as La and Ce are generally low, at detection limit. Plagioclase (Plag) and orthopyroxene (Opx) average are from this study.

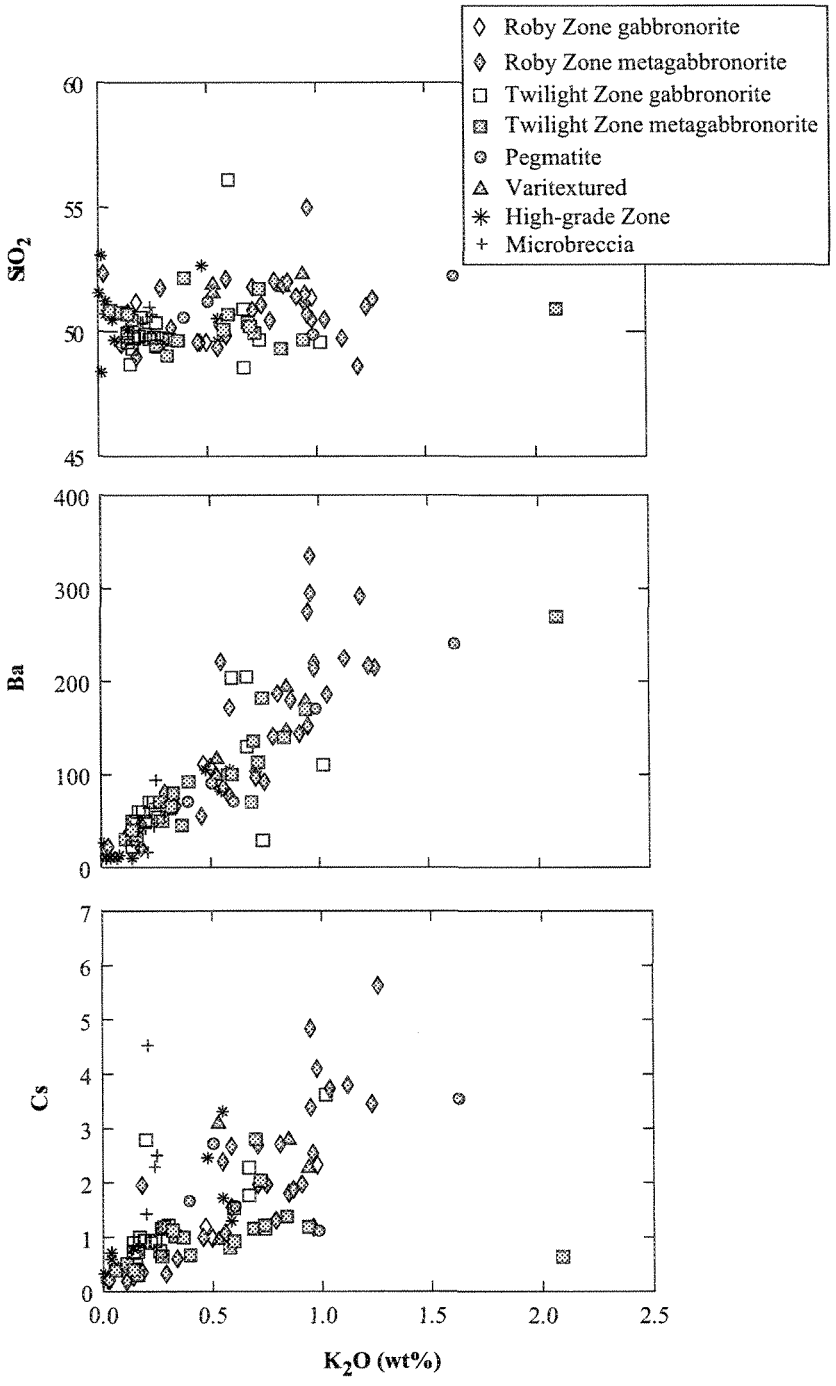

Figure 4.8. Variation diagrams of SiO_2 (wt%), and selected trace elements in ppm versus K_2O (wt%). Note the positive correlation between Cs, Ba and K_2O (wt%).

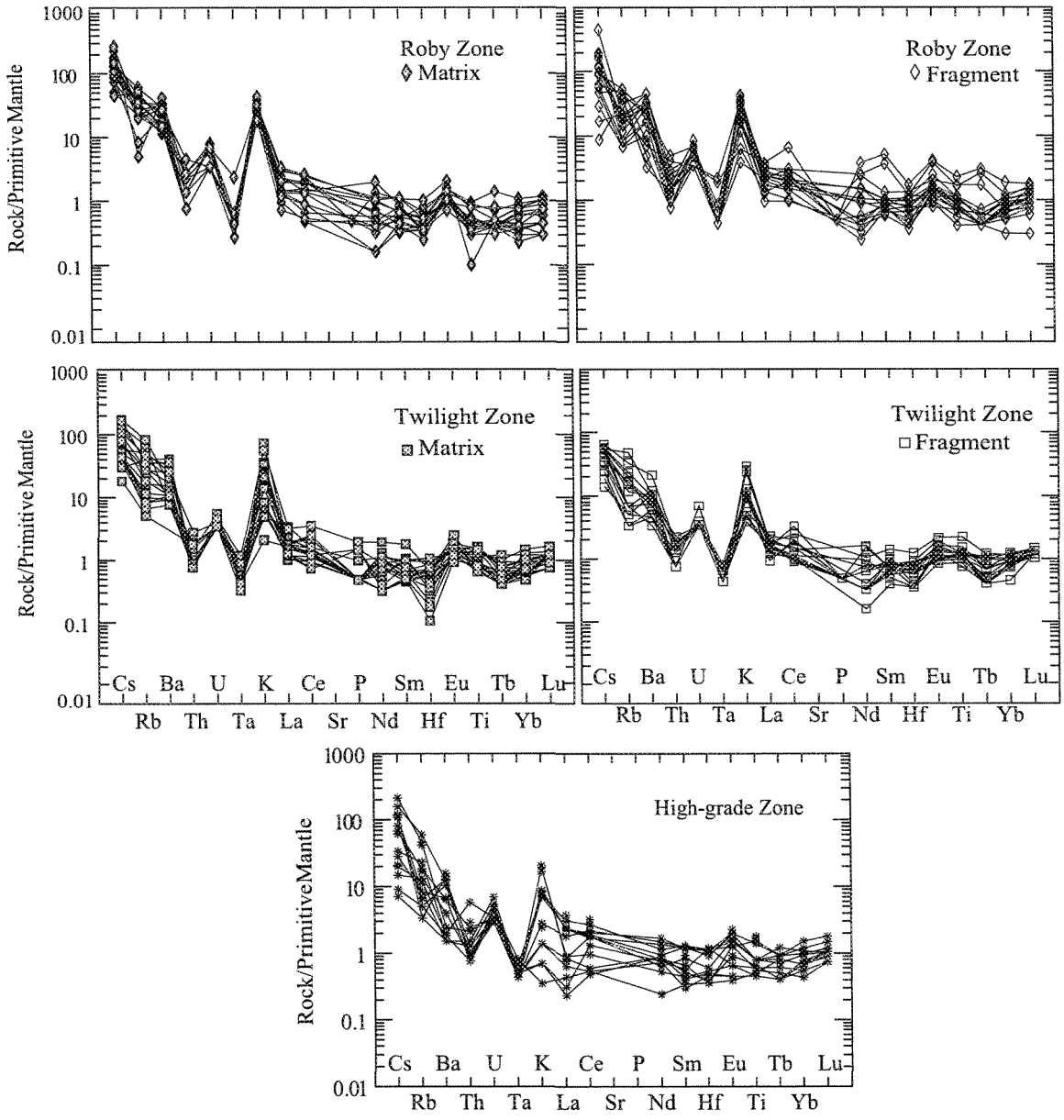

Figure 4.9. Rare earth and trace element spider diagrams for the fragment and matrix samples of the Roby and Twilight Zones along with High-grade Zone samples. Primitive mantle values after McDonough and Sun (1995).

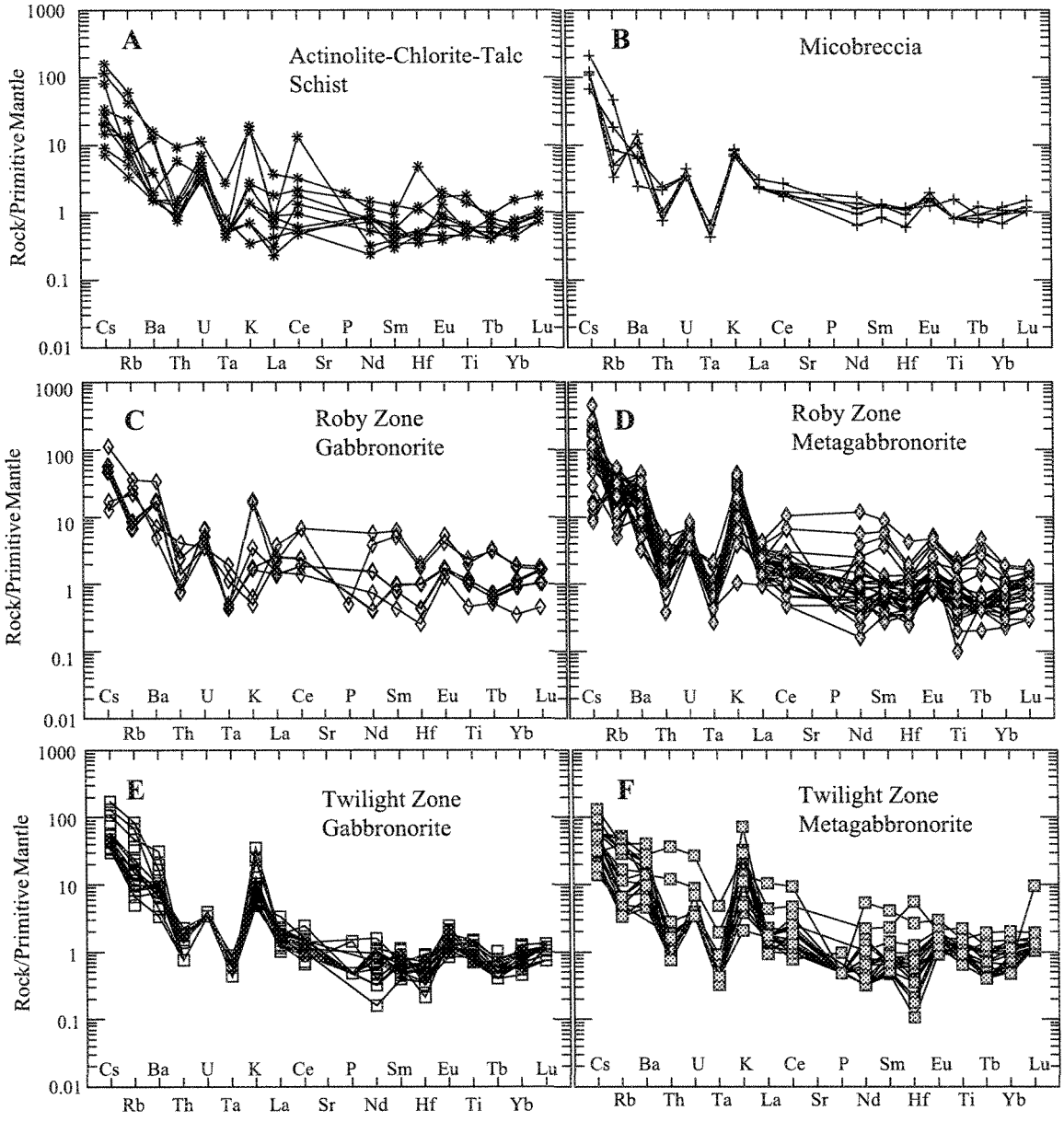

Figure 4.10. Spidergrams of the High-grade Zone (actinolite-chlorite-talc schist and microbreccia), Roby and Twilight Zone gabbronorite and metagabbronorite samples. Note: the similarity in concentration and pattern between the gabbronorite and metagabbronorite samples within the Zones. Primitive Mantle from McDonough and Sun (1995).

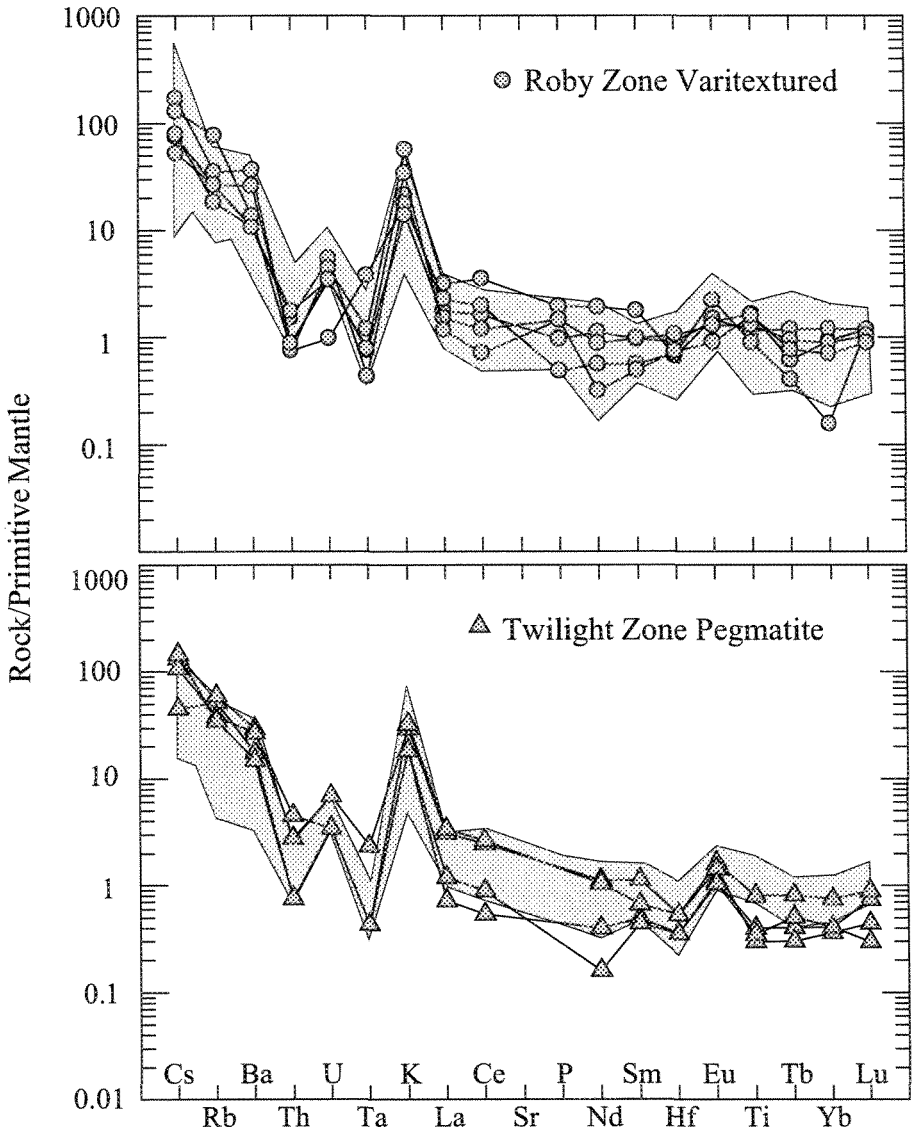

Figure 4.11. Spidergrams of the varitextured gabbro from the Roby Zone and pegmatite from the Twilight Zone. There is a similarity in pattern and normalised values to the Roby and Twilight Zone gabbronorite and metagabbronorite samples of Figure 4.9. The shaded area represents the Roby and Twilight Zones from Figure 4.9. for comparison purposes. Primitive Mantle values are from McDonough and Sun (1995).

4.3. Trace element Characteristics of the Silicate Minerals

4.3.1. Orthopyroxene

The compositions of orthopyroxene grains from the Roby and Twilight Zones were determined to see if they varied between the Zones and with alteration. Two samples Rz-30 (gabbronorite matrix) and Rz-33 (leucogabbro fragment) from the Roby Zone were selected for analysis (Table 4.7). The Roby Zone is altered to a higher degree and hence there are fewer fresh orthopyroxene grains present than in the Twilight Zone. No fresh orthopyroxene grains were found in the High-grade Zone. Samples from the Twilight Zone that contain orthopyroxene are Tz-7 (gabbronorite fragments) and Tz-8 (gabbronorite matrix) and the compositions are given in Table 4.7. All of the pyroxene crystals are enstatite (Fig. 4.12) with little to no variation in composition between the different zones (Roby and Twilight) and between fragments and matrix. The sample Tz-8, although altered, does not contain pyroxene grains that are of different composition to those in the unaltered samples. Alteration may also affect the concentration of REE in pyroxenes. Samples Rz-30 and Rz-33 are altered and unaltered respectively and this may have affected the REE concentrations (Fig. 4.13). Samples Rz-33 and Tz-7 show lower orthopyroxene concentrations than the rest of the samples as they fall outside of the enstatite field.

Table 4.7. Average trace element contents for orthopyroxene from the samples Rz-30 and 33 of the Roby Zone. Full analytical results are in Appendix II

Sample	**Rz-30**		**Rz-33**	
Occurence	**Matrix**		**Fragment**	
Lithology	**gabbro-norite**		**leuco-gabbronorite**	
n	**7**	**σ**	**3**	**σ**
CaO (wt%)	1.8	0	0.96	0.22
Ba (ppm)	1.60	1.39	0.91	0.82
Ce	0.43	0.09	0.30	0.32
Co	130	9	34	5
Cr	493	111	106	30
Cu	4.42	3.04	5.71	0
Cs	0.16	0.09	0.01	0
Dy	0.47	0.05	0.15	0.11
Er	0.51	0.09	0.14	0.06
Eu	0.03	0.00	0.02	0.02
Gd	0.21	0.05	0.08	0.00
Hf	0.23	0.09	0.08	0.02
Ho	0.14	0.02	0.04	0.02
La	0.22	0.11	0.09	0.07
Lu	0.14	0.02	0.03	0.00
Nb	0.08	0.05	0.01	0.01
Nd	0.32	0.04	0.20	0.28
Ni	615	59	99	29
Pb	0.26	0.08	0.09	0.03
Pr	0.06	0.01	0.04	0.06
Rb	0.28	0.20	0.05	0.08
Sb	0.03	0.02	0.00	0.00
Sc	81.0	14.3	10.6	4.2
Sm	0.12	0.02	0.08	0.10
Sr	0.94	0.42	1.00	1.35
Ta	0.004	0.00	0.001	0.00
Tb	0.05	0.01	0.02	0.00
Tm	0.09	0.02	0.02	0.01
V	197	24	42	7
Yb	0.79	0.14	0.20	0.02
Y	3.67	0.42	1.04	0.54
Zr	8.55	3.59	2.61	1.24

Emslie (1975), as quoted by Ashwal (1993), noted that at 5 kbars the Al_2O_3 content in orthopyroxene averages 3.1% and that it increases significantly with increase in pressure. The Al_2O_3 concentrations observed in the orthopyroxene grains studied here fall within the range 1.8 to 2.2 wt%, suggesting that crystallisation pressures were below 5 kbars. Brügmann et al. (1997) suggest that the magma crystallised in the continental crust at pressures corresponding to depths from 5 to 8 km, which would broadly correspond to pressures of 1.5 to 2.4 bars.

The Roby and the Twilight Zone samples (Fig. 4.13) generally have very low REE concentrations, which reflect the fact that REE do not partition into orthopyroxene (Bédard et al. in press). The patterns show depletion in LREE and enrichment in HREE [$La/Lu_{[n]}$ on average 0.12 – 0.81 for the Roby Zone]. All of the patterns show negative Eu anomalies [Eu* = 0.6 – 2.3]. This indicates that orthopyroxene and plagioclase were on the liquidus together.

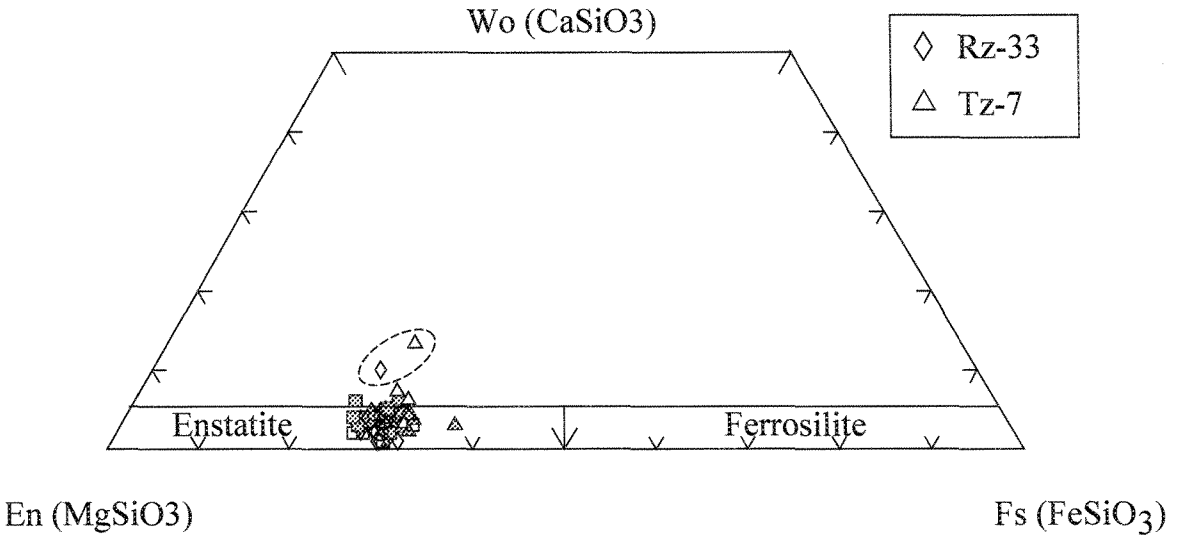

Figure 4.12. Classification of pyroxenes obtained by EMPA from thin sections. Most samples plot within the enstatite field. There is no variation in opx composition between the Roby and Twilight Zones, between fragments and matrix, or with degree of alteration.

4.3.2. Plagioclase

The Plagioclase grains in one sample each from the from the Roby, Twilight and High-grade Zones were analysed, a total of 17 points by EMPA for the major element oxide composition and 28 by ICPMS for the trace element compositions from representative samples. The average concentrations of trace elements are listed in Table 4.8. In the case of the High-grade Zone, remnants of igneous plagioclase were located in the microbreccia sample. The Roby Zone sample is a fragment of metagabbro and that from the Twilight Zone is a representative fragment from a gabbronorite (Tz-7). All plagioclase crystals have patterns that show an enrichment of LREE (1 to 5 times primitive mantle) over HREE (0.01

to 0.2 times primitive mantle) and strong positive Eu anomalies (Fig. 4.14). The plagioclase with the highest average trace element concentrations, especially for Rb, Sr, and Ba, is a metagabbronorite from the Roby Zone. All analysed samples show depletion in HREE (Gd to Lu) with these elements almost at the detection limit.

Trace element concentrations of plagioclase show less variations than for orthopyroxene (Fig. 4.14). The REE patterns are similar for all the analysed samples and are characterised by enrichment in LREE and strong depletion in HREE with [$La/Lu_{[n]}$ = 20 to 89] and a strong positive Eu/Eu* ratios, 5.6 to 26 (Fig. 4.14). There is little variation between samples from the Roby and Twilight Zones or between fragments and matrix samples from these zones with respect to trace element contents. Sample Rz-9 from the High-grade Zone shows moderately lower HREE element concentrations compared to the other samples. Although considerable care was taken to analyse the centre of the plagioclase grains, there is the possibility that alteration was more pervasive and did in some way affect the compositions of the grains' cores.

Table 4.8. Average trace element concentrations form the plagioclase grains analysed. Full analytical results are in Appendix II

Sample	**Rz-9**		**Rz-33**		**Tz-7**	
Occurence	**Micro-breccia**		**Fragment**		**Fragment**	
Lithology			**leuco-gabbronorite**		**gabbro-norite**	
n	**8**	**σ**	**3**	**σ**	**6**	**σ**
CaO (wt%)	12.4	0.06	13.4	(n=1)	12.4	(n=1)
Ba (ppm)	77.4	19.7	161	17.9	108	14.4
Ce	1.80	0.96	2.49	0.59	4.31	0.66
Co	0.74	1.25	1.61	0.75	0.44	0.19
Cr	7.24	11.3	27.3	2.88	6.10	4.49
Cu	8.18	16.7	11.3	0.36	3.81	2.63
Cs	0.45	0.31	0.65	0.24	0.10	0.07
Dy	0.02	0.01	0.06	0.02	0.06	0.01
Er	0.008	0.00	0.04	0.00	0.02	0.01
Eu	0.23	0.06	0.43	0.04	0.35	0.05
Gd	0.07	0.01	0.08	0.00	0.09	0.02
Hf	0.01	0.00	0.00	0.00	0.07	0.06
Ho	0.00	0.00	0.01	0.00	0.01	0.00
La	1.09	0.69	1.22	0.27	2.34	0.25
Lu	0.00	0.00	0.00	0.00	0.00	0.00
Nb	0.02	0.02	0.08	0.01	0.03	0.03
Nd	0.51	0.26	0.85	0.17	1.34	0.16
Ni	14	23	46	7	23	7
Pb	0.95	0.17	7.00	4.50	2.19	0.28
Pr	0.16	0.08	0.25	0.05	0.40	0.05
Rb	0.93	0.63	3.66	3.37	0.94	0.59
Sb	0.01	0.01	0.04	0.01	0.03	0.02
Sc	11.3	11.5	33.2	2.56	9.88	4.63
Sm	0.06	0.04	0.16	0.03	0.18	0.03
Sr	350	59.7	556	30	377	48.1
Ta	0.001	0.00	0.00	0.00	0.004	0.00
Tb	0.02	0.00	0.02	0.00	0.02	0.00
Tm	0.001	0.00	0.00	0.00	0.00	0.00
V	5.98	8.12	29.1	4.04	5.01	3.95
Yb	0.01	0.00	0.01	0.01	0.02	0.00
Y	0.11	0.04	0.35	0.03	0.27	0.05
Zr	1.31	2.10	0.38	0.13	2.90	2.53

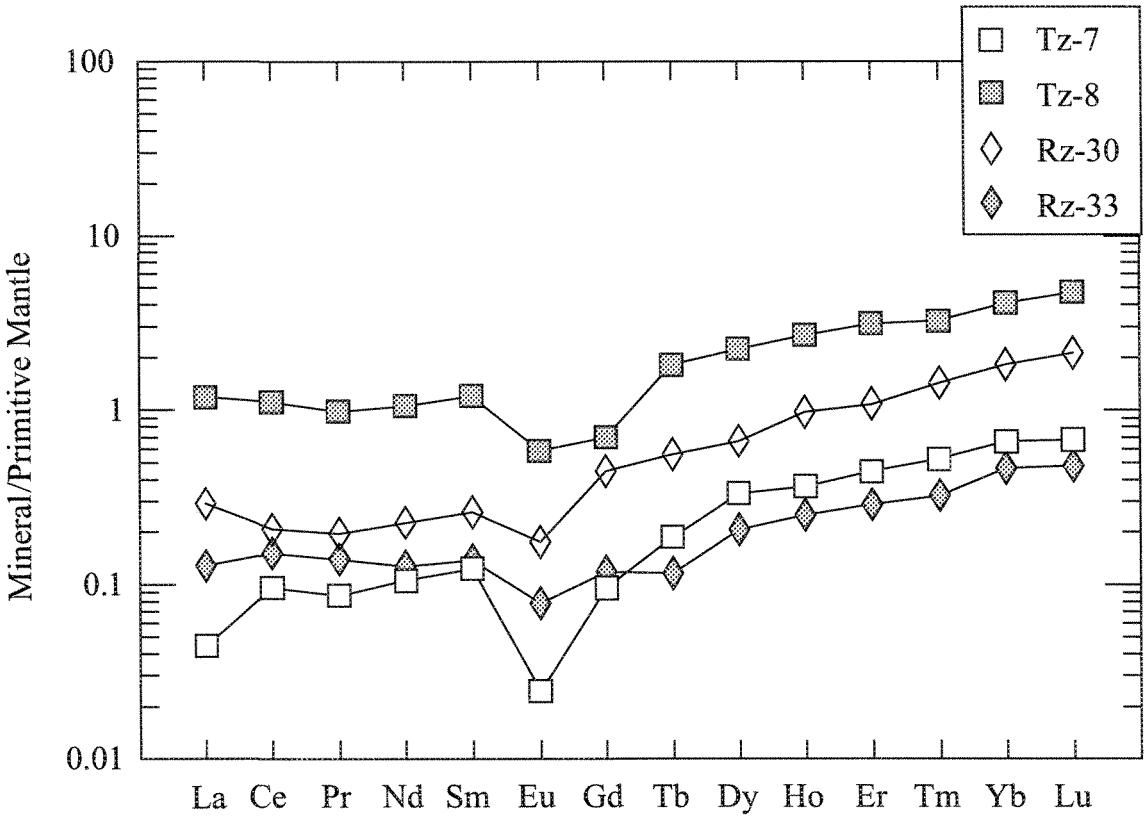

Figure 4.13. Average rare earth element (REE) diagram for orthopyroxene grains in the Roby and Twilight Zones. Note the enrichment in HREE for the majority of the samples. Primitive mantle values are from McDonough and Sun (1995).

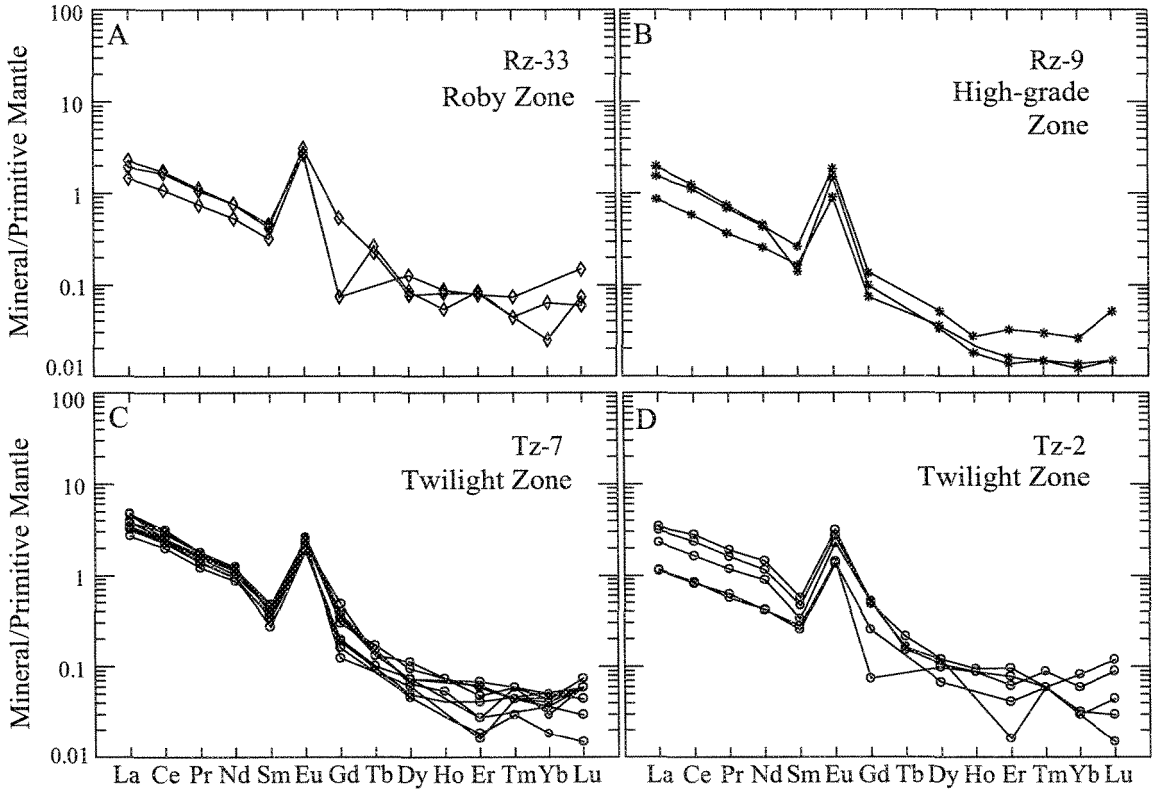

Figure 4.14. Rare earth element diagram for plagioclase from: (a) the Roby (Rz-33), (b) the High-grade (Rz-9), and the Twilight Zone (c) Tz-7, and (d) Tz-2. Note the enrichment in LREE, strong depletion in HREE, and positive Eu anomaly in all of the samples. Primitive mantle values are from McDonough and Sun (1995).

4.3.3. Amphibole

The classification by major element indicates that the fibrous grains that pseudomorph pyroxene and the amphibole minerals are primarily magnesio-hornblende and tremolite-actinolite (Fig 4.15. and APPENDIX II). The presence of igneous hornblende in the gabbros (Brügmann et al. 1997) indicates that water was present in the parental magma.

This concentration of H_2O in the magma increased during crystallisation favouring the eventual appearance of hornblende as a liquidus phase.

Average trace element concentrations of selected amphiboles are shown in Table 4.9 (a) and (b). The partition coefficients for the REE into hornblende are approximately 0.3 LREE to 1 HREE in basaltic systems (Rollinson 1993), therefore, the measured concentrations suggest a magma that had a concentration of REE of 10 to 2 times chondrite. But this is not consistent with the results from the orthopyroxene and plagioclase REE. However, two types of REE patterns can be discerned from the suite of amphiboles that were analysed. Most of the magnesio-hornblendes (Type I) have patterns that are between 1 and 10 times mantle and show a slight enrichment of the middle REE and have negative Eu anomalies. These grains could be igneous, as their REE patterns are similar to that of igneous hornblende (Rollinson 1993). These grains imply a magma with 10-20 times chondrite abundances of REE, which is consistent with the data for orthopyroxene and plagioclase. Other hornblendes (Type II) have slight Eu anomalies and have lower REE concentrations. These minerals could be metamorphic (Fig. 4.16). These amphibole patterns closely resemble the orthopyroxene patterns, supporting the proposition that they may be derived from the orthopyroxene minerals by alteration.

The grains of actinolite share similar ranges between 1 and 10 times mantle, this may be because they formed by alteration of hornblende. Trace element variations for the different generations of amphibole that are identified and analysed (Fig. 4.17) resemble the

patterns from the orthopyroxene. Some of the actinolites (Type III) have patterns with positive Eu anomalies and enrichment in LREE (Fig. 4.17). It is possible that these actinolite crystals formed from the replacement of plagioclase as they have similar REE patterns.

Table 4.9. (a) Trace element average values for the amphibole samples analysed. The full analytical results are in Appendix III

Sample	**Rz-1**		**Rz-2**		**Rz-33**	
Occurrence			**Micro-breccia**		**Fragment**	
Lithology	**Meta-gabbro**				**Meta-gabbronorite**	
Mineral			**Magnesio-hornblende**			
n	**12**	**σ**	**13**	**σ**	**6**	**σ**
CaO (wt%)	11.7	0.15	11.5	0.20	12.0	0.08
Ba (ppm)	12.6	137	26.9	21.6	20.8	5.86
Ce	10.3	6.58	7.54	3.89	8.59	2.34
Co	54.0	26.6	68.2	5.86	55.3	3.89
Cr	118	106	185	57	533	139
Cu	1280	2446	0.41	0.31	715	1008
Cs	0.10	0.88	0.07	0.05	0.17	0.06
Dy	3.76	2.61	2.27	1.04	2.79	0.64
Er	2.14	1.37	1.38	0.62	1.89	0.50
Eu	0.52	0.23	0.52	0.24	0.51	0.12
Gd	0.15	0.30	0.10	0.06	0.08	0.00
Hf	1.15	1.02	0.97	0.49	1.10	0.20
Ho	0.77	0.53	0.47	0.21	0.62	0.16
La	3.58	2.16	2.35	1.25	3.23	0.80
Lu	0.28	0.14	0.20	0.08	0.30	0.08
Nb	0.81	0.48	1.36	1.47	1.79	1.02
Nd	10.1	6.63	6.12	3.07	6.50	1.59
Ni	434	161	245	43	478	51
Pb	13.5	26.2	0.23	0.07	2.14	1.93
Pr	1.89	1.22	1.24	0.64	1.34	0.36
Rb	0.55	17.2	3.15	2.74	1.16	0.28
Sb	ND	ND	ND	ND	0.05	0.02
Sc	85.4	106	72.8	19.8	107	16.9
Sm	2.95	2.00	1.72	0.82	1.79	0.42
Sr	6.85	36.5	14.3	7.46	15.2	2.53
Ta	0.04	0.03	0.09	0.10	0.12	0.05
Tb	0.55	0.38	0.33	0.15	0.38	0.09
Tm	0.29	0.17	0.20	0.09	0.29	0.08
V	665	474	278	59.1	370	76.0
Yb	1.97	1.09	1.42	0.60	2.04	0.57
Y	20.3	13.3	12.3	5.67	16.4	4.41
Zr	15.5	53.0	25.8	14.3	29.4	7.63

Table 4.9. (b) Trace element average values for the amphibole samples analysed. The full analytical results are in Appendix III

Sample	**Rz-1**		**Rz-2**		**Rz-9**	
Occurrence			**Micro-breccia**		**Micro-breccia**	
Lithology	**Meta-gabbronorite**					
Mineral			**Actinolite**			
n	**15**	**σ**	**6**	**σ**	**6**	**σ**
CaO (wt%)	11.72	0.15 (n=12)	12.50	0.10	12.01	0.08 (n=5)
Ba (ppm)	11.72	7.66	3.04	1.01	20.88	5.86
Ce	11.32	7.01	0.01	1.08	8.59	2.34
Co	54.22	7.74	115.02	23.84	55.38	3.89
Cr	69	102	22	119	533	139
Cu	425	833	4	1.53	715	1008
Cs	0.07	0.03	0.24	0.10	0.17	0.06
Dy	4.36	1.59	0.08	0.81	2.79	0.64
Er	2.55	0.74	0.17	0.41	1.89	0.50
Eu	0.50	0.19	0.01	0.08	0.51	0.12
Gd	0.13	0.19	0.07	0.01	0.08	0.00
Hf	1.27	0.78	0.01	0.29	1.10	0.20
Ho	0.88	0.28	0.03	0.16	0.62	0.16
La	3.57	2.31	0.02	0.29	3.23	0.80
Lu	0.32	0.08	0.20	0.14	0.30	0.08
Nb	0.96	0.86	0.06	0.01	1.79	1.02
Nd	11.09	5.87	0.01	1.69	6.50	1.59
Ni	545	105.49	278	54.81	478	51
Pb	62.95	224.83	0.07	0.02	2.14	1.93
Pr	2.09	1.18	0.00	0.25	1.34	0.36
Rb	0.44	0.33	0.17	0.06	1.16	0.28
Sb	ND	ND	0.08	0.04	0.05	0.02
Sc	110	4.58	52	40.83	108	16.98
Sm	3.33	1.61	0.02	0.56	1.79	0.42
Sr	6.07	2.31	3.68	0.37	15.21	2.53
Ta	0.06	0.04	0.00	0.00	0.12	0.05
Tb	0.63	0.25	0.02	0.11	0.38	0.09
Tm	0.35	0.08	0.05	0.04	0.29	0.08
V	396	315.62	46	121.34	371	76.07
Yb	2.36	0.58	0.69	0.35	2.04	0.57
Y	23.43	7.01	1.02	4.12	16.46	4.41
Zr	16.83	13.89	2.78	5.91	29.46	7.63

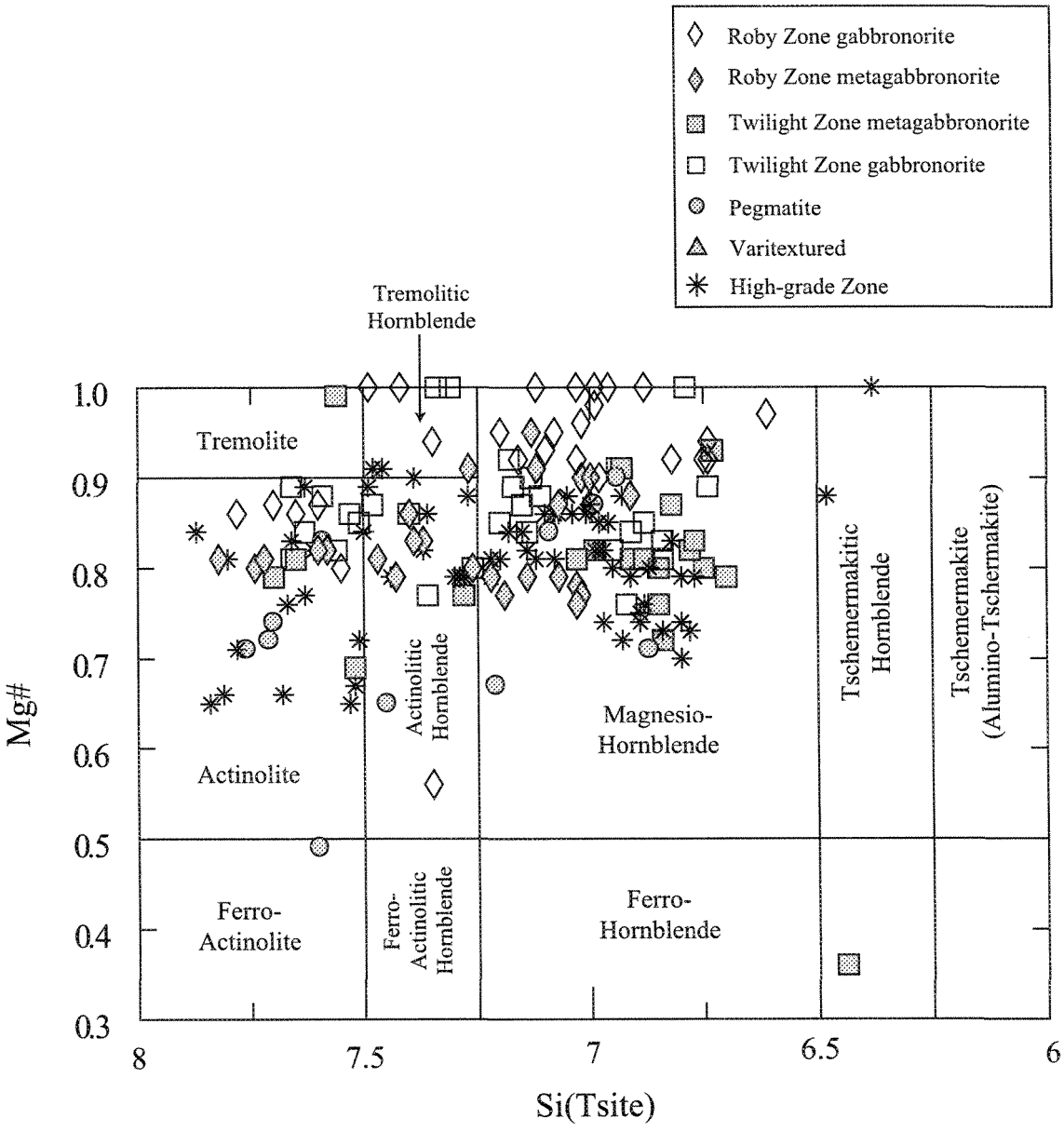

Figure 4.15. Classification diagram for calcic amphiboles where (Na+K)A < 0.50 and Ti < 0.50 modified from Leake et al. (1997).

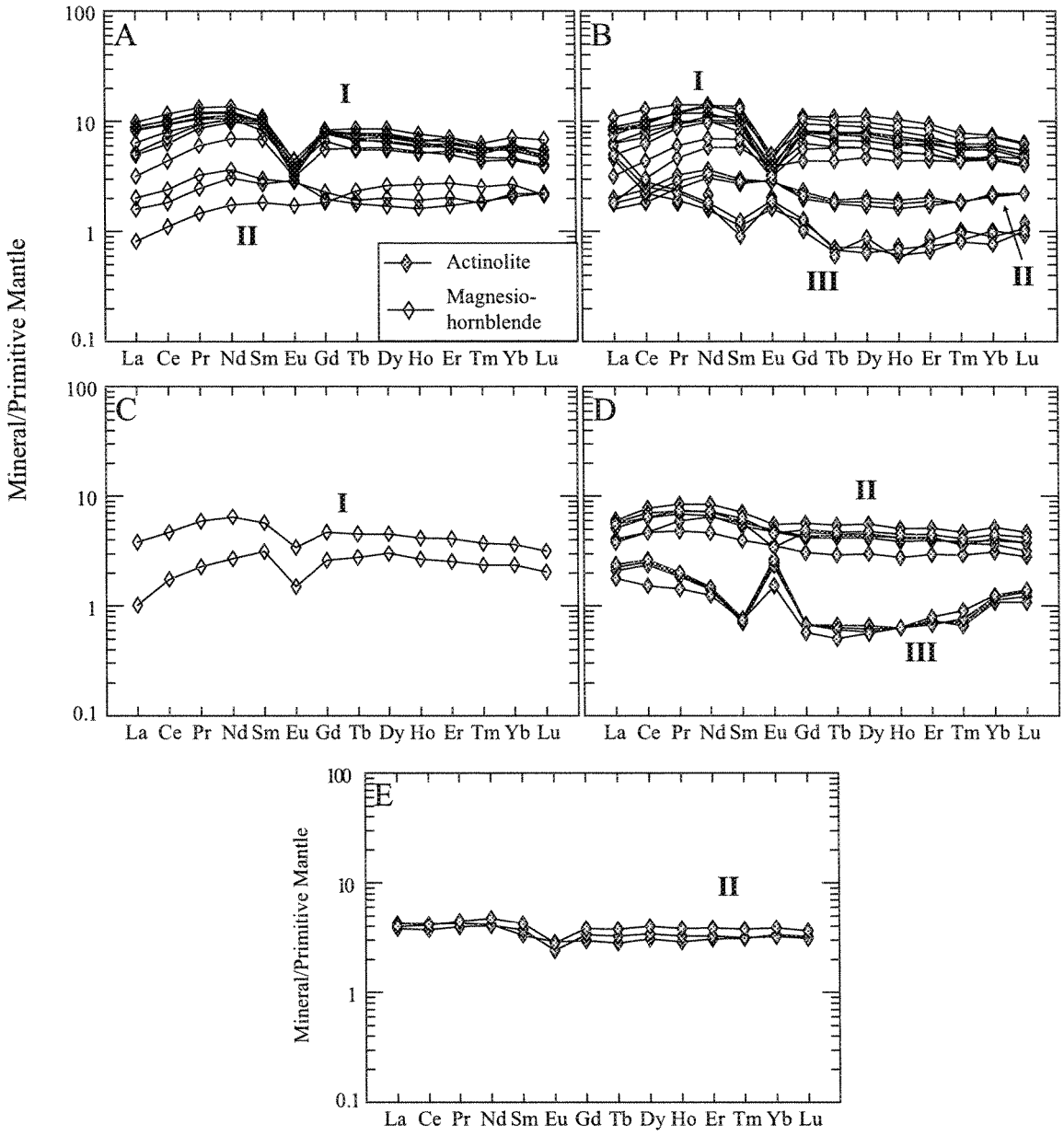

Figure 4.16. Representative REE patterns for magnesiohornblende and actinolite from the High-grade Zone: (a and b) Rz-1 and (c and d) Rz-2 and the Roby Zone (e) Rz-33. See text for Types I to III. Primitive Mantle values are from McDonough and Sun (1995).

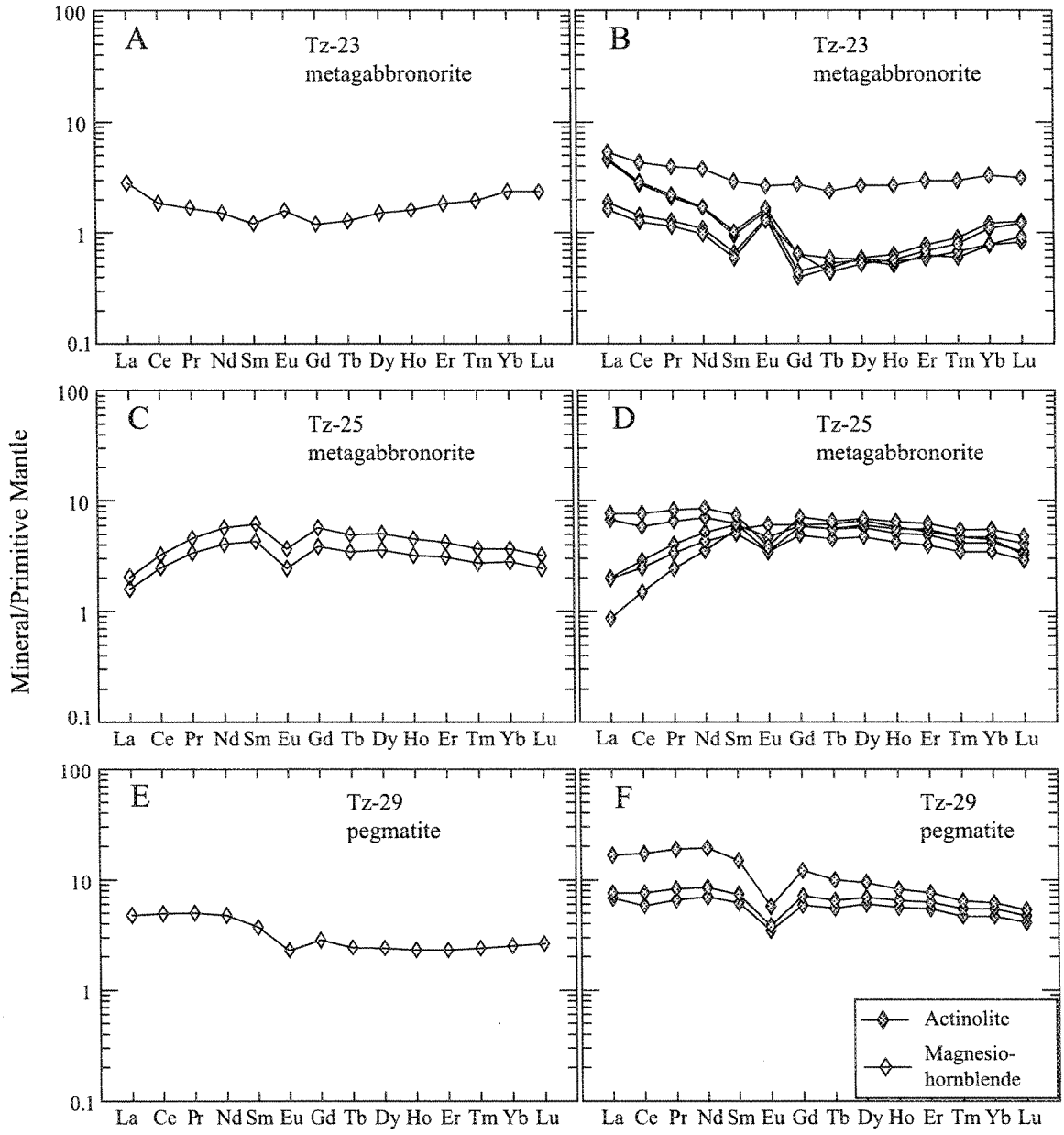

Figure 4.17. Representative magnesiohornblende and actinolite REE trends for the Twilight Zone: (a and b) Tz-23, (c and d) Tz-25 and (e and f) Tz-29. Primitive Mantle values are from McDonough and Sun (1995).

4.4. Parental Magma Signature

Brügmann et al. (1997) noted that the εNd(t) values of the LDIC indicate that the magma was derived from a depleted mantle reservoir that had assimilated continental crust, possibly tonalite gneiss. They suggested a destructive plate margin as the tectonic setting. Hinchey et al. (2005) noted low degrees of REE fractionation for the whole rock and the calculated parental magma and suggested that the magma was from a moderately refractory mantle that had suffered previous partial melting that lowered the LREE concentrations. Hinchey et al. (2005) suggested that the MgO values of the samples they analysed indicated a primary melt similar to picritic or komatiitic basalts that formed by high degrees of partial melting in the mantle.

A direct estimate of the composition of the magma from which the rocks formed cannot be made from the whole rock compositions due to the low fraction of trapped melt in the rocks, i.e. most of the rocks are essentially orthopyroxene and plagioclase meso- to adcumulates. The percentage of mafic phases present other than orthopyroxene is low apart from the 12 samples that contained normative olivine and/or clinopyroxene and which will be discussed in a later section. The range in Mg# for the rocks is 0.61 to 0.78, with the vast majority of the samples in the 0.66 to 0.74 range (Fig. 4.5). Thus, the magma that formed most of the rocks had plagioclase and orthopyroxene on the liquidus and the Mg# of the orthopyroxene was in the 0.66 to 0.74 range. Plagioclase compositions as determined by EPMA are in the range of An 54 to 61 and the estimates based on norm calculations are An

63 to 77. Assuming the K_D for $FeO/MgO_{(opx/liquid)}$ was 0.3 (Rollinson 1993) for the rocks with the highest Mg# (0.78), implies the Mg# of the magma was at least 0.51 and evolved to approximately 0.32. These compositions imply that the magma that formed the Roby and Twilight Zones was fairly evolved, i.e. it is not a primary mantle melt, contrary to (Hinchey et al. 2005) suggestions that the magma from which the Roby Zone formed was not primary.

Given the age of the arc tectonic setting and the relatively low Mg# of the orthopyroxene, the average island-arc andesite from the GEOROC database was used to model the composition of the liquid which formed the Roby and Twilight Zones. Modelling of the starting liquid with fO_2 at FMQ buffer, a pressure of 2kb, and low water content, 0.6 wt% has orthopyroxene and plagioclase on the liquidus (Table 4.10). The An and En compositions were within the range observed at LDIC. It was found that the addition of H_2O to 2 and 3wt% put clinopyroxene and olivine, respectively, on the liquidus much earlier (Table 4.11). When there was no water in the system the plagioclase was too sodic for similar orthopyroxene values. It is possible then that the bulk of the samples crystallized from relatively dry magmas, while the twelve clinopyroxene and olivine rich samples formed from magma of a similar composition except that it contained more H_2O.

Table 4.10. Summary result from the numerical simulation of crystallisation of a magma of island arc andesite composition using the programme PELE (Boudreau 2006). Average andesite composition values are from GEOROC.

STARTING LIQUID COMPOSITION (wt%)

SiO_2	TiO_2	Al_2O_3	Fe_2O_3	Cr_2O_3	FeO	MnO	MgO	CaO	Na_2O	K_2O	P_2O_5	H_2O	CO_2	S
59.45	0.73	16.78	0.92	0.00	5.51	0.14	3.36	6.80	3.07	1.42	0.15	0.60	0.00	0.00

CONSTRAINTS	Log $f(O_2)$	LIQUIDUS TEMP (°C)	PRESSURE (bars)	**LIQUID:**	MASS	VOLUME	DENSITY	VISCOSITY
At STEP 8	-10.29	1040.19	2000		65.67 g	26.26 cm3	2.50 g/cm3	2.76 log (poise)

LIQUID COMPOSITION (wt%)

SiO_2	TiO_2	Al_2O_3	Fe_2O_3	Cr_2O_3	FeO	MnO	MgO	CaO	Na_2O	K_2O	P_2O_5	H_2O	CO_2	S
63.956	1.77	13.45	1.27	0.00	6.61	0.23	1.59	5.37	2.87	2.29	0.24	0.97	0.00	0.00

SATURATED PHASES:

BULK MASS:	BULK VOLUME	BULK DENSITY
3.65 g	1.30 cm3	2.81 g/cm3

PHASE	**MASS**	**TOTAL MASS**	**COMPOSITION**	
Plagioclase	2.65	28.17	an : 0.55	ab : 0.44
Orthopyroxene	1.00	8.73	en : 0.65	fs : 0.32

Table 4.11. Summary result from the numerical simulation of crystallisation of a magma of island arc andesite composition using the programme PELE (Boudreau 2006), this system is enriched in water at 2 wt% . Average andesite composition values are from GEOROC.

STARTING LIQUID COMPOSITION (wt%)

SiO_2	TiO_2	Al_2O_3	Fe_2O_3	Cr_2O_3	FeO	MnO	MgO	CaO	Na_2O	K_2O	P_2O_5	H_2O	CO_2	S
59.45	0.73	16.78	0.92	0.00	5.51	0.14	3.36	6.80	3.07	1.42	0.15	2.00	0.00	0.00

CONSTRAINTS	Log f (O_2)	LIQUIDUS TEMP (°C)	PRESSURE (bars)	**LIQUID:**	MASS	VOLUME	DENSITY	VISCOSITY
At STEP 7	-11.11	987.10	2000		77.18 g	31.99cm^3	2.41 g/cm^3	2.46 log (poise)

LIQUID COMPOSITION (wt%)

SiO_2	TiO_2	Al_2O_3	Fe_2O_3	Cr_2O_3	FeO	MnO	MgO	CaO	Na_2O	K_2O	P_2O_5	H_2O	CO_2	S
61.82	0.99	14.81	1.15	0.00	5.76	0.19	1.58	5.56	3.27	1.93	0.20	2.72	0	0

SATURATED PHASES

BULK MASS:	BULK VOLUME	BULK DENSITY
3.64 g	1.28 cm^3	2.85 g/cm^3

PHASE	**MASS**	**TOTAL MASS**	**COMPOSITION**	
Clinopyroxene	0.28	0.28	di : 0.73	hd : 0.27
Plagioclase	2.49	18.71	an : 0.65	ab : 0.34
Orthopyroxene	0.87	7.79	en : 0.68	fs : 0.32

4.4.1. Methodology

Trace element concentrations of minerals may be changed considerably by the alteration of the minerals, therefore, samples with the least alteration of their constituent minerals were selected to calculate the parental magma composition. A sample from the Roby Zone (Rz-33) which represents the gabbronorite fragments was selected because it is representative and contains very fresh plagioclase and very fresh orthopyroxene. A leuco-gabbronorite sample from the Twilight Zone (Tz-7) was selected because it is representative and contains very fresh plagioclase and very fresh orthopyroxene. A sample from the High-grade Zone (Rz-9) was selected because it contains moderately fresh plagioclase, but no fresh orthopyroxene was observed. Whole rock data for the samples analysed are shown in Table 4.12 (a-c).

There are several sources of error in carrying out the inversion. The element may not actually partition into the crystal lattice of mineral and the observed trace element concentrations may actually be due inclusions in the mineral. The element may be present at such low concentrations that there are large analytical errors in determining its concentration. The element concentrations may be much higher at the margins of the grain than in the core, i.e. the mineral may be compositionally zoned. Finally, partition coefficients for incompatible elements are inaccurately known, and may change significantly with magma composition.

Plagioclase and orthopyroxene were on the liquidus together and hornblende may be a late crystallizing phase. In order to make a reliable estimate of the magma composition it is necessary to determine which phase controls each element. Mass balance calculations using whole rock data were used to determine the weight fraction of each element within each mineral. The weight fraction of element *i* in each mineral F was calculated by:

$$F^i = (F_x C^i_x / C_{wr})$$

Where; F_x is the weight fraction of each mineral x, from the norm calculation. C^i_x is the concentration of element *i* in the mineral x, C_{wr} is the concentration of element *i* in the whole rock. This equation indicates which mineral accommodates each element under consideration.

The values for the partition coefficients must be as representative as possible of the type of parental magma that would likely crystallise the minerals observed. Partition coefficients from Bedard (2001) for mafic magma were used, as the trace element concentrations are comparable to those calculated using the partition coefficients from the GEOROC database for an average andesite of continental arc, island arc (calc-alkaline), and continental . Table 4.12 shows the mass balance calculations and the mineral partition coefficients for the samples represented.

Table 4.12. (a) Mass balance calculation for the parental magma signature for Rz-9. Partition coefficients are from Bedard (2001)

SAMPLE	Rz-9	PLAG		Bedard (2001) Partition Coefficients	
Element Fraction ($F_{(x)}$)	Whole Rock (C_{WR})	0.43	Mass fraction of element in rock ($C_{(i)}$)	Element	PLAG
SiO_2	50.5	51.3	43.6		
TiO_2	0.16	0.01	2.15	Ti	0.045
Al_2O_3	17.2	30.1	75.1		
MgO	8.89	0.00	0.00		
CaO	10.4	12.4	51.4		
MnO	0.15	0.00	0.00		
FeO	10.3	0.07	0.29		
Na_2O	2.12	4.47	90.6		
K_2O	0.24	0.03	4.81	K	0.036
H_2O (LOI)	2.00	-	-		
Ba	44	77.4	75.6	Ba	0.9
La	1.49	1.09	31.5	La	0.042
Ce	2.9	1.80	26.7	Ce	0.036
Pb	N/A	0.95	-	Pb	1.07
Sr	N/A	350.	-	Sr	0.3
Nd	1.7	0.52	13.1	Nd	0.029
Sm	0.48	0.07	5.90	Sm	0.022
Eu	0.23	0.22	42.0	Eu	0.22
Gd	N/A	0.05	-	Gd	0.014
Tb	0.09	0.01	3.05	Tb	0.013
Dy	N/A	0.02	-	Dy	0.013
Y	N/A	0.11	-	Y	0.01
Ho	N/A	0.00	-	Ho	0.013
Er	N/A	0.01	-	Er	0.012
Tm	N/A	0.00	-	Tm	0.012
Yb	0.43	0.01	0.70	Yb	0.012
Lu	0.08	0.00	0.82	Lu	0.012

PLAG = Plagioclase. Note: for this sample, the plagioclase concentration is used to calculate the primary magma signature.

Table 4.12. (a) Mass balance calculation for the parental magma signature for Rz-33

SAMPLE Element	Whole Rock (C_{WR})	Mass Fraction ($F_{(x)}$)	OPX	PLAG	Total	% of element in:			Bedard (2001) Partition Coeffiencts		
			0.18	**0.58**		OPX	PLAG	SUM	Element	OPX	PLAG
SiO_2	50.3		52.1	50.4	38.6	18.6	58.1	76.7			
TiO_2	0.11		0.12	0.04	0.05	20.0	22.1	42.2	Ti	**0.086**	0.045
Al_2O_3	18.4		2.15	30.7	18.2	2.10	96.6	98.7			
MgO	9.94		24.6	-	4.43	44.6	0.00	44.6			
CaO	10.1		0.96	13.4	8.00	1.69	76.8	78.5			
MnO	0.12		0.34	0.02	0.08	51.3	11.6	62.9			
FeO	7.17		18.1	0.13	3.35	45.6	1.07	46.7			
Na_2O	2.22		0.02	3.82	2.22	0.16	99.7	99.8			
K_2O	0.75		0.01	0.06	0.04	0.14	4.56	4.70	K	0.006	**0.036**
H_2O	2.53	-		-	-	-	-	-			
Ba	92		0.91	161	93.7	0.18	101	101	Ba	0.0006	**0.9**
La	0.95		0.09	1.22	0.73	1.68	74.7	76.4	La	0.016	**0.042**
Ce	2.60		0.30	2.49	1.50	2.08	55.5	57.6	Ce	0.04	**0.036**
Pb	N/A		0.09	7.00	4.07	-	-	-	Pb	0.0121	**1.07**
Sr	N/A		1.00	556	322	-	-	-	Sr	**0.062**	0.3
Nd	1.20		0.20	0.85	0.53	2.94	41.1	44.1	Nd	**0.037**	0.029
Sm	0.28		0.08	0.16	0.11	5.21	33.4	38.7	Sm	**0.054**	0.022
Eu	0.15		0.02	0.43	0.25	2.20	167	169	Eu	**0.063**	0.22
Gd	N/A		0.03	-	-	-	-	-	Gd	**0.097**	0.014
Tb	<0.04		0.02	0.02	0.02	-	-	-	Tb	**0.094**	0.013
Dy	N/A		0.15	0.06	0.07	-	-	-	Dy	**0.1621**	0.013
Y	N/A		1.04	0.35	0.39	-	-	-	Y	0.17	**0.01**
Ho	N/A		0.04	0.01	0.01	-	-	-	Ho	**0.1633**	0.013
Er	N/A		0.14	0.04	0.05	-	-	-	Er	**0.1816**	0.012
Tm	N/A		0.02	0.00	0.01	-	-	-	Tm	**0.259**	0.012
Yb	0.30		0.20	0.01	0.04	11.8	2.51	14.33	Yb	**0.2605**	0.012
Lu	0.08		0.03	0.00	0.01	6.90	2.18	9.08	Lu	**0.318**	0.012

OPX = Orthopyroxene, PLAG = Plagioclase,

Note: because of the differences in the abundances of different trace elements in opx and plag for the primary magma the partition coefficient in bold is the concentration used to calculate the primary magma composition.

Table 4.12. (b) Mass balance calculation for the parental magma signature for Tz-07

SAMPLE Element	Whole Rock (C_{WR})	Mass Fraction ($F_{(x)}$)	OPX	PLAG	Total	% of element in:			Bedard (2001) Partition Coeffiencts		
			0.36	0.43		OPX	PLAG	SUM	Element	OPX	PLAG
SiO_2	49.4		52.6	51.3	41.0	38.3	44.6	83.0			
TiO_2	0.30		0.25	0.01	0.09	30.1	1.15	31.2	Ti	**0.086**	0.045
Al_2O_3	12.6		2.13	30.1	13.7	6.07	102	108			
MgO	13.1		23.2	0.00	8.35	63.5	0.01	63.5			
CaO	7.90		1.95	12.4	6.06	8.87	67.8	76.6			
MnO	0.19		0.36	0.00	0.13	67.2	0.00	67.2			
FeO	14.4		18.8	0.07	6.81	46.9	0.21	47.1			
Na_2O	1.21		0.04	4.47	1.94	1.21	158	159			
K_2O	0.19		0.00	0.03	0.01	0.69	0.07	36.9	K	0.006	**0.036**
H_2O	0.81		-	-	-	-	-	-			
Ba	60		1.10	108	46.9	0.66	77.6	78.2	Ba	0.0006	**0.9**
La	1.44		0.11	2.34	1.05	2.78	69.7	72.5	La	0.016	**0.042**
Ce	2.5		0.35	4.31	1.98	5.02	74.0	79.0	Ce	0.04	**0.036**
Pb	N/A		0.11	2.19	0.98	-	-	-	Pb	0.0121	**1.07**
Sr	145		0.84	377	162	0.21	112	112	Sr	**0.062**	0.3
Nd	1.4		0.34	1.34	0.70	8.77	41.2	50.0	Nd	**0.037**	0.029
Sm	0.37		0.14	0.18	0.12	13.2	20.3	33.6	Sm	**0.054**	0.022
Eu	0.28		0.03	0.35	0.16	3.73	53.6	57.3	Eu	**0.063**	0.22
Gd	N/A		0.23	-	0.12	-	-	-	Gd	**0.097**	0.014
Tb	0.08		0.05	0.01	0.03	24.2	11.4	35.6	Tb	**0.094**	0.013
Dy	N/A		0.46	0.06	0.19	-	-	-	Dy	**0.1621**	0.013
Y	N/A		3.19	0.27	1.26	-	-	-	Y	0.17	**0.01**
Ho	N/A		0.12	0.01	0.05	-	-	-	Ho	**0.1633**	0.013
Er	N/A		0.43	0.02	0.16	-	-	-	Er	**0.1816**	0.012
Tm	N/A		0.08	0.00	0.03	-	-	-	Tm	**0.259**	0.012
Yb	0.43		0.60	0.02	0.23	50.6	1.77	52.4	Yb	**0.2605**	0.012
Lu	0.08		0.11	0.00	0.04	48.7	2.36	51.0	Lu	**0.318**	0.012

OPX = Orthopyroxene, PLAG = Plagioclase,

Note: because of the differences in the abundances of different trace elements in opx and plag for the primary magma the partition coefficient in bold is the concentration used to calculate the primary magma composition.

Table 4.13. Calculated parental magma composition compared with modern andesite.

	Parental Magma			Whole Rock Compositions		
	Rz-09	Rz-33	Tz-07	Continental arc calc-alkali*	Island - arc calc –alkali*	Continenal Flood Basalt*
Element				(ppm)	(ppm)	(ppm)
Ba (ppm)	86.0	179	120	750	381	260
K	7453	13605	7454	30090	12106	10884
La	26.0	29.1	55.6	43	15	13
Ce	36.0	49.8	86.1	93	41	31
Pb	0.89	7.25	8.79	21	14	2
Sr	175	278	188.	356	295	244
Nd	17.8	29.3	46.3	41	18	20
Sm	2.99	7.35	7.97	7.6	4.1	5.6
Eu	1.02	1.97	1.59	1.8	1.0	1.6
Gd	5.26	5.71	6.36	2.0	4.2	6.5
Ti	1820	4539	9288	5381	4286	5349
Tb	1.54	1.54	1.54	1.0	0.6	ND
Dy	1.84	4.97	4.87	4.6	4.3	7.1
Y	10.8	34.9	26.7	29	27	37
Ho	0.31	0.24	0.72	ND	ND	ND
Er	0.66	2.94	2.38	1.1	2.8	4.4
Tm	0.12	0.31	0.29	ND	ND	ND
Yb	0.58	1.08	2.32	2.0	2.6	4.3
Lu	0.13	0.25	0.34	0.3	0.4	0.6

* Averages from GEOROC
ND = No Data

4.4.2. Results

Compositions normalized to the primitive mantle are shown in Fig. 4.18 which summarizes the distinctive features shared by the rocks of the Roby and Twilight Zones. There is an overall enrichment in High Field Strength Elements (HFSE) and depletion in LILE. There is comparative enrichment in Nd and Pb with depletion in Sr and Ti with relatively flat REE trends. There is a general enrichment in LREE relative to HREE $La/Lu_{[n]}$ = 12 (Rz-5) and 17 (Tz-4).

The sample from the High-grade Zone (Rz-9) is more depleted in Pb, Sm, Eu, Ti and HREE relative to the samples from the Roby and Twilight Zones. The fact that no orthopyroxene remains and that the magma composition was determined from plagioclase may account for the difference in the level of REE concentration. Alteration may have modified the REE concentrations in the analysed plagioclase grains. Enrichment in HREE relative to LREE is greater than that of the samples from the Roby and Twilight Zones ($La/Lu_{[n]}$ = 15).

The calculated parental magma concentrations were compared with modern arc-type rocks. Figure 4.19 (a-c) shows the calculated magma composition plotted with continental-, island- arc andesites and tholeiite continental flood basalts. The samples show comparable trends to the arc calc-andesite trends (Fig. 4.19 (a) and (b)). The calculated LDI magma hasslightly depleted HREE but with a similar overall flat profile to arc-andesite and

tholeiite continental flood basalt. The positive anomaly for Pb and negative Ti anomaly in the arc-type magmas are reflected in samples Rz-33 and Tz-7. There is no negative Ti anomaly in the continental flood basalts and Rz-33 and Tz-7 show slight enrichment in Pb (Fig. 4.19c). Compared to the arc tholeiites (Fig. 4.19d) the samples are enriched in K, La, Ce, Pb, and Nd and depleted in HREE. If the arc andesite was the magma, it would have to have been contaminated by a contaminate that would increase the concentrations of the LILE and decrease the concentration of HREE. Brügmann et al. (1997) suggests that tonalite was ingested during ascent of the magma, and that their chemical contribution would be that of increasing the LILE and decreasing the HREE concentration. These observations led Brügmann et al. (1997) to conclude that the LDIC shows similar characteristics to rock assemblages created at destructive plate boundaries, i.e. magmatic arcs or subduction zones. The enrichment in LILE and U could be the product of greenschist metamorphism (Brügmann et al. 1997), which is consistent with the regional metamorphism or indicative of an island-arc or back-arc setting deduced from the regional tectonic framework. This is consistent with the tectonic setting close to the Quetico volcanic and sedimentary units (Stone et al. 2003), which are interpreted to be the result of island-arc activity. In this study the LILE are enriched in the igneous minerals which suggest an island-arc or back-arc setting.

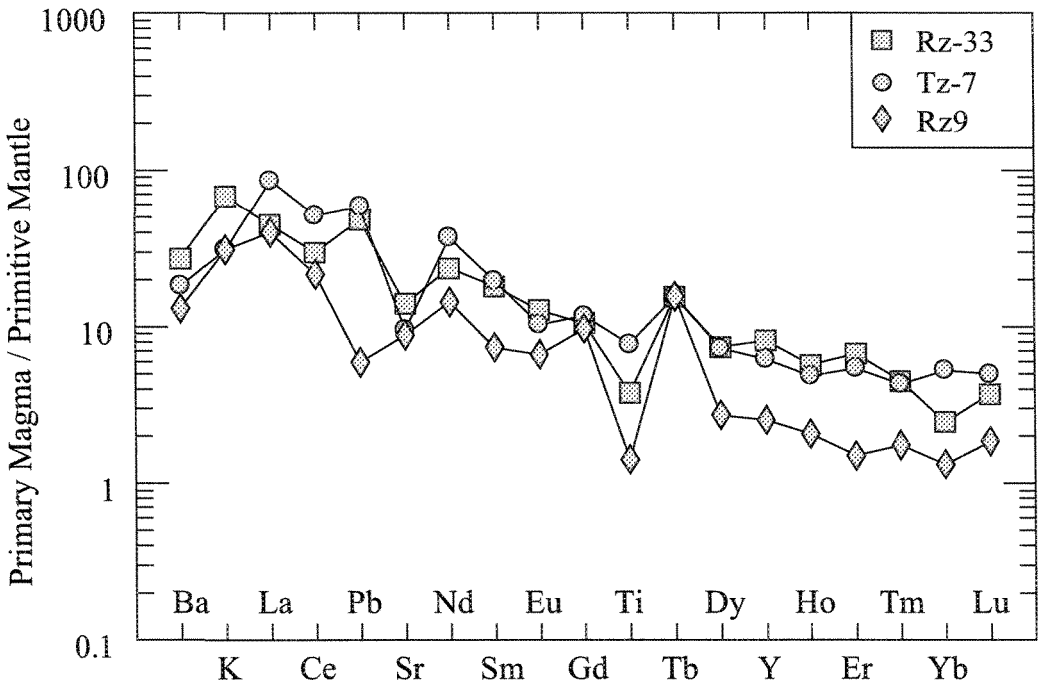

Figure 4.18. Calculated primary magma composition normalised to primitive mantle for samples Rz-33 from the Roby Zone, Rz-9 from the High-grade Zone and Tz-7 from the Twilight Zone. Primitive mantle values are from McDonough and Sun (1995).

This conclusion contrasts with that of Hinchey et al. (2005) who also used the whole rock geochemistry and the modal concentrations of the cumulate minerals to calculate the REE compositions for the parental magma of the Roby and Twilight Zones. Their results show low degrees of REE fractionation for both the bulk rock and the calculated melt and correspond to those of enriched mid-oceanic ridge basalts. Hinchey et al. (2005) suggest that the high MgO values of clinopyroxenite indicate a primary melt similar to picritic or komatiitic basalts that form by high degrees of partial melting in the mantle.

The calculations carried out by Hinchey et al. (2005) are based on the whole-rock clinopyroxenite composition and not on clinopyroxene composition. They assumed that the the composition of what they classififed as clinopyroxene to represent the liquid. As was shown in chapter 3 there are no clinopyroxenites in the samples from Hinchey et al. (2005) but they are adcumulates.

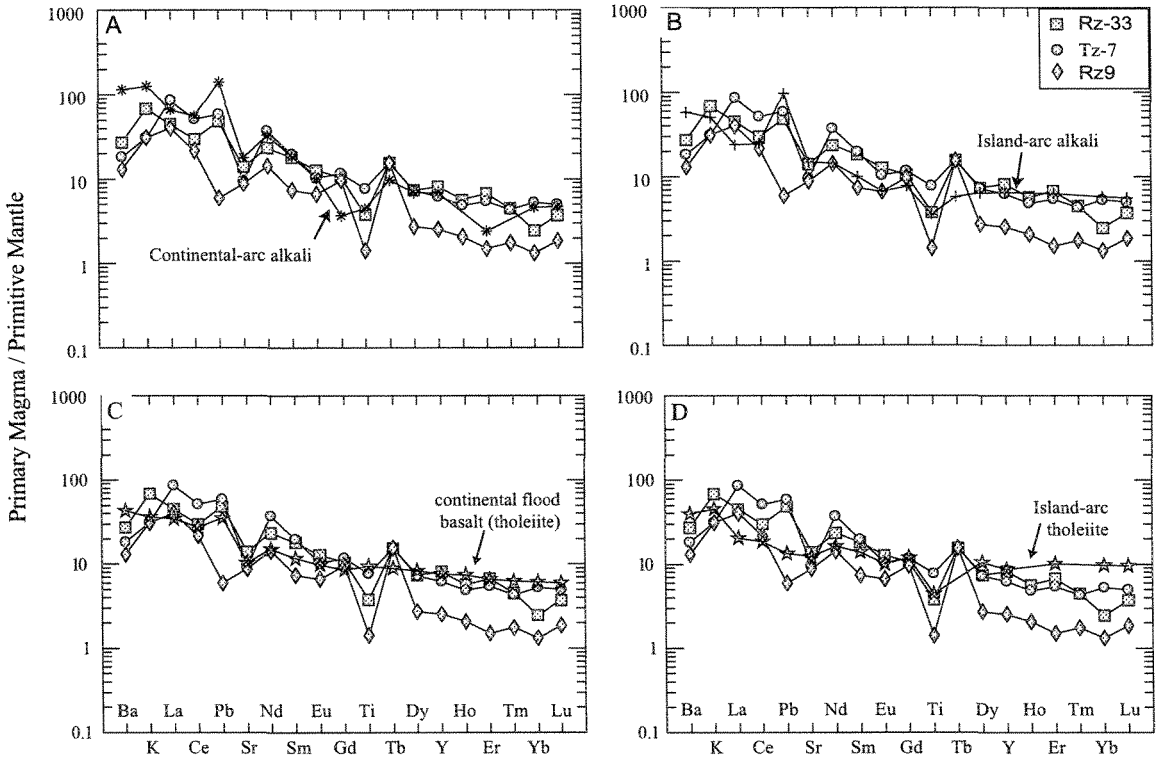

Figure 4.19. Calculated primary magma composition compared to: a) continental-arc calc-alkali, b) island-arc calc-alkali, c) continental flood basalt (tholeiitic), and d) island-arc tholeiite. The average arc and flood basalt values were taken from the GEOROC database. Primitive mantle values are from McDonough and Sun (1995).

4.5. Summary

Compositionally the main rock type found in all the three of the zones is gabbronorite. Most of the samples are plagioclase-orthopyroxene adcumulates. Twelve are olivine or olivine plus clinopyroxene cumulates. These twelve are completely altered and are now either metagabbronorite or chlorite-actinolite schists. The High-grade Zone is slightly more mafic than the Roby and Twilight Zones. The matrix is slightly more mafic than the fragments and the pegmatites and varitextured rocks are the most felsic. Despite these differences in the averages, the range of compositions covers all three zones and all textures. The altered samples are richer in H_2O, Rb, Na, K, and Cs.

The lithophile geochemistry of the samples analysed in this study indicates that the matrix material is simply a finer-grained equivalent of the fragments and is not a silicate liquid component. The overall low levels of incompatible elements (apart from LILE and U) indicates that there was very little trapped liquid component in either the fragments or the matrix. This also rules out the possibility that the matrix represents a frozen liquid as suggested by most previous authors (Lavigne and Michaud (2001) and Watkinson et al., (2002)). This observation implies that the fractionated liquid has been squeezed out of the breccia. The matrix petrographically represents a fine-grained component of either the Roby or Twilight zones. The magma source is the same even for the wherlites and 'pyroxenite', which is believed to correspond to the clinopyroxene and olivine rich rocks. Crystallisation of a dry Si-rich mafic magma favours crystallisation of orthopyroxene.

The plagioclase-orthopyroxene cumulates from all three zones appear comagmatic. The olivine-clinopyroxene cumulates could have crystallized from the same magma if H_2O was present at the time. The alteration of plagioclase results in some redistribution of the trace elements, therefore, alteration did affect the whole rock compositions. However, alteration is not restricted to a specific zone. The whole-rock trace element data highlights the low fraction of trapped melt in rocks of the LDIC and the matrix is not a liquid component of the LDIC.

The enrichment in LILE in the igneous minerals suggests that the rocks formed in an island-arc or back-arc setting. The petrographic observations in this study correspond with Brügmann et al. (1997). The compositions of the minerals suggest a magma that underwent fluid saturation during crystallization. The whole-rock composition from an average andesite from GEOROC was used to simulate the crystallisation of the parental magma to the LDIC. A magma enriched in water favoured the crystallisation of clinopyroxene instead of orthopyroxene. This may explain the presence of clinopyroxene-rich cumulates from water enriched magma and orthopyroxene-plagioclase cumulates from the dry magma. The mineral chemistry does not show extreme variation between the fragments, matrix, gabbro and metagabbro and between the different zones.

The presence of pegmatites and varitextured rocks suggests the presence of a high-temperature fluid, however, there is no difference in whole rock geochemistry between the pegmatite and other rock types. Therefore the pegmatitic textures must represent the

recrystallized component of the whole rock assemblage. In most hydrothermally altered systems the fluid is, in most cases, externally derived and is enriched in dissolved elements, these are generally LILE and some mobile LREE. These elements would be subsequently enriched in the altered rock assemblage, for example lode Au, VMS, or as in porphyry-Cu deposits. These deposits also show characteristic alteration halos where the fluids interacted with the host rock. The LILE enrichment in the Roby, Twilight and High-grade Zones does not show signs of fluid involvement and there is no evidence of alteration halos within the samples. The REE patterns for the pegmatite or varitextured samples do not show enrichment relative to the other rock types and the PGE mineralisation is also not greater in these rocks. This may be explained by the involvement of a fluid that is in equilibrium with the system. An externally-derived fluid would have likely not have been in equilibrium with the system, resulting in depletion, or enrichment, of elements as it passed through as in the case of lode Au, VMS and porphyry-Cu deposits.

5.
CHALCOPHILE AND SIDEROPHILE GEOCHEMISTRY

5.1. Analytical Methods

PGE were analysed by INAA. The PGE were pre-concentrated from 20 g of sample powder, in a Ni-sulphide fire-assay bead with a flux containing 12g of $NaCO_3$ and 24g $NaBO_3$ with total 4.4g of Ni and 3.3g of S, following the method developed by Gingras (2002) as modified after Robert et al. (1971) and Steele et al. (1975). The beads were placed in HCl, which dissolved the Ni, S, and most of the chalcophile elements leaving behind a residue of noble metals. The metals were collected on millipore filter paper (dia. 25mm, 0.45μm), which was irradiated at Ecole Polytechnique, Montreal with a neutron flux of 5 x 10^{15} $m^{-2}s^{-1}$. After an initial irradiation, which lasted for 3 minutes, produced the spectra for the determination of Rh were counted using a planar Ge detector in Montreal. The samples were then irradiated for a further 4 hours. The spectra for Pd determinations were counted between 20 and 30 hours after this second irradiation also using a planar detector in Montreal. The spectra for determining the remaining PGE were collected between 5 and 7 days after irradiation using a semi-planar detector at UQAC. In general, Au concentrations obtained by this method were systematically lower than those obtained by INAA on 2g of whole-rock powder. This is attributed to loss of Au during the dissolution step of the fire-assay procedure. Thus, the Au reported here is that determined from the whole-rock powder and not after the fire assay. A blank included in each run was

created by using 20 g of silica in place of a sample during the analysis of PGE. Certified rock standard LDI1 and in-house standards AX-90 and KPT-1 were used to monitor accuracy (Table 5.1 (a)). All of the noble metals were found to be below detection levels in the blank samples.

Table 5.1(a). Standards LDI-1, Ax90 and KPT-1 accepted PGE values compared with results obtained at UQAC. OGS = Ontario Geological Survey

Standard	LDI-1 UQAC		LDI-1 Accepted		Ax90 UQAC		Ax90 Internal		KPT-1 UQAC		KPT-1 Internal	
n	4	σ	OGS	σ	4	σ	Standard	σ	1	σ	Standard	σ
Element												
Os (ppb)	<0.9	0.23	<0.9	-	1.5	0.6	2.65	0.45	N/A	-	0.0028	0.0015
Ir	0.13	0.03	0.08	0.01	2.6	0.2	3.15	0.26	N/A	-	0.0068	0.0015
Ru	<3	0.5	0.32	0.02	6.2	1.4	15.6	3.3	N/A	-	0.017	0.002
Rh	0.56	0.11	0.7	0.03	12.5	1.2	12.1	1	N/A	-	0.017	0.001
Pt	106	12	98	11	139	6	142	12	N/A	-	0.07	0.02
Pd	814	50	833	26	311	40	353	28	N/A	-	0.15	0.04
Au	71.8	1.6	84	12	4.9	0.4	5	0.77	N/A	-	0.04	0.02
Re	<0.15	0.55	N/A	-	1.7	0.3	1.6	0.36	N/A	-		-
As	<0.12	-	N/A	-	N/A	-	0.41	0.33	1.97	0.12	2.2	0.53
Co	57	0.2	52	2	N/A	-	255	11	80	0.3	79	6
Sb	0.04	0.02	n.a	-	N/A	-	0.13	0.31	12	0.33	10	1
Ni (ppm)	643	10	656	14	N/A	-	7400	374	1174	16	1093	71
Cu	412	1.06	413	12	N/A	-	832	70	N/A	-	1112	102
S (wt%)	0.13	0.01	0.12	0.01	N/A	-	3.27	0.14	N/A	-	N/A	-

N/A = not analysed

In situ distribution of PGE specifically Pd and Pt in the sulphides of the High-grade, Roby and Twilight Zones were made on four thick sections (100 μm thick) using LA-ICP-MS at UQAC. All elements were measured using a 10 ms dwell time. Using Thermo Elemental PlasmaLab "time-resolved analysis" (TRA) data acquisition software allowing about 30 s for background counting followed by 60 s for laser ablation. Po52 synthetic iron sulphide was used for instrument calibration, and Po62 synthetic iron sulphide and PGE-a nickel sulphide were used as secondary standards. Accepted trace element concentrations for Po62 and averaged measured concentrations determined during this study are shown in Table 5.1(b). Sulphur was used as an internal standard to correct the ablation yield differences between and during individual analyses on both the samples and the standards. The S concentrations were determined by EPMA in the standard, and stoichiometric values were used to normalise for changes in the ablation yield. Data processing was carried out using the PlasmaLab software. Platinum group minerals were quantitatively analysed from selected representative thin section samples from the High-grade, Roby, and Twilight Zones with a Cameca SX100 electron microprobe at Laval University, Québec.

Table 5.1(b). Accepted values for the standards Po52 and Po62 compared to the PGE values obtained at UQAC using LA-ICP-MS analysis. ND = not detected

Standard	Po52 UQAC		Po52 Standard addition UQAC		Po62 UQAC		Po62 Accepted	
n	28	σ		σ	10	σ	4	σ
^{59}Co	14.5	0.9	14.4	2.3	18.0	4.3	ND	-
^{61}Ni	0.02	0.02	122	35.5	0.04	0.02	ND	-
^{65}Cu	4.97	3.01	98.1	1.57	10.5	7.35	ND	-
^{66}Zn	289	563	134	18.8	275	509	ND	-
^{101}Ru	5.29	0.49	9.91	2.08	1.21	0.42	1.41	0.83
^{103}Rh	6.64	0.43	7.44	0.89	1.38	0.21	ND	-
^{108}Pd	8.67	0.59	9.89	0.99	1.95	0.36	1.58	2.01
^{107}Ag	0.33	0.24	0.24	0.14	0.14	0.13	ND	-
^{111}Cd	0.45	0.56	0.16	0.05	0.37	0.54	ND	-
^{185}Re	0.004	0.002	0.011	0.006	0.4	0.07	0.49	0.75
^{192}Os	11.5	1.24	23.7	18.5	2.08	0.4	1.59	0.01
^{193}Ir	4.36	0.37	9.71	1.75	0.95	0.17	1.53	0.01
^{195}Pt	8.99	0.68	8.33	0.33	2.18	0.31	1.64	0.01

5.2. Distribution of Chalcophile Elements

The concentrations of S, Sb, As, Ag, Au, Co, Cu, and the PGE are summarised in Table 5.2, to 5.6 for the different zones, breccia components, altered, and non-altered rocks. The average S content in all zones is similar and very low, between 0.1 to 0.3 wt%, which represents approximately 0.5 - 0.8 % sulphide minerals in the rock Table 5.2. The microbreccia has the lowest S content (0.1 wt%) compared to the rest of the samples from the High-grade, Roby, and Twilight Zones. The concentrations of S, Ni, Cu, Co, Ir, and Rh are similar for all zones Table 5.2. In contrast, the Pd, Pt, Au, As, and Sb concentrations are 2 – 5 times higher in the High-grade Zone than in the Roby and Twilight Zones, which have similar concentrations of these elements. The Ni, Cu, Ir, Pd, Pt, Au, As, and Sb concentrations are 4 – 80 times higher in the actinolite-chlorite schist than in the microbreccia (Table 5.6). Silver, Os, and Ru concentrations are very low in all zones and are close to detection limits, so these elements will not be discussed further.

The primitive mantle-normalized graphs for the Roby, Twilight, and High-grade Zones (Fig. 5.1) show that the zones have similar patterns. This pattern shows low Os, Ir Ru, and (IPGE) concentrations and high Pt, Pd (PPGE). There is an extreme fractionation of IPGE from PPGE. Overall, the High-grade Zone shows higher Pd and Au peaks compared to samples from the Roby and Twilight Zones (Fig. 5.1).

Table 5.2. Average concentrations of chalcophile elements in the Roby, Twilight and High-grade Zones. Full data list is given in Appendix III

Zone	High-grade			Roby			Twilight		
n	17	σ	Range	36	σ	Range	40	σ	Range
Ag (ppm)	0.96	0.98	0.5 - 4.4	0.76	0.73	0.50 - 3.40	0.75	0.52	0.5-2.9
As	0.76	0.92	0.2 - 3.2	0.52	0.35	0.10 - 1.60	0.43	0.26	0.10-1.20
Au	0.72	2.31	0.01 - 9.95	0.15	0.22	0.004 - 1.18	0.19	0.28	0.002-1.37
Co	77	28	35 - 174	64	30	24 - 167	73	20	27.0-104
Cu	557	893	2 - 2756	543	771	11 - 3465	841	953	31-3369
Ni	767	697	171 - 2684	624	581	106 - 3285	773	561	18-2671
Sb	0.37	0.48	0.02 - 1.66	0.13	0.08	0.03 - 0.32	0.07	0.07	0.02-0.48
Zn	45	26	4 - 1475	41	58	4 - 280	63	24	4-106
S (wt%)	0.23	0.44	0.01 - 1.75	0.21	0.30	0.01 - 1.48	0.27	0.31	0.01-1.33
Ir (ppb)	0.17	26.3	0.02 - 0.81	0.17	0.26	0.01 - 1.12	0.28	0.28	0.02-0.95
Rh	0.57	2.16	0.1 - 9.2	1.62	2.32	0.30 - 11.8	1.92	2.30	0.1-11.4
Pt	390	719	5 - 3078	146	293	1 - 1669	186	213	2-905
Pd	5510	12041	69 - 52316	1071	2164	3 - 12441	1272	1509	7-5446
Re	0.62	1.11	0.1 - 3.9	0.43	0.58	0.10 - 3.10	0.60	0.74	0.1-3.0
Pd/Ir	21975	19037	607 - 64587	6282	5623	18- 21760	5496	6413	607-64587
Pd/Pt	10	5	3 - 21	6	3	0.5 - 16	6	3	4-21

Table 5.3. Average concentration of chalcophile elements in matrix and fragment samples from the Roby and Twilight Zones. Full data list is given in Appendix III

Zone	Roby			Roby Matrix			Twilight			Twilight Matrix		
Occurence	Frag						Frag					
n	17	σ	Range	19	σ	Range	16	σ	Range	19	σ	Range
Ag (ppm)	0.61	0.27	0.5 - 1.5	1.11	0.90	0.5 - 3.4	0.68	0.34	0.5 - 2.9	0.83	0.65	0.5 - 2.0
As	0.43	0.21	0.2 – 1.0	0.61	0.43	0.1 - 1.6	0.47	0.26	0.2 - 1.1	0.39	0.29	0.1 - 1.2
Au	0.06	0.04	0.02 -0.16	0.24	0.28	0.01 - 1.18	0.26	0.36	0.01 - .37	0.13	0.17	0.01 - 0.44
Co	54	18.6	24 - 100	78	33.4	28 - 167	67	17	27 - 103	81	20	67 - 104
Cu	260	211	51 - 694	891	951	11 - 3465	750	763	31 - 3369	954	1122	47 - 3160
Ni	392	178	106 - 705	898	702	224 - 3285	681	375	18 - 2671	870	708	332 - 2330
Sb	0.10	0.05	0.03 - 0.21	0.14	0.09	0.04 - 0.32	0.07	0.04	0.02 - 0.17	0.08	0.10	0.02 - 0.48
Zn	38	26	4 - 104	67	72	4 - 280	59	21	4 - 106	66	27	4 - 106
S (wt%)	0.12	0.12	0.03 - 1.48	0.33	0.38	0.01 - 0.45	0.20	0.21	0.01 - 1.33	0.35	0.39	0.01 - 0.95
Ir (ppb)	0.07	0.14	0.01 - 0.61	0.28	0.31	0.02 - 1.12	0.25	0.25	0.02 - 0.95	0.30	0.30	0.02 - 0.86
Rh	0.7	0.6	0.3 - 2.5	2.53	2.93	0.4 - 11.8	1.93	1.61	0.1 - 4.5	2.32	2.82	0.4 - 11.4
Pt	32	36	1 - 114	251	367	4 - 1669	131	159	2 - 632	240	256	11 - 905
Pd	238	303	5 - 1088	1784	2764	3 - 12441	936	1338	7 - 5446	1557	1699	19 - 5419
Re	0.32	0.29	0.1 - 1.23	0.57	0.73	0.1 - 3.1	0.42	0.56	0.1 - 2.4	0.85	0.88	0.1 - 3
Pd/Ir	5492	6157	125 - 21760	6324	5029	18 - 16537	4213	2701	217 - 7556	4664	3196	475-10180
Pd/Pt	4	2	1 - 8	7	3	0.5 - 16	6	2	0.4 - 17	6	4	2 - 8

Table 5.4. Average concentrations of chalcophile elements in the varitextured and pegmatite samples from the Roby and Twilight Zones. Full data list is given in Appendix III

Zone	Roby			Twilight		
Texture	Varitextured			Pegmatites		
n	4	σ	Range	5	σ	Range
Ag (ppm)	0.55	0.09	0.5 - 0.7	0.70	0.40	0.50 - 1.5
As	0.33	0.13	0.2 - 0.5	0.40	0.11	0.20 - 0.5
Au	0.03	0.01	0.02 - 0.05	0.19	0.25	0.01 - 0.69
Co	44	12	24 - 53	58	13	46 - 81
Cu	123	19	110 - 155	701	727	79 - 2060
Ni	268	127	106 - 460	694	300	311 - 1130
Sb	0.10	0.03	0.06 - 0.12	0.06	0.04	0.02 - 0.12
Zn	35	17	7 - 52	63	22	40 - 100
S (wt%)	0.04	0.02	0.01 - 0.07	0.20	0.17	0.01 - 0.52
Ir (ppb)	0.03	0.02	0.01 - 0.05	0.27	0.25	0.07 - 0.73
Rh	0.90	0.92	0.3 - 2.5	0.34	0.68	1.70 - 1.7
Pt	12	10	4 - 26	153	102	24 - 335
Pd	34	34	10 - 89	1261	923	53 - 2800
Re	0.10	0.00	0.1 - 0.1	0.23	0.11	0.10 - 0.4
Pd/Ir	1975	1359	200 - 3500	12509	14258	72 - 40000
Pd/Pt	3	1	2 - 3	7	3	2 - 10

Table 5.6. Average concentrations of chalcophile elements in the High-grade Zone. Full data list is given in Appendix III

Texture	Schist			Microbreccia		
n	12	σ	Range	5	σ	Range
Ag (ppm)	1.04	1.15	0.5 - 4.4	0.8	1.04	0.5 – 1.83
As	0.98	1.07	0.2 - 3.2	0.2	0.98	0.20 - 0.40
Au	1.01	2.82	0.02 -9.95	0.02	1.01	0.01 - 0.03
Co	83	32	35 - 174	61	83	54 - 76
Cu	727	1044	2 - 2756	87	727	82 - 97
Ni	300	740	382 - 2684	206	300	171 - 257
Sb	0.51	0.54	0.04 - 1.66	0.05	0.51	0.02 - 0.07
Zn	54	30	4 - 96	45	54	10 - 64
S (wt%)	0.31	0.53	0.01 - 1.75	0.05	0.31	0.03 - 0.06
Ir (ppb)	0.21	0.25	0.04 - 0.81	0.07	0.21	0.02 - 0.17
Rh	9.2	0	9.2	0.10	0.77	0.10 - 0.40
Pt	542	844	18 - 3078	23	542	5 -43
Pd	7765	14325	69 - 52316	97	7765	82 -143
Re	0.70	1.25	0.1 - 3.9	0.20	0	0.20
Pd/Ir	28591	18313	1500 - 64587	1350	28591	607 - 4100
Pd/Pt	12	5	4 - 21	6	12	3 - 16

Table 5.6. Average concentrations of chalcophile elements in the High-grade Zone. Full data list is given in Appendix III

Texture	Schist			Microbreccia		
n	12	σ	Range	5	σ	Range
Ag (ppm)	1.04	1.15	0.5 - 4.4	0.8	1.04	0.5 – 1.83
As	0.98	1.07	0.2 - 3.2	0.2	0.98	0.20 - 0.40
Au	1.01	2.82	0.02 -9.95	0.02	1.01	0.01 - 0.03
Co	83	32	35 - 174	61	83	54 - 76
Cu	727	1044	2 - 2756	87	727	82 - 97
Ni	300	740	382 - 2684	206	300	171 - 257
Sb	0.51	0.54	0.04 - 1.66	0.05	0.51	0.02 - 0.07
Zn	54	30	4 - 96	45	54	10 - 64
S (wt%)	0.31	0.53	0.01 - 1.75	0.05	0.31	0.03 - 0.06
Ir (ppb)	0.21	0.25	0.04 - 0.81	0.07	0.21	0.02 - 0.17
Rh	9.2	0	9.2	0.10	0.77	0.10 - 0.40
Pt	542	844	18 - 3078	23	542	5 -43
Pd	7765	14325	69 - 52316	97	7765	82 -143
Re	0.70	1.25	0.1 - 3.9	0.20	0	0.20
Pd/Ir	28591	18313	1500 - 64587	1350	28591	607 - 4100
Pd/Pt	12	5	4 - 21	6	12	3 - 16

Hinchey et al. (2005) suggest that the leucocratic fragments are depleted in PGE with the matrix being sulphide and PGE enriched. In order to characterise the components of the Roby and Twilight Zones' breccia components, the samples were separated into fragments and matrix (Fig. 5.1). On average, the fragments in both the Roby and Twilight Zones are poorer in S and all the chalcophile elements than the matrix (Table 5.3). However, the matrix samples have a wider range in concentrations for all elements. Thus, despite the differences in average composition there is an overlap in the content of chalcophile elements between the rocks of the different zones, and between the fragments and the matrix (Fig. 5.1). This overlap is similar to that which was observed for the major-element oxides.

Lavigne and Michaud (2001) and Michaud (1998) proposed that a gabbroic magma rich in PGE and volatiles brecciated the already emplaced gabbroic rocks that make up the MBI. Such a scenario should result in a matrix material that is enriched in PGE compared to the fragment component in the breccia-type ore. Lavigne and Michaud (2001) and Michaud (1998) noted that the sulphide minerals associated with the alteration assemblage show evidence of alteration of fine intergrowths between silicates and sulphides. It is possible that the fluids exsolved from the intruding gabbroic magma (i.e., which constitutes the matrix of the breccia) permeated throughout the Complex favouring the formation of varitextured rocks, Pd-rich pegmatites, and causing hydrothermal alteration. If this was the case, the rocks that have textures modified by the passage of fluids, such as pegmatites and varitextured rocks should, therefore, be enriched in Pd. In this scenario, fluid flow was

limited on one side by the impermeable East Gabbro and was focussed in the area where a 15-20 m wide zone of alteration and Pd-rich mineralisation formed (the High-grade Zone) (Lavigne and Michaud 2001).

In order to test whether the varitextured and pegmatite samples have different Pd content from other zones, their average compositions and primitive mantle-normalised patterns were compared to those in the Roby, Twilight, and High-grade Zones. The varitextured samples from the Roby Zone (Table 5.4) have overall, lower concentrations (Fig. 5.2) and the varitextured fragments display flatter patterns (with low variation) between Rh and Au compared to the fragments from the Roby Zone (Fig. 5.1 and Fig. 5.2). The lowest Ir concentration is in a varitextured fragment. The pegmatite samples from the Twilight Zone (Table 5.4) have values close to those of the metagabbronorite (Table 5.5). One pegmatite sample shows a pattern similar to the varitextured fragments from the Roby Zone; it has a flatter pattern between Rh and Au (Fig. 5.2) compared to the rest of the pegmatites (Fig. 5.2). The overall fractionation between the IPGE (Ru, Os, and Ir) and PPGE (Pt and Pd) that is observed in the Roby and Twilight Zones (Fig. 5.1) is displayed in these samples. The varitextured and pegmatite samples show an overlap and no significant enrichment in Pd compared to the fragments of the Roby and Twilight Zones.

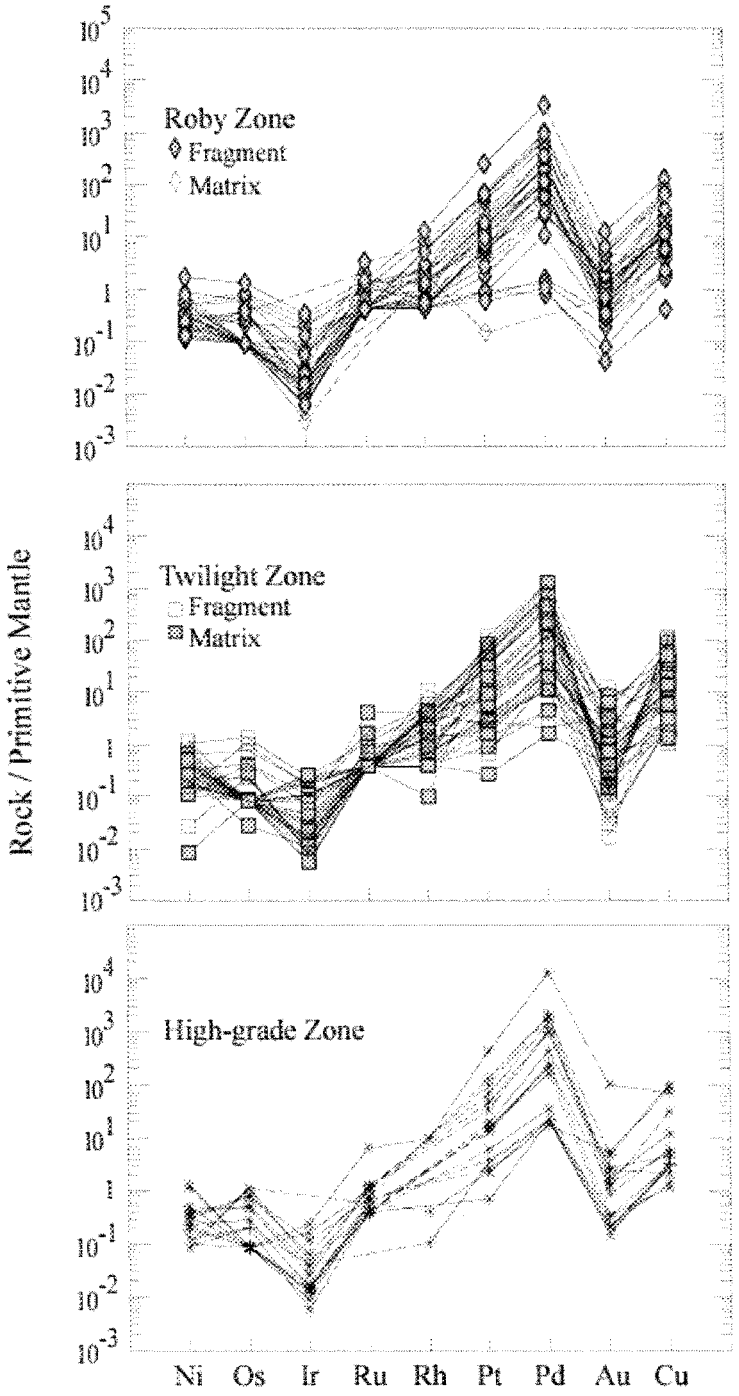

Figure 5.1. Primitive mantle normalised concentrations of the chalcophile elements in the Roby, Twilight and High-grade Zones. Primitive mantle values are from Barnes et al., (1999).

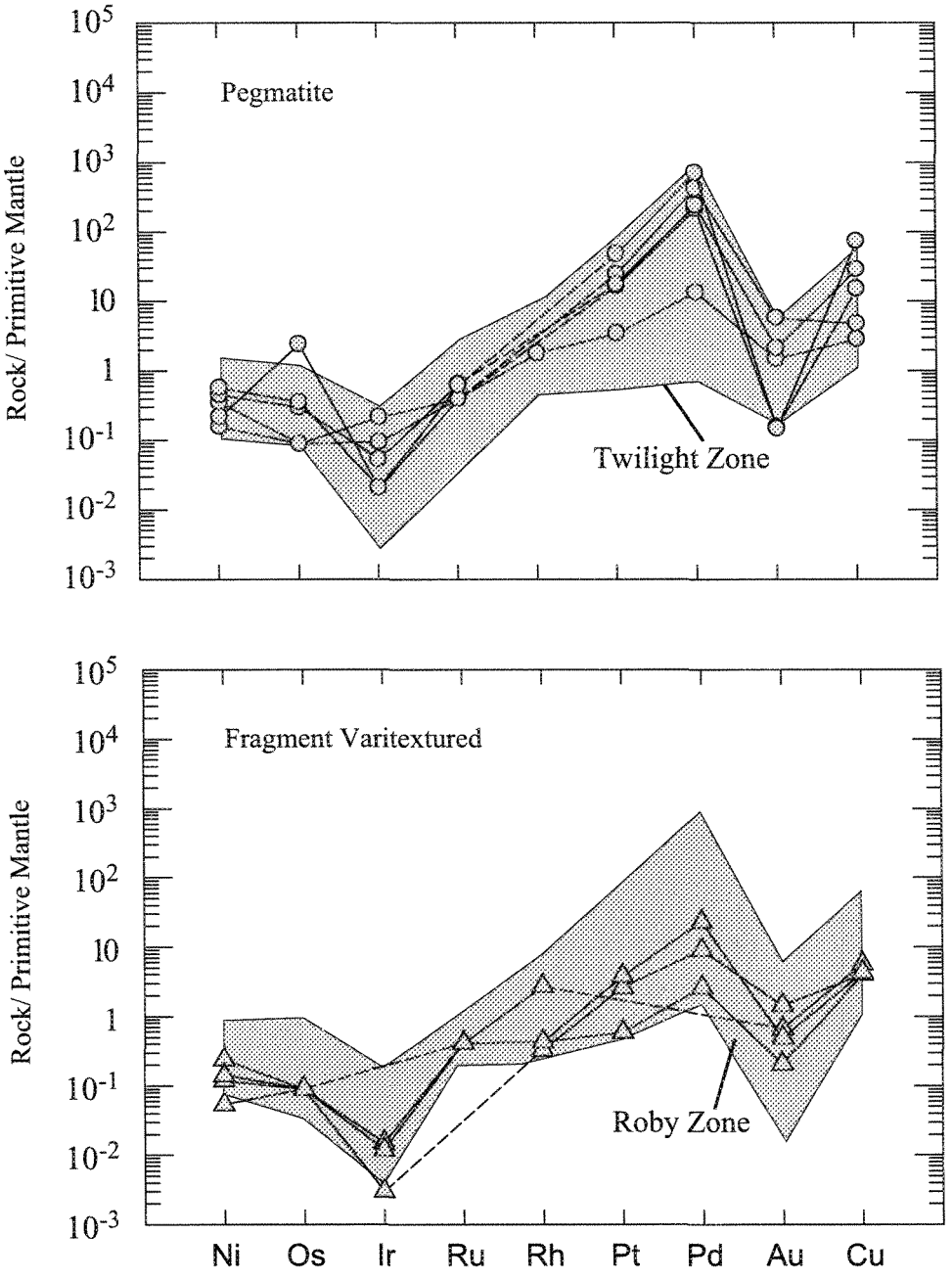

Figure 5.2. Primitive mantle normalised chalcophile element concentrations from the pegmatite of the Twilight Zone and varitextured fragments from the Roby Zone. Primitive mantle values are from Barnes et al. (1999). The shaded area shows the zone for the samples from the Twilight and Roby Zone respectively.

As mentioned earlier the high Pd/Ir ratio and extensive alteration has led to the suggestion that fluids played a role in the formation of the deposit. In order to determine the affects of alteration on the chalcophile elements the gabbronorite and metagabbronorite samples were compared (Fig. 5.3). The gabbronorite has slightly higher S concentrations than the metagabbronorite (Table 5.5). The gabbronorite samples fall within the range of the metagabbronorite samples creating an overlap in concentration (Fig. 5.3). Thus, there does not appear to be any connection between degree of alteration and chalcophile element content.

The concentration of siderophile elements in the microbreccia and schist of the High-grade Zone are given in Table 5.6. The microbreccia samples lie within the lower ranges of the High-grade Zone for their concentration of chalcophile elements and they have lower Pd/Ir averages compared to the schist. The microbreccia samples resemble the varitextured rocks. The identification of the High-grade Zone based on its texture does not show significant differences between the High-grade Zone and any of the other zones. The samples can be divided into two main groups, samples that have a similar trend and chalcophile element concentrations to those of the Roby and Twilight Zones and samples of samples that have higher Pd/Pt ratios than the average values. The averages are shown in Table 5.7. The primitive mantle-normalised plots show that the samples that have the higher Pd/Pt ratios are significantly enriched in Pt, Pd, and Rh (Fig. 5.4). The Pd concentrations are the highest and this accounts for the higher Pd/Pt ratios in these samples.

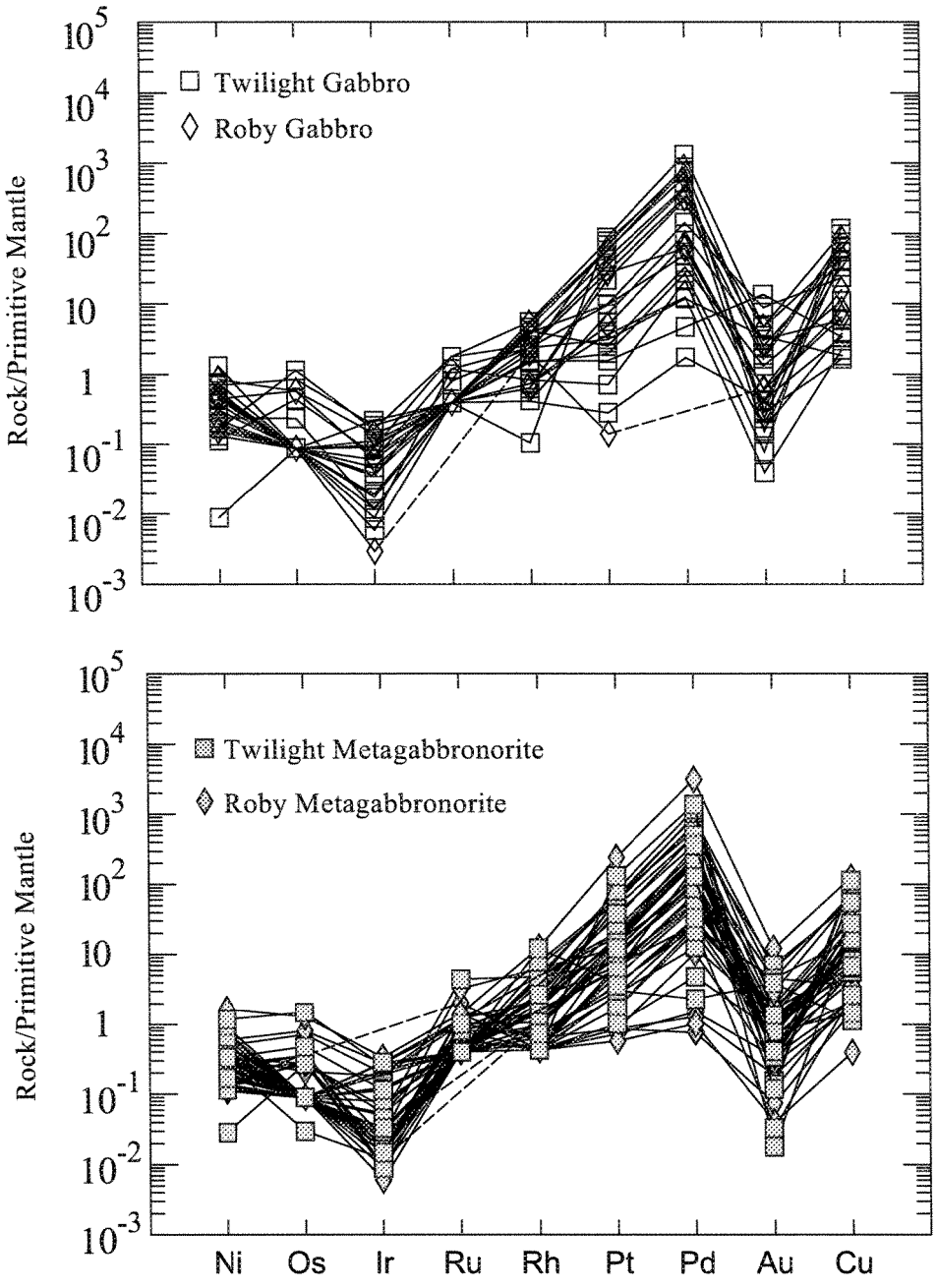

Figure 5.3. Primitive mantle normalised concentrations of the chalcophile elements in Roby, Twilight Zone gabbronorite and metagabbronorite samples. Primitive mantle values are from Barnes et al. (1999).

Table 5.7. Average concentrations of the siderophile elements in the High-grade Zone divided into high Pd and low Pd groups. Full data list is documented in Appendix III

Sample	High-grade High Pd Group			High-grade Low Pd Group		
n	7	σ	Range	10	σ	Range
Ag (ppm)	0.76	0.52	0.50 - 2.00	1.10	1.18	0.50 - 4.40
As	1.11	0.85	0.40 - 3.10	0.52	0.90	0.20 - 3.20
Au	1.59	3.42	0.06 - 9.95	0.11	0.16	0.01 - 0.54
Co	95	32	75 - 174	63	13	35 - 80
Cu	745	967	2 - 2503	426	812	32 - 2756
Ni	1283	792	604 - 2684	406	262	171 - 1033
Sb	0.66	0.58	0.04 - 1.66	0.17	0.25	0.02 - 0.90
Zn	2430	34	4 - 96	194	19	10 - 73
S (wt%)	0.41	0.62	0.01 - 1.75	0.11	0.16	0.01 - 0.59
Ir (ppb)	0.33	0.25	0.09 - 0.81	0.06	0.05	0.02 - 0.17
Rh	1.31	3.22	9.20	0.05	0.12	0.10 - 0.40
Pt	863	932	237 - 3078	57	45	5 - 136
Pd	12695	16246	4103 - 52316	480	544	69 - 1760
Re	1.13	1.47	0.10 - 3.90	0.19	0.14	0.10 - 0.50
Pd/Ir	38138	17229	13698 - 64587	7927	9995	607 - 29891
Pd/Pt	14	4	9 - 21	7	4	3 - 16

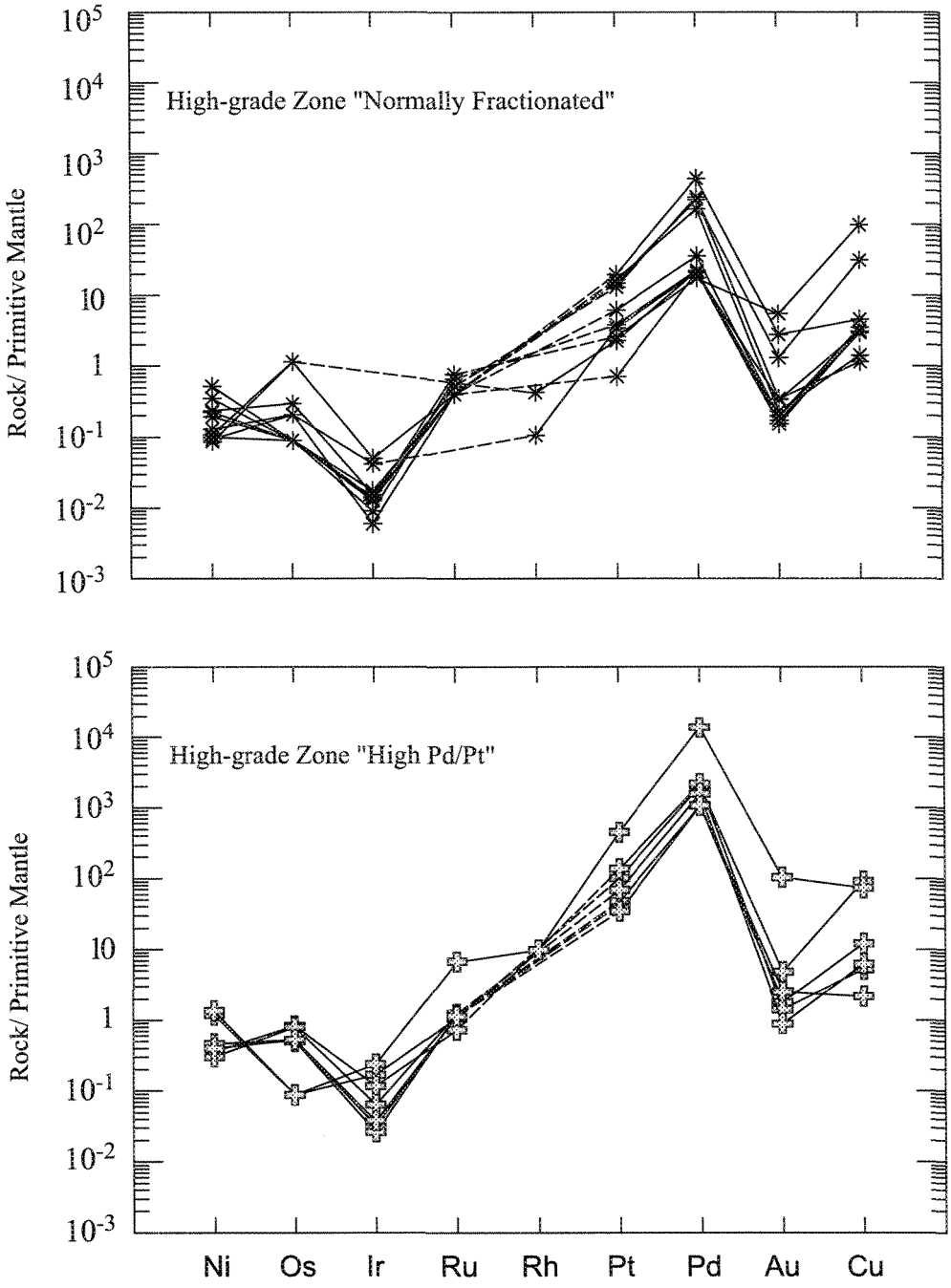

Figure 5.4. Primitive mantle normalised chalcophile element concentrations from the High-grade Zone. The high grade samples have ratios Pd/Pt from 4 to 23. Primitive mantle values are from Barnes et al. (1999).

The rest of the elements occur at concentrations that are comparable to those of the rest of the High-grade, Roby, and Twilight Zones. The greater enrichment in Pd and the lesser enrichment of Ir accounts for the higher Pd/Ir ratio determined for these samples (Fig. 5.4).

Compared with most magmatic PGE deposits the data from the LDIC show extreme fractionation of the IPGE from the PPGE, with Pd/Ir ratios of 1000 to 34000 (Tables 5.2 to 5.6) (Brügmann et al. 1989; Hinchey et al. 2005). Of PGE-dominated ores, only rocks from the JM-reef at Pd/Ir = 905 approach these values, (Table 1.1). The Cu-rich veins at Sudbury and Cu-rich massive ores at Noril'sk also have high Pd/Ir ratios, and on the Ni/Cu versus Pd/Ir plot LDIC samples fall in the Cu-rich sulphide field (Fig. 5.5). Furthermore, the metal ratios in Cu-rich veins associated with basaltic komatiites of the Cape Smith belt (Barnes et al. 1992) also approach our values from the LDIC. All of these types of ore except the J-M reef, however, generally have much more Cu than Ni and contain >10 % sulphides and are, therefore, not good analogues for the rocks of the LDIC. The fractionation of the PGE, Ni, and Cu may also be considered by normalising the data to the composition of the primitive mantle (Fig. 5.1 and 5.2). In all three zones the metal plots are relatively unfractionated from Ni to Ru with values in the 0.001 to 1 range. Values then rise steeply through Rh and Pt to peak at Pd in the 10 to 104 range before dropping by two orders of magnitude (200) to Cu. The varitextured samples from the Roby Zone show similarly shaped patterns as the matrix and the fragments, but their absolute concentrations are lower, ranging from 0.001 to 0.1 times mantle from Ni to Ru and peaking at around 10 times mantle for Pd. Copper values are approximately one order of magnitude lower than the Pd values (Fig. 5.2).

Pegmatite samples from the Twilight Zone have broadly similar concentrations as the matrix and fragments from this locality (Fig. 5.2). The shape of the patterns for the fragments and the matrix is similar to the Roby and Twilight Zones, the main difference being that some matrix samples are richer in PGE than the fragments.

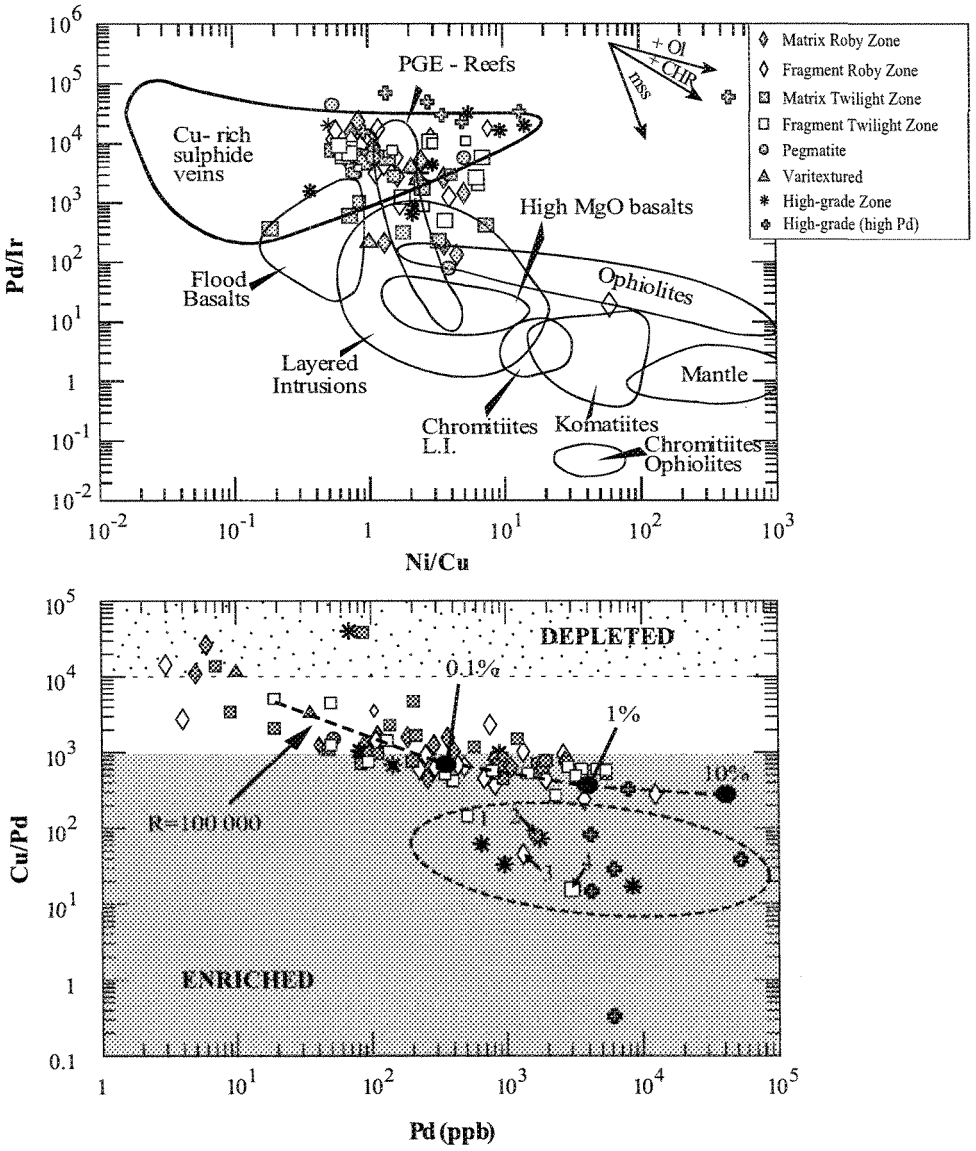

Figure 5.5. a) Pd/Ir versus Ni/Cu plot modified after (modified after Barnes 1990) and b) Cu/Pd versus Pd plot for all samples from the High-grade, Roby, and Twilight Zones, R-values for the Bushveld Complex are taken from Barnes and Maier (1999). The values 0.1, 1 and 10 % relate to the percentage of sulphide present in the system. 1 = Tz-36, 2 = Tz-20, 3 = Rz-51, 4 = Tz-41.

5.3. Interpretation of the Data

5.3.1. Roby and Twilight Zones

The phase that most commonly controls the concentrations of chalcophile and siderophile elements in magmatic processes is a base metal sulphide liquid. In order to assess whether a sulphide liquid controlled the distribution of chalcophile elements and PGE (Ir, Rh, Pt, Pd and Re) were plotted against S (Fig. 5.6 a and b). The elements, Au, As, Sb, and Zn do not appear to correlate with S (Fig. 5.6 (a)) and, therefore, do not appear to have been controlled by a base metal sulphide liquid. Nickel, Co, Cu, Ir, Pt, Pd, Au, Rh, and Re (Co, not shown) all show a positive correlation with S for samples containing >0.1 wt% S (Fig. 5.6). Most samples from the Roby and Twilight Zones fall on the same trend lines, and this suggests that the distribution of these metals is controlled by sulphide liquid, and that the composition of the sulphide liquid was similar in both zones.

Both the fragments and the matrix from the Twilight and Roby Zones breccias plot along the same trend on the S versus metal plots (Fig. 5.6). This suggests that in both the fragments and the matrix the phase controlling the metal concentrations was a sulphide liquid. On average the fragments have lower metal and S contents than the matrix samples (Table 5.3), but the fragments and matrix also show a considerable overlap in composition. This could be because there were a number of injections (i.e. pulses) of magma into both zones, thus some fragments probably represent matrix material from an earlier injection of magma (Fig. 2.4).

The varitextured rocks and the pegmatites plot along the same trend as the rocks from the breccia zones (Fig. 5.6). This suggests that in these rocks the metals are also controlled by the sulphides, and that these sulphides are similar in composition to those in the breccia. This observation is significant because some authors, for example Talkington and Watkinson (1984b), Macdonald (1988), Watkinson et al (2002) and Michaud and Lavigne (2003) have interpreted the presence of the pegmatites and the varitextured rocks as an indication for the action of a high temperature fluid during the formation of the ores. In their models the fluid also introduced the PGE into the system. This study shows that the varitextured and the pegmatitic rocks fall on the same trend-line as non-pegmatitic and non-varitextured rocks. Such a relationship suggests that, while a high temperature fluid could have had an effect on the textures with the development of pegmatoidal textures and varitextured gabbronorites, it did not change the PGE, S, and base metal concentrations of the rocks. (Hinchey and Hattori 2005) reached a similar conclusion from their data.

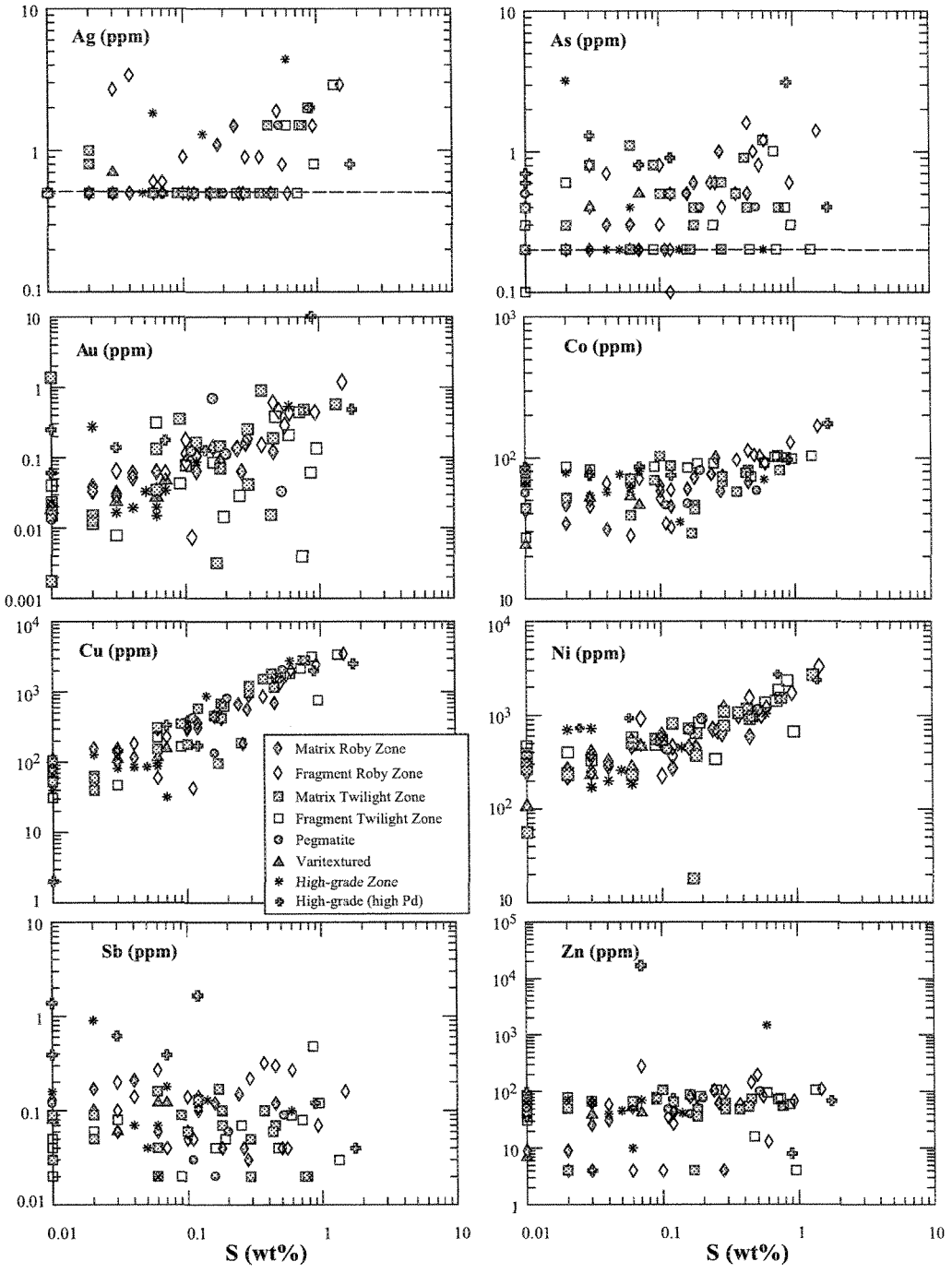

Figure 5.6(a). Chalcophile elements plotted versus S (wt%) of the High-grade, Roby and Twilight Zones. Note Au, Co, Cu and Ni correlate with S indicating sulphides control the element concentration. Some samples from the High-grade Zone show poor correlation for all elements. lld = lower limit of detection.

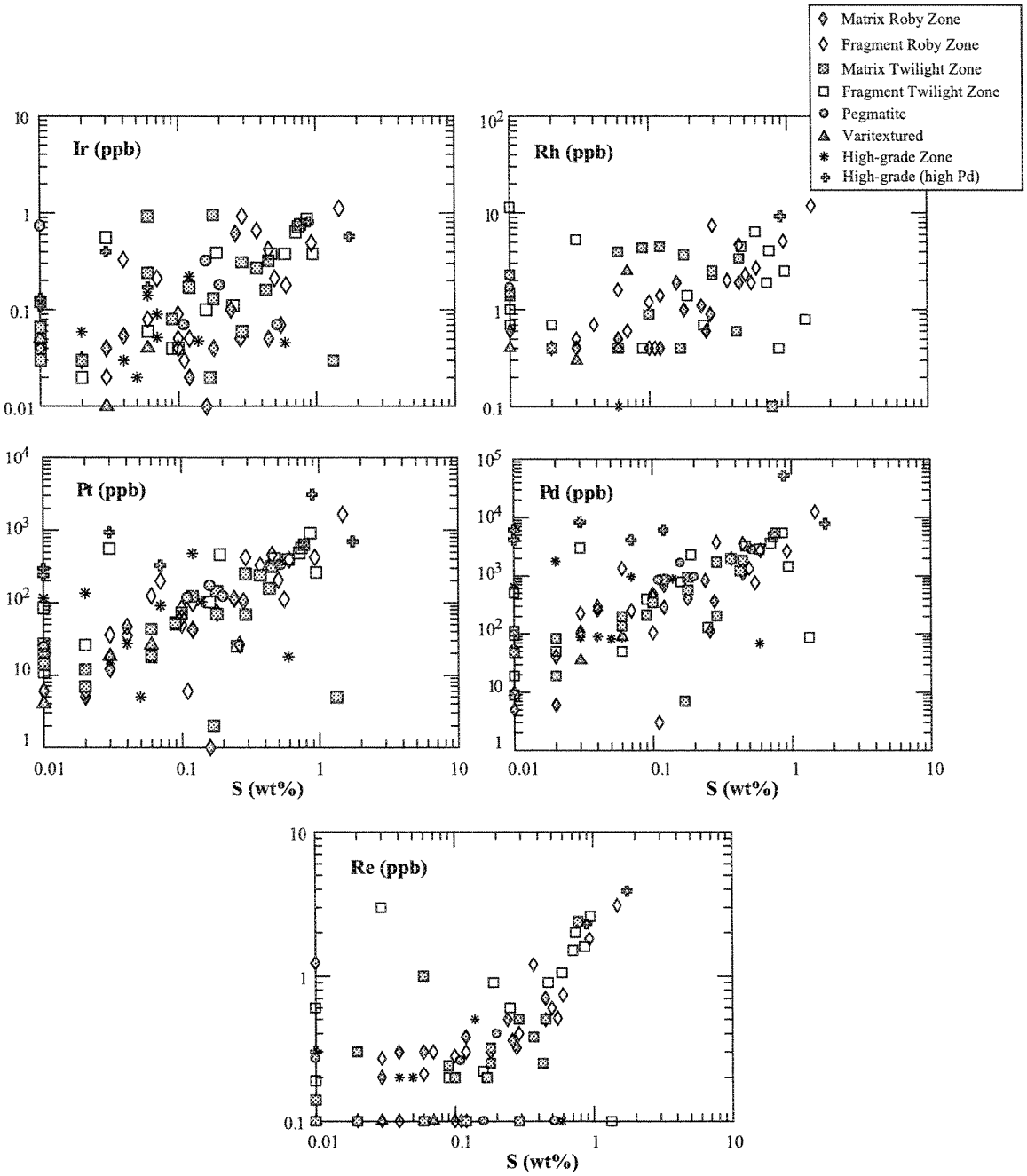

Figure 5.6(b). Plots of the chalcophile elements versus S (wt%) of the High-grade, Roby and Twilight Zones. Note Pt, Pd and Re correlate with S indicating sulphides control the element concentration. Some samples from the High-grade Zone show poor correlation for all elements.

Talkington and Watkinson (1984b), Macdonald (1988), Watkinson et al. (2002), and Michaud and Lavigne (2003) also drew a connection between the alteration of the LDIC and the mineralisation. In order to test the affects of alteration on the relationship between chalcophile elements and S, the gabbro and metagabbronorite samples from the Roby and Twilight are compared on Fig. 5.7. The gabbro and metagabbronorite samples plot along the same trend for Ni, Cu, Ir, Pt, Pd, Au, Rh, and Re. The metagabbronorite samples from the Roby and the Twilight Zones show the same variations as the gabbro samples (Fig. 5.7). This indicates that the chalcophile elements are not significantly redistributed during alteration of gabbronorite to metagabbronorite.

A plot of Cu/Pd versus Pd (Fig. 5.5) may be used to model how much sulphide the rocks contained and the R-factor (the mass ratio of silicate to sulphide liquid, Campbell and Naldrett 1979) that would be required to form these rocks (Barnes et al. 1993). The initial magma was assumed to be a moderate degree partial melt of the mantle which might be expected to contain approximately 10 – 15 ppb Pd and 100 ppm Cu (Barnes and Lightfoot 2005). The Roby and Twilight Zone samples fall along a mixing line between silicate and sulphide liquid formed at an R-factor of 100 000, with most samples containing <1 wt% sulphide component consistent with the petrographic observations. Many of the High-grade Zone samples do not, however, fall along the model lines.

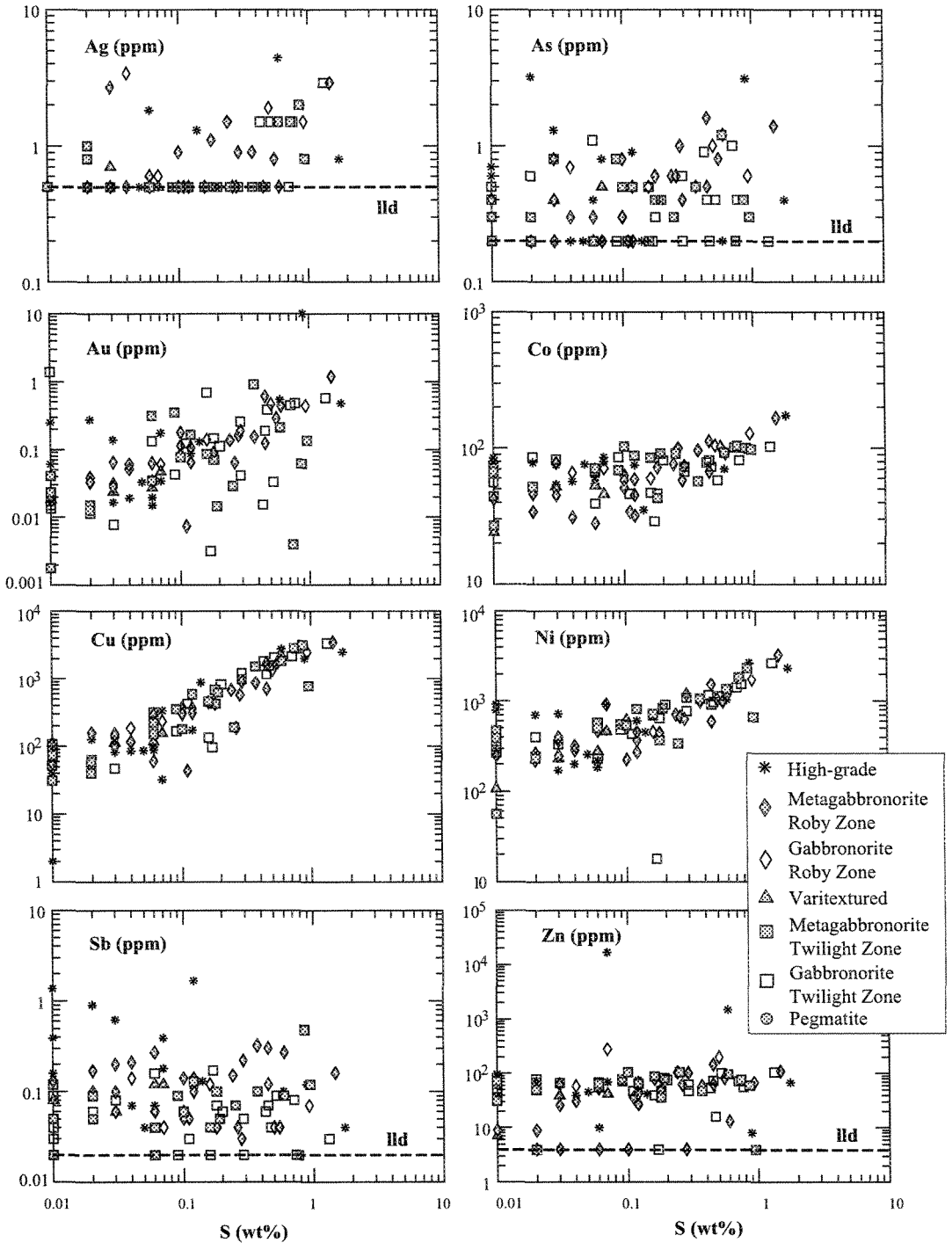

Figure 5.7(a). The metals Ag, As, Au, Co, Cu, Ni, Sb, and Zn plotted versus S (wt%) for the gabbronorite and metagabbronorite of the Roby and Twilight Zone breccia. The High-grade Zone schist is also represented. lld = lower limit of detection.

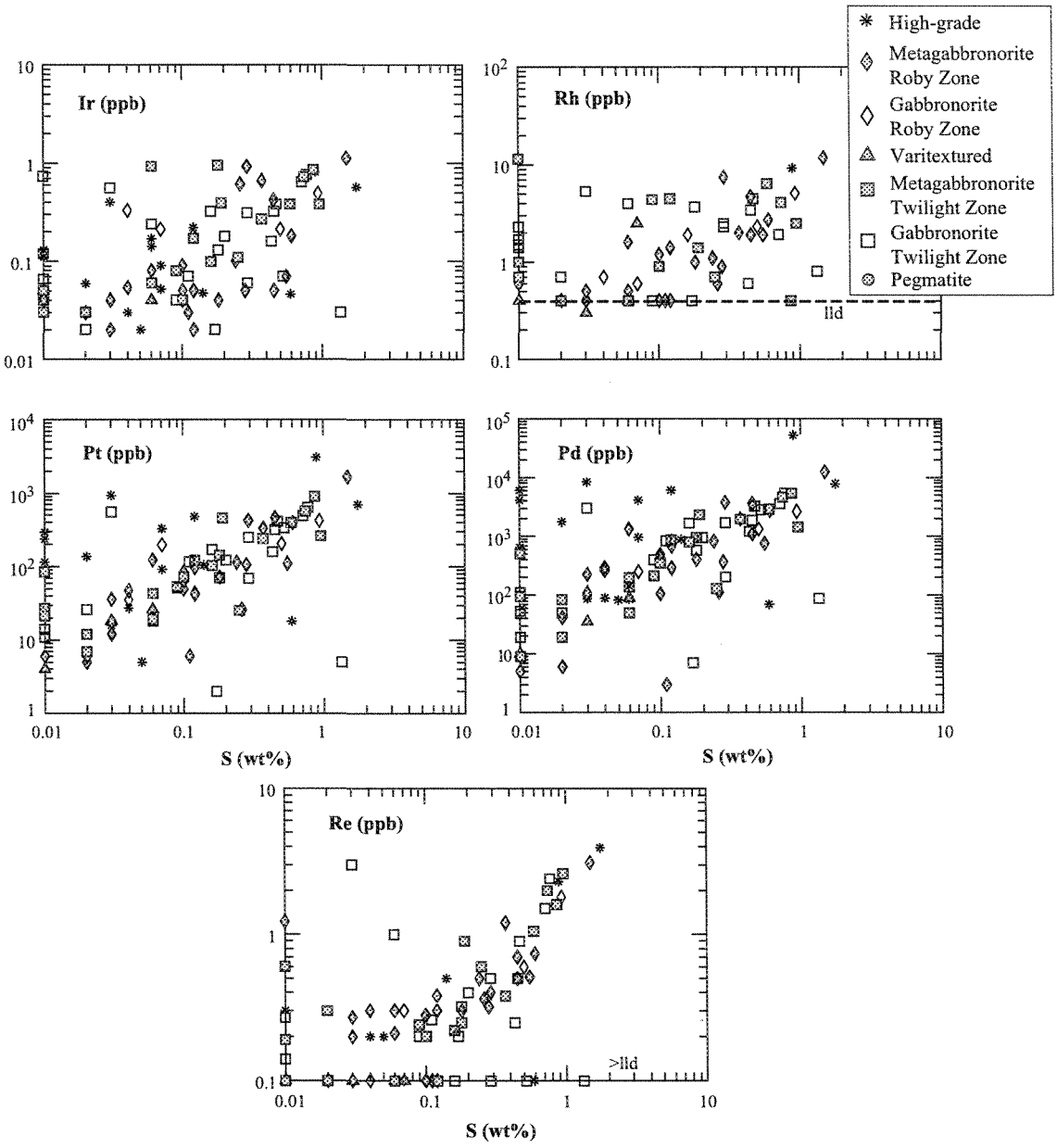

Figure 5.7(b). Plots of platinum-group elements versus S (wt%) showing the gabbronorite and metagabbronorite of the Roby and Twilight Zone breccia. The High-grade Zone schist is also represented.

Detailed mapping of part of the Roby Zone by Hinchey et al. (2005) revealed that the bulk of the PGE mineralisation occurs in late melanocratic rocks and that hydrothermal activity could not explain the preferential enrichment of Pd in the mafic rocks. Hinchey and Hattori (2005) noted that the sulphur contents have a positive correlation with PGE contents, Se and Te. This indicates a magmatic origin for the sulphides of the LDIC. Their determinations of $\delta^{34}S$ contents suggest that the S was derived from the mantle. An unfractionated crustal source cannot be excluded, but is not required for such low abundances. The High-grade Zone shows low correlation between S and Se and, furthermore, the pyrite grains from the three zones have lower $\delta^{34}S$ values than chalcopyrite which indicates hydrothermal activity and recrystallization of the sulphide minerals over a wide temperature range. This hydrothermal activity is interpreted to have been responsible for the enrichment of Pd by 40 ppm in the High-grade Zone (Hinchey and Hattori 2005). The parental magma was volatile-rich, as evidenced by the breccia and pegmatite structures. These volatiles, along with aqueous fluids, were interpreted to have been released during solidification of the LDIC intrusion. The fluids are interpreted to have collected near the impermeable East Gabbro and deposited minerals from solution in the fluids, as mentioned earlier. Hinchey and Hattori (2005) concluded that hydrothermal fluids do not significantly contribute to the Pd mineralisation in the southern Roby and Twilight Zones, but that Pd was enriched by the assimilation of sulphide melt contained in earlier magmas.

The composition of the whole rock sulphide fraction was calculated for samples containing >0.1 wt % S and it is similar on average for both the Roby and Twilight Zones

(Table 5.8). The sulphides contain approximately 6 – 9 wt% Ni and 7 – 10 wt% Cu, which implies that approximately 20 – 30 % of the sulphides are chalcopyrite and pentlandite, which is consistent with the petrographic observations. The Ni and Cu contents of the sulphide fraction are not particularly unusual for sulphides formed from a mafic magma (Naldrett 2004). The IPGE are in the range of 20 to 100 ppb, which is also not unusual. The PPGE concentrations are in the 17 – 180 ppm range which is higher than most magmatic sulphides (Naldrett 2004), with the exception of reef-type ores in large layered intrusions. It is the extreme fractionation of IPGE from Pt, Pd and Au and Pt from Pd that is unusual. No primary magmas have such extremely high Pd/Ir and Pd/Pt ratios (Maier et al. 2004) and, as experimental work to date indicates that the partition coefficients of the individual PGE into sulphide liquid are approximately the same (Fleet et al. 1999), these high ratios represent a challenge to the sulphide-collection model.

It has been suggested that Pd, Pt and Au were introduced by a low temperature fluid (Watkinson and Dunning 1979). Plots of Au versus loss on ignition (LOI) and Pd/Pt versus LOI are used to investigate this possibility. No correlation is evident between LOI and PGE contents, i.e., LOI-rich and LOI-poor samples from the Roby and Twilight Zones have similar Au and Pd/Pt ratios (Fig 5.8). Naldrett (2004) and Hinchey et al. (2005) have also made this observation. This plot is not particularly useful due to the composition of the rocks. The rocks range from leucogabbro (enriched in plagioclase) to melanogabbronorite (enriched in orthopyroxene, olivine and clinopyroxene) and during alteration the pyroxene and olivine will alter to hydrated minerals such as amphibole and chlorite whereas the

plagioclase is more resistant to alteration. The degree of hydration of plagioclase is minor and therefore the total H_2O added is lower in plagioclase rich rocks. Therefore the melanocratic samples will naturally have higher LOI than the leucocratic samples. The lack of correlation between Pd/Pt and Au versus LOI cannot be regarded as a definitive test that there was no deposition of Pd, Pt and Au by a low temperature fluid.

Another test whether alteration mobilized Pd would be to ratio a mobile element likes Cs, Rb or K with an immobile element of broadly similar magmatic compaitibilities like Th, Ta or La. With decreasing concentration of the mobile element during alteration there is an increase in the ratio value. Figure 5.8 shows Pd versus Cs/Th, it is expected that the samples that have the highest Cs/Th values should also have the highest Pd concentration if alteration mobilized Pd. However, the graph shows that the samples show no correlation between Cs/Th and Pd. The samples with the highest Cs/Th values are not the ones with the highest Pd concentrations. The High-Pd grade samples have the highest concentration but they do not have the highest Cs/Th as expected. Thus the low temperature alteration observed in the High-grade samples (schist) does not play a major role in the concentration of Pd.

Table 5.8. Calculated composition of the sulphide fraction in each zone and for different textures

Zone	High-grade	Roby	Twilight	Roby	Roby	Twilight	Twilight	Twilight
Texture				Fragment	Matrix	Fragment	Matrix	Pegmatite
n	5	22	25	7	15	11	10	4
Element								
S (wt %)	36.1	36.6	36.1	36.8	36.5	36.1	36.4	35.5
Fe	42.2	45.2	42.6	46.4	44.7	42.3	44.0	39.9
Cu	10.7	7.43	10.0	7.07	7.60	11.0	8.92	10.2
Ni	7.61	6.12	8.94	5.16	6.57	7.06	9.28	13.2
Co	0.32	0.35	0.37	0.45	0.31	0.29	0.57	0.1
Re (ppb)	60	50	61	57	47	48	86	38
Ir	25	28	35	18	32	40	30	33
Rh	75	185	41	167	194	13	87	<72
Pt	61709	17416	25540	8977	21355	20375	29439	29998
Pd	865304	126349	177367	64330	155291	142104	186627	251193
Au	101627	24747	19612	18617	27607	19325	20837	17338

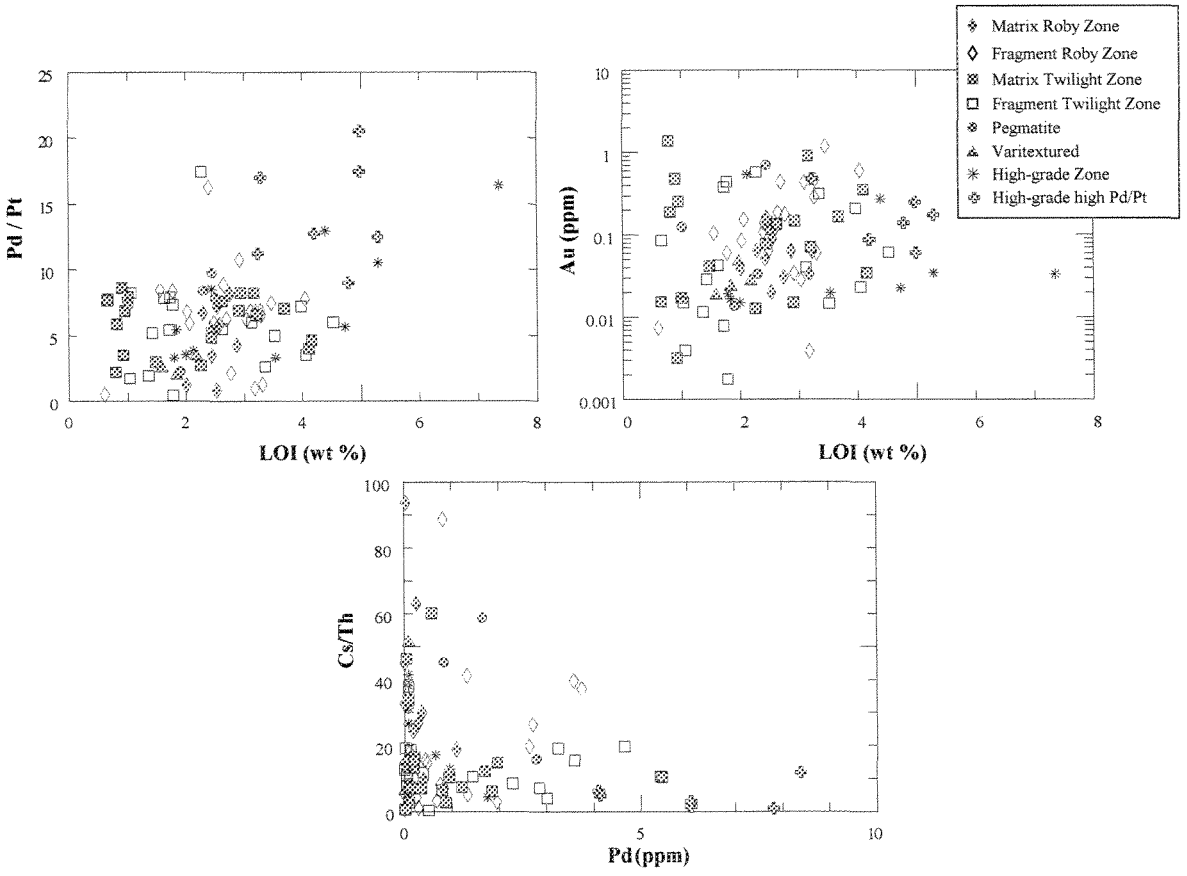

Figure 5.8. Variation diagrams for Pd/Pt ratio, Au versus loss on ignition (LOI) and Cs/Th versus Pd for the Roby and Twilight Zone fragments, matrix, pegmatite and varitextured components along with the High-grade Zone.

5.3.2. High Grade Zone

On the Ni, Cu, Co, Ir, Rh, Re versus S plots the samples from the High-grade Zone fall along the same trend as samples from the Roby and Twilight Zones (Fig. 5.6). Furthermore, the average concentration of these elements calculated to be in the sulphide fraction is similar to that calculated for the Roby and Twilight Zones (Table 5.8). This suggests that these elements were controlled by sulphides in all the zones. In contrast, Pd, Au and Pt values in about half of the samples do not correlate with S in the High-grade Zone (Fig. 5.6). Inspection of data from Hinchey and Hattori (2005) indicates that in about 75 % of their high-grade samples Pd also does not correlate with S. The sample set in this study shows that the samples that display no correlation between Pd and S have the highest Pd/Pt ratio. Furthermore, the calculated concentrations of Pd, Pt, and Au in the samples of this study are 5 to 10 times higher in the average sulphide fraction from the High-grade Zone than in the sulphide fraction from either the Roby or the Twilight Zones (Table 5.8).

Inspection of the distribution of samples from the High-grade Zone on the metal versus S plots shows that approximately half of the samples fall on the trend defined by the Twilight and Roby Zones (Fig. 5.6). These samples are interpreted to contain sulphides with compositions similar to those in the Twilight and Roby Zones. The other half of the samples have very low S contents, and yet they still have high Au, Pd, and Pt contents. All of these are High-grade Zone actinolite-chlorite-talc schists. The LDI area underwent greenschist metamorphism (Brügmann et al. 1997; Stone et al. 2003) and these assemblages

could reflect the regional metamorphism. It could be suggested that samples with low S and high Pd, Pt and Au content have undergone S-loss during metamorphism, and that the high Pd, Pt and Au contents simply reflect the presence of sulphides that were resorbed during metamorphism (Li et al. 2004). This would require that the low-S samples lost one order of magnitude of S (Fig. 5.6). In view of the well-defined correlation between Cu and S (Fig. 5.6, and 5.7) this would require that a similar amount of Cu was lost. Cu loss is supported by the fact that on the Cu/Pd versus Pd plot these samples plot well below the magma-sulfide mixing line (Fig. 5.5).

For samples with low S it is possible to conceive that sulphur and Cu were lost from the system leaving behind the Pd in the form of PGM. To test this possibility, Pd-rich, S-poor samples were subjected to image analysis to quantify the loss in sulphur. To place the S-poor, Pd-rich samples on the trend line followed by the rest of the samples (Fig. 5.6), the concentration of S would have to increase by approximately one order of magnitude (Fig. 5.6), i.e. the samples would have lost about 90 % of their sulphides. Gray-scale images of sulphide grains show a dark halo of alteration material around the sulphide grains (Fig. 5.9). This contrast in colour was used to calculate the average ratio between unaltered sulphide to alteration material using the programme 3-D Doctor (Able Software Corp) and the percentage of sulphides lost was estimated from this. The samples analysed show between 33 and 64 % loss of sulphide minerals (Table 5.9), which is somewhat less than required by the sulphide loss model. Thus, there is evidence of sulphur loss, but there is not enough S

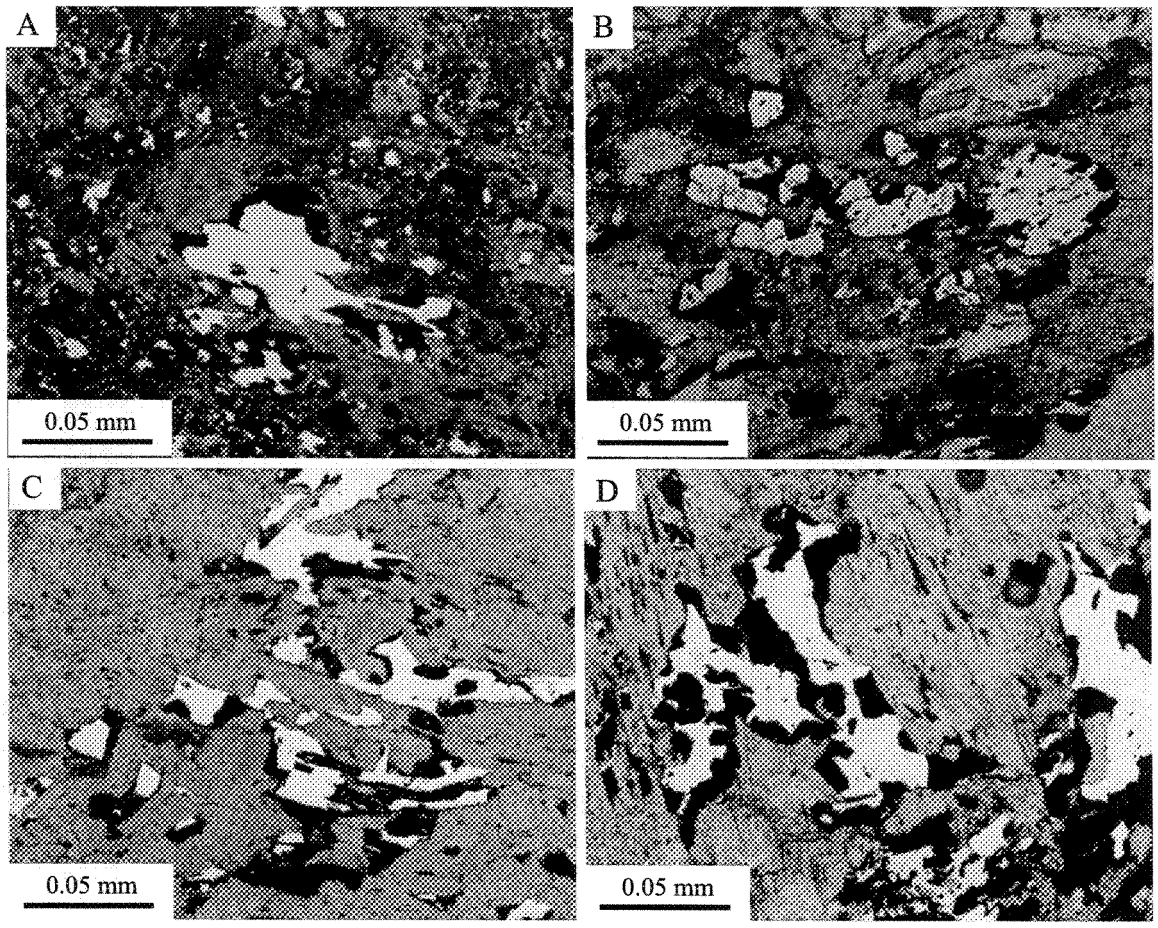

Figure 5.9. Sample showing sulphide alteration halo (a) Rz-1, (b) Rz-3, (c) Rz-6 and (d) Rz-7. These sections have alteration material content of between 20 and 40%.

loss from the samples to account for 5 to 10 fold enrichment of Pd and Au found in the samples. Thus, loss of Cu and S will not account for the low S and Cu in Pd-rich samples. Hinchey and Hattori (2005) reached a similar conclusion based on the strong correlation between Cu and Se (an element considered to be less mobile than S) in their samples. It is possible that there was a reaction between the silicates and the Fe-rich sulfides which liberated the S from the system in a reaction:

$$FeS + \text{low-Fe silicates} = \text{Fe-rich silicates} + S\uparrow$$

Table 5.9. Calculated sulphide loss determined using 3-D Doctor Software.

Sample Name	Number of grains	Average % loss
Rz1	3	64
Rz3	2	37
Rz-5	7	51
Rz-6	6	34
RZ-7	6	58
RZ-16	3	66
RZ-12	5	43
Rz-17	6	33

The weight of evidence suggests that some process other than accumulation of sulphide liquid added Au, Pd, and Pt to the High-grade Zone. In order to consider this process, data from the High-grade Zone was inspected for correlations between Au, Pd, Pt and major and trace elements. Three elements were found to correlate: MgO, Sb, and As (Fig. 5.10). There is no correlation between Pd and these elements when samples from all the other zones are considered (not shown), thus the process appears to be unique to the

High-grade Zone. The samples in which there is no correlation between S and Pd, Pt and Au tend to be richest in Sb-, As- and MgO (Fig. 5. 10). These samples are those that have the highest Pd/Pt ratio and lowest S concentration. There is a lack of correlation with S in some samples which may reflect a limited availability of Fe, S loss, and/or fixation of Pd by other magmatic components. In this case Cl may have been the ligand.

In the case of alteration, orthopyroxene is more susceptible to hydration/alteration than plagioclase. Therefore, the lack of correlation between LOI, Pd/Pt, and Au does not demonstrate that hydrothermal transportation of metals is not a viable mechanism and most of the data is consistent with the magmatic origin of the mineralisation. The involvement of transportation ligands (S. Wood, personal communication, 2006) such as chlorides or bisulphides within the transporting fluid is supported by the correlation between Pd, Sb, and Cu. These ligands may exist in significant concentrations during the oxidation of sulphide bodies that they can transport significant amounts of Pd, Pt, and Au (Wood 2002). The amphibole chemistry, those that were determined to be formed from alteration, show that the hydrothermal fluid was in equilibrium with the magmatic system, indicative of a deuteric fluid. Therefore the process of transportation is less important than the process of deposition. The accumulation of Pd at the High-grade Zone is due to the presence of a fixant that would draw out the Pd from the circulating fluid. This fixant would be present throughout the complex Roby and Twilight Zones, but in lower concentrations which would explain the correlation between S and Pd in these samples.

Thin sections of samples from the High-grade Zone (Rz-3, -6 and -17) were imaged in backscattered electron mode on an EPMA to search for the occurrence of PGM. Rz-3 and Rz-17 have very low S concentration and they show a correlation between Pd and Sb, As, and MgO. Rz-6 has S concentrations comparable to the Roby and Twilight Zones and contains abundant pyrite. Most of the PGM observed in Rz-6 were associated with the sulphides, either wedged between pentlandite and chalcopyrite (Fig. 5.11a) or included in pyrite (Fig. 5.11b). In these cases palladium occurs as Vysotskite (PdS), other PGM were only rarely observed.

In samples Rz-3 and -17 there are few occurrences of PGEs associated with pyrite (Fig. 5.12(a)) or included in other sulphide minerals (Fig. 5.13(a)), similar to the occurrences observed in Rz-6. Palladium is geochemically associated with As (Fig. 5.11(b)), Te (Fig 5.12(b) and (c)), Sb (Fig. 5.11(a)), Bi (Fig. 3.), and as S (Fig. 5.11(c) and Fig. 5.12(d)). PGMs containing Pd or Pt associated with Te are common throughout the sections (Fig. 3.14) in most cases the various minerals are linked to each other to form mineral aggregates. These aggregates typically comprise a large grain of one phase (for example PdSbAs) with other PGMs located along its edges or as inclusions (Fig. 3.14 (a) – (c)). As reported by Hinchey and Hattori (2005) and Watkinson et al. (2002) these grains are most commonly located in the hydrated material assemblage, (in this case actinolite, chlorite, and talc), are sometimes associated with minor chalcopyrite and pyrite, but most commonly occur without associated sulphides. There is minimal pyrite present, which is abundant in the metagabbronorite of the Twilight and Roby Zones. Most of the pyrite

grains are 5 to 10 μm in size, but some grain aggregates are as large as 300 μm (Fig. 3.14 (a)). This occurrence of PGM is unusual; most PGMs occur as small inclusions within sulphides, mainly pyrite, as a result of the mobilisation of S and Cu during alteration. The analysed High-grade Zone samples do not show this simple relationship, and that indicates that the mineralisation was due to more than the loss of S and Cu from the system.

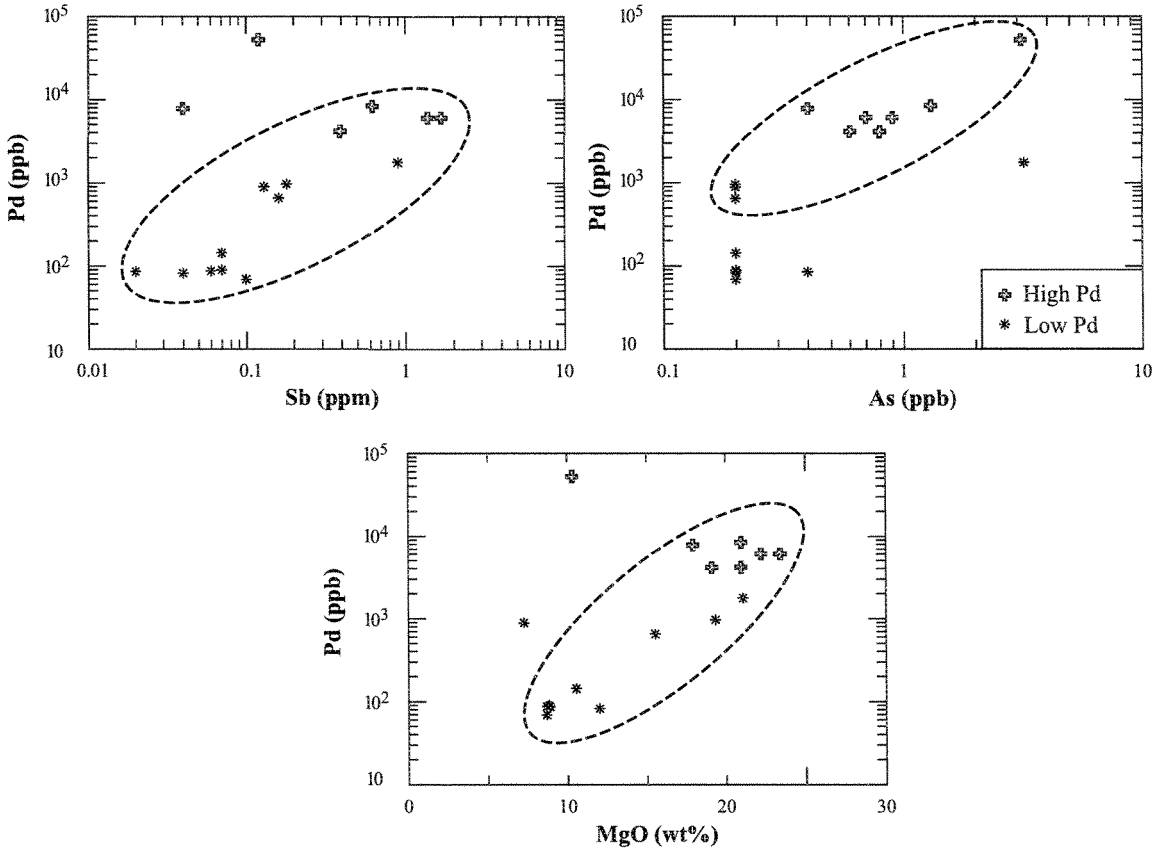

Figure 5.10. Variation diagrams for Pd versus Sb, As, and MgO for the High-grade Zone samples.

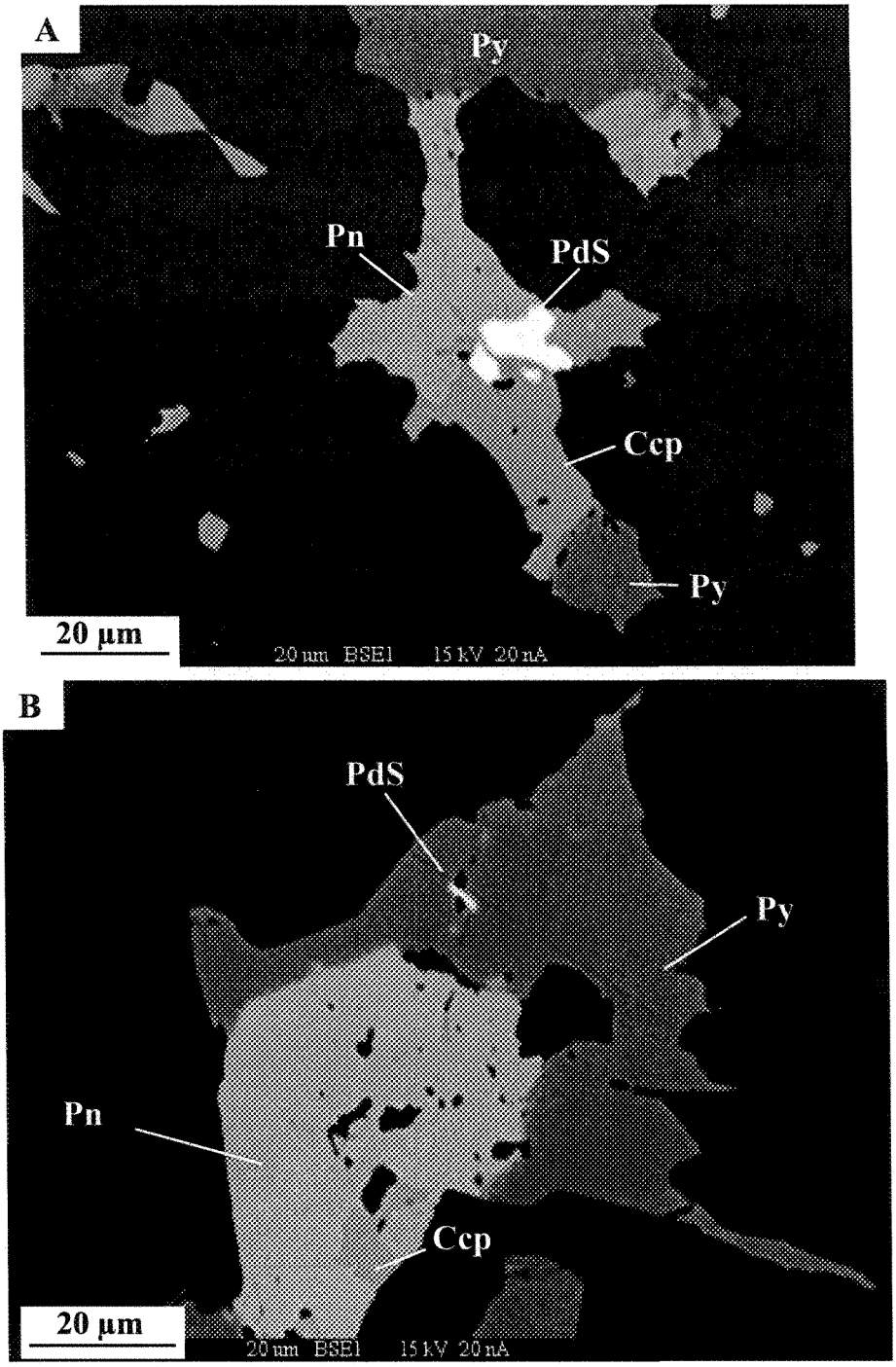

Figure 5.11. Backscattered electron images of sulphide minerals and PGM in a High-grade Zone microbreccia (Rz-6) with Pd and S values comparable to the Roby and Twilight Zones.

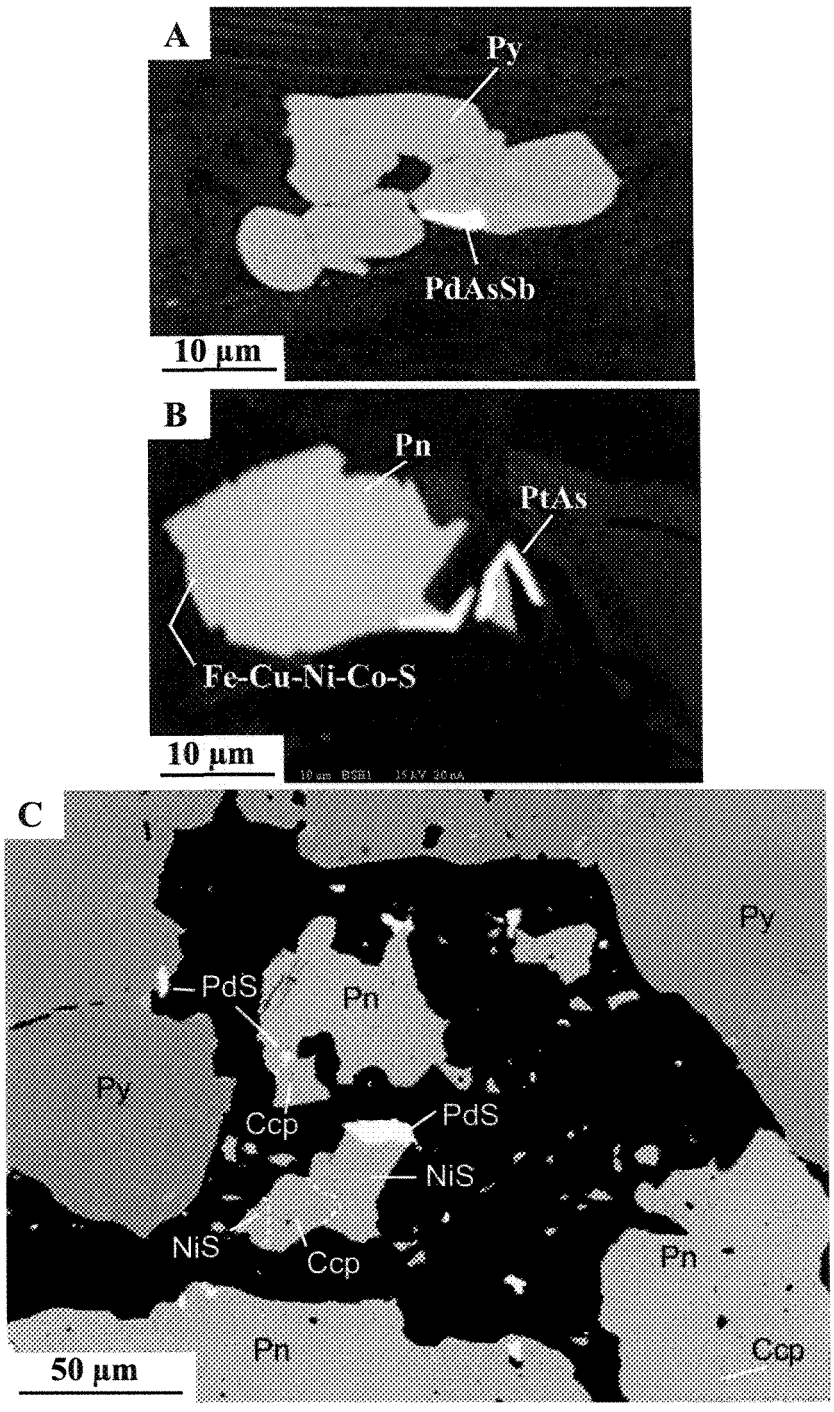

Figure 5.12. Backscattered electron imagesof the High-grade Zone showing PGM minerals in sample Rz-3. This sample has high Pd/Pt ratio and low S concentration.

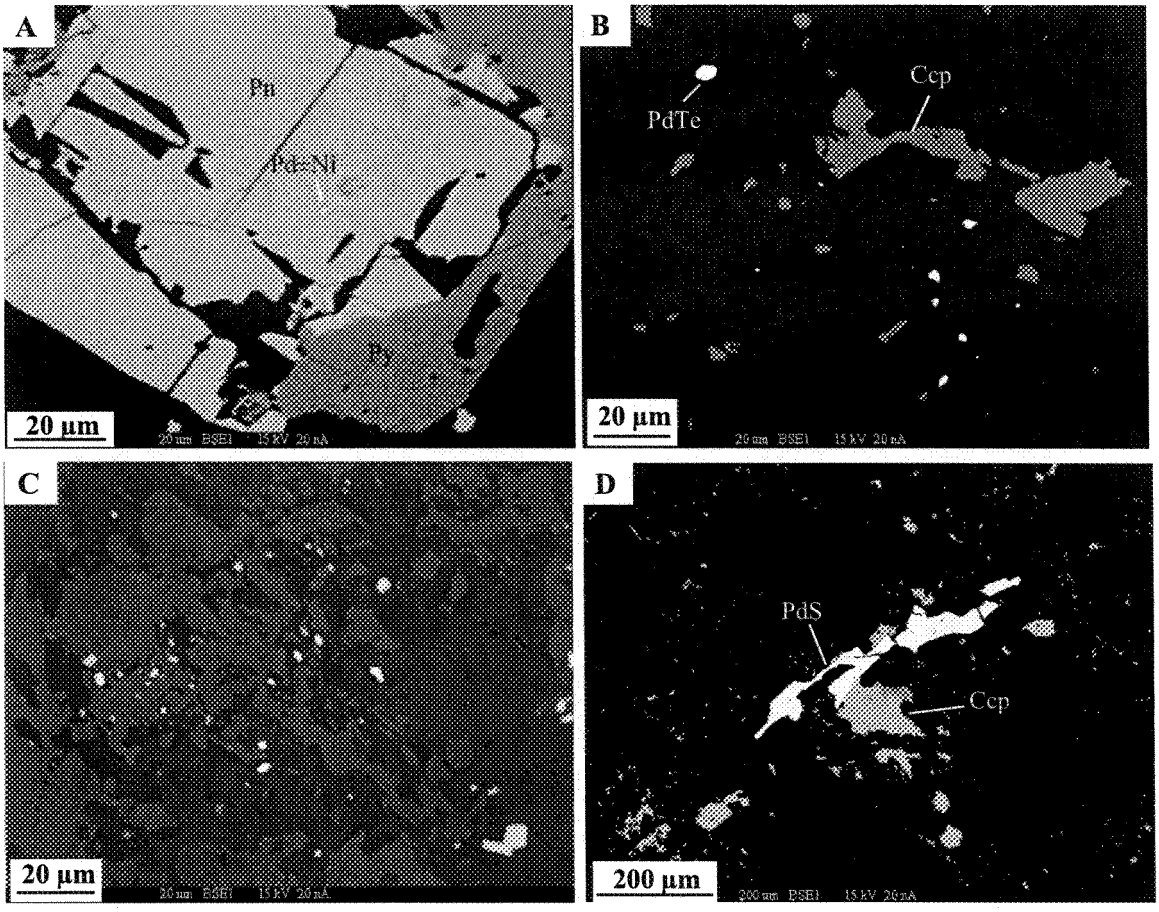

Figure 5.13. Backscattered electron image of PGM minerals in the High-grade Zone (Rz-17). This sample is a high Pd/Pt low S sample. (a) Rare occurrence of PGM mineralisation within pentlandite (Pn) grains. (b) shows PdTe grains associated with silicate and chalcopyrite (Ccp). (c) shows PdTe grains scattered throughout silicate alteration assemblage. (d) Vysotskite (PdS) mineralisation associated with chalcopyrite.

5.4. Summary

Control of the distribution of metals by a sulphide liquid explains much of the variation in metal content observed in all of the samples from the Roby, and Twilight Zones, and about half of the samples from the High-grade Zone. The partition coefficients for the PGEs into sulphide liquid are thought to be similar for all of the PGE, thus their collection by a sulphide liquid will not explain the extreme fractionation of IPGE from PPGE or Pt from Pd. All of the rocks in this study show very strong fractionation of Pd from Pt and Ir and, as yet, no rocks that are enriched in Pt and depleted in Pd have been found anywhere in the intrusion. The distribution of chalcophile elements underscores that there is no difference between the Roby and the Twilight Zones. The varitextured and pegmatite fragments are not enriched in chalcophile elements, as would be expected in a model where a fluid favoured the development of pegmatitic textures and deposited Pd. Therefore, with respect to the first objective, the PGE and chalcophile element contents of the Twilight and Roby Zones are essentially the same. There is considerable overlap between the compositions of the fragments and matrix samples, and this can be attributed to numerous injections of magma into both the zones. Therefore, some fragments probably represent matrix component of the breccia from an early magma injection.

In approximately half of the samples from the High-grade Zone Au, Pd, and Pt do not appear to have been controlled by a sulphide liquid and are enriched by factors of 5 to 10 over the samples from the Twilight and Roby Zones. These samples also show no

correlation between their Pd, Pd/Pt, and S concentrations, and have very low S concentrations. The mass balance calculations together with the results from the image analysis indicate that S removal alone cannot account the low S contents. Thus, sulphide collection alone cannot explain the observed PGE distributions in the High-grade Zone and a secondary process must be responsible for the enrichment of Pd within the LDIC. The correlation of Pd with As, Sb, and Pd in the High-grade Zone indicates that this process also enriched these elements. A hydrothermal process involving a fluid enriched in Au, Pd, and Pt coming into contact with Fe-rich As, Sb, Te bearing-rock can be used to explain this trend. These elements subsequently formed 'insoluble' compounds that are observed in most of the High-grade Zone samples. Hinchey and Hattori (2005) also identified a correlation between Se, Te, and S and they suggest that hydrothermal activity resulted in the enrichment of Pd by up to 40 ppm.

The unusual presence of PGMs isolated from sulphides or pyrite mineralisation and located within the secondary hydrous minerals in the High-grade Zone supports the hypothesis of fluids removing some S. The extent of pyrite mineralisation correlates with the degree of alteration, which confirms the mobility of S. Therefore the alteration was accompanied by the addition of water (to hydrate the igneous silicate phases) into the system and previous authors have linked this step to the mobilization and concentration of Pd. A deuteric origin for the fluid that remobilized the magmatic sulphides and the deposition of metals in the gabbroic unit has been proposed by Michaud and Lavigne (2001) and Watkinson and Lavigne (2002). Watkinson and Dunning (1979) suggested that the

silicate alteration, in their case amphibolitisation of pyroxenite, led to the mobilization and concentration of Pd at Lac Des Îles. This alteration is accompanied by the addition of H_2O to the system and has been linked to the mobilization and concentration of Pd.

The presence of a fluid that was in equilibrium with the system was suggested in the previous chapter from the observations of the major and trace element composition of the rocks. It is suggested that this fluid would be a deuteric fluid that evolved as the magma crystallised (Michaud 1998; Michaud and Lavigne 2003). The amphibole chemistry indicates that the hydrothermal fluid was most probably a deuteric fluid. Therefore the process of transportation is less important that the process of deposition. Regional metamorphism overprints the deuteric fluid alteration and constitutes the second alteration (hydration) event at LDIC. The most significant enrichment observed is in Pd, and associated elements, As, Sb, and Te. A deuteric fluid in equilibrium with the system would promote recrystallisation, creating the pegmatite patches, but there would be no significant change in the trace element composition of the recrystallised rock. A PGE-enriched deuteric fluid in a closed system would explain these observations, and is in accordance with the conclusions of Brügmann et al. (1997) and Sutcliffe et al.(1989). However, instead of the fluid creating a melanocratic residue, the rock is simply partially hydrated and recrystallized.

6.
DISCUSSION AND CONCLUSIONS

The objectives of this study were three fold. Firstly, the study aimed to establish whether there are petrographic and/or compositional differences between the High-grade, Roby, and Twilight Zones of the Lac des Îles Complex. The second objective was to investigate whether there are petrographic and compositional differences between the fragments and their matrix. Finally, the Complex has been affected by late magmatic alteration and subsequent regional metamorphism, thus the third objective was to determine whether there is a relationship between alteration and the mineralisation. The objectives became the base for developing a model for the emplacement of the LDIC.

6.1. Formation of the Mine Block Intrusion

Any model for the formation of the Pd-Pt enrichment in the MBI must consider the following observations. The deposits are located in zones of magmatic breccia that underwent deformation at high temperature. There were repeated injections of magma into these zones. Each injection caused fragmentation of the rocks already there. The rocks are essentially orthopyroxene-plagioclase cumulates with a very low component of trapped liquid component. The matrix material does not represent a silicate liquid composition, but is a finer-grained equivalent of the fragments. The similarity in composition between the fragments and the matrix also implies that they are co-magmatic. The presence of mafic

pegmatites and varitextured rocks suggests the presence of a late magmatic high-temperature aqueous fluid, however there is no difference between the whole-rock geochemistry of the pegmatites and the matrix or the fragment samples. Therefore, the coarse-grained textures are interpreted to be recrystallised of the whole rock assemblages. Although the presence of pegmatites and varitextured rocks suggests the presence of a high-temperature fluid, the pegmatitic rocks are neither enriched nor depleted in PGE, thus this fluid did not play a role in the mineralisation of the pegmatites. Much of the variation in metal content observed in the Roby, Twilight, and about half the High-grade Zone samples is controlled by sulphides. However, the extreme fractionation of IPGE from PPGE or Pt from Pd cannot be accounted for by collection of PGE by sulphide liquid. No rocks enriched in Pt and depleted in Pd have been found, and this indicates that the process of PGE fractionation took place elsewhere (presumably below the LDIC). Furthermore, for approximately half of the samples from the High-grade Zone, the Au, Pd, and Pt contents do not appear to have been controlled by a sulphide liquid, and are enriched in Pd by factors of 5 to 10 over the samples from the Twilight and Roby Zones. The High-grade Zone samples are hydrated to a greenschist facies mineral assemblage, and appear to be located close to, or within, a shear zone.

Considering all of these factors we suggest a model with a minimum of two magma chambers, as shown in Figure 6.1(a). The upper chamber consisted of partially consolidated leucogabbronorite emplaced on either side of the East Gabbro, the proto MBI. This leucogabbronorite originated from a second, deeper, feeder chamber. In the first step (Fig.

6.1(b)) a new magma was introduced from the feeder chamber into the semi-consolidated leucogabbronorite of the upper chamber. The intrusion was undergoing shearing as the magma was emplaced and the combined effect of the injection of the new magma and the shearing resulted in the formation of breccia. The semi-consolidated leucogabbronorite formed the fragments and the intruding gabbronorite which crystallised orthopyroxene and plagioclase formed the matrix. As the system crystallised the fractionated liquid was effectively squeezed out by deformation. The loss of the liquid resulted in the formation of the adcumulate composition and textures in both the fragments and matrix. Some magma remained in the deeper feeder chamber and segregated disseminated base metal sulphides with a normal Pd/Pt and Pd/Ir ratio.

In the second step (Fig. 6.1(c)) the magma in the lower chamber became fluid saturated as crystallisation progressed and this fluid dissolved the segregated disseminated sulphides. By analogy with experimental work of Peregoedova et al. (2004) it is suggested that when S was removed from the disseminated sulphides a Cu-Pd rich fluid, mss and Pt-Fe alloy all formed (Fig. 6.1(c)). The fluid rose into the MBI and was focused around the East Gabbro where it interacted with the rocks there and resulted in the formation of the Roby and Twilight Zones. Mss and Pt-Fe remained in the feeder chamber.

At high temperature the aqueous fluid did not cause any alteration of the silicate rocks but it did induce a change in crystallisation to form pegmatioids and varitextured rocks. Sulphur and the elements Pd, Fe and Cu, were precipitated amongst the cumulate

silicate grains, mainly as sulphides, but some fluid penetrated into the fragments and sulphides were also precipitated within the fragments.

The formation of the High-grade Zone occurred as the temperature decreased and the fluid could no longer penetrate pervasively but became channelled into the shear zone next to the East Gabbro (Fig 6.1(d)). Palladium, Pt and Au continued to be precipitated from the fluid, but they were accompanied by Sb and As, rather than S and so creating the low-S, Pd-rich High-grade Zone. The focusing of the lower temperature aqueous fluid and the continuing shearing and fracturing accentuated the level of alteration in this zone by providing a large surface area for the fluid to interact with. The correlation between Pd and Sb, the low Cu content and the enrichment in Au observed in the High-grade Zone rocks, all suggest that a process of deposition occurred involving Sb, Te and As. The presence of these elements resulted in the precipitation of Pd as tellurides, selenides and arsenides that are not spatially associated with the sulphide mineralisation.

In an alternative hybrid model, initially there were two magma chambers. Partially consolidated leucogabbronorite was present in both chambers. In the lower chamber disseminated sulphides with a normal magmatic composition were present (Fig. 6.2(a)). A new S-undersaturated magma was introduced into the lower chamber and this partially dissolved the disseminated sulphide to form IPGE-rich mss, an Fe-Pt alloy and a magma enriched in Cu-Pd. (Fig. 6.2(b)). This magma was then injected into the overlying chamber concurrent with shearing there and formed the breccia zones (Fig. 6.2(c)). A Cu-Pd rich

sulphide liquid segregated from this magma and precipitated among the cumulate grains to form the Roby and Twilight Zones. The same steps as outlined in the fluid model would subsequently be required to form the High-grade Zone (Fig. 6.1(d)).

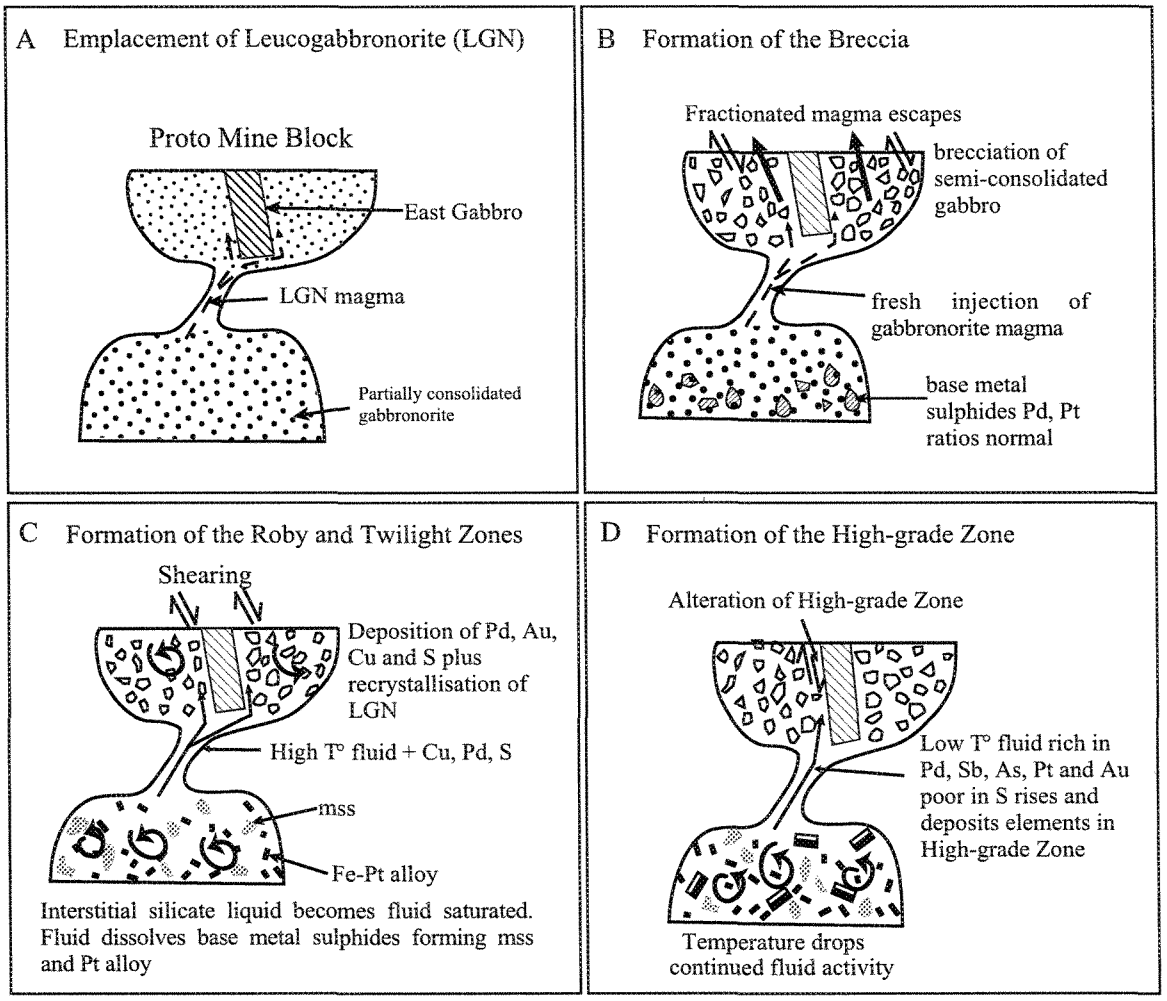

Figure 6.1. A Proposed model for the formation of the LDIC. See text for details.

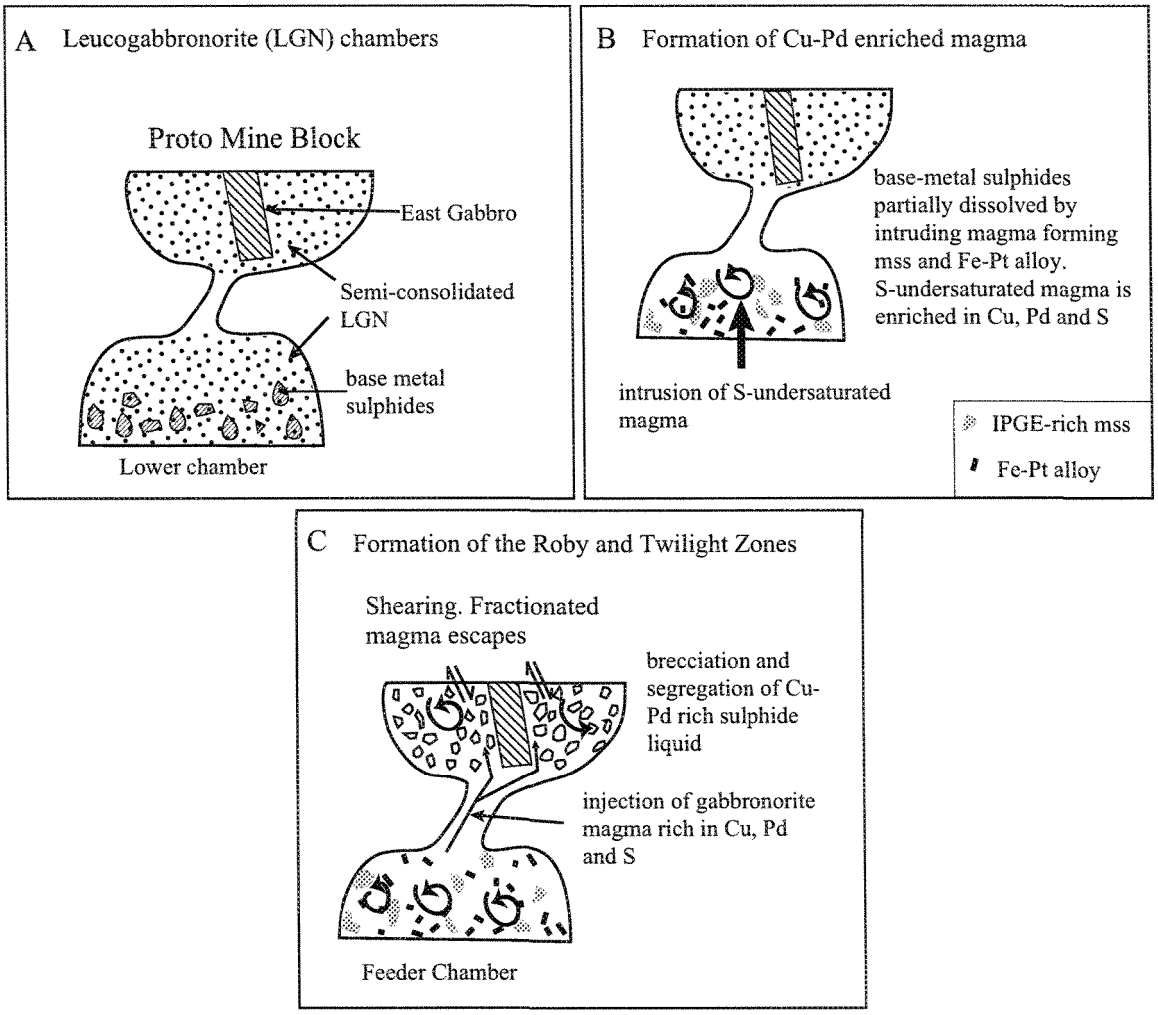

Figure 6.2. An alternative proposed model for the formation of the LDIC. See text for details.

6.2. Conclusions

The following conclusions were reached in accordance with the objectives of this study, to determine whether there is a difference between the zones and between the breccia components (fragments and the matrix) and whether alteration of the Complex correlates with the distribution of the mineralisation.

The rock types that are found as fragments and matrix from both the Roby and Twilight Zones are generally the same: leuco to melagabbronorites. Petrographically and geochemically the fragments and matrix are both plagioclase-orthopyroxene adcumulates. The zones, fragments and the matrix are similar both in terms of their mineral modal proportions and their major and trace element compositions. The breccia cannot, therefore, have formed completely from the forceful injection of magma. A model that is based on the injection or exsolution of a volatile phase derived from a deeper magma chamber brecciating a partially consolidated gabbroic rock in the LDIC is preserved. This fluid promoted the recrystallisation of what would become the matrix, and accelerated crystal growth giving rise to the pegmatitic pods observed in the varitextured units.

In the Twilight and Roby Zones, PGE correlate with S and appear to be controlled by sulphides. The matrix has higher PGE concentrations than the fragments, but the sulphide compositions are the same in both the fragments and the matrix. The matrix samples simply have higher sulphide contents than the fragments. The extremely high Pd/Ir

and Pd/Pt ratios of these rocks cannot be modelled by sulphide segregation from a primary magma. It is suggested that the normal disseminated magmatic sulphides formed in the feeder chamber and that the later magma pulses partially dissolved the disseminated sulphides leaving an IPGE-rich mss and some Pt in the feeder chamber. The later magmatic, or aqueous fluid pulses, transported the base metals S, Au, Pd and a little Pt to the Roby and Twilight Zones, where the elements were deposited along with base metal sulphides.

About half of the High-grade Zone samples can be explained by the model proposed above. However, for the other half Au, Pt, and Pd do not correlate with S. Although the rocks have undergone low temperature alteration, the lack of a correlation with S cannot simply be the result of S loss during alteration, because in these samples Au, Pd, and Pt do not correlate with the other chalcophile elements, such as Cu. Also, the petrographic observations indicate less loss of S than the mass balance calculations require. Further, Pd/Ir and Pd/Pt ratios are higher in the High-grade Zone than in the Roby and Twilight Zones, which indicates that Pd has been preferentially enriched in this zone. There is no correlation between alteration and a high concentration of Pd throughout the complex. There is no alteration halo that is typical of deposits created by the interaction of externally derived fluids, for example Cu-porphyry deposits. Palladium and Pt show a correlation with Sb and As in the High-grade Zone suggesting that these elements acted as a fixing agent for Pd and Pt in the system. This indicates a fluid that was in equilibrium with the system transported the Pd in solution.

7.
REFERENCES

Alapieti TT, Lahtinen JJ (1986) Stratigraphy, petrology, and platinum-group element mineralization of the early Proterozoic Penikat layered intrusion, northern Finland. Economic Geology 81: 1126-1136.

Ashwal LD (1993) Anorthosites. Springer-Verlag, New York, Berlin, Heidelberg.

Barnes S-J (1990) The Use of Metal Ratios in Prospecting for Platinum-Group Element Deposits in Mafic and Ultramafic Intrusions. Journal of Geochemical Exploration 37: 91-99.

Barnes S-J, Couture JF, Sawyer EW, Bouchaib C (1993) Nickel-Copper Occurrences in the Belleterre-Angliers Belt of the Pontiac Subprovince and the Use of Cu-Pd Ratios in Interpreting Platinum-Group Element Distributions. Economic Geology 88: 1402-1418.

Barnes S-J, Lightfoot PC (2005) Formation of Magmatic Nickel-Sulfide Ore Deposits and Processes Affecting Their Copper and Platinum-Group Element Contents In: Hedenquist JW, Thompson JFH, Goldfarb RJ, Richards JP (eds) Economic Geology 100th Aniversary Volume. pp 179-214.

Barnes S-J, Maier WD (1999) The Fractionation of Ni, Cu and Noble Metals in Silicate and Sulphide Liquids. In: Keays RR, Lesher CM, Lightfoot PC, Farrow CEG (eds) Dynamic Processes in Magmatic Ore Deposits and their Application in Mineral Exploration. Geological Association of Canada, Short Course, pp 69-106.

Barnes S-J, Maier WD (2002) Platinum-group elements and microstructures of normal Merensky Reef from Impala Platinum Mines, Bushveld Complex. Journal of Petrology 43: 103-128.

Barnes S-J, Picard C, Giovenazzo D, Tremblay C (1992) The composition of nickel-copper sulphide deposits and their host rocks from the Cape Smith Fold Belt, northern Quebec. Australian Journal of Earth Sciences 39: 335-347.

Barnes SJ, Hoatson DM (1994) The Munni-Munni Complex, Western-Australia - Stratigraphy, Structure and Petrogenesis. Journal of Petrology 35: 715-751.

Barnes SJ, Naldrett AJ (1985) Geochemistry of the J-M (Howland) Reef of the Stillwater Complex, Minneapolis Adit Area .1. Sulfide Chemistry and Sulfide-Olivine Equilibrium. Economic Geology 80: 627-645.

Bedard JH (2001) Parental magmas of the Nain Plutonic Suite anorthosites and mafic cumulates: a trace element modelling approach. Contributions to Mineralogy and Petrology 141: 747-771.

Bédard L, Savard D, Barnes S-J (in press) Total sulphur concentration in geological reference materials by elemental infrared analyzer. Geostandard Newsletter.

Bedard LP, Barnes S-J (2002) A comparison of the capacity of FA-ICP-MS and FA-INAA to determine platinum-group elements and gold in geological samples. Journal of Radioanalytical and Nuclear Chemistry 254: 319-329.

Boudreau A (2006) PELE Duke University, www.nicholas.duke.edu/eos.

Brügmann GE, Arndt NT, Hofmann AW, Tobschall HJ (1987) Noble metal abundances in komatiite suites from Alexo, Ontario and Gorgona Island, Columbia. Geochimica Et Cosmochimica Acta 51: 2159-2169.

Brügmann GE, Naldrett AJ, Macdonald AJ (1989) Magma Mixing and Constitutional Zone-Refining in the Lac-Des-Iles Complex, Ontario - Genesis of Platinum-Group Element Mineralization. Economic Geology 84: 1557-1573.

Brügmann GE, Reischmann T, Naldrett AJ, Sutcliffe RH (1997) Roots of an Archean volcanic arc complex : the Lac des Îles area in Ontario, Canada. Precambrian Research 81: 223-239.

Campbell IH, Naldrett AD (1979) The influence of silicate: sulfide ratios on the geochemistry of magmatic sulfides. Economic Geology 74: 1530-1505.

Davis DW, Stutcliff RH, Trowell NF (1988) Geochronological constraints on the tectonic evolution of a late Archean greenstone belt, Wabigoon subprovince, northwest Ontario. Precambrian Research 39.

Dionne-Foster C (2002) Étude Minéragraphique et Pétrologique de la Zone Twilight, Complexe du Lac des Îles, Ontario. Sciences de la Terre. Projet de fin d'études: pp 86.

Dunning GR (1979) The Geology and Platinum-group mineralization of the Roby Zone, Lac des Îles Complex, Northwestern Ontario. M. Sc.: pp 129.

Eberl DD, Środoń J, Lee M, Nadeau PH, Northrop HR (1987) Sericite from the Silverton caldera, Colorado: Correlation among structure, composition, origin, and particle thickness. American Mineralogist 72: 914-934.

Emslie RF (1975) High pressure pyroxene megacrysts from anorthosite rocks and their bearing on genesis of parent magma. Geological Society of America 7: 752-753.

Ernst WG, Liu J (1998) Experimental phase-equilibrium study of Al- and Ti-contents of calcic amphibole in MORB – a semiquantitative thermobarometer. American Mineralogist 83.

Findlay DC (1969) Origin of the Tulameen ultramafic gabbro complex, southern British Columbia. Canadian Journal of Earth Science 6: 399-425.

Fleet ME, Crocket JH, Liu M, Stone WE (1999) Laboratory partitioning of platinum-group elements (PGE) and gold with application to magmatic sulfide-PGE deposits. Lithos 47: 127-142.

Gingras P (2002) Développement d'un processus analytique de préconcentration pour les éléments du group du platine et l'or. Sciences de la terre. Projet de fin d'études: pp 46.

Halkoaho TAA, Alapieti TT, Lahtinen JJ (1989a) The Ala-Penikka PGE mineralizations in the Penikat layered intrusion, northern Finland. 5th international platinum symposium; Guide to the post-symposium field trip; I, The Tornio-Narankavaara intrusion belt; II, Kuhmo-Koli-Enonkoski sites Opas - Geologian Tutkimuskeskus 29: 93-122.

Halkoaho TAA, Alapieti TT, Lahtinen JJ (1989b) The Sompujarvi PGE mineralization in the Penikat layered intrusion, northern Finland. 5th international platinum symposium; Guide to the post-symposium field trip; I, The Tornio-Narankavaara

intrusion belt; II, Kuhmo-Koli-Enonkoski sites Opas - Geologian Tutkimuskeskus 29: 71-92.

Hinchey J (2003) Preliminary report of field descriptions and contact relationships of lithological units in the South Roby and Twilight zones, Lac des Iles Deposit, northwestern Ontario. Open File Report - Ontario Geological Survey.

Hinchey JG, Hattori KH (2005) Magmatic mineralization and hydrothermal enrichment of the High Grade Zone at the Lac des Iles Palladium mine, northern Ontario, Canada. Mineralium Deposita 40: 13-23.

Hinchey JG, Hattori KH, Lavigne MJ (2005) Geology, petrology, and controls on PGE mineralization of the southern Roby and Twilight zones, Lac des Îles mine, Canada. Economic Geology 100: 43-61.

Hoatson DM, Keays RR (1989) Formation of Platiniferous Sulfide Horizons by Crystal Fractionation and Magma Mixing in the Munni-Munni Layered Intrusion, West Pilbara Block, Western-Australia. Economic Geology 84: 1775-1804.

Huhtelin TA, Alapieti TT, Lahtinen JJ (1989) The Paasivaara PGE mineralization in the Penikat layered intrusion, northern Finland. 5th international platinum symposium; Guide to the post-symposium field trip; I, The Tornio-Narankavaara intrusion belt; II, Kuhmo-Koli-Enonkoski sites Opas - Geologian Tutkimuskeskus 29: 123-144.

Lavigne MJ, Michaud MJ (2001) Geology of North American Palladium Ltd.'s Roby Zone Deposit, Lac des Iles. Exploration and Mining Geology 10: 1-17.

Leake BE, Woolley AR, Arps CES, Birch WD, Gilbert MC, Grice JD, Hawthorne FC, Kato A, Kisch HJ, Krivovichev VG, Linthout K, Laird J, Mandarino J, Maresch WV,

Nickel EH, Rock NMS, Schumacher JC, Smith DC, Stephenson NCN, Ungaretti L, Whittaker EJW, Youzhi G (1997) Nomenclature of Amphiboles: Report of the Subcommittee on Amphiboles of the International Mineralogical Association, Commission on New Minerals and Mineral Names. Canadian Mineralogist 35: 219-246.

Li C, Ripley EM, Merino E, Maier WD (2004) Replacement of base metal sulfides by actinolite, epidote, calcite, and magnetite in the UG2 and Merensky Reef of the Bushveld Complex, South Africa. Economic Geology 99: 173-184.

Macdonald AJ (1988) Platinum-Group Element Mineralisation and the Relative Importance of Magmatic and Deuteric Processes: Field Evidence from the Lac des Iles Deposit, Ontario, Canada In: Prichard HM, Potts PJ, Bowles JFW, Cribb SJ (eds) GeoPlatinum '87. Elsevier, London, pp 215-236.

Maier WD, Gomwe T, Barnes S-J, Li C, Theart H (2004) Platinum group elements in the Uitkomst Complex, South Africa. Economic Geology 99: 499-516.

McDonough WF, Sun SS (1995) The Composition of the Earth. Chemical Geology 120: 223-253.

Michaud MJ (1998) The Geology, Petrology, Geochemistry and Platinum-Group Element-Gold-Copper-Nickel Ore Assemblage of the Roby Zone, Lac des Îles Mafic-Ultramafic Complex, Northwestern Ontario. M. Sc.

Michaud MJ, Lavigne MJ (2003) Distinguishing ore types at the Lac des Iles PGE-gold-copper-nickel mine, Ontario: Implications for resource modelling, mining and processing. CIM Bulletin 96: 44-47.

Naldrett A (2004) Magmatic sulfide deposits: geology, geochemistry and exploration. Springer-Verlag, Heidelberg, Berlin.

Naldrett AD, Gasparini EC, Barnes S-J, Von Gruenewaldt G, Sharpe MR (1986) The Upper Critical Zone of the Bushveld Complex and the origin of the Merensky-type ores. Economic Geology 81: 1105-1117.

Naldrett AJ (1981) Platinum-group element deposits In: Cabri LJ (ed) Platinum-group elements: Mineralogy, geology, recovery. Canadian Institute Mining Metallurgy, pp 197-232.

Nielsen TFD (2001) The Palladium Potential of the Skaergaard Intrusion, South-East Greenland GEUS, Volume 23. Geological Society of Denmark and Greenland, pp 33.

Nixon GT, Cabri LJ, Laflamme GJH (1990) Platinum-Group-Element Mineralization in Lobe and Placer Deposits Associated with the Tulameen Alaskan-type Complex, British Columbia. Canadian Mineralogist 28: 503-535.

Pearce NJG, Perkins WT, Westgate JA, Gorton MP, Jackson EE, Neal CR, Chenery SP (1997) A compilation of new and published major and trace element data for NIST SRM 610 and NIST SRM 612 glass reference materials. Geostandard Newsletter 21: 115-144.

Percival JA, Williams HR (1989) Late Archean Quetico accretionary complex, Superior province, Canada. Geology 17: 23-25.

Peregoedova A, Barnes S-J, Baker DR (2004) The formation of Pt-Ir alloys and Cu-Pd-rich sulfide melts by partial desulfurization of Fe-Ni-Cu sulfides: results of experiments and implications for natural systems. Chemical Geology 208: 247-264.

Pettigrew NT, Hattori KH (2001) Geology of the palladium-rich Legris Lake mafic-ultramafic complex, western Wabigoon subprovince, north-western Ontario. Exploration and Mining Geology 10: 35-49.

Prendergast MD, Keays RR (1989) Controls of platinum-group element mineralization and the origin of the PGE-rich main sulphide zone in the Wedza Subchamber of the Great Dyke, Zimbabwe; implications for the genesis of, and exploration for, stratiform PGE mineralization in layered intrusions In: Prendergast MS, Jones MJ (eds) Magmatic sulfides; the Zimbabwe volume. Inst. Min. and Metall., London, United Kingdom, Harare, pp 43-69.

Pye EG (1968) Geology of the Lac des Îles area, District of Thunderbay. Ontario. Department of Mines Geology Report, pp 64-47.

Robert RVD, Van Wyk E, Palmer R (1971) Concentration of the Noble Metals by a Fire Assay Technique Using Nickel Sulfide as the Collector. National Institute of Metallogeny, South Africa Report 1371: 1-14.

Rollinson HR (1993) Using geochemical data: evaluation, presentation, interpretation. Longman, Edinburgh Gate.

Sage RP (1998) Operation Ignace-Armstrong Obanga Lake-Lac des Îles area, Geology of Area II : Part2 - Granites; granite - supercrustal relationships Open file Report 5978. Ontario Geological Survey, pp 226.

Sheridan JP (1987) The Lac-Des-Iles Complex, Thunder-Bay, Ontario. Journal of Metals 39: A68-A68.

Steele TW, Levin J, Copelowitz I (1975) Preparation and certification of a reference sample of a precious metal ore. National Institute for Metallurgy Report pp 1696-1975.

Stone D, Lavigne MJ, Schnieders B, Scott J, Wagner D (2003) Regional Geology of the Lac des Iles Area. Summary of Field Work and Other Activities Open File Report 6120. Ontario Geological Survey, pp 15-11 - 15-25.

Streckeisen A (1975) To Each Plutonic Rock Its Proper Name. Earth Science Reviews 12: 1-33.

Sutcliffe R (1987) PGE Geology of the Lac-Des-Iles-Complex, Ontario. Geoscience Canada 14: 177-179.

Sutcliffe RH (1989) Magma Mixing in Late Archean Tonalitic and Mafic Rocks of the Lac Des Iles Area, Western Superior Province. Precambrian Research 44: 81-101.

Sutcliffe RH, Sweeny JM, Edgar AD (1989) The Lac-Des-Iles Complex, Ontario - Petrology and Platinum-Group-Elements Mineralization in an Archean Mafic Intrusion. Canadian Journal of Earth Sciences 26: 1408-1427.

Talkington RW, Watkinson DH (1984a) Trends in the Distribution of the Precious Metals in the Lac-Des-Iles Complex, Northwestern Ontario. Canadian Mineralogist 22: 125-136.

Talkington RW, Watkinson DH (1984b) Trends in the Distribution of the Precious Metals in the Lac-Des-Iles Complex, Northwestern Ontario. Canadian Mineralogist 22: 125-136.

Tomlinson KY, Davis DW, Stone D, Hart TR (2003) U-Pb age and Nd isotopic evidence for Archean terrane development and crustal recycling in the south-central Wabigoon subprovince, Canada. Contributions to Mineralogy and Petrology 144: 684-702.

Valli F, Guillot S, Hattori KH (2004) Source and tectono-metamorphic evolution of mafic and pelitic metasedimentary rocks from the central Quetico metasedimentary belt, Archean Superior Province of Canada. Precambrian Research 132: 155-177.

Von Gruenewaldt G, Hatton CJ, Merkle RKW, Gain SB (1986) Platinum-group element chromitite associations in the Bushveld Complex. Economic Geology 81: 1067-1079.

Watkinson DH, Dunning GR (1979) Geology and platinum-group mineralization, Lac des Îles Complex, northwestern Ontario. Canadian Mineralogist 17: 453-462.

Watkinson DH, Lavigne MJ, Fox PE (2002) Magmatic-Hydrothermal Cu- and Pd-rich Deposits in Gabbroic Rocks from North America In: Cabri LJ (ed) The Geology, Geochemistry, Mineralogy and Mineral Beneficiation of Platinum-Group Elements. Canadian Institute of Mining, Metallurgy and Petroleum, pp 299-320.

Wood SA (2002) The aqueous geochemistry of the Platinum-group elements with applications to the ore deposits In: Cabri LJ (ed) The Geology, Geochemistry, Mineralogy and Mineral Beneficiation of Platinum-Group Elements. Canadian Institute of Mining, Metallurgy and Petroleum, pp 211-249.

Zientek ML, Cooper RW, Corson SR, Geraghty EP, Cabri LJ (2002) Platinum-group element mineralization in the Stillwater Complex, Montana In: Cabri LJ (ed) The

Geology, Geochemistry, Mineralogy and Mineral Beneficiation of Platinum-Group Elements. Canadian Institute of Mining and Metallurgy, pp 459-481.

APPENDIX I

Whole Rock Data

Abbreviations used:

Rz	= Roby Zone (High-grade Zone samples are from Rz-01 to Rz17, inclusive)
Tz	= Twilight Zone
Chlor-act	= chlorite-actinolite schist
Meta-gabnor	= metagabbronorite
Leuco-gabnor	= leucogabbronorite
Gabnor	= gabbronorite
ND	= not detected
DL	= detection limit
Frag	= fragment
Mat	= matrix
Peg	= pegmatite
Frag-vari-	= varitextured fragment

Note: mineral abundances are in percent

A-1 UTM co-ordinates of Samples

ROBY ZONE

Sample Number	Mine Sample Name	UTM_east	UTM_north
Rz-18	266N 214E	309429	5449383
Rz-19	L270N 225E	309432.1	5449384
Rz-20	L265N 220E	309430.5	5449383
Rz-21	265N 205E	309425.9	5449383
Rz-22	260N 255E	309442.6	5449381
Rz-23	260N 255E	3094343	5449381
Rz-24	265N 200E	309424.4	5449383
Rz-25	264N 255E	3094343	5449382
Rz-26	L240N 235E	309434.8	5449375
Rz-27	L260N 230E	309433.5	5449381
Rz-28	L260N 230E	309464	5449380
Rz-29	L265N 215E	309429	5449383
Rz-30	272N 220E	309430.5	5449385
Rz-31	L260N 210E	309427.4	5449381
Rz-32	L250N 205E	309425.2	5449378
Rz-33	L260N 240E	309436.6	5449381
Rz-34	L170N 350E	309469.1	5449352
Rz-35	L265N 240E	309436.6	5449382
Rz-36	L245N 220E	309430.3	5449377
Rz-38	L215N 230E	309433	5449367
Rz-39	273N 311E	309458	5449383
Rz-40	L190N 295E	309452.5	5449359
Rz-41	L265N 235E	309435.1	5449383
Rz-42	L180N 270E	309444.8	5449356
Rz-43	L270N 300E	309454.9	5449383
Rz-44	L200N 310E	309457.2	5449362
Rz-45	137N 360E	309474.1	5449342
Rz-46	L235N 215E	309428.6	5449373
Rz-47	L250N 220E	309430.3	5449378
Rz-48	L230N 325E	309462.1	5449371
Rz-49	L165N 295E	309452.3	5449351
Rz-50	212N 325E	309461.9	5449365
Rz-51	L275N 300E	309454.9	5449385
Rz-52	L255N 235E	309435	5449379
Rz-53	L125N 380E	309477.7	5449338
Rz-54	L220N 275E	309446.8	5449368
Rz-55	L175N 305E	309455.4	5449354

Twilight Zone

Sample Number	Mine Sample Name	UTM_east	UTM_north
Tz-1	L4800 5940C	309655.5	5449538
Tz-2	TZG-01-001	309659.8	5449537
Tz-3	TZG-01-002	309661.5	5449537
Tz-4	L4790 5935	309653.8	5449535
Tz-5	L4790 5950	309658.4	5449535
Tz-6	L4790 5965	309663	5449535
Tz-7	L4790 5970	309664.5	5449535
Tz-8	L4780 5975	309665.9	5449532
Tz-9	TZG-01-003	309669.7	5449531
Tz-10	L4780 5940	309655.3	5449532
Tz-11	L4790 5975	309666	5449535
Tz-12	L4770 5935	309653.6	5449529
Tz-13	L4720 5940	309654.6	5449514
Tz-14	L4770 5980	309667.3	5449528
Tz-15	L4770 6000	309673.4	5449528
Tz-16	TZG-01-009	309661.6	5449526
Tz-17	L4760 5970	309664.2	5449525
Tz-19	L4740 5965	309662.4	5449519
Tz-21	L4730 5940	309654.7	5449517
Tz-22	L4730 5945	309656.3	5449517
Tz-23	L4770 5940	309655.1	5449529
Tz-24	L4720 5945	309656.1	5449514
Tz-25	L4710 5930	309651.5	5449511
Tz-26	5990-4710	309671.4	5449511
Tz-30	H40-99-022	309707.7	5449454
Tz-31	L4790 5980	309667.6	5449534
Tz-32	L4630- 5970	309662.8	5449486
Tz-33	4610/6013	309675.7	5449479
Tz-34	4470/6100	309700.7	5449436
Tz-35	4370/5975E	309661.6	5449407
Tz-36	4370/5865E	309628.1	5449408
Tz-37	4340/5970E	309659.7	5449398
Tz-38	4270/6150	309712.8	5449374
Tz-41	L4780 6000	309673.5	5449531

For samples Tz-27 to Tz-29 locations were not provided ref: (Dionne-Foster 2002)

A-2 Summary of High-grade Zone logs

Sample Name Rz1

Location (Mine grid) NORTHING: 104463.99
EASTING: 104674.65

Mine sample Name 99-052

Unit Name Pyroxenite

Unit Depth (ft) 42.35 to 159.65

Depth Sampled (ft) 120 to 121

Description

GABBRO

medium to coarse varitextured average medium/coarse grained, locally fine grained pegmatitic

Assay Results

FROM	TO	Pd/Pt	Cpy:Po	Pd opt	Au opt	Pt opt	Cu wt%	Ni wt%	Co wt%
62.35	72.35	13	1.25	0.092	0.012	0.007	0.128	0.104	0.004

Sample Name Rz 2

Location (Mine grid) NORTHING: 105795.467
EASTING: 105470.401

Mine Sample Name 99-096

Unit Name Varitextured gabbro

Unit Depth 619.1 to 683.3

Depth Sampled 646-650

Description

VARITEXTURED GABBRO
- finer medium grained to locally coarse grained
- medium to dark grey-green

- 40-45% plagioclase, 55-60% Clinopyroxene
- unit is moderately to strongly altered increasing down section as does sulfides
- Clinopyroxene to actinolite, plagioclase-smoky grey
- last 15 feet intensely altered with Clinopyroxene crystals up to 2 cm. Strongly mineralized, moderately foliated at 63° to core axis locally, weak epidote
- 0.25 to 2.0% Po-Cpy blebs
- occasional milky, white quartz veins with 4% Cpy (5 cm)
- sharp lower contact at approximately 45° to core axis

Assay Results

FROM	TO	Pd/Pt	Cpy:Po	Pd opt	Au opt	Pt opt	Cu wt%	Ni wt%	Co wt%
619.1	629.4		0.25	0.002	0.001	<0.001	0.022	0.013	0.002

Sample Name	Rz 3
Location (Mine grid)	NORTHING: 106094.155
	EASTING: 105255.607
Mine Sample Name	98-012
Unit Name	Varitextured gabbro
Unit Depth	94.2 to 193.3
Depth Sampled	107 to 112

Description

PYROXENITE AND MELANOGABBRO
>90% pyroxenite between 94.2 -147ft. rest is 70% pyroxenite, ~30% melanogabbro medium grained, Unit marked by numerous discrete shear and fracture/fault zones. Local patchy, strong epidote, saussurite, talc alteration.
occasional hornblende stringers.
Opx often appears relatively fresh.
At 106 - 123 - sheared, broken core, local intense serpentine or slikenslide faces. Trace pyrite.
At 110 - 111.7 - quartz vein, weak fault at 111.7 - 112.7m
At 187.3 - 192.2 - weak fault with coarser sulphides in melanogabbro sections.

Assay Results

FROM	TO	Pd/Pt	Cpy:Po	Pd opt	Au opt	Pt opt	Cu wt%	Ni wt%	Co wt%
107.00	112.00	80	1.25	0.483	0.020	0.006	0.004	0.025	0.002

Sample Name Rz-4

Location (Mine grid) NORTHING: 105024.256

EASTING: 105077.275

Mine Sample Name 99-075

Unit Name Pyroxenite – Shear ore type

Unit Depth 207.60 to 263.20

Depth Sampled 227 to 230

Description

Shear ore type dark green to green foliated 45-35° to core axis
cpx 90-100%; plag <10-0%
25.0-226.4 talcose pyroxene dark green blue
243.3 sheared granite (0.2) 65° to core axis
254.0(0.2) quartz with epidote halo (0.8')
257.7 (0.2) quartz bull white
258.3-260.1 altered leucogab to quartz diorite contacts sharp 40° to core axis

Assay Results

FROM	TO	Pd/Pt	Cpy:Po	Pd opt	Au opt	Pt opt	Cu wt%	Ni wt%	Co wt%
226.90	231.70	16	1.00	0.153	0.007	0.010	0.032	0.040	0.005

Sample Name Rz- 5

Location (Mine grid) NORTHING: 105024.256

EASTING: 105077.275

Mine Sample Name 99-075

Unit Name Pyroxenite

Unit Depth 494.90 to 519.20

Depth Sampled 516.0 to 519.8

Description

PYROXENITE
shear ore type
massive to foliation 30° to core axis, grad upper contact from breccia with melanogabbro over 6 feet
dark green; fine grained net textured pyrrhotite, chalcopyrite with minor talcose
foliation 30-50° to core axis
lower contact 25° to melanogabbro grad over 1.5 feet

Assay Results

FROM	TO	Pd/Pt	Cpy:Po	Pd opt	Au opt	Pt opt	Cu wt%	Ni wt %	Co wt%
513.80	519.20	18	1.00	0.052	0.001	0.003	0.015	0.019	0.004

Sample Name Rz-6

Location (Mine grid) NORTHING: 105024.256
EASTING: 105077.275

Mine Sample Name 99-075

Unit Name Pyroxenite

Unit Depth 207.60 to 263.20

Depth Sampled 217.7 to 219.7

Description See Rz-5

Assay Results

FROM	TO	Pd/Pt	Cpy:Po	Pd opt	Au opt	Pt opt	Cu wt%	Ni wt%	Co wt%
217.10	221.90	14	2.00	0.015	0.001	0.001	0.019	0.024	0.006

Sample Name Rz-7

Location (Mine grid) NORTHING: 105675.596

EASTING: 105376.374

Mine Sample Name 99-092

Unit Name Pyroxenite – Shear ore type

Unit Depth 488.9- 507.6

Depth Sampled 501-505

Description

PYROXENITE
Shear ore type
Dark green, massive foliation 70° to core axis, weak
Fine grained chalcopyrite pyrrhotite and blebs chalcopyrite pyrrhotite to medium grained size; patchy distortions
Zoned/euhedral chalcopyrite pyrrhotite blebs
95% Opx
Crenulate Plagioclase from 503.6'
Lower contact 40° to core axis

Assay Results

FROM	TO	S wt%	Cpy:Po	Pd opt	Au opt	Pt opt	Cu wt%	Ni wt%	Co wt%
498.30	502.90	4.60	0.75	0.081	0.003	0.006	0.058	0.044	0.005
502.90	507.60	4.70	0.75	0.051	0.005	0.006	0.030	0.034	0.004

Sample Name Rz 8

Location (Mine grid) NORTHING: 105024.256

EASTING: 105077.275

Mine Sample Name 99-075

Unit Name Pyroxenite

Unit Depth 494.90 to 519.20

Depth Sampled 509 to 512

Description See Rz-5

Assay Results

FROM	TO	Pd/Pt	Cpy:Po	Pd opt	Au opt	Pt opt	Cu wt%	Ni wt%	Co wt%
509.30	513.80	21	1.00	0.327	0.006	0.016	0.054	0.075	0.006

Sample Name Rz-9

Location (Mine grid) NORTHING: 105795.467

EASTING: 105470.401

Mine Sample Name 99-096

Unit Name Varitextured gabbro

Unit Depth 619.1 to 683.3

Depth Sampled 637 to 639

Description See Rz-2

Assay Results

FROM	TO	Pd/Pt	Cpy:Po	Pd opt	Au opt	Pt opt	Cu wt%	Ni wt%	Co wt%
629.4	639.8		tr	0.003	<0.001	<0.001	0.008	0.007	0.002

Sample Name Rz-10

Mine Sample Name 99-075

Unit Name Pyroxenite

Unit Depth 494.90 to 519.20

Depth Sampled 505.9 to 509

Description See Rz-5

PYROXENITE

Assay Results

FROM	TO	Pd/Pt	Cpy:Po	Pd opt	Au opt	Pt opt	Cu wt%	Ni wt%	Co wt%
504.70	509.30	20	1.50	0.329	0.009	0.016	0.093	0.075	0.006

Sample Name Rz-11

Mine Sample Name 99-096

Unit Name Varitextured gabbro

Unit Depth 619.1 to 683.3

Depth Sampled 659 – 669.3

Description See – Rz-2

Assay Results

FROM	TO	Pd/Pt	Cpy:Po	Pd opt	Au opt	Pt opt	Cu wt%	Ni wt%	Co wt%
659.4	669.3	15.82448	0.25	0.043	0.002	0.003	0.019	0.012	0.002

Sample Name Rz-12

Mine Sample Name 99-012

Unit Name Varitextured gabbro

Unit Depth 94.2 – 193.3

Depth Sampled 102-107

Description See – Rz-3

Assay Results

FROM	TO	Pd/Pt	Cpy:Po	Pd opt	Au opt	Pt opt
102	107	69	2	0.275	0.017	0.004

Sample Name Rz 13

Mine Sample Name 99-075

Unit Name Pyroxenite

Unit Depth 207.60 to 263.20

Depth Sampled 220 to 226

Description See Rz-5

Assay Results

FROM	TO	Pd/Pt	Cpy:Po	Pd opt	Au opt	Pt opt	Cu wt%	Ni wt%	Co wt%
221.90	226.90	19	0.25	0.124	0.008	0.006	0.022	0.032	0.004

Sample Name Rz-14

Mine Sample Name 99-096

Unit Name Pyroxenite

Unit Depth 683.90 to 692.40

Depth Sampled 689 to 692

Description

PYROXENITE

- dark green
- medium to coarse grained
- 0-10% plag, 90-100% Cpx
- moderately soft, moderately foliated at 41° to core axis
- strongly altered with Cpx to actinolite, tremolite and local talc alteration
- Cpx up to 1.5 cm (crystals, anhedral)
- moderate serpentine along fractures
- locally fractured at 45° to core axis
- local block chlorite
- 0.25% cubic pyrite, 0.25% Po-Cpy - small blebs
- sharp lower contact at 43° to core axis

Assay Results

FROM	TO	Pd/Pt	Cpy:Po	Pd opt	Au opt	Pt opt	Cu wt%	Ni wt%	Co wt%
689	692.40	19	0.5	0.264	0.005	0.014	0.013	0.035	0.004

Sample Name Rz-15

Mine Sample Name 99-103

Unit Name Melagabbronorite (pyroxenite)

Unit Depth 449.3 to 499.5

Depth Sampled 637 to 639

Description

MELANOGABBRONORITE

medium to coarse grained
- dark green to very dark green, black patches
- medium to coarse grained
- 5-20% plag, 80-95% Cpx
- unit consists mainly of pyroxenite with patches of melanogabbro (15-25% plag)
- moderately foliated
- strongly altered with Cpx to actinolite-tremolite, plagioclase moderately saussaurtized
- mottled texture with black patches with green pyroxenite
- local talc and serpentine along fractures
- strongly to moderately fractured with several granitic and tonalitic dikes up to 3 feet at shallow irregular angles to core axis
- sharp lower contact at 80° to core axis
- weakly mineralized with tr - 0.25% disseminated pyrrhotite

759.9 to 761.1 Tonalite dyke at 15° to core axis
766.2 to 768.8 Granitic dike with gabbro xenoliths, brecciated

Assay Results

FROM	TO	Pd/Pt	Cpy:Po	Pd opt	Au opt	Pt opt	Cu wt%	Ni wt%	Co wt%
768.9	775.8	17	tr	0.069	<0.001	0.004	<0.001	0.029	0.004

Sample Name Rz-16

Mine Sample Name 99-105

Unit Name Melagabbro breccia

Unit Depth 449.3 to 499.5

Depth Sampled 492.3 to 494

Description

MELAGABBRO BRECCIA

- mixture of fine medium grained, melanogabbro, brecciated gabbro, varitextured gabbro, gabbro norite
- weak to moderate breccia

451.8(0.3) - wehrlite band, 70° to core axis
465.2(0.9) - granitic dike, 40° to core axis
485.0 to 487.0 Quartz vein
495.5(0.1) Fracture quartz calcite filled, 70° to core axis

Assay Results

FROM	TO	Pd/Pt	Cpy:Po	Pd opt	Au opt	Pt opt	Cu wt%	Ni wt%	Co wt%
492.1	499.50	6	1.5	0.057	0.006	0.010	0.078	0.071	0.004

Sample Name Rz-17

Mine sample Name 99-096

Depth analysed 683 to 686

Description See Rz-5

Assay Results

FROM	TO	Pd/Pt	Cpy:Po	Pd opt	Au opt	Pt opt	Cu wt%	Ni wt%	Co wt%
683.3	689.00	23	0.5	0.785	0.011	0.035	0.042	0.070	0.005

A-3 Whole Rock Composition

SAMPLE	Rz-01	Rz-02	Rz-03	Rz-04	Rz-05	Rz-06	Rz-07	Rz-08	Rz-09	Rz-10
Rock Type	Chlor-act schist	micro-breccia	Chlor-act schist	Chlor-act schist	Chlor-act schist	Micro-breccia	Chlor-act schist	Chlor-act schist	micro-breccia	micro-breccia
SiO_2	50.6	50.5	48.3	50.4	49.6	50.3	50.4	50.6	50.9	50.3
TiO_2	0.34	0.16	0.09	0.12	0.28	0.31	0.12	0.09	0.16	0.16
Al_2O_3	18.2	17.3	8.07	10.1	5.06	10.3	13.1	8.92	17.2	14.4
Fe_2O_3 (Total)	7.77	9.56	9.85	10.6	18.6	13.8	9.31	10.0	9.45	10.4
Fe_2O_3	6.78	9.46	9.86	10.5	15.1	13.7	9.28	9.98	9.3	10.2
Fe(s)	0.69	0.07	0	0.07	2.4	0.09	0.02	0.03	0.1	0.1
MnO	0.13	0.15	0.17	0.18	0.32	0.19	0.15	0.19	0.15	0.16
MgO	8.69	8.82	23.4	19.1	17.9	12.0	15.5	20.9	8.89	10.5
CaO	10.2	10.4	7.19	5.03	5.53	7.28	6.19	5.63	10.4	9.5
Na_2O	2.17	2.26	0.27	0.85	0.44	1.3	1.52	0.77	2.12	2.17
K_2O	0.59	0.25	0.02	0.07	0.08	0.21	0.55	0.04	0.24	0.2
P_2O_5	0.01	ND	ND	ND	ND	ND	ND	ND	ND	ND
LOI	2.13	1.8	4.99	5.29	3.24	7.36	4.73	4.79	2	3.54
S	0.59	0.04	0.01	0.07	1.75	0.05	0.01	0.03	0.06	0.06
Total	**100.42**	**101.00**	**100.00**	**98.64**	**100.45**	**99.10**	**98.72**	**99.38**	**101.24**	**99.42**
Mg#	0.72	0.65	0.82	0.78	0.7	0.63	0.77	0.81	0.65	0.67
Ag (ppm)	4.4	0.5	0.5	0.5	0.8	0.5	0.5	0.5	0.5	1.83
As	0.2	0.2	0.7	0.8	0.4	0.2	0.2	1.3	0.4	0.2
Au	0.54	0.02	0.06	0.17	0.47	0.03	0.02	0.14	0.01	0.02
Ba	105	94	10	10	13	16	84	12	44	42
Ce	4.4	3.2	2.2	22.1	3.6	4.5	1.6	0.9	2.9	3
Co	70	57	80	86	174	76	67	75	55	61
Cr	178	175	912	493	457	270	232	779	165	229
Cs	1.29	2.49	0.15	0.44	0.42	4.52	1.71	0.71	2.29	1.42
Cu	2756	85	2	334	2503	86	40	144	87	97
Eu	0.35	0.3	0.1	0.13	0.31	0.19	0.1	0.07	0.23	0.24
La	2.04	1.50	0.20	0.49	1.16	1.97	0.58	0.41	1.49	1.56
Lu	0.05	DL	DL	DL	0.12	0.10	DL	DL	DL	DL
Nd	1.64	1.18	0.95	0.40	1.84	1.41	0.66	0.90	1.70	0.80
Ni	1033	200	916	913	2350	257	382	718	184	217
Rb	10	2	2	4	7	28	4	14	5	11
Sb	0.1	0.07	1.37	0.39	0.04	0.04	0.16	0.62	0.02	0.07
Sc	29.4	38.8	42.0	36.2	54.6	44.1	33.2	37.8	38.7	35.8
Hf	0.30	0.26	0.34	0.14	0.31	0.32	<0.1	0.13	0.31	0.17
Sm	0.48	0.50	0.23	0.16	0.51	0.53	0.18	0.12	0.48	0.34
Ta	0.06	0.016	0.02	0.016	0.016	0.024	0.016	0.016	0.016	0.016
Tb	0.07	0.12	0.04	0.04	0.09	0.09	0.06	0.04	0.09	0.08
Th	0.23	0.06	0.10	0.07	0.46	0.17	0.10	0.06	0.06	0.19
U	0.25	0.09	0.11	0.06	0.07	0.07	0.07	0.07	0.07	0.07
W	2.8	4	4.8	2.2	3.9	3	1.2	3.9	1.8	2.4
Yb	0.05	0.47	0.34	0.28	0.67	0.52	0.24	0.24	0.43	0.3
Zn	ND	40	37	ND	68	46	65	4	10	64

$Fe_{(s)} = (1.527*S-0.6592*(Cu-70)/10000-0.5285*(Ni-450)/10000$

SAMPLE Rock Type	Rz-11 Micro-breccia	Rz-12 Chlor-act schist	Rz-13 Chlor-act schist	Rz-14 Chlor-act schist	Rz-15 Chlor-act schist	Rz-16 Chlor-act schist	Rz-17 Chlor-act schist
SiO_2	50.6	53.0	51.1	51.5	50.0	52.6	49.5
TiO_2	0.16	0.09	0.13	0.1	0.12	0.36	0.11
Al_2O_3	17.3	6.5	8.23	7.18	10.3	21.2	17.9
Fe_2O_3 (Total)	9.46	9.41	11.0	10.0	10.4	4.97	8.07
Fe_2O_3	9.37	9.17	11.0	10	10.2	4.75	6.49
Fe(s)	0.06	0.17	0.01	0.01	0.1	0.15	1.11
MnO	0.15	0.15	0.18	0.18	0.17	0.08	0.12
MgO	8.7	22.2	20.9	21.0	19.3	7.26	10.3
CaO	10.4	6.74	5.32	7.47	6.01	9.23	9.83
Na_2O	2.27	0.23	0.36	0.16	0.43	2.71	1.3
K_2O	0.25	0.02	0.04	0.01	0.14	0.48	0.55
P_2O_5	ND	ND	ND	ND	ND	0.04	ND
LOI	1.84	4.21	4.98	4.4	5.29	2.45	3.29
S	0.03	0.12	0.01	0.02	0.07	0.14	0.89
Total	**100.6**	**100.8**	**99.74**	**99.74**	**99.38**	**100.4**	**99.94**
Mg#	0.65	0.83	0.79	0.81	0.79	0.75	0.76
Ag (ppm)	0.5	0.5	0.5	0.5	0.5	1.3	2
As	0.2	0.9	0.6	3.2	0.2	0.2	3.1
Au	0.02	0.09	0.25	0.27	0.03	0.13	9.95
Ba	69	12	10	26	10	105	82
Ce	3.4	0.8	1	0.9	0.6	5.4	3
Co	54	75	85	78	80	35	96
Cr	171	841	577	816	594	95	239
Cs	2.5	0.19	0.59	0.31	0.78	2.45	3.3
Cu	82	172	60	127	32	869	1998
Eu	0.25	0.07	0.14	0.06	0.06	0.26	0.2
La	1.47	0.15	0.55	0.28	0.02	2.40	0.54
Lu	DL	0.06	0.06	DL	DL	DL	DL
Nd	2.10	1.10	1.10	0.30	0.50	1.40	1.00
Ni	171	604	793	697	465	450	2684
Rb	3	3	5	8	14	25	36
Sb	0.06	1.66	0.39	0.9	0.18	0.13	0.12
Sc	38.5	40.7	40.0	42.3	40.3	18.5	28.3
Hf	0.33	0.14	0.11	0.10	0.11	1.35	0.10
Sm	0.47	0.17	0.21	0.14	0.01	0.38	0.27
Ta	0.02	0.02	0.02	0.03	0.02	0.10	0.02
Tb	0.07	0.04	0.04	0.08	0.07	0.07	0.05
Th	0.08	0.06	0.12	0.07	0.06	0.73	0.07
U	0.07	0.1	0.14	0.09	0.07	0.23	0.06
W	3.2	2.5	4.1	3.2	3.8	2.4	0.1
Yb	0.41	0.34	0.3	0.3	0.29	0.24	0.19
Zn	64	75	96	73	70	42	8

$Fe_{(s)} = (1.527*S-0.6592*(Cu-70)/10000-0.5285*(Ni-450)/10000$

SAMPLE Rock Type	Rz-18 frag meta-gabnor	Rz-19 frag meta-gabnor	Rz-20 frag meta-gabnor	Rz-21 frag-vari meta-gabnor	Rz-22 frag leuco-gabnor	Rz-23 frag meta-gabnor	Rz-24 frag-vari meta-gabnor	Rz-25 frag meta-gabnor	Rz-26 frag meta-gabnor	Rz-27 frag meta-gabnor
SiO_2	49.7	49.7	50.2	51.8	51.3	50.8	51.7	51.1	51.4	52.3
TiO_2	0.06	0.19	0.18	0.08	0.09	0.16	0.16	0.09	0.02	0.14
Al_2O_3	24.5	12.1	13.3	17.0	19.9	12.2	18.1	19.2	18.8	3.44
Fe_2O_3 (Total)	4.50	10.9	10.9	7.32	7.59	9.57	7.25	7.03	7.80	10.8
Fe_2O_3	4.40	10.5	10.5	7.24	7.29	9.48	7.11	6.13	7.56	10.2
Fe(s)	0.07	0.31	0.24	0.05	0.21	0.07	0.10	0.63	0.17	0.37
MnO	0.08	0.19	0.19	0.14	0.12	0.17	0.13	0.13	0.14	0.2
MgO	5.93	13.0	12.9	9.9	8.37	15.0	8.28	9.27	7.97	21.6
CaO	10.6	9.27	8.25	10.5	8.56	7.56	9.98	9.31	9.22	9.90
Na_2O	2.38	1.89	1.84	2.16	2.23	1.43	2.74	1.89	2.62	0.32
K_2O	1.12	0.59	0.56	0.53	0.98	0.71	0.85	0.95	0.95	0.03
P_2O_5	ND	ND	ND	ND	ND	ND	ND	ND	0.01	ND
LOI	2.43	2.5	2.55	1.84	2.42	3.24	1.98	2.61	2.29	2.87
S	0.04	0.24	0.18	0.03	0.16	0.06	0.07	0.45	0.12	0.26
Total	**100.4**	**99.16**	**99.69**	**101.0**	**100.8**	**98.77**	**100.5**	**101.0**	**100.3**	**100.4**
Mg#	0.73	0.71	0.71	0.73	0.69	0.76	0.7	0.74	0.72	0.81
Ag (ppm)	0.5	1.5	1.1	0.7	0.5	0.5	0.5	0.5	0.5	0.5
As	0.3	0.6	0.6	0.4	0.5	0.3	0.5	0.5	0.5	0.6
Au	0.05	0.14	0.09	0.02	0.14	0.06	0.05	0.12	0.06	0.06
Ba	225	76	86	116	220	103	194	152	275	22
Ce	1.1	3.2	3.3	0.9	2.3	2.4	4.1	3.4	4.2	2.4
Co	31	76	72	52	60	70	46	67	45	100
Cr	118	323	307	215	171	251	156	282	147	1067
Cs	3.78	1.54	1.07	0.94	2.32	2.68	2.78	3.38	4.83	0.2
Cu	116	671	417	111	445	293	155	694	361	183
Eu	0.16	0.24	0.21	0.17	0.19	0.15	0.25	0.21	0.32	0.14
La	0.89	1.28	1.47	0.47	0.96	1.57	2.00	1.32	1.93	0.63
Lu	DL	DL	DL	DL	DL	DL	DL	DL	DL	DL
Nd	0.70	1.30	0.60	0.50	0.90	2.50	1.40	0.80	1.70	1.00
Ni	285	705	444	230	452	525	460	590	272	665
Rb	13	16	13	31	21	22	36	27	3	29
Sb	0.21	0.15	0.04	0.06	0.12	0.06	0.12	0.12	0.14	0.04
Sc	13.6	45.6	39.3	35.8	21.2	38.7	33.5	24.1	30.1	66.0
Hf	0.10	0.19	0.09	0.10	0.07	0.10	0.15	0.23	0.29	0.36
Sm	0.13	0.46	0.33	0.20	0.17	0.35	0.46	0.22	0.44	0.38
Ta	0.016	0.016	0.016	0.016	0.018	0.023	0.087	0.017	0.016	0.016
Tb	0.04	0.14	0.07	0.04	0.05	0.05	0.08	0.05	0.05	0.05
Th	0.06	0.22	0.11	0.06	0.11	0.11	0.22	0.18	0.18	0.06
U	0.07	0.16	0.14	0.07	0.07	0.16	0.14	0.12	0.07	0.07
W	0.8	1.1	1.4	1.8	1.3	3.1	2.9	1.8	2.6	12.7
Yb	0.1	0.48	0.4	0.18	0.15	0.34	0.33	0.19	0.35	0.40
Zn	31	104	51	39	80	53	42	63	47	62

$Fe_{(s)} = (1.527*S-0.6592*(Cu-70)/10000-0.5285*(Ni-450)/10000$

SAMPLE	Rz-28	Rz-29	Rz-30	Rz-31	Rz-32	Rz-33	Rz-34	Rz-35	Rz-36	Rz-38
Rock Type	frag-vari meta-gabnor	frag meta-gabnor	mat gabnor	frag-vari meta-gabnor	frag meta-gabnor	frag leuco-gabnor	frag meta-gabnor	frag meta-gabnor	mat meta-gabnor	mat gabnor
SiO_2	52.2	51.9	49.5	51.5	51.8	51.0	51.2	51.7	52.0	51.1
TiO_2	0.06	0.09	0.2	0.07	0.08	0.11	0.07	0.1	0.04	0.46
Al_2O_3	23.8	16.8	9.92	16.6	18.0	18.4	20.4	17.8	24.0	5.82
Fe_2O_3 (Total)	3.58	6.84	14.6	8.35	6.97	6.49	6.44	6.38	4.51	12.4
Fe_2O_3	3.55	6.79	12.9	8.22	6.43	6.45	6.38	6.32	4.28	12.3
Fe(s)	0.02	0.03	1.19	0.09	0.38	0.03	0.04	0.04	0.16	0.06
MnO	0.07	0.12	0.21	0.16	0.11	0.12	0.13	0.12	0.07	0.21
MgO	4.14	9.28	15.7	10.4	9.44	9.94	7.81	10.9	4.24	16.3
CaO	11.6	11.3	6.36	9.03	9.07	10.1	7.66	9.15	10.1	12.1
Na_2O	3.47	2.35	0.98	2.53	2.65	2.22	3.53	2.09	3.68	0.75
K_2O	0.94	0.81	0.47	0.53	0.85	0.75	1.26	0.71	0.59	0.18
P_2O_5	ND	ND	ND	ND	ND	ND	ND	ND	ND	0.01
LOI	1.59	2.01	2.7	2.18	2.45	2.53	3.19	2.75	1.56	1.78
S	0.01	0.02	0.93	0.06	0.28	0.01	0.02	0.03	0.12	0.04
Total	**101.4**	**101.3**	**99.62**	**100.7**	**100.8**	**101.1**	**100.4**	**100.8**	**100.4**	**100.8**
Mg#	0.7	0.73	0.71	0.72	0.74	0.75	0.71	0.77	0.66	0.72
Ag (ppm)	0.5	0.50	1.5	0.5	0.50	0.50	0.50	0.5	0.5	3.4
As	0.2	0.20	0.6	0.2	1.00	0.40	0.20	0.4	0.1	0.7
Au	0.02	0.04	0.44	0.03	0.16	0.02	0.03	0.03	0.10	0.06
Ba	178	187	111	98	146	92	215	97	172	46
Ce	4.4	1.50	3.1	1.5	0.80	2.60	0.80	2.2	1.1	10.9
Co	24	46.00	128	53	58.00	42.00	34.00	50	32	66
Cr	100	153	370	162	133	227	132	262	32	1421
Cs	2.26	2.70	1.18	3.07	1.80	1.96	5.62	1.96	2.66	0.35
Cu	110	157	2470	117	569	55	51	100	307	184
Eu	0.22	0.15	0.25	0.16	0.15	0.15	0.11	0.17	0.17	0.63
La	2.18	0.89	0.88	0.77	0.62	0.95	0.62	0.88	0.86	2.39
Lu	DL	DL	0.07	DL	DL	DL	DL	DL	0.02	0.12
Nd	1.30	0.50	1.90	0.20	0.60	1.20	0.20	0.40	0.80	4.70
Ni	106	219	1719	275	628	247	261	362	368	317
Rb	23	12.00	5	21	5.00	17.00	16.00	21	5	13
Sb	0.08	0.10	0.07	0.12	0.03	0.13	0.17	0.06	0.11	0.14
Sc	20.9	39.2	45.3	29.9	24.6	28.1	20.0	27.1	12.7	52.2
Hf	0.15	0.16	0.12	0.10	0.12	0.15	0.10	0.13	0.10	0.49
Sm	0.27	0.27	0.31	0.18	0.14	0.28	0.14	0.23	0.11	2.05
Ta	0.016	0.01	0.016	0.016	0.02	0.02	0.02	0.016	0.016	0.07
Tb	0.03	0.04	0.06	0.05	0.04	0.04	0.04	0.04	0.02	0.30
Th	0.36	0.06	0.06	0.06	0.06	0.06	0.06	0.06	0.03	0.32
U	0.07	0.07	0.13	0.07	0.07	0.07	0.07	0.07	0.07	0.07
W	1.2	0.10	10.7	0.5	0.80	0.70	0.70	0.7	0.1	2.6
Yb	0.16	0.28	0.4	0.18	0.16	0.30	0.13	0.24	0.1	0.83
Zn	7	4.00	68	52	dl	9.00	9.00	26	27	59

$Fe_{(s)} = (1.527*S-0.6592*(Cu-70)/10000-0.5285*(Ni-450)/10000$

SAMPLE	Rz-39	Rz-40	Rz-41	Rz-42	Rz-43	Rz-44	Rz-45	Rz-47	Rz-48	Rz-49
Rock Type	mat meta-gabnor	mat gabnor	mat gabnor	mat meta-gabnor	mat meta-gabnor	mat meta-gabnor	mat meta-gabnor	mat meta-gabnor	mat meta-gabnor	mat meta-gabnor
SiO_2	50.1	50.7	49.5	49.4	50.4	50.4	48.9	50.6	50.4	51.7
TiO_2	0.14	0.39	0.23	0.33	0.17	0.34	0.22	0.15	0.14	0.36
Al_2O_3	10.0	6.53	12.2	6.21	17.2	17.4	7.98	15.1	19.1	6.41
Fe_2O_3 (Total)	11.1	10.6	12.3	12.1	8.44	9.17	15.9	12.4	9.27	7.52
Fe_2O_3	11.0	10.5	11.4	11.4	8.21	8.68	13.2	12.1	9.09	7.35
Fe(s)	0.04	0.06	0.64	0.48	0.16	0.34	1.89	0.19	0.13	0.12
MnO	0.2	0.18	0.21	0.19	0.14	0.14	0.24	0.16	0.13	0.16
MgO	16.4	19.3	13.4	17.8	10.1	9.94	16.6	10.4	9.27	19.5
CaO	8.45	9.29	7.46	11.5	8.76	8.66	6.55	8.91	8.89	9.52
Na_2O	0.98	0.5	1.4	0.76	2.24	1.93	0.79	2.58	2.48	0.74
K_2O	0.34	0.14	0.5	0.11	0.79	0.98	0.18	0.96	1.04	0.29
P_2O_5	ND	ND	ND	ND	0.01	0.02	ND	ND	0.01	ND
LOI	3.04	3.31	3.29	2.07	2.4	2.65	3.47	2.58	2.77	3.18
S	0.03	0.07	0.5	0.37	0.12	0.29	1.48	0.10	0.10	
Total	**98.8**	**99.0**	**98.8**	**99.5**	**99.1**	**100.9**	**99.7**	**99.2**	**100.9**	**99.3**
Mg#	0.75	0.78	0.7	0.76	0.71	0.69	0.71	0.70	0.71	0.8
Ag (ppm)	2.7	0.6	1.9	0.9	0.5	0.9	2.9	0.90	0.50	0.5
As	0.8	0.2	1	0.5	0.2	0.4	1.4	0.80	0.30	0.2
Au	0.03	0.06	0.46	0.15	0.11	0.19	1.18	0.11	0.18	0.00
Ba	66	32	108	32	141	214	21	295	186	80
Ce	1.6	11	4	5	4.3	5	3.5	3.50	3.40	17.2
Co	78	71	104	96	59	74	167	63	58	62
Cr	423	1474	317	1111	206	264	427	198	135	1441
Cs	0.6	0.26	0.98	0.18	1.3	4.09	1.95	2.53	3.72	0.32
Cu	136	231	1360	862	309	893	3465	318	371	11
Eu	0.19	0.79	0.26	0.59	0.24	0.31	0.38	0.23	0.17	0.72
La	0.61	1.37	1.62	1.38	2.17	2.02	0.83	1.85	1.54	2.74
Lu	DL	0.11	DL	0.10	DL	DL	0.09	DL	DL	0.12
Nd	0.50	7.00	0.50	3.10	1.90	3.00	1.80	1.10	0.70	14.70
Ni	397	915	1038	980	456	1178	3285	503	612	657
Rb	4	16	4	22	26	9	23	19.00	5.00	12
Sb	0.2	0.04	0.04	0.32	0.1	0.22	0.16	0.14	0.06	0.04
Sc	43.8	26.6	39.6	46.6	26.2	33.2	45.3	37.2	27.1	24.5
Hf	0.10	0.55	0.28	0.34	0.21	0.38	0.30	0.16	0.33	1.19
Sm	0.23	2.46	0.39	1.47	0.41	0.53	0.41	0.36	0.32	3.53
Ta	0.016	0.041	0.016	0.016	0.031	0.024	0.016	0.08	0.02	0.016
Tb	0.04	0.32	0.07	0.26	0.04	0.17	0.05	0.04	0.04	0.46
Th	0.06	0.06	0.19	0.06	0.39	0.11	0.10	0.17	0.11	0.06
U	0.07	0.07	0.1	0.1	0.14	0.13	0.12	0.07	0.07	0.07
W	2.5	2.7	5.5	6.5	3.9	13.6	8.7	0.40	0.30	0.7
Yb	0.35	0.77	0.48	0.54	0.35	0.31	0.42	0.27	0.32	0.83
Zn	63	280	197	59	43	101	110	4.00	4.00	14

$Fe_{(s)} = (1.527*S-0.6592*(Cu-70)/10000-0.5285*(Ni-450)/10000$

SAMPLE Rock Type	Rz-50 mat meta- gabnor	Rz-51 mat meta- gabnor	Rz-52 mat meta- gabnor	Rz-53 mat meta- gabnor	Rz-54 mat meta- gabnor	Rz-55 mat meta- gabnor
SiO_2	49.5	48.5	51.9	51.3	50.9	49.3
TiO_2	0.23	0.08	0.11	0.14	0.18	0.18
Al_2O_3	11.9	25.9	19.1	17.8	16.6	10.6
Fe_2O_3 (Total)	12.7	4.26	6.53	7.60	9.81	12.7
Fe_2O_3	11.7	4.14	6.33	7.54	8.75	11.9
Fe(s)	0.70	0.08	0.14	0.04	0.74	0.52
MnO	0.21	0.07	0.12	0.15	0.14	0.20
MgO	13.7	4.03	8.60	9.25	10.5	15.8
CaO	7.47	11.5	9.28	9.35	7.28	6.39
Na_2O	1.30	3.05	2.79	2.42	2.11	1.16
K_2O	0.46	1.19	0.87	0.91	1.23	0.55
P_2O_5	ND	ND	ND	ND	ND	ND
LOI	3.28	2.92	2.03	2.49	3.11	4.05
S	0.55	0.06	0.1	0.03	0.6	0.45
Total	**99.1**	**100.5**	**100.8**	**100.5**	**101.3**	**98.7**
Mg#	0.7	0.66	0.73	0.71	0.7	0.72
Ag (ppm)	0.8	0.6	0.5	0.5	0.5	0.5
As	0.8	0.3	0.3	0.2	1.2	1.6
Au	0.29	0.03	0.08	0.06	0.43	0.60
Ba	55	292	180	144	217	221
Ce	2.8	3.2	2.4	2.5	3.3	1.7
Co	102	28	51	45	91	112
Cr	314	155	96	156	175	351
Cs	0.99	9.45	1.87	1.97	3.44	2.38
Cu	1757	60	296	153	2033	1707
Eu	0.17	0.14	0.15	0.12	0.25	0.21
La	1.44	1.54	1.10	1.25	1.58	0.89
Lu	<0.08	<0.08	<0.08	<0.08	<0.08	<0.08
Nd	1.30	0.60	0.30	1.20	0.60	0.40
Ni	983	465	224	248	1188	1523
Rb	31	12	11	32	7	12
Sb	0.04	0.27	0.05	0.1	0.27	0.3
Sc	39.6	10.0	26.1	30.2	28.1	39.2
Hf	0.27	0.19	0.14	0.22	0.23	0.10
Sm	0.40	0.25	0.28	0.28	0.36	0.32
Ta	0.016	0.016	0.016	0.016	0.016	0.016
Tb	0.05	0.04	0.04	0.06	0.04	0.04
Th	0.12	0.23	0.12	0.11	0.13	0.06
U	0.07	0.1	0.07	0.07	0.17	0.07
W	0.8	0.7	0.9	0.5	0.1	0.6
Yb	0.46	0.13	0.22	0.23	0.3	0.37
Zn	82	dl	dl	dl	13	145

$Fe_{(s)} = (1.527*S-0.6592*(Cu-70)/10000-0.5285*(Ni-450)/10000$

SAMPLE	Tz-1	Tz-2	Tz-3	Tz-4	Tz-5	Tz-6	Tz-7	Tz-8	Tz-9	Tz-10
Rock Type	frag gabnor	frag leuco-gabnor	frag gabnor	frag gabnor	frag leuco-gabnor	mat gabnor	frag gabnor	mat gabnor	peg meta gabnor	frag gabnor
SiO_2	48.66	49.86	49.70	49.27	50.87	49.67	49.78	50.32	50.62	49.54
TiO_2	0.23	0.14	0.17	0.15	0.14	0.29	0.3	0.22	0.33	0.18
Al_2O_3	15.73	19.61	15.63	16	17.62	10.32	12.66	13.74	13.62	14.27
Fe_2O_3 (Total)	12.11	8.05	11.49	10.37	6.39	15.52	13.81	12.13	11.12	11.86
Fe_2O_3	10.80	8.03	10.94	9.89	6.28	14.25	12.96	12.05	11.10	11.09
Fe(s)	0.92	0.01	0.38	0.33	0.08	0.89	0.60	0.06	0.01	0.54
MnO	0.15	0.11	0.17	0.14	0.12	0.21	0.19	0.17	0.17	0.16
MgO	11.03	8.9	11.23	12.71	6.82	14.68	13.15	13.39	11.66	13.43
CaO	9.32	10.71	8.78	9.13	13.59	6.71	7.9	7.97	9.37	8.17
Na_2O	1.3	1.67	1.43	1.18	2.21	0.79	1.21	1.12	1.42	1.12
K_2O	0.15	0.22	0.17	0.16	0.67	0.24	0.19	0.27	0.61	0.14
P_2O_5	0.03	0.01	0.01	0.01	0.01	0.03	0.01	0.01	0.02	0.01
LOI	0.9	1	1.48	0.95	2.62	1.78	0.81	1.03	1.91	0.65
S	0.77	0.01	0.29	0.29	0.06	0.71	0.45	0.01	0.01	0.43
Total	**100.02**	**99.68**	**99.76**	**100.03**	**99.70**	**100.16**	**100.11**	**99.85**	**99.90**	**99.53**
Mg#	0.67	0.69	0.67	0.72	0.68	0.67	0.67	0.67	0.68	0.7
Ag (ppm)	1.5	0.5	0.5	0.5	0.5	0.5	0.5	0.5	0.5	1.5
As	0.4	0.2	0.2	0.6	1.1	1	0.4	0.1	0.5	0.9
Au	0.48	0.02	0.04	0.25	0.13	0.44	0.19	0.02	0.01	0.02
Ba	50	70	60	50	130	70	60	50	70	50
Ce	1.9	2.2	1.5	1.9	1.1	1.2	2.5	1.5	2.7	2.6
Co	81	44	67	73	39	101	81	69	56	78
Cr	338	260	384	300	370	433	418	388	380	398
Cs	0.63	0.89	0.99	0.73	1.76	0.93	0.93	1.15	1.55	0.89
Cu	2800	107	969	1215	314	2150	1155	97	79	1815
Eu	0.3	0.23	0.19	0.16	0.33	0.18	0.28	0.17	0.22	0.18
La	1.13	1.10	0.80	0.75	0.66	0.82	1.44	1.06	1.15	2.19
Lu	<0.08	<0.08	<0.08	<0.08	<0.08	<0.08	<0.08	<0.08	<0.08	0.09
Nd	0.80	1.30	1.00	0.90	0.60	0.50	1.40	0.40	1.40	0.70
Ni	1530	268	765	1080	229	1405	909	355	311	1160
Rb	3	7	5	4	22	5	6	4	16	4
Sb	0.02	0.03	0.05	0.02	0.16	0.08	0.07	0.04	0.12	0.06
Sc	31.61	24.1	30.1	28.78	44.88	43.91	36.42	39.76	42.01	37.25
Hf	0.14	0.06	0.16	0.16	0.17	0.12	0.13	0.25	0.26	0.09
Sm	0.29	0.25	0.20	0.18	0.46	0.31	0.37	0.29	0.39	0.43
Ta	0.016	0.022	0.016	0.016	0.281	0.033	0.016	0.016	0.016	0.024
Tb	0.04	0.06	0.04	0.07	0.10	0.08	0.08	0.05	0.06	0.05
Th	0.06	0.12	0.06	0.06	0.25	0.06	0.15	0.06	0.12	0.12
U	0.07	0.07	0.07	0.07	0.6	0.07	0.07	0.07	0.11	0.07
W	0.4	<0.1	0.1	0.2	2.6	3	1.7	0.4	1	1.1
Yb	0.34	0.25	0.30	0.24	0.53	0.45	0.43	0.35	0.41	0.57
Zn	56	44	62	48	68	72	74	68	52	54

$Fe_{(s)} = (1.527*S-0.6592*(Cu-70)/10000-0.5285*(Ni-450)/10000$

SAMPLE	Tz-11	Tz-12	Tz-13	Tz-14	Tz-15	Tz-16	Tz-17	Tz-19	Tz-20	Tz-21
Rock Type	frag gabnor	frag leuco-gabnor	frag meta-gabnor	frag meta-gabnor	mat meta-gabnor	mat meta-gabnor	mat meta-gabnor	mat meta-gabnor	peg leuco-gabnor	mat meta-gabnor
SiO_2	50.5	49.5	50.8	50.0	49.6	50.7	50.4	49.3	52.1	49.3
TiO_2	0.29	0.14	0.27	0.2	0.2	0.25	0.22	0.24	0.23	0.23
Al_2O_3	12.1	19.5	6.42	14.1	11.1	6.83	12.2	10.1	18.1	9.31
Fe_2O_3 (Total)	13.8	8.09	15.6	11.2	13.7	15.9	11.8	4.02	15.6	7.05
Fe_2O_3	13.8	7.79	15.4	11.1	12.6	15.5	11.8	3.75	14.4	6.72
Fe(s)	0.00	0.21	0.12	0.08	0.77	0.25	0.01	0.19	0.84	0.23
MnO	0.21	0.12	0.24	0.17	0.19	0.25	0.17	0.21	0.12	0.21
MgO	14	8.42	18.0	13.2	14.4	18.3	14.2	15.6	7.67	14.9
CaO	6.92	9.41	5.98	7.22	6.85	4.9	6.67	6.49	8.73	7.17
Na_2O	1.19	1.85	0.09	0.89	0.58	0.29	1.56	0.81	2.72	0.22
K_2O	0.2	1.02	0.06	0.58	0.33	0.11	0.16	0.28	1.63	0.27
P_2O_5	0.01	0.01	0.01	0.02	0.01	0.01	0.01	0.01	0.04	0.01
LOI	0.79	2.94	3.69	4.11	3.98	3.52	4.06	1.06	2.46	4.53
S	0.01	0.18	0.12	0.09	0.59	0.19	0.01	0.74	0.16	0.86
Total	**99.7**	**99.68**	**99.20**	**99.90**	**99.51**	**99.42**	**99.30**	**100.5**	**99.65**	**99.90**
Mg#	0.67	0.68	0.7	0.7	0.69	0.7	0.7	0.68	0.69	0.69
Ag (ppm)	0.5	0.5	0.5	0.5	1.5	0.5	0.5	1.5	0.5	2
As	0.4	0.3	0.5	0.8	1.2	0.4	0.3	0.2	0.5	0.4
Au	1.37	0.15	0.16	0.35	0.21	0.01	0.02	0.00	0.69	0.06
Ba	50	110	<10	100	80	30	30	50	240	70
Ce	2.1	2.6	4.1	1.3	3.2	5.5	3.4	1.6	5.9	1.7
Co	74	46	88	69	92	91	71	104	47	100
Cr	366	194	425	258	390	520	312	431	181	456
Cs	2.78	3.61	0.38	0.8	1.01	0.51	0.29	1.18	3.52	0.64
Cu	52	676	583	354	1835	618	71	2810	133	3160
Eu	0.24	0.32	0.2	0.2	0.14	0.15	0.25	0.3	0.23	0.24
La	1.12	1.12	1.05	0.92	0.60	1.02	1.48	1.14	2.04	0.79
Lu	0.05	<0.08	0.11	<0.08	<0.08	<0.08	<0.08	0.09	<0.08	<0.08
Nd	1.20	1.20	0.70	0.40	0.40	1.90	0.80	0.80	2.40	1.00
Ni	389	640	811	552	1355	829	466	1845	694	2330
Rb	41	50	3	7	4	2	3	4	21	3
Sb	0.09	0.07	0.13	0.09	0.09	0.05	0.02	0.02	0.02	0.48
Sc	23.66	31.23	60.8	32.67	45.91	41.52	58.19	54.31	48.56	41.06
Hf	0.20	0.17	0.27	0.06	0.17	0.16	0.16	0.26	0.19	0.10
Sm	0.21	0.26	0.40	0.21	0.23	0.28	0.39	0.32	0.72	0.30
Ta	0.016	0.016	0.016	0.016	0.016	0.016	0.016	0.016	0.044	0.016
Tb	0.05	0.04	0.10	0.04	0.07	0.04	0.11	0.09	0.12	0.04
Th	0.06	0.06	0.14	0.06	0.14	0.06	0.10	0.06	0.06	0.06
U	0.07	0.07	0.07	0.07	0.07	0.07	0.07	0.07	0.09	0.07
W	0.7	0.3	0.3	1	0.7	1.7	0.8	0.5	0.2	0.2
Yb	0.27	0.39	0.64	0.29	0.40	0.37	0.51	0.55	0.53	0.38
Zn	82	48	66	72	96	82	64	76	40	60

$Fe_{(s)} = (1.527*S-0.6592*(Cu-70)/10000-0.5285*(Ni-450)/10000$

SAMPLE	Tz-22	Tz-23	Tz-24	Tz-25	Tz-26	Tz-27	Tz-28	Tz-29	Tz-30	Tz-31
Rock Type	frag meta lecuo-gabnor	mat meta-gabnor	frag meta-gabnor	mat meta-gabnor	mat meta-melagn	peg leuco-gabnor	peg ganor	peg leuco-gabnor	mat leuco-gabnor	mat gabnor
SiO_2	49.63	50.35	50.64	50.89	50.68	51.15	50.52	49.83	49.63	49.72
TiO_2	0.15	0.24	0.17	0.18	0.25	0.18	0.26	0.32	0.15	0.25
Al_2O_3	19.56	12.15	11.2	21.9	8.09	19.7	9.88	19.2	18.8	11.7
Fe_2O_3 (Total)	8.49	11.6	12.4	5.76	16.1	7.84	13.5	8.53	9.67	14.1
Fe_2O_3	7.88	11.4	12.3	5.39	15.8	7.63	13.2	7.60	8.84	14.1
Fe(s)	0.43	0.08	0.08	0.26	0.20	0.15	0.22	0.65	0.58	0.03
MnO	0.12	0.18	0.2	0.09	0.24	0.11	0.2	0.16	0.14	0.21
MgO	8.17	14.3	15.1	5.53	17.6	7.87	15.8	6.03	9.76	14.8
CaO	9.15	7.51	6.61	9.03	5.45	10.02	6.58	10.26	8.93	6.46
Na_2O	1.83	1.09	0.6	2.6	0.67	1.74	0.84	2.52	1.59	1.21
K_2O	0.94	0.69	0.6	2.09	0.14	0.51	0.4	0.99	0.74	0.3
P_2O_5	0.01	0.01	0.01	0.01	0.01	0.01	0.03	0.03	ND	ND
LOI	3.17	3.36	4.16	3.21	0.66	1.02	2.52	2.31	1.73	1.36
S	0.37	0.06	0.06	0.18	0.16	0.11	0.2	0.52	0.47	0.02
Total	**100.2**	**100.0**	**99.82**	**99.78**	**99.83**	**99.62**	**99.37**	**99.41**	**101.0**	**99.18**
Mg#	0.67	0.71	0.71	0.67	0.69	0.67	0.7	0.61	0.94	0.68
Ag (ppm)	0.5	0.5	0.5	0.5	0.5	0.5	0.5	1.5	0.5	0.5
As	0.5	0.2	0.2	0.4	0.2	0.2	0.4	0.4	0.2	0.6
Au	0.91	0.31	0.03	0.07	0.09	0.12	0.11	0.03	0.38	0.01
Ba	170	70	100	270	40	90	70	170	29	63
Ce	2	2.5	1.6	2.1	1.9	3.3	2	1.2	1.9	2.5
Co	57	68	71	43	85	46	81	58	73	86
Cr	166	380	423	118	497	196	363	150	296	469
Cs	1.18	1.15	0.92	0.63	0.39	2.7	1.65	1.1	1.15	1.21
Cu	1525	224	153	425	452	423	812	2060	1580	63
Eu	0.26	0.2	0.15	0.18	0.14	0.34	0.2	0.14	0.2	0.21
La	1.17	1.14	0.65	1.08	1.01	1.48	0.98	0.76	1.07	1.20
Lu	<0.08	<0.08	<0.08	<0.08	0.09	<0.08	0.07	0.06	<0.08	<0.08
Nd	0.80	0.40	0.40	0.40	0.40	0.70	1.10	0.40	1.20	0.90
Ni	1050	577	501	366	717	431	906	1130	968	399
Rb	31	29	10	24	2	46	11	16	12	14
Sb	0.1	0.02	0.04	0.1	0.04	0.03	0.06	0.09	0.04	0.06
Sc	22.9	41.5	37.5	28.4	46.6	7.76	43.9	38.3	25.2	40.9
Hf	0.20	0.11	0.03	0.05	0.19	0.20	0.30	0.21	0.10	0.20
Sm	0.26	0.37	0.19	0.20	0.29	0.23	0.39	0.20	0.20	0.34
Ta	0.016	0.016	0.016	0.016	0.027	0.14	0.028	0.029	0.016	0.03
Tb	0.04	0.10	0.04	0.04	0.10	0.04	0.09	0.08	0.04	0.07
Th	0.08	0.15	0.06	0.06	0.06	0.06	0.14	0.07	0.06	0.11
U	0.07	0.07	0.07	0.07	0.07	0.02	0.07	0.07	0.07	0.08
W	0.2	0.4	0.1	0.1	0.2	<0.1	<0.1	0.1	0.7	2.8
Yb	0.28	0.40	0.33	0.24	0.44	0.07	0.39	0.31	0.20	0.40
Zn	48	58	66	36	88	48	76	100	16	78

$Fe_{(s)} = (1.527*S-0.6592*(Cu-70)/10000-0.5285*(Ni-450)/10000$

SAMPLE	Tz-32	Tz-33	Tz-34	Tz-35	Tz-36	Tz-38	Tz-39	Tz-40	Tz-41	Tz-42
Rock Type	frag meta leuco-gabnor	mat gabnor	frag meta-gabnor	mat meta-gabnor	mat meta-gabnor	frag meta-gabnor	mat meta-gabnor	mat meta-gabnor	mat gabnor	mat leuco-gabnor
SiO_2	49.9	49.9	49.6	50.1	51.6	52.1	49.2	48.9	49.7	48.5
TiO_2	0.13	0.17	0.22	0.18	0.19	0.31	0.45	0.31	0.20	0.16
Al_2O_3	19.5	13.0	7.51	24.1	11.8	7.19	14.8	10.8	12.5	21.0
Fe_2O_3 (Total)	8.16	12.0	16.2	5.56	10.8	11.4	9.40	12.9	15.0	12.7
Fe_2O_3	8.11	11.8	16.0	5.52	10.8	11.0	9.34	10.9	14.4	12.6
Fe(s)	0.03	0.12	0.14	0.03	0.02	0.27	0.04	1.39	0.37	0.05
MnO	0.12	0.16	0.24	0.09	0.18	0.16	0.18	0.22	0.18	0.10
MgO	9.38	15.1	18.3	4.37	13.7	15.9	9.84	13.8	15.2	7.12
CaO	9.03	6.74	4.94	10.9	6.82	11.9	9.15	7.73	6.77	9.68
Na_2O	1.71	1.19	1.26	3.12	1.93	1.09	1.74	1.33	1.15	1.9
K_2O	0.72	0.14	0.37	0.7	0.74	0.4	0.84	0.32	0.26	0.67
P_2O_5	ND	ND	ND	0.01	ND	0.01	ND	ND	ND	0.01
LOI	2.91	1.63	2.44	1.78	3.13	2.26	2.63	1.43	1.72	2.28
S	0.02	0.09	0.1	0.01	0.01	0.02	0.95	0.25	0.03	1.33
Total	**100.3**	**98.87**	**100.0**	**100.4**	**98.99**	**99.30**	**101.8**	**98.98**	**99.25**	**99.95**
Mg#	0.7	0.72	0.98	0.7	0.72	0.77	0.64	0.65	0.7	0.68
Ag (ppm)	1	0.5	0.5	0.5	0.5	0.8	0.8	0.5	0.5	2.9
As	0.3	0.2	0.5	0.2	0.3	0.2	0.3	0.3	0.8	0.2
Au	0.01	0.04	0.08	0.00	0.04	0.01	0.13	0.03	0.01	0.57
Ba	113	22	45	136	182	92	140	65	54	205
Ce	2.2	1.7	1.7	3.6	7.9	15.7	4.2	3.1	2.3	4.1
Co	52	86	103	27	67	52	98	91	83	103
Cr	256	443	545	109	380	1133	235	383	483	213
Cs	2.03	0.71	0.99	2.79	1.21	0.66	1.37	1.12	0.74	2.27
Cu	59	167	179	31	73	40	767	188	47	3369
Eu	0.19	0.13	0.15	0.28	0.3	0.46	0.33	0.25	0.18	0.38
La	0.99	0.83	0.95	1.16	2.86	6.78	1.14	0.61	1.34	1.18
Lu	<0.08	<0.08	<0.08	<0.08	0.10	0.13	0.09	0.09	<0.08	<0.08
Nd	0.40	0.20	0.40	1.60	2.80	6.70	1.30	0.50	2.00	0.90
Ni	242	480	541	56	388	230	663	337	332	2671
Rb	17	4	9	24	17	4	20	7	10	28
Sb	0.05	0.02	0.06	0.05	0.05	0.09	0.12	0.07	0.08	0.03
Sc	22.9	35.2	44.7	19.0	36.4	66.5	46.5	48.3	17.5	37.9
Hf	0.10	0.10	0.19	0.24	1.58	0.76	0.35	0.21	0.26	0.18
Sm	0.21	0.16	0.26	0.28	0.94	1.66	0.57	0.36	0.28	0.23
Ta	0.012	0.016	0.016	0.034	0.178	0.072	0.016	0.016	0.024	0.016
Tb	0.04	0.04	0.05	0.06	0.14	0.19	0.12	0.07	0.04	0.05
Th	0.06	0.06	0.14	0.22	2.89	0.95	0.13	0.06	0.18	0.06
U	0.07	0.07	0.07	0.08	0.55	0.18	0.07	0.14	0.07	0.07
W	4.7	2.9	6	2.1	5	0.1	0.7	11.8	7.6	5
Yb	0.22	0.32	0.43	0.21	0.66	0.89	0.51	0.50	0.20	0.34
Zn	50	79	106	31	72	4	4	106	67	106

$Fe_{(s)} = (1.527*S-0.6592*(Cu-70)/10000-0.5285*(Ni-450)/10000$

Sample Rock Type	Rz-01 Chlor-act schist	Rz-02 micro-breccia	Rz-03 Chlor-act schist	Rz-04 Chlor-act schist	Rz-05 Chlor-act schist	Rz-06 micro-breccia	Rz-07 Chlor-act schist	Rz-08 Chlor-act schist	Rz-09 micro-breccia	Rz-10 Micro-breccia
Au (ppb)	5381	192	605	1740	4736	328	226	1382	149	195
Ir	0.05	0.03	0.11	0.09	0.57	0.02	0.04	0.40	0.14	0.17
Os	0.3	0.3	1.8	1.7	0.3	0.7	0.3	2.8	0.7	3.9
Pd	69	89	6057	4103	7808	82	650	8391	85	143
Pt	18	27	295	329	696	5	115	933.8	24	43
Re	0.1	0.2	0.3	0.1	3.9	0.2	0.1	ND	ND	ND
Rh	ND	ND	ND	ND	ND	ND	ND	ND	0.1	ND
Ru	3.8	3.3	5.8	6.1	5.3	2	2	3.6	ND	2
Pd/Pt	3.8	3.3	20.5	12.5	11.2	16.4	5.7	9.0	3.5	3.3
Pd/Ir	1500	2967	55064	45589	13698	4100	15318	20978	607	841
CIPW NOWM $FE^{+2}/Fe^{+3} = 0.8$										
Orthoclase	3.63	1.51	0.13	0.45	0.52	1.37	3.50	0.25	1.45	1.25
Albite	19.0	19.4	2.42	7.79	4.05	12.1	13.8	6.95	18.2	19.3
Anorthite	39.7	37.0	22.0	25.5	12.6	24.1	29.2	22.1	37.5	30.7
An'	0.68	0.66	0.90	0.77	0.76	0.67	0.68	0.76	0.67	0.61
Plagioclase	58.8	56.4	24.4	33.3	16.6	36.3	43.1	29.1	55.7	50.1
Nepheline	0.01	0	0	0	0	0	0	0	0	0
Diopside	10.2	12.8	12.5	1.15	13.8	12.7	2.94	6.08	12.1	15.3
Hypersthene	22.6	22.9	38.3	53.9	61.7	44.2	36.1	51.1	27.6	22.4
Olivine	2.1	3.14	21.3	7.58	0	0	11.2	10.2	0	7.46
Magnetite	2.04	2.79	3.04	3.32	4.79	4.39	2.89	3.09	2.74	3.14
Chromite	0.04	0.04	0.21	0.11	0.11	0.06	0.05	0.18	0.04	0.05
Ilmenite	0.67	0.31	0.18	0.25	0.58	0.65	0.24	0.18	0.31	0.32
Apatite	0.02	0	0	0	0	0	0	0	0	0
Total	**100**	**100**	**100**	**100**	**100**	**100**	**100**	**100**	**100**	**100**

Sample Rock Type	Rz-11 micro- breccia	Rz-12 Chlor- act schist	Rz-13 Chlor- act schist	Rz-14 Chlor- act schist	Rz-15 Chlor-act schist	Rz-16 Chlor-act schist	Rz-17 Chlor-act schist
Au (ppb)	166	871	2491	2733	343	1291	99510
Ir	ND	0.22	0.13	0.06	0.05	0.05	0.81
Os	3.9	2.7	1.8	0.3	1	0.3	0.3
Pd	87	6054	4133	1760	957	886	52316
Pt	16	475	237	136	91	104	3078
Re	ND	0.1	0.1	0.1	0.1	0.5	2.3
Rh	0.4	ND	ND	ND	ND	ND	9.2
Ru	ND	6.1	5.7	2	2.6	2	33
Pd/Pt	5.4	12.7	17.4	12.9	10.5	8.5	17.0
Pd/Ir	-	27518	31792	29891	18452	18700	64588
CIPW NOWM $FE^{+2}/Fe^{+3} = 0.8$							
Orthoclase	1.51	0.12	0.25	0.06	0.89	2.92	3.46
Albite	19.6	2.03	3.25	1.43	3.91	23.5	11.6
Anorthite	37.1	17.4	22.0	19.9	27.7	45.5	44.2
An'	0.65	0.90	0.87	0.93	0.88	0.66	0.79
Plagioclase	56.7	19.4	25.3	21.3	31.6	69.1	55.9
Nepheline	0	0	0	0	0	0.03	0
Diopside	12.6	13.9	4.81	15.3	3.42	1.03	6.09
Hypersthene	23.2	62.5	63.2	58.1	54.4	23.3	31.6
Olivine	2.80	0	2.8	1.88	6.16	0	1.02
Magnetite	2.77	2.78	3.41	3.07	3.2	1.42	2.0
Chromite	0.04	0.19	0.13	0.19	0.14	0.02	0.05
Ilmenite	0.31	0.18	0.26	0.2	0.24	0.7	0.22
Apatite	0	0	0	0	0	0.1	0
Total	**100**	**100**	**100**	**100**	**100**	**100**	**100**

Sample	Rz-18	Rz-19	Rz-20	Rz-21	Rz-22	Rz-23	Rz-24	Rz-25	Rz-26	Rz-27
Rock Type	frag meta-gabnor	frag meta lecuo-gabnor	frag meta gabnor	frag-vari meta gabnor	frag leuco-gabnor	frag meta-gabnor	frag-vari meta gabnor	frag meta-gabnor	frag meta gabnor	frag meta-gabnor
Au (ppb)	512	1357	880	234	1398	627	468	1223	641	634
Ir	0.05	0.1	0.04	0.01	0.01	0	0	0.05	0.02	0.61
Os	0.9	0.3	0.3	0.3	0.3	1.2	0.3	0.3	0.3	0.7
Pd	259	822	405	35	ND	185	ND	1088	288	111
Pt	47	114	72	18	1	ND	ND	ND	43	26
Re	0.3	0.5	0.3	0.1	ND	0.3	0.1	0.7	0.38	0.36
Rh	ND	1.1	1	0.3	1.9	0.5	2.5	1.9	0.4	0.6
Ru	4.26	0	0	0	0	10	2	2	2	5
Pd/Pt	5.5	7.2	5.6	1.9	-	-	-	-	6.7	4.3
Pd/Ir	4812	8220	10125	3500	-	-	-	21760	14400	182
CIPW NORM	**FE^{+2}/Fe^{+3} = 0.8**									
Orthoclase	6.80	3.67	3.46	3.18	5.95	4.44	5.14	5.81	5.79	0.18
Albite	20.6	16.7	16.2	18.5	19.3	12.7	23.7	16.5	22.8	2.82
Anorthite	54.2	24.2	27.6	35.7	42.5	26.3	35.5	42.6	37.8	8.18
An'	0.72	0.59	0.63	0.66	0.69	0.67	0.60	0.72	0.62	0.74
Plagioclase	74.9	40.9	43.8	54.3	61.8	39.1	59.2	59.1	60.6	11
Nepheline	0	0	0	0	0	0	0	0	0.01	0
Diopside	0.06	19.3	12.1	14.1	0.88	10.6	12.2	4.05	7.47	34.1
Hypersthene	7.55	18.4	27.3	24.1	27.1	33.4	14.4	27.9	17.9	48.9
Olivine	9.30	14.0	9.73	2.04	1.93	9.21	6.68	1.09	5.94	2.47
Magnetite	1.31	3.21	3.2	2.13	2.17	2.9	2.11	1.84	2.26	3.1
Chromite	0.03	0.07	0.07	0.05	0.04	0.06	0.03	0.06	0.03	0.24
Ilmenite	0.12	0.38	0.36	0.15	0.18	0.32	0.31	0.18	0.04	0.28
Apatite	0	0	0	0	0	0	0	0	0.02	0
Total	**100**	**100**	**100**	**100**	**100**	**100**	**100**	**100**	**100**	**100**

SAMPLE	Rz-28	Rz-29	Rz-30	Rz-31	Rz-32	Rz-33	Rz-34	Rz-35	Rz-36	Rz-38
Rock Type	frag-vari meta-gabnor	frag meta - gabnor	mat gabnor	frag-vari meta-gabnor	frag meta-gabnor	frag leuco-gabnor	frag meta-gabnor	frag meta-gabnor	mat meta-gabnor	mat gabnor
Au (ppb)	182	385	4391	270	1603	199	8000	306	1041	601
Ir	0.05	0.03	0.49	0.04	0.05	0.04	0.03	0.04	0.05	0.33
Os	0.3	0.30	2	0.3	0.30	1.30	0.30	0.3	0.3	0.3
Pd	10	6.00	2636	89	366.00	5.00	41.00	98	819	293
Pt	4	5.00	421	26	105.00	6.00	6.00	12	97	35
Re	0.1	0.10	1.8	0.1	0.32	1.23	0.10	0.2	0.1	0.1
Rh	0.4	0.40	5.1	0.4	0.90	0.60	0.40	0.4	0.4	0.7
Ru	2	4.00	2	2	3.00	2.00	2.00	2	2	2
Pd/Pt	2.5	1.2	6.3	3.4	3.5	0.8	6.8	8.2	8.4	8.4
Pd/Ir	200	200	5380	2225	7320	125	1367	2450	16380	888
CIPW NOWM $FE^{+2}/Fe^{+3} = 0.8$										
Orthoclase	5.59	4.86	2.97	3.21	5.18	4.52	7.71	4.31	3.56	1.09
Albite	29.5	20.1	8.84	21.8	23.1	19.1	30.9	18.1	31.6	6.48
Anorthite	46.8	33.4	22.7	33.2	35.9	39.0	37.5	38.2	48.2	12.2
An'	0.61	0.62	0.72	0.60	0.61	0.67	0.55	0.68	0.60	0.65
Plagioclase	76.3	53.6	31.5	55.1	59.0	58.1	68.4	56.3	79.8	18.7
Nepheline	0	0	0	0	0	0	0	0	0	0.01
Diopside	8.94	18.9	8.84	10.1	8.3	10.0	1.48	6.68	2.51	39.3
Hypersthene	2.33	15.5	48.8	21.7	18.9	17.7	2.62	26.4	7.67	34.4
Olivine	5.70	4.94	3.65	7.23	6.59	7.48	17.7	4.16	5.10	1.75
Magnetite	1.03	1.99	4.01	2.44	1.92	1.91	1.91	1.88	1.26	3.66
Chromite	0.02	0.03	0.08	0.04	0.03	0.05	0.03	0.06	0.01	0.31
Ilmenite	0.11	0.17	0.41	0.14	0.16	0.21	0.14	0.19	0.08	0.89
Apatite	0	0	0	0	0	0	0	0	0	0.02
Total	**100**	**100**	**100**	**100**	**100**	**100**	**100**	**100**	**100**	**100**

SAMPLE Rock Type	Rz-39 mat meta- gabnor	Rz-40 mat gabnor	Rz-41 mat gabnor	Rz-42 mat meta- gabnor	Rz-43 mat meta- gabnor	Rz-44 mat meta- gabnor	Rz-46 mat meta gabnor	Rz-47 mat meta- gabnor	Rz-48 mat meta- gabnor	Rz-49 mat meta- gabnor
Au (ppb)	281	602	4646	1524	1075	1862	11806	1129	1764	38
Ir	0.02	0.21	0.21	0.66	0.18	0.92	1.12	0.09	0.04	0.22
Os	0.3	2	0.3	2.4	0.9	2.7	4.3	0.30	0.30	0.9
Pd	225	251	1332	1952	682	3747	12441	488.00	105.00	4
Pt	36	198	204	330	42	423	1669	84.00	49.00	4
Re	0.1	0.3	0.6	1.2	0.3	0.4	3.1	0.10	0.10	0.2
Rh	0.4	0.6	2.3	2	1.4	7.4	11.8	ND	0.40	0.4
Ru	2	2	6	6	4	5	7	16.00	7.00	3
Pd/Pt	6.3	1.3	6.5	5.9	16.2	8.9	7.5	5.8	2.1	1.0
Pd/Ir	11250	1195	6343	2958	3789	4073	11108	5422	2625	18
CIPW NOWM $FE^{+2}/Fe^{+3} = 0.8$										
Orthoclase	2.12	0.88	3.17	0.68	4.88	5.98	5.73	5.94	6.32	1.80
Albite	8.74	4.47	12.6	6.72	19.7	16.8	33.3	22.8	21.5	6.56
Anorthite	23.3	16	27.5	13.8	36.2	37.0	25.3	28.2	39.0	13.9
An'	0.73	0.78	0.68	0.67	0.65	0.69	0.43	0.55	0.64	0.68
Plagioclase	32.0	20.4	40.1	20.5	56.0	53.9	58.6	51	60.5	20.5
Nepheline	0	0	0	0	0.01	0.01	0.17	0	0.01	0
Diopside	16.7	26.0	9.75	36.6	7.32	5.77	5.37	14.5	5.05	28.2
Hypersthene	36.8	42.2	36.0	26.3	19.4	26.3	17.2	10.7	14.1	39
Olivine	8.61	6.43	6.98	11.8	9.60	4.82	0	14.8	11.5	6.86
Magnetite	3.39	3.24	3.56	3.47	2.48	2.60	3.55	2.75	2.19	2.86
Chromite	0.10	0.33	0.07	0.25	0.05	0.06	0	0.04	0.03	0.32
Ilmenite	0.28	0.78	0.47	0.65	0.34	0.67	2.35	0.3	0.27	0.72
Apatite	0	0	0	0	0.02	0.05	0.62	0	0.02	0
Total	**100**	**100**	**100**	**100**	**100**	**100**	**100**	**100**	**100**	**100**

SAMPLE Rock Type	Rz-50 mat meta- gabnor	Rz-51 mat meta- gabnor	Rz-52 mat meta- gabnor	Rz-53 mat meta- gabnor	Rz-54 mat meta- gabnor	Rz-55 mat meta- gabnor
Au (ppb)	2861	339	847	646	4334	6041
Ir	0.07	0.08	0.05	0.02	0.18	0.42
Os	0.3	1.2	0.3	0.3	0.3	0.3
Pd	757	1323	435	108	2714	3583
Pt	110	123	64	18	396	461
Re	0.51	0.21	0.28	0.27	0.74	0.5
Rh	1.9	1.6	1.2	0.5	2.7	4.7
Ru	2	2	7	2	2	2
Pd/Pt	6.9	10.8	6.8	6.0	6.9	7.8
Pd/Ir	10814	16538	8700	5400	15078	8531
CIPW NOWM $FE^{+2}/Fe^{+3} = 0.8$						
Orthoclase	2.91	7.26	5.25	5.53	7.57	3.51
Albite	11.7	19.1	24.1	21.0	18.5	10.5
Anorthite	27.1	55.2	37.8	36.1	33.5	24.0
An'	0.70	0.74	0.61	0.63	0.64	0.69
Plagioclase	38.8	74.3	61.9	57.1	52.1	34.6
Nepheline	0	4.05	0	0	0	0
Diopside	10.1	2.92	7.31	9.27	3.23	8.17
Hypersthene	38.4	0	17.3	18.7	28.6	38.9
Olivine	5.84	10.1	6.15	6.88	5.62	10.8
Magnetite	3.63	1.24	1.87	2.24	2.64	3.74
Chromite	0.07	0.03	0.02	0.03	0.04	0.08
Ilmenite	0.47	0.16	0.21	0.27	0.36	0.37
Apatite	0	0	0	0	0	0
Total	**100**	**100**	**100**	**100**	**100**	**100**

SAMPLE Rock Type	Tz-01 frag gabnor	Tz-02 frag leuco-gabnor	Tz-03 frag gabnor	Tz-04 frag gabnor	Tz-05 frag leuco-gabnor	Tz-06 mat gabnor	Tz-07 frag gabnor	Tz-08 mat gabnor	Tz-09 peg meta-gabnor	Tz-10 frag gabnor
Au (ppb)	478	17	41	254	132	440	188	15	13	15
Ir	0.76	0.066	0.06	0.31	0.24	0.64	0.32	0.04	0.73	0.16
Os	0.3	0.3	0.3	0.3	1.5	2.9	0.3	0.3	0.3	0.3
Pd	5446	111	205	1705	137	3593	1849	19	53	1209
Pt	632	14	69	249	18	490	316	11	24	158
Re	2.4	0.14	0.1	0.5	1	1.5	0.5	0.1	0.27	0.25
Rh	0.1	1.4	2.3	2.5	4	1.9	3.4	1.5	1.7	0.6
Ru	2	2	2	9	2	2	2	2	2	2
Pd/Pt	8.6	7.9	3.0	6.8	7.6	7.3	5.9	1.7	2.2	7.7
Pd/Ir	7166	1685	3417	5500	571	5614	5778	475	73	7556
CIPW NOWM	**$FE^{+2}/Fe^{+3} = 0.8$**									
Orthoclase	0.92	1.33	1.04	0.97	4.12	1.49	1.16	1.63	3.72	0.86
Albite	11.4	14.4	12.5	10.2	19.4	7.02	10.5	9.69	12.3	9.80
Anorthite	38.1	46.3	37.0	38.9	37.5	25.1	29.4	32.4	29.8	34.6
An'	0.77	0.76	0.75	0.79	0.66	0.78	0.74	0.77	0.71	0.78
Plagioclase	49.5	60.7	49.5	49.1	56.9	32.1	40.0	42.0	42.2	44.4
Nepheline	0.02	0.01	0.01	0.01	0.01	0.02	0.01	0.01	0.01	0.01
Diopside	7.93	6.36	6.51	6.07	26.1	7.82	8.83	6.45	14.4	5.81
Hypersthene	37.9	28.6	39.1	38.3	5.56	52.1	45.0	45.3	34.4	45.2
Olivine	0	0.33	0	2.32	5.07	0	0	0	1.11	0.09
Magnetite	3.25	2.38	3.3	2.95	1.89	4.34	3.88	3.59	3.32	3.34
Chromite	0.08	0.06	0.09	0.07	0.08	0.10	0.09	0.09	0.08	0.09
Ilmenite	0.45	0.27	0.33	0.29	0.28	0.58	0.59	0.43	0.65	0.35
Apatite	0.07	0.02	0.02	0.02	0.02	0.07	0.02	0.02	0.05	0.02
Total	**100**	**100**	**100**	**100**	**100**	**100**	**100**	**100**	**100**	**100**

SAMPLE Rock Type	Tz-11 frag gabnor	Tz-12 frag leuco- gabnor	Tz-13 frag meta- gabnor	Tz-14 frag meta- gabnor	Tz-15 mat meta- gabnor	Tz-16 mat meta- gabnor	Tz-17 mat meta- gabnor	Tz-19 mat meta- gabnor	Tz-20 peg leuco- gabnor	Tz-21 Mat meta- gabnor
Au (ppb)	1372	146	164	351	209	14	23	3	691	61
Ir	0.12	0.13	0.17	0.08	0.38	0.39	0.05	0.72	0.32	0.86
Os	0.3	0.3	0.3	0.3	0.3	0.3	0.3	0.3	0.3	5
Pd	48	577	866	212	2857	2291	95	4646	1662	5419
Pt	22	70	123	53	396	459	27	565	171	905
Re	0.1	0.32	0.1	0.24	1.05	0.9	0.19	2	0.1	1.6
Rh	2.3	3.7	4.5	4.4	6.4	1.4	11.4	4.1	ND	0.4
Ru	4	2	22	2	2	2	2	2	2	2
Pd/Pt	2.2	8.2	7.0	4.0	7.2	5.0	3.5	8.2	9.7	6.0
Pd/Ir	400	4438	5094	2650	7518	5874	1900	6453	5194	6301
CIPW NOWM	**$FE^{+2}/Fe^{+3} = 0.8$**									
Orthoclase	1.22	6.33	0.38	3.63	2.10	0.69	1.0	1.72	10.0	1.74
Albite	10.3	16.3	0.81	7.96	5.29	2.61	14.0	7.12	23.9	2.03
Anorthite	27.9	43.9		34.7	28.8	18.1	27.5	24.1	33.7	25.7
An'	0.73	0.73		0.81	0.85	0.87	0.66	0.77	0.58	0.93
Plagioclase	38.2	60.2	0.81	42.7	34.1	20.7	41.5	31.2	57.6	27.7
Nepheline	0.01	0	0.01	0.01	0.01	0.01	0.01	0.01	0.03	0
Diopside	5.75	4.02	10.8	2.42	6.21	6.20	6.05	7.5	8.99	10.5
Hypersthene	49.2	19.7	61.8	47.3	51.8	65.1	42.3	54.6	13.8	52.9
Olivine	0	7.07	0	0	0	0	4.93	0	7.09	0
Magnetite	4.11	2.36	4.77	3.4	3.97	4.81	3.65	4.35	2.03	4.2
Chromite	0.08	0.04	0.10	0.06	0.09	0.12	0.07	0.10	0.04	0.11
Ilmenite	0.56	0.28	0.55	0.4	0.41	0.5	0.44	0.47	0.45	0.48
Apatite	0.02	0	0.03	0.05	0.03	0.03	0.03	0.02	0.10	0
Total	**100**	**100**	**100**	**100**	**100**	**100**	**100**	**100**	**100**	**100**

SAMPLE Rock Type	Tz-22 frag meta- gabnor	Tz-23 mat meta- gabnor	Tz-24 frag meta- gabnor	Tz-25 mat meta- gabnor	Tz-26 mat meta- gabnor	Tz-27 peg leuco- gabnor	Tz-28 peg gabnor	Tz-29 peg leuco- gabnor	Tz-30 mat leuco- gabnor	Tz-31 mat gabnor
Au (ppb)	906	313	34	70	85	123	111	32	19000	115
Ir	0.27	0.06	0.92	0.95	0.1	0.07	0.18	0.07	0.38	0.02
Os	0.3	0.3	0.3	0.3	0.3	8.2	1	1.2	0.3	0.3
Pd	1964	50	200	940	790	840	950	2800	3242	50
Pt	239	19	43	144	102	115	122	335	411	26
Re	0.38	0.1	0.1	0.25	0.22	0.26	0.4	0.1	0.9	0.1
Rh	ND	0.4	ND	ND	ND	ND	0	ND	4.5	0.7
Ru	2	2	2	ND	2	2	3.2	3.1	2	2
Pd/Pt	8.2	2.6	4.7	6.5	7.7	7.3	7.8	8.4	7.9	1.9
Pd/Ir	7274	833	217	989	7900	12000	5278	40000	8532	2500
CIPW NOWM $FE^{+2}/Fe^{+3} = 0.8$										
Orthoclase	5.84	4.28	3.76	12.9	0.85	3.11	2.49	6.16	4.49	1.84
Albite	16.2	9.66	5.38	23.0	5.82	15.0	7.47	22.4	13.7	10.5
Anorthite	44.4	27.4	27.8	44.1	19.1	45.6	23.1	40.4	43.1	26.5
An'	0.73	0.74	0.84	0.66	0.77	0.75	0.76	0.64	0.76	0.71
Plagioclase	60.7	37.1	33.2	67.1	24.9	60.7	30.6	62.8	56.9	37.1
Nepheline	0.01	0.01	0.01	0	0.01	0	0.02	0.02	0	0
Diopside	2.53	9.25	5.49	2.3	6.9	4.29	8.86	10.5	1.81	5.35
Hypersthene	24.3	41.3	52.6	5.33	60.8	27.0	53.4	10.9	31.9	46.6
Olivine	4.04	4.11	0	10.4	0	0	0	6.56	2	4.36
Magnetite	2.40	3.49	3.78	1.63	4.73	2.27	4.03	2.33	2.63	4.24
Chromite	0.04	0.09	0.10	0.03	0.11	0.04	0.08	0.03	0.07	0.10
Ilmenite	0.30	0.48	0.34	0.36	0.49	0.35	0.52	0.64	0.29	0.49
Apatite	0.02	0.02	0.03	0	0.02	0	0.07	0.07	0	0
Total	**100**	**100**	**100**	**100**	**100**	**100**	**100**	**100**	**100**	**100**

SAMPLE Rock Type	Tz-32 frag meta- gabnor	Tz-33 mat gabnor	Tz-34 frag meta- gabnor	Tz-35 mat meta- gabnor	Tz-36 mat meta- gabnor	Tz-38 frag meta- gabnor	Tz-39 mat meta- gabnor	Tz-40 mat meta- gabnor	Tz-41 mat gabnor	Tz-42 mat leuco - gabnor
Au (ppb)	149	426	768	17	401	126	1344	288	5725	78
Ir	0.03	0.04	0.04	0.03	0.05	ND	0.38	0.11	0.56	0.03
Os	1	0.8	0.1	0.9	0.3	0.3	1.6	0.3	3.9	0.3
Pd	83	399	347	9	509	19	1445	130	3012	87
Pt	12	51	72	21	85	7	262	25	557	5
Re	0.1	0.2	0.2	0.1	0.6	0.3	2.6	0.6	3	0.1
Rh	0.4	0.4	0.9	0.7	1	0.4	2.5	0.7	5.3	0.8
Ru	2	2	2	4	5	2	2	2	9	6
Pd/Pt	6.9	7.8	4.8	0.4	6.0	2.7	5.5	5.2	5.4	17.4
Pd/Ir	2767	9975	8675	300	10180	-	3803	1182	5379	2900
CIPW NOWM $FE^{+2}/Fe^{+3} = 0.8$										
Orthoclase	4.40	0.86	2.28	4.22	4.61	3.59	2.46	5.18	1.98	1.60
Albite	14.9	10.4	11.1	26.8	17.2	33.9	9.58	15.3	11.7	10.0
Anorthite	45.1	31.0	14.3	50.8	22.6	26.8	14.0	31.4	23.7	29.2
An'	0.75	0.75	0.56	0.65	0.57	0.44	0.60	0.67	0.67	0.74
Plagioclase	60.0	41.5	25.4	77.7	39.8	60.7	23.6	46.8	35.5	39.3
Nepheline	0	0	0	0.01	0	0.20	0.01	0	0	0
Diopside	1.02	3.02	9.03	3.59	10.4	3.69	37.9	12.8	13.1	4.48
Hypersthene	28.1	46.7	46.1	3.77	34.2	16.6	28.4	27.9	37.1	45.3
Olivine	3.81	3.97	12.0	8.68	7.24	0	3.96	3.08	7.20	5.01
Magnetite	2.43	3.59	4.85	1.63	3.30	3.24	2.81	3.31	4.38	3.81
Chromite	0.06	0.1	0.12	0.02	0.09	0	0.25	0.05	0.09	0.11
Ilmenite	0.26	0.34	0.43	0.35	0.38	2.31	0.61	0.89	0.61	0.39
Apatite	0	0	0	0.02	0	0.7	0.02	0	0	0
Total	**100**	**100**	**100**	**100**	**100**	**100**	**100**	**100**	**100**	**100**

APPENDIX

II

Mineral Data

Abbreviations used:

Rz	= Roby Zone (High-grade Zone samples are from Rz-01 to Rz17, inclusive)
Tz	= Twilight Zone
Chlor-talc	= chlorite-talc schist
Sch	= Schist
Meta-gabnor	= metagabbronorite
Leucogabnor	= leucogabbronorite
Leucogab	= leucogabbro
Gabnor	= gabbronorite
ND	= not detected
N/A	= not analysed
Frag	= fragment
Mat	= matrix
Peg	= pegmatite
Frag-vari-	= varitextured fragment

B-1 PLAGIOCLASE

Microprobe Analyses

SAMPLE	RZ9-1 1	RZ9-1 2	RZ9-2 1	RZ9 C1b	RZ33-6 1	RZ33 C6 a	RZ33 C6 b	RZ33 C6 c
SiO_2 (%)	51.67	52.38	50.75	52.05	50.43	51.18	49.82	50.04
TiO_2	ND	ND	ND	0.09	0.042	ND	ND	ND
Al_2O_3	30.35	30.03	30.12	29.28	30.79	31.29	31.05	31.22
MgO	ND	0.001	0.005	ND	ND	ND	0.019	ND
CaO	12.38	12.55	12.48	12.72	13.493	13.51	13.83	13.94
FeO	0.07	0.04	0.08	0.18	0.13	0.18	0.2	0.18
Na_2O	4.51	4.41	4.46	4.54	3.82	3.77	3.38	3.65
K_2O	0.027	0.029	0.026	0.027	0.059	0.14	0.17	0.09
Total	**98.99**	**99.44**	**97.92**	**98.99**	**98.75**	**100.14**	**98.59**	**99.2**
Si	2.37	2.39	2.35	4.97	2.32	3.83	4.03	4.26
Al	1.64	1.61	1.65	5.59	1.67	4.68	5.02	5.31
Mg	-	0.0001	0.0003	-	-	-	0.002	-
Ca	0.61	0.61	0.62	1.21	0.67	1.01	1.12	1.19
Fe	0.003	0.0015	0.003	0.017	0.005	0.01	0.016	0.02
Na	0.4	0.39	0.4	0.87	0.34	0.56	0.55	0.62
K	0.0016	0.002	0.002	0.005	0.0034	0.02	0.026	0.02
An	60.18	61.03	60.65	58.21	65.93	63.33	66.1	65.06

SAMPLE	Tz7-1a	Tz7-4a	Tz7-4b	Tz7-5a	Tz7-5b	Tz7-6a	TZ29 C4 c
SiO_2	52.76	52.12	51.75	48.78	52.71	51.82	53.42
TiO_2	0.02	ND	0.03	0.03	0.04	0.06	0.09
Al_2O_3	30.07	30.68	30.67	32.66	30.86	30.5	29.29
MgO	0.001	0.005	ND	0.015	0.83	0.02	0.018
CaO	12.68	13.24	13.47	15.85	12.89	13.14	11.65
FeO	0.17	0.15	0.26	0.31	0.15	0.13	0.15
Na_2O	4.5	4.13	3.97	2.61	4.21	4.18	4.81
K_2O	0.06	0.1	0.15	0.07	0.07	0.09	0.06
Total	**100.45**	**100.52**	**100.34**	**100.41**	**101.79**	**100.02**	**99.68**
Si	2.48	2.68	2.91	2.96	3.42	3.65	4.8
Al	2.82	3.16	3.45	3.96	3.99	4.3	5.27
Mg		0.0002		0.001	0.05	0.0015	0.0016
Ca	0.59	0.68	0.76	0.96	0.84	0.93	1.05
Fe	0.0081	0.0077	0.014	0.018	0.0099	0.0092	0.013
Na	0.42	0.42	0.45	0.32	0.55	0.59	0.87
K	0.0057	0.01	0.016	0.0088	0.0093	0.012	0.01
An	58.15	61	62.07	74.42	60.05	60.61	54.45

PLAGIOCLASE

LA-ICP-MS Analyses

SAMPLE	Rz9 c1-1	Rz9 c2-1	Rz9 c2-2	Rz9 c2-3	Rz9 c5-1	Rz9 c5-2	Rz 9 point 1-1	Rz 9 point 1-2	Rz33 c6-1	Rz33 c6-2	Rz33 c6-3
Ca (%)	12.71	12.37	12.55	12.51	12.51	12.51	12.37	12.55	13.51	13.82	13.93
^{85}Rb (ppm)	0.90	1.91	0.91	1.49	0.13	1.38	0.29	0.41	3.02	0.64	7.29
^{88}Sr	395	288	309	412	280	302	405	408	538	540	589
^{89}Y	0.09	0.07	0.08	0.12	0.08	0.07	0.17	0.17	0.36	0.31	0.36
^{133}Cs	0.62	0.42	0.51	0.53	0.11	1.04	0.11	0.22	0.66	0.41	0.88
^{137}Ba	71	71	73	104	61	47	102	89	158	144	180
^{139}La	1.91	0.58	0.91	2.33	0.44	0.56	1.26	0.72	1.48	0.94	1.24
^{140}Ce	2.67	1.08	1.76	3.45	0.75	0.98	2.43	1.28	2.88	1.81	2.76
^{141}Pr	0.25	0.11	0.15	0.31	0.075	0.09	0.22	0.12	0.28	0.18	0.27
^{146}Nd	0.77	0.28	0.47	0.95	0.25	0.32	0.66	0.42	0.94	0.66	0.95
^{147}Sm	0.07	0.03	0.06	0.08	0.01	0.06	0.12	0.08	0.18	0.12	0.17
^{153}Eu	0.23	0.19	0.21	0.29	0.17	0.13	0.29	0.27	0.40	0.42	0.47
^{157}Gd	0.08	0.04	0.04	0.08	0.04	0.04	0.07	0.07	0.04	0.04	0.28
^{159}Tb	DL	DL	DL	DL	DL	DL	DL	0.01	DL	0.02	0.02
^{163}Dy	0.025	0.012	0.02	0.03	0.002	0.02	0.03	0.03	0.08	0.05	0.05
^{165}Ho	0.005	0.001	0.001	0.006	<0.001	<0.001	<0.001	<0.001	0.013	<0.001	0.01
^{166}Er	0.003	0.003	0.01	0.005	0.007	0.007	0.01	0.01	0.03	0.03	0.03
^{169}Tm	0.001	<0.001	0.001	0.002	0.002	<0.001	0.002	0.002	0.005	0.003	0.003
^{172}Yb	0.006	0.008	<0.001	0.008	0.005	0.006	0.006	0.017	<0.001	0.02	0.011
^{175}Lu	0.001	0.001	0.001	0.001	0.001	0.001	0.002	0.005	0.01	0.004	0.005
^{181}Ta	0.001	0.001	0.001	0.001	0.001	0.004	0.001	0.001	0.004	0.003	0.003
^{208}Pb	1.02	0.67	1.03	1.08	0.71	0.95	1.09	1.07	5.55	3.39	12.0

Ca – value is obtained by microprobe analysis and used as internal standard in ICPMS trace element analysis

SAMPLE	Tz7 c1-3	Tz7 c1-4	Tz7 c1-5	Tz7 c4-2	Tz7 c4-4	Tz7 c5-3	Tz7 c6-2	Tz7 c6-3	Tz7 c6-6
Ca (%)	12.68	12.68	12.68	13.24	13.47	12.89	13.14	13.14	13.14
^{85}Rb (ppm)	0.16	0.41	0.65	2.00	1.58	0.84	7.98	0.37	0.84
^{88}Sr	399	400	344	417	411	291	343	389	322
^{89}Y	0.22	0.32	0.22	0.23	0.27	0.16	0.17	0.18	0.22
^{133}Cs	0.13	0.13	0.37	0.55	0.14	0.23	1.86	0.05	0.02
^{137}Ba	93	108	60	146	123	112	104	110	93
^{139}La	3.08	2.55	3.01	3.03	2.41	2.15	1.74	2.22	2.05
^{140}Ce	4.74	4.11	4.15	5.22	5.04	3.99	3.30	4.11	3.76
^{141}Pr	0.45	0.41	0.42	0.45	0.45	0.36	0.31	0.39	0.35
^{146}Nd	1.54	1.39	1.43	1.43	1.47	1.17	1.08	1.27	1.17
^{147}Sm	0.15	0.19	0.16	0.16	0.20	0.11	0.15	0.17	0.14
^{153}Eu	0.37	0.38	0.33	0.40	0.38	0.28	0.30	0.36	0.28
^{157}Gd	0.20	0.19	0.26	0.21	0.16	0.10	0.09	0.07	0.11
^{159}Tb	0.01	0.01	0.01	0.02	0.02	DL	DL	DL	0.01
^{163}Dy	0.05	0.08	0.05	0.04	0.06	0.03	0.031	0.041	0.05
^{165}Ho	<0.001	0.01	<0.001	0.01	0.01	0.00	0.001	0.001	0.001
^{166}Er	0.03	0.02	0.03	0.01	0.03	0.02	0.008	0.007	0.005
^{169}Tm	0.003	0.004	0.004	<0.001	<0.001	<0.001	0.002	0.003	DL
^{172}Yb	0.02	0.02	0.02	0.01	0.02	<0.001	0.008	0.005	0.016
^{175}Lu	0.002	0.005	0.003	<0.001	<0.001	<0.001	0.001	0.004	0.004
^{181}Ta	0.002	0.003	0.005	0.01	0.01	<0.001	0.004	0.006	0.004
^{208}Pb	2.32	1.93	1.79	4.45	2.49	2.46	2.68	4.16	2.15

Ca – value is obtained by microprobe analysis and used as internal standard in ICPMS trace element analysis

B-2 PYROXENE

Microprobe Analyses

SAMPLE	RZ30-3 1	RZ30-1 1	RZ30-6 1	RZ30-7 1	RZ30-8 1	RZ30-10 1	RZ30-11 1
SiO_2	52.66	52.85	50.24	52.70	51.84	52.88	55.78
TiO_2	0.14	0.18	0.10	0.15	0.26	0.09	0.01
Al_2O_3	1.98	1.70	2.24	1.43	2.48	2.38	0.42
Cr_2O_3	0.06	0.051	0.17	0.09	0	0.13	0.07
FeO	17.58	17.66	17.00	18.48	18.50	17.26	17.30
MnO	0.36	0.31	0.32	0.39	0.37	0.31	0.43
MgO	24.34	24.31	25.43	24.40	24.45	24.73	21.88
CaO	1.80	1.90	1.65	1.22	0.86	2.04	0.59
Na_2O	0.017	0.028	0.026	0.023	0.018	0.027	0.03
K_2O	ND	ND	ND	ND	ND	ND	ND
Total	**101.05**	**101.11**	**97.18**	**98.88**	**98.77**	**99.85**	**96.50**
Mg#	0.71	0.71	0.73	0.70	0.70	0.72	0.69
Ca (%)	1.29	1.35	1.18	0.87	0.62	1.46	0.42
Wo	4	4	3	2	2	4	1
En	68	68	70	68	69	69	67
Fs	28	28	26	29	30	27	31
Ac	0.1	0.10	0.10	0.10	0.10	0.10	0.10
Total	**100**	**100**	**99**	**99**	**101**	**100**	**99**
Si	1.95	1.95	1.90	1.96	1.93	1.93	2.09
Al (iv)	0.05	0.05	0.10	0.05	0.08	0.07	-
Al (vi)	0.03	0.03	-	0.02	0.03	0.04	0.10
Fe(iii)	0.02	0.02	0.15	0.03	0.04	0.03	-
Cr	0.002	0.001	0.005	0.003	-	0.004	0.002
Ti	0.004	0.005	0.003	0.004	0.007	0.003	-
Fe(ii)	0.52	0.53	0.38	0.54	0.53	0.49	0.55
Mn	0.01	0.01	0.01	0.012	0.012	0.009	0.01
Mg	1.34	1.34	1.43	1.35	1.35	1.35	1.22
Ca	0.07	0.08	0.07	0.05	0.03	0.08	0.02
Na	0.001	0.002	0.002	0.002	0.001	0.002	0.002
K	0	0	0	0	0	0	0
Total	**4.01**	**4.00**	**4.04**	**4.01**	**4.01**	**4.01**	**3.92**

SAMPLE	RZ33-1-1	RZ33-2-1	RZ33-3-1	RZ33-4-1	RZ33-5-1	RZ33-5-2	RZ33-5-3	RZ33-5-4	RZ33-5-5	RZ33-5-6
SiO_2	52.33	51.73	53.79	52.91	52.99	52.21	53.55	53.17	53.09	53.62
TiO_2	0.14	0.11	0.14	0.10	0.16	0.20	0.21	0.14	0.10	0.11
Al_2O_3	1.73	2.28	1.67	1.81	1.91	1.95	2.16	1.85	2.18	1.71
Cr_2O_3	0.11	0.12	0.12	0.03	0.08	0.05	0	0	0.015	0.06
FeO	18.43	18.35	17.25	18.11	17.88	18.37	15.50	18.17	18.44	18.33
MnO	0.33	0.35	0.34	0.37	0.33	0.37	0.27	0.34	0.32	0.32
MgO	24.80	24.56	24.11	25.02	24.77	25.21	23.23	25.25	25.02	24.79
CaO	0.63	0.83	2.53	1.25	1.21	0.49	4.89	0.44	0.49	0.62
Na_2O	0.02	0.02	0.019	0.017	0.03	0.016	0.076	0.025	0.029	0.002
K_2O	ND	0.005	0.004	0.002	0.007	ND	ND	ND	ND	0.001
Total	**98.50**	**98.33**	**99.96**	**99.60**	**99.36**	**98.87**	**99.88**	**99.38**	**99.68**	**99.57**
Mg#	0.71	0.70	0.71	0.71	0.71	0.71	0.73	0.71	0.71	0.71
Ca (%)	0.45	0.59	1.81	0.89	0.86	0.35	3.49	0.31	0.35	0.45
Wo	1	2	5	2	2	1	10	1	1	1
En	69	70	67	69	69	70	65	70	70	69
Fs	29	29	28	28	28	29	25	29	29	29
Ac	0.1	0.1	0.1	0.1	0.1	0.1	0.3	0.1	0.1	0
Total	**99**	**101**	**100**	**99**	**99**	**100**	**100**	**100**	**100**	**99**
Si	1.95	1.93	1.97	1.94	1.95	1.93	1.96	1.95	1.95	1.97
Al (iv)	0.06	0.07	0.04	0.06	0.05	0.07	0.05	0.05	0.05	0.04
Al (vi)	0.02	0.03	0.04	0.02	0.03	0.02	0.05	0.03	0.04	0.04
Fe(iii)	0.04	0.05	0	0.04	0.02	0.06	0	0.02	0.02	0
Cr	0.003	0.004	0.003	0.001	0.002	0.001	0	0	0	0.002
Ti	0.004	0.003	0.004	0.003	0.004	0.005	0.006	0.004	0.003	0.003
Fe(ii)	0.54	0.52	0.53	0.51	0.53	0.51	0.47	0.54	0.55	0.56
Mn	0.01	0.01	0.01	0.01	0.01	0.01	0.008	0.01	0.01	0.01
Mg	1.37	1.37	1.313	1.37	1.36	1.39	1.26	1.38	1.37	1.36
Ca	0.03	0.03	0.10	0.05	0.05	0.02	0.19	0.02	0.02	0.02
Na	0.001	0.001	0.001	0.001	0.002	0.001	0.005	0.002	0.002	0
K	0	0.0002	0.0002	0.0001	0.0003	0	0	0	0	0
Total	**4.01**	**4.02**	**4.00**	**4.01**	**4.01**	**4.02**	**4.00**	**4.01**	**4.01**	**4.00**

SAMPLE	TZ7-1 1	TZ7-1 3	TZ7-2 1	TZ7-4 1	TZ7-4 2	TZ7-4 3	TZ7-5 1	TZ7-5 2
SiO_2	53.50	52.98	51.78	50.86	52.31	50.73	52.17	51.94
TiO_2	0.17	0.11	0.14	0.24	0.43	0.17	0.16	0.19
Al_2O_3	1.90	1.23	2.06	2.15	2.36	2.37	2.15	1.95
Cr_2O_3	0.08	0	0.15	0.09	0.10	0.102	0.05	0.08
FeO	18.00	18.38	18.99	19.21	19.30	19.59	19.20	19.82
MnO	0.37	0.36	0.35	0.36	0.34	0.36	0.36	0.38
MgO	23.06	23.88	23.27	23.14	23.26	23.33	23.28	23.57
CaO	2.85	1.57	1.93	1.90	1.47	1.76	1.53	0.93
Na_2O	0.04	0.03	0.047	0.041	0.044	0.047	0.038	0.012
K_2O	0.001	ND	ND	ND	0.007	ND	0.003	0
Total	**99.96**	**98.54**	**98.71**	**97.98**	**99.61**	**98.45**	**98.94**	**98.86**
Mg#	0.70	0.70	0.69	0.68	0.68	0.68	0.68	0.68
Ca (%)	2.04	1.12	1.38	1.35	1.05	1.26	1.09	0.66
Wo	6	3	4	4	3	4	3	2
En	65	67	65	65	66	65	66	66
Fs	29	30	30	31	31	31	40	32
Ac	0.1	0.1	0.2	0.2	0.20	0.2	0.1	0
Total	**100**	**100**	**99**	**100**	**100**	**100**	**109**	**100**
Si	1.96	1.97	1.94	1.92	1.93	1.91	1.94	1.94
Al (iv)	0.04	0.03	0.07	0.08	0.07	0.09	0.06	0.06
Al (vi)	0.05	0.03	0.03	0.02	0.04	0.01	0.04	0.03
Fe(iii)	0	0.000	0.05	0.08	0.01	0.10	0.02	0.04
Cr	0.002	0.000	0.005	0.003	0.003	0.003	0.002	0.002
Ti	0.005	0.003	0.004	0.01	0.01	0.005	0.004	0.005
Fe(ii)	0.55	0.57	0.55	0.53	0.59	0.51	0.58	0.58
Mn	0.01	0.01	0.01	0.01	0.011	0.01	0.011	0.01
Mg	1.26	1.32	1.30	1.30	1.28	1.31	1.29	1.31
Ca	0.11	0.06	0.08	0.08	0.06	0.07	0.06	0.04
Na	0.003	0.002	0.003	0.003	0.003	0.003	0.003	0.001
K	0	0	0	0	0.0003	0	0.0001	0
Total	**3.99**	**4.00**	**4.01**	**4.02**	**4.00**	**4.03**	**4.01**	**4.01**

SAMPLE	TZ2-1 1	TZ2-2 1	TZ2-3 1	TZ2-3 2	TZ2-3 3	TZ2-4 1
SiO_2	51.72	48.39	51.35	52.80	53.53	52.44
TiO_2	0.16	0.12	0.19	0.14	0.13	0.08
Al_2O_3	2.40	1.67	2.70	2.50	2.30	2.68
Cr_2O_3	0.11	0.08	0.18	0.19	0.10	0.12
FeO	18.35	21.02	16.86	16.08	16.73	18.07
MnO	0.34	0.38	0.32	0.25	0.29	0.29
MgO	23.86	23.87	25.39	25.05	25.86	24.76
CaO	2.00	1.28	1.25	2.20	1.03	0.64
Na_2O	0.03	0.02	0.01	0.01	0.02	0.02
K_2O	ND	ND	ND	0.01	0.01	0.01
Total	**98.97**	**96.83**	**98.24**	**99.23**	**99.99**	**99.10**
Mg#	0.70	0.67	0.73	0.74	0.73	0.71
Ca (%)	1.43	0.91	0.89	1.57	0.74	0.46
Wo	4	3	2	4	2	1
En	67	65	71	70	72	70
Fs	29	32	27	26	26	30
Ac	0.1	0.1	0.1	0	0.1	0
Total	**100**	**100**	**100**	**100**	**100**	**101**
Si	1.92	1.87	1.91	1.93	1.94	1.93
Al (iv)	0.08	0.08	0.09	0.07	0.06	0.07
Al (vi)	0.03	0	0.03	0.04	0.04	0.05
Fe(iii)	0.06	0.25	0.08	0.02	0.01	0.02
Cr	0.003	0.003	0.005	0.005	0.003	0.003
Ti	0.005	0.004	0.005	0.004	0.004	0.002
Fe(ii)	0.51	0.42	0.44	0.47	0.49	0.54
Mn	0.01	0.01	0.01	0.008	0.009	0.009
Mg	1.32	1.38	1.41	1.37	1.40	1.36
Ca	0.08	0.05	0.05	0.08	0.04	0.025
Na	0.002	0.001	0.001	0.001	0.001	0.001
K	0	0	0	0.0004	0.0004	0.0006
Total	**4.02**	**4.07**	**4.02**	**4.01**	**4.00**	**4.01**

SAMPLE	TZ8-1 1	TZ8-2 1	TZ8-2 2	TZ8-3 1	TZ8-4 1
SiO_2	51.83	51.99	52.20	53.19	51.31
TiO_2	0.17	0.69	0.35	0.16	0.20
Al_2O_3	2.21	2.05	2.66	2.15	2.31
Cr_2O_3	0.15	0.13	0.13	0.12	0.14
FeO	19.11	18.86	16.42	17.84	17.54
MnO	0.38	0.35	0.30	0.28	0.30
MgO	23.45	22.37	20.97	24.14	22.50
CaO	1.51	2.77	6.62	1.60	3.62
Na_2O	0.02	0.06	0.15	0.04	0.11
K_2O	0.01	0.01	0.01	ND	ND
Total	**99.07**	**97.49**	**99.99**	**99.38**	**97.47**
Mg#	0.69	0.68	0.69	0.71	0.70
Ca (%)	1.08	1.98	4.73	1.14	2.59
Wo	3	6	13	3	7
En	66	64	59	68	64
Fs	31	30	27	29	28
Ac	0.1	0.2	0.5	0.2	0.4
Total	**100**	**100**	**100**	**100**	**99**
Si	1.93	1.93	1.93	1.95	1.93
Al (iv)	0.07	0.07	0.07	0.05	0.07
Al (vi)	0.03	0.02	0.05	0.05	0.03
Fe(iii)	0.04	0.005	0.018	0	0.05
Cr	0.004	0.004	0.004	0.004	0.004
Ti	0.005	0.019	0.01	0.004	0.006
Fe(ii)	0.56	0.58	0.49	0.55	0.50
Mn	0.01	0.01	0.009	0.009	0.009
Mg	1.30	1.24	1.16	1.32	1.26
Ca	0.06	0.11	0.26	0.06	0.15
Na	0.002	0.004	0.01	0.003	0.008
K	0.0004	0.0005	0.0004	0.0000	0.0000
Total	**4.01**	**4.00**	**4.01**	**4.00**	**4.01**

SAMPLE	TZ10-1 1	TZ10-1 2	TZ10-1 3	TZ10-1 4	TZ10-2 1	TZ10-2 2	TZ10-3 1	TZ10-3 2
SiO_2	52.64	51.02	52.76	52.52	51.30	52.99	52.05	52.58
TiO_2	0.17	0.16	0.13	0.16	0.06	0.12	0.21	0.09
Al_2O_3	2.11	1.92	2.39	2.25	2.44	2.82	2.63	2.45
Cr_2O_3	0.16	0.03	0.17	0.21	0.14	0.17	0.12	0.09
FeO	17.63	18.77	19.01	17.76	16.31	15.64	15.38	15.59
MnO	0.30	0.36	0.33	0.29	0.28	0.27	0.24	0.24
MgO	23.63	24.36	24.16	23.51	25.53	25.35	25.13	25.82
CaO	2.38	0.86	1.01	2.61	1.39	1.78	3.24	1.92
Na_2O	0.06	0.01	0.02	0.06	0.01	0.02	0.06	0.02
K_2O	ND	ND	ND	ND	ND	ND	ND	ND
Total	**99.07**	**97.49**	**99.99**	**99.38**	**97.47**	**99.16**	**99.06**	**98.81**
Mg#	0.70	0.70	0.69	0.70	0.74	0.74	0.74	0.75
Ca (%)	1.70	0.62	0.72	1.86	0.99	1.27	2.32	1.38
Wo	5	2	2	5	3	4	6	4
En	67	68	68	66	71	71	69	71
Fs	28	30	30	28	26	25	24	25
Ac	0.2	0	0.1	0.2	0	0.1	0.2	0.1
Total	**100**	**100**	**100**	**99**	**100**	**100**	**99**	**100**
Si	1.95	1.93	1.94	1.94	1.92	1.93	1.91	1.93
Al (iv)	0.05	0.07	0.06	0.06	0.08	0.07	0.09	0.07
Al (vi)	0.04	0.01	0.04	0.04	0.02	0.06	0.03	0.04
Fe(iii)	0.01	0.08	0.02	0.02	0.08	0	0.07	0.05
Cr	0.005	0.001	0.005	0.006	0.004	0.005	0.003	0.003
Ti	0.005	0.005	0.004	0.004	0.002	0.003	0.006	0.002
Fe(ii)	0.54	0.51	0.56	0.53	0.43	0.48	0.40	0.43
Mn	0.009	0.012	0.010	0.009	0.009	0.008	0.007	0.007
Mg	1.302	1.37	1.32	1.29	1.42	1.38	1.38	1.41
Ca	0.09	0.04	0.04	0.10	0.06	0.07	0.13	0.08
Na	0.004	0.001	0.001	0.004	0.001	0.002	0.004	0.001
K	0	0	0.0001	0	0.0002	0	0	0
Total	**4.00**	**4.02**	**4.01**	**4.01**	**4.02**	**4.00**	**4.02**	**4.01**

SAMPLE	TZ41-1 4	TZ41-2 1	TZ41-2 2	TZ41-3 1	TZ41-4 1	TZ41-6 1
SiO_2	51.46	50.43	51.62	51.82	52.93	52.80
TiO_2	0.14	0.18	0.10	0.17	0.09	0.15
Al_2O_3	2.33	2.30	2.16	2.44	2.48	2.33
Cr_2O_3	0.14	0.14	0.12	0.13	0.15	0.10
FeO	17.31	17.53	18.19	17.99	17.82	17.73
MnO	0.31	0.32	0.29	0.32	0.31	0.34
MgO	24.25	24.31	24.86	24.25	24.78	24.98
CaO	2.23	1.86	1.18	1.43	0.82	1.00
Na_2O	0.05	0.06	0.03	0.05	0.02	0.02
K_2O	ND	ND	ND	ND	ND	ND
Total	**98.21**	**97.12**	**98.55**	**98.58**	**99.39**	**99.44**
Mg#	0.71	0.71	0.71	0.71	0.71	0.72
Ca (%)	1.59	1.33	0.84	1.02	0.58	0.71
Wo	4	4	2	3	2	2
En	68	68	69	68	69	69
Fs	27	28	29	29	28	28
Ac	0.2	0.2	0.1	0.2	0.1	0.1
Total	**99**	**100**	**100**	**100**	**99**	**99**
Si	1.92	1.91	1.92	1.93	1.94	1.94
Al (iv)	0.08	0.09	0.08	0.07	0.06	0.06
Al (vi)	0.02	0.01	0.02	0.03	0.05	0.04
Fe(iii)	0.07	0.11	0.08	0.045	0.002	0.02
Cr	0.004	0.004	0.004	0.004	0.004	0.003
Ti	0.004	0.005	0.003	0.005	0.002	0.004
Fe(ii)	0.47	0.44	0.48	0.512	0.54	0.52
Mn	0.01	0.01	0.009	0.010	0.01	0.01
Mg	1.35	1.37	1.38	1.34	1.35	1.37
Ca	0.09	0.08	0.05	0.057	0.03	0.04
Na	0.004	0.005	0.002	0.003	0.001	0.001
K	0	0	0	0	0	0
Total	**4.02**	**4.03**	**4.02**	**4.01**	**4.00**	**4.01**

Trace Element
LA-ICP-MS Analyses

SAMPLE	Rz33 c2-1	Rz33 c2-21	Rz33 c5-1
CaO (wt%)	0.83	0.83	1.21
^{137}Ba (ppm)	0.92	0.08	1.73
^{140}Ce	0.10	0.13	0.68
^{59}Co	38	37	28
^{52}Cr	89	88	141
^{65}Cu	5.71	ND	ND
^{163}Dy	0.08	0.10	0.28
^{166}Er	0.10	0.10	0.20
^{153}Eu	0.01	0.01	0.04
^{157}Gd	0.08	0.08	0.08
^{178}Hf	0.06	0.09	0.10
^{165}Ho	0.03	0.03	0.06
^{139}La	0.03	0.07	0.17
^{175}Lu	0.03	0.03	0.03
^{93}Nb	0.02	0.01	0.01
^{146}Nd	0.05	0.02	0.51
^{60}Ni	120	109	66
^{208}Pb	0.06	0.08	0.12
^{141}Pr	0.01	0.01	0.11
^{85}Rb	0.14	0.01	0.00
^{45}Sc	12.25	13.85	5.88
^{147}Sm	0.01	ND	0.16
^{88}Sr	0.21	0.23	2.56
^{181}Ta	0.001	0.000	0.003
^{159}Tb	0.02	0.02	0.02
^{232}Th	0.12	0.10	0.04
^{169}Tm	0.02	0.02	0.03
^{51}V	46	48	35
^{172}Yb	0.18	0.20	0.21
^{89}Y	0.70	0.76	1.67
^{91}Zr	1.47	2.41	3.94

Ca – value is obtained by microprobe analysis and used as internal standard in ICPMS trace element analysis

SAMPLE	Rz 30 point 1-1	Rz 30 point 1-2	Rz 30 point 3-1	Rz 30 point 3-2	Rz 30 point 3-3	Rz 30 point 3-4
CaO (wt%)	1.80	1.80	1.80	1.80	1.80	1.80
^{137}Ba (ppm)	4.18	2.16	0.08	0.36	2.01	0.82
^{140}Ce	0.35	0.59	0.50	0.40	0.40	0.35
^{59}Co	128	140	115	128	142	128
^{52}Cr	446	501	343	412	681	576
^{65}Cu	9.58	7.65	1.92	2.12	3.04	2.19
^{163}Dy	0.43	0.54	0.49	0.52	0.39	0.45
^{166}Er	0.59	0.66	0.43	0.49	0.42	0.47
^{153}Eu	0.03	0.02	0.03	0.03	0.03	0.03
^{157}Gd	0.12	0.20	0.22	0.28	0.19	0.24
^{178}Hf	0.34	0.35	0.19	0.24	0.12	0.12
^{165}Ho	0.11	0.17	0.13	0.15	0.13	0.15
^{139}La	0.25	0.45	0.17	0.14	0.15	0.19
^{175}Lu	0.16	0.17	0.10	0.12	0.12	0.14
^{93}Nb	0.18	0.10	0.04	0.08	0.05	0.02
^{146}Nd	0.26	0.29	0.37	0.36	0.34	0.28
^{60}Ni	551	726	593	626	638	558
^{208}Pb	0.26	0.29	0.37	0.31	0.13	0.21
^{141}Pr	0.05	0.07	0.07	0.07	0.05	0.05
^{85}Rb	0.60	0.47	0.04	0.11	0.28	0.16
^{45}Sc	98.99	101	62.14	70.77	76.18	76.75
^{147}Sm	0.11	0.14	0.14	0.10	0.14	0.11
^{88}Sr	0.79	1.42	0.39	0.45	1.26	1.34
^{181}Ta	0.009	0.004	0.002	0.002	0.002	0.003
^{159}Tb	0.04	0.06	0.05	0.05	0.04	0.06
^{232}Th	0.21	0.28	0.12	0.22	0.07	0.17
^{169}Tm	0.10	0.13	0.09	0.07	0.08	0.10
^{51}V	220	217	191	224	170	164
^{172}Yb	0.89	1.04	0.63	0.71	0.67	0.80
^{89}Y	3.55	4.52	3.38	3.70	3.18	3.69
^{91}Zr	13.35	13.71	6.26	7.36	5.30	5.30

Ca – value is obtained by microprobe analysis and used as internal standard in ICPMS trace element analysis

Note : For CaO wt% value an average value of 1.80 was used as the internal standard for this sample.

SAMPLE	Tz7 c1-6	Tz7 c4-3	Tz7 c5-4
CaO (wt%)	2.85	1.47	1.53
^{137}Ba (ppm)	1.56	0.65	ND
^{140}Ce	0.50	0.29	0.25
^{59}Co	149	97	48
^{52}Cr	925	574	265
^{65}Cu	6.88	0.04	ND
^{163}Dy	0.82	0.28	0.29
^{166}Er	0.77	0.27	0.26
^{153}Eu	0.06	0.02	0.01
^{157}Gd	0.50	0.10	0.05
^{178}Hf	0.24	0.04	0.07
^{165}Ho	0.21	0.07	0.07
^{139}La	0.17	0.08	0.09
^{175}Lu	0.19	0.07	0.06
^{93}Nb	0.12	0.03	ND
^{146}Nd	0.62	0.20	0.21
^{60}Ni	714	425	205
^{208}Pb	0.175	0.084	0.06
^{141}Pr	0.11	0.04	0.03
^{85}Rb	0.53	0.14	ND
^{45}Sc	99.08	35.90	21.64
^{147}Sm	0.26	0.08	0.07
^{88}Sr	1.02	1.33	0.18
^{181}Ta	0.009	0.001	ND
^{159}Tb	0.10	0.03	0.02
^{232}Th	0.39	0.034	0.144
^{169}Tm	0.13	0.05	0.04
^{51}V	259	141	78
^{172}Yb	1.02	0.44	0.36
^{89}Y	5.58	2.11	1.89
^{91}Zr	8.22	1.29	3.07

Ca – value is obtained by microprobe analysis and used as internal standard in ICPMS trace element analysis

B-3 AMPHIBOLE

SAMPLE NAME	Tz-1 amph	Tz-1 amph	Tz-1 amph1	Tz-1 amph2	Tz-1 amph2	Tz-2 c1 amph1 frag	Tz-2 c1 amph2 frag	Tz-2 c2 amph1 frag	Tz-2 c2 amph2 frag	Tz-2 c4 amph frag	Tz-2 c6 amph1 frag	Tz-2 c6 amph2 frag	Tz-2 c6 amph3 frag
Rock Type	Frag gabnor	Frag gabnor	Frag gabnor	Frag gabnor	Frag gabnor	leuco-gabnor	leuco-gabnor	leuco-gabnor	leuco-gabnor	leuco-gabnor	leuco-gabnor	leuco-gabnor	leuco-gabnor
Mineral Type	M-H	Act	Act	M-H	Act	M-H	M-H	M-H	Act	M-H	M-H	M-H	M-H
SiO_2	46.15	53.14	53.88	45.90	53.42	47.35	46.73	50.66	51.74	46.62	48.13	46.60	41.57
TiO_2	1.34	0.09	0.08	1.37	0.05	0.25	0.47	0.31	0.55	0.45	0.30	0.46	0.03
Al_2O_3	7.38	2.38	2.52	7.20	2.14	6.35	8.46	5.29	3.85	8.79	8.34	9.35	9.48
Cr_2O_3	0.26	0.10	0.14	0.2	0.08	ND	0.015	0.049	0.13	ND	0.02	ND	ND
MgO	15.57	16.78	17.36	15.66	16.44	15.08	13.24	15.04	15.02	13.22	14.26	13.46	5.66
CaO	11.96	12.00	10.22	11.92	11.92	11.99	12.24	12.15	13.28	11.48	11.42	11.34	11.55
MnO	0.08	0.27	0.27	0.10	0.24	0.18	0.15	0.2	0.15	0.21	0.18	0.18	0.25
FeO	10.98	11.57	11.36	11.02	11.30	12.44	14.283	12.766	11.80	13.54	13.04	13.85	26.97
Na_2O	1.098	0.25	0.25	0.99	0.31	0.78	0.95	0.519	0.35	1.14	1.11	1.19	1.23
K_2O	0.78	0.02	0.03	0.72	0.04	0.07	0.17	0.09	0.05	0.11	0.08	0.07	0.31
H_2O	1.89	2.06	2.07	1.96	1.94	1.98	2.007	2.055	2.05	1.94	1.99	1.98	1.78
F	0.22	0.01	ND	0.06	0.16	ND	ND	ND	0.02	0.06	0.09	0.07	ND
Cl	0.07	0.03	0.03	0.07	0.18	0.07	0.06	0.02	0.03	0.18	0.08	0.08	0.45
Total	**97.80**	**98.67**	**98.20**	**97.16**	**98.21**	**96.54**	**98.77**	**99.14**	**99.00**	**97.73**	**99.04**	**98.63**	**99.27**
Mg#	0.82	0.83	0.99	0.84	0.79	0.82	0.72	0.77	0.69	0.76	0.81	0.80	0.36
$Fe^{3+}/(Fe^{3+}+[6]Al)$	0.92	1.00	1.00	0.98	0.88	0.90	0.68	0.76	0.00	0.67	0.73	0.73	0.87
Si	6.78	7.59	7.56	6.76	7.70	6.99	6.84	7.28	7.52	6.85	6.91	6.75	6.44
Al(iv)	1.22	0.40	0.42	1.24	0.30	1.01	1.16	0.72	0.48	1.15	1.09	1.25	1.56
Al(vi)	0.05	0.00	0.00	0.01	0.06	0.10	0.29	0.18	0.18	0.37	0.32	0.35	0.17
Fe(iii)	0.62	0.64	1.28	0.71	0.44	0.83	0.63	0.56	0.00	0.73	0.86	0.94	1.13
Ti	0.15	0.01	0.01	0.15	0.01	0.03	0.05	0.03	0.06	0.05	0.03	0.05	0.00
Cr	0.03	0.01	0.02	0.02	0.01	0.00	0.00	0.01	0.01	0.00	0.00	0.00	0.00
Fe(ii)	0.73	0.74	0.05	0.64	0.92	0.71	1.12	0.97	1.43	0.93	0.71	0.74	2.36
Mn	0.01	0.03	0.03	0.01	0.03	0.02	0.02	0.02	0.02	0.03	0.02	0.02	0.03
Mg	3.41	3.57	3.63	3.44	3.53	3.32	2.89	3.22	3.25	2.89	3.05	2.91	1.31
Ca	1.88	1.84	1.54	1.88	1.84	1.90	1.92	1.87	2.07	1.81	1.76	1.76	1.92
Na	0.31	0.07	0.07	0.28	0.09	0.22	0.27	0.14	0.10	0.32	0.31	0.33	0.37
K	0.15	0.00	0.01	0.14	0.01	0.01	0.03	0.02	0.01	0.02	0.01	0.01	0.06
TOTAL	**15.34**	**14.91**	**14.61**	**15.30**	**14.93**	**15.13**	**15.22**	**15.03**	**15.14**	**15.15**	**15.08**	**15.11**	**15.35**

SAMPLE NAME	TZ2-2 2 frag	TZ2-5 1 frag	TZ2-5 2 frag	TZ2-6 1 frag	TZ2-8 1 frag	TZ2-8 2 frag	Tz7 c6	TZ8 c	TZ8 e	Tz-22 c1	Tz-22 c4	Tz-23 c1 mat	Tz-23 c2b mat
Rock Type	leuco-gabnor	leuco-gabnor	leuco-gabnor	leuco-gabnor	leuco-gabnor	leuco-gabnor	Frag gabnor	mat gabnor	mat gabnor	frag meta-gabnor	frag meta-gabnor	meta-gabnor	meta-gabnor
Mineral Type	Edenite	M-H	M-H	M-H	M-H	M-H	M-H	M-H	M-H	M-H	M-H	Trem	Actt
SiO_2	49.871	45.53	47.05	47.24	46.19	47.47	50.61	49.30	48.34	48.10	47.14	53.88	52.80
TiO_2	0.59	1.67	1.11	0.38	0.30	1.13	0.79	0.88	0.96	0.796	1.21	0.08	0.09
Al_2O_3	3.10	8.28	7.50	8.80	8.04	7.90	5.57	6.61	6.83	6.49	7.338	2.521	2.75
Cr_2O_3	0.18	0.06	0.02	0.00	0.02	0.14	0.07	0.09	0.09	0.04	0.16	0.14	0.043
MgO	14.74	14.32	15.70	13.50	15.12	14.87	17.31	16.85	16.66	15.33	15.62	17.36	17.20
CaO	22.06	11.71	11.66	11.15	11.16	11.79	11.98	11.84	11.90	11.95	11.85	10.22	11.31
MnO	0.16	0.13	0.11	0.20	0.15	0.12	0.10	0.08	0.10	0.12	0.13	0.27	0.16
FeO	7.75	12.25	11.34	13.68	12.76	11.63	9.59	11.14	10.6	11.54	10.74	11.36	10.14
Na_2O	0.33	0.84	0.85	1.13	1.02	0.77	0.65	0.74	0.71	0.74	1.02	0.25	0.36
K_2O	0.01	0.98	0.74	0.10	0.16	0.60	0.22	0.38	0.46	0.50	0.47	0.03	0.02
H_2O	1.95	1.95	1.95	1.99	1.90	2.03	2.07	2.08	2.04	1.98	2.02	2.07	2.05
F	0.26	0.00	0.11	0.00	0.20	0.00	0.03	-	0.04	0.07	-	-	-
Cl	0.004	0.24	0.13	0.16	0.03	0.05	0.01	0.012	0.03	0.04	0.04	0.03	0.02
Total	**101.0**	**97.96**	**98.26**	**98.32**	**97.05**	**98.51**	**98.99**	**100.1**	**98.98**	**97.70**	**97.72**	**98.20**	**96.95**
Mg#	0.77	0.79	0.87	0.80	0.93	0.81	0.89	0.91	0.90	0.81	0.84	0.99	0.88
$Fe^{3+}/(Fe^{3+}+[6]Al)$	-	0.82	0.90	0.72	0.92	0.74	0.87	0.96	0.94	0.81	0.83	1.00	0.93
Si	7.22	6.70	6.82	6.85	6.73	6.88	7.17	6.94	6.91	7.03	6.87	7.56	7.59
Al(iv)	0.53	1.30	1.18	1.15	1.27	1.12	0.83	1.06	1.09	0.97	1.13	0.42	0.41
Al(vi)	0.00	0.14	0.10	0.36	0.11	0.23	0.10	0.04	0.06	0.15	0.13	0.00	0.06
Fe(iii)	0.00	0.66	0.85	0.91	1.29	0.65	0.69	0.98	0.89	0.61	0.64	1.28	0.74
Ti	0.06	0.19	0.12	0.04	0.03	0.12	0.08	0.09	0.10	0.09	0.13	0.01	0.01
Cr	0.02	0.01	0.00	0.00	0.00	0.02	0.01	0.01	0.01	0.00	0.02	0.02	0.00
Fe(ii)	0.94	0.85	0.53	0.75	0.26	0.76	0.45	0.33	0.38	0.80	0.67	0.05	0.48
Mn	0.02	0.02	0.01	0.02	0.02	0.01	0.01	0.01	0.01	0.01	0.02	0.03	0.02
Mg	3.18	3.14	3.39	2.92	3.28	3.21	3.66	3.54	3.55	3.34	3.39	3.63	3.69
Ca	3.42	1.85	1.81	1.73	1.74	1.83	1.82	1.79	1.82	1.87	1.85	1.54	1.74
Na	0.09	0.24	0.24	0.32	0.29	0.22	0.18	0.20	0.20	0.21	0.29	0.07	0.10
K	0.00	0.18	0.14	0.02	0.03	0.11	0.04	0.07	0.08	0.09	0.09	0.01	0.00
TOTAL	**15.49**	**15.27**	**15.19**	**15.07**	**15.06**	**15.16**	**15.04**	**15.06**	**15.10**	**15.17**	**15.23**	**14.61**	**14.85**

SAMPLE NAME	Tz-23 c3	TZ23 C3 c	Tz-23 c4	TZ23 C4 a	Tz-23 c5	Tz-23 c8	TZ23 C8 a	TZ23 C6 a	TZ23 C7 a	TZ23 C7 b	TZ23 C3 a	TZ23 C3 b	Tz-25 c1
Rock Type						**Matrix metagabbronorite**							
Mineral Type	**Act**	**M-H**	**Act**	**M-H**	**M-H**	**M-H**	**M-H**	**M-H**	**M-H**	**Act**			**M-H**
SiO_2	52.51	53.14	52.92	52.55	47.95	49.91	46.51	48.20	52.95	54.32	53.53	52.83	49.41
TiO_2	0.10	0.12	0.25	0.04	1.39	0.97	1.32	1.41	0.13	0.09	0.12	0.07	0.52
Al_2O_3	2.82	3.45	3.13	2.76	7.28	5.60	7.27	7.55	3.74	2.29	3.08	2.61	6.15
Cr_2O_3	0.10	0.05	0.11	0.11	0.14	0.19	0.21	0.17	0.11	0.09	0.14	0.09	0.14
MgO	17.62	17.21	17.01	17.85	16.12	17.28	16.46	16.31	16.97	17.88	17.23	17.78	12.65
CaO	12.17	11.86	11.94	10.44	11.88	12.04	12.05	12.13	12.00	12.38	12.41	8.94	12.26
MnO	0.14	0.19	0.18	0.28	0.073	0.08	0.10	0.08	0.19	0.09	0.15	0.37	0.31
FeO	9.96	11.00	11.02	12.38	10.05	9.63	10.58	10.11	11.96	10.39	10.66	13.24	14.63
Na_2O	0.35	0.39	0.24	0.29	1.08	0.72	0.98	0.88	0.47	0.32	0.40	0.30	0.68
K_2O	0.03	0.035	0.05	0.02	0.58	0.38	0.65	0.6	0.04	0.03	0.03	0.03	0.11
H_2O	2.06	2.03	2.04	2.06	2.04	2.00	2.03	2.08	2.08	2.09	2.07	2.03	2.01
F	-	0.14	0.08	-	0.02	0.15	-	-	0.06	0.05	0.07	0.06	-
Cl	0.02	0.012	0.01	0.04	0.02	0.01	0.03	0.03	0.03	0.001	0.02	0.02	0.10
Total	**97.86**	**99.931**	**98.993**	**98.96**	**98.61**	**98.94**	**98.45**	**100.02**	**100.951**	**100.15**	**100.25**	**98.47**	**98.96**
Mg#	0.86	0.87	0.85	1.00	0.84	0.88	0.89	0.85	0.86	0.84	0.82	1.00	0.64
$Fe^{3+}/(Fe^{3+}+[6]Al)$	1.00	0.93	0.95	1.00	0.79	0.93	1.00	0.80	0.98	0.99	0.87	1.00	0.40
Si	7.53	7.48	7.51	7.34	6.91	7.11	6.74	6.88	7.40	7.63	7.56	7.31	7.26
Al(iv)	0.47	0.52	0.49	0.45	1.09	0.89	1.24	1.12	0.60	0.37	0.44	0.43	0.74
Al(vi)	0.00	0.05	0.03	0.00	0.15	0.05	0.00	0.15	0.02	0.01	0.07	0.00	0.32
Fe(iii)	0.60	0.74	0.68	1.65	0.55	0.67	0.83	0.60	0.82	0.52	0.47	2.19	0.22
Ti	0.01	0.01	0.03	0.00	0.15	0.10	0.14	0.15	0.01	0.01	0.01	0.01	0.06
Cr	0.01	0.01	0.01	0.01	0.02	0.02	0.02	0.02	0.01	0.01	0.02	0.01	0.02
Fe(ii)	0.59	0.55	0.62	0.00	0.67	0.48	0.45	0.61	0.58	0.70	0.79	0.00	1.58
Mn	0.02	0.02	0.02	0.03	0.01	0.01	0.01	0.01	0.02	0.01	0.02	0.04	0.04
Mg	3.76	3.61	3.60	3.71	3.46	3.67	3.56	3.47	3.54	3.74	3.63	3.67	2.77
Ca	1.87	1.79	1.82	1.56	1.83	1.84	1.87	1.85	1.80	1.86	1.88	1.33	1.93
Na	0.10	0.11	0.07	0.08	0.30	0.20	0.28	0.24	0.13	0.09	0.11	0.08	0.19
K	0.00	0.01	0.01	0.00	0.11	0.07	0.12	0.11	0.01	0.00	0.00	0.00	0.02
TOTAL	14.97	14.90	14.89	14.85	15.24	15.10	15.27	15.21	14.93	14.95	14.99	15.07	15.14

SAMPLE NAME	Tz-25 c2	Tz-25 c2	Tz-25 c3	Tz-25 c4	Tz25 c1	TZ25 C2 a	TZ25 C2 b	TZ25 C2 c	TZ25 C2 d	Tz-26 c2	Tz-26 c3	Tz-26 c4	Tz-27 c4
Rock Type	mat meta-gabnor	mat meta-gabnor	mat meta-gabnor	mat meta-gabnor	mat meta-gabnor	mat meta-gabnor	mat meta-gabnor	mat meta-gabnor	mat meta-gabnor	mat meta-gabnor	mat meta-gabnor	mat meta-gabnor	peg leuco-gabnor
Mineral Type	M-H	Act	M-H	M-H	M-H	Act	M-H	M-H	M-H	M-H	M-H	M-H	M-H
SiO_2	45.44	53.98	46.72	38.82	49.41	54.21	47.12	50.65	50.52	46.46	46.83	48.31	47.75
TiO_2	1.14	0.10	0.26	0.36	0.52	0.18	4.12	0.28	0.82	1.24	0.50	0.52	0.82
Al_2O_3	7.30	1.37	7.50	12.93	6.15	2.18	3.36	3.86	3.49	6.96	6.98	6.92	5.80
Cr_2O_3	0.14	0	0	0	0.14	0.04	0.10	0.24	0.05	0.20	0.08	0.22	0.00
MgO	13.79	17.88	13.30	10.15	12.65	17.60	14.49	15.80	16.16	15.51	17.31	16.62	16.08
CaO	11.92	12.70	12.44	12.57	12.26	12.66	11.71	12.70	12.57	11.86	10.95	11.87	11.88
MnO	0.26	0.20	0.24	0.16	0.31	0.17	0.24	0.15	0.15	0.12	0.15	0.13	0.15
FeO	13.59	9.88	14.47	17.13	14.63	10.43	14.87	12.17	13.05	11.21	9.91	10.28	11.33
Na_2O	0.92	0.18	0.95	1.95	0.68	0.27	0.45	0.41	0.41	1.07	0.94	0.99	0.77
K_2O	0.58	0.05	0.34	1.47	0.11	0.09	0.04	0.06	0.02	0.57	0.24	0.27	0.13
H_2O	1.97	2.08	1.94	1.88	2.01	2.10	1.91	2.02	2.04	2.00	1.99	2.03	2.01
F	-	-	0.09	-	-	-	0.20	-	0.02	0.01	0.02	-	-
Cl	0.04	0.004	0.09	0.13	0.10	0.02	0.02	0.08	0.03	0.02	0.04	0.07	0.01
Total	97.09	98.40	98.33	97.55	98.96	100	98.98	98.60	99.43	97.21	95.93	98.23	96.71
Mg#	0.76	0.82	0.70	0.57	0.64	0.81	0.76	0.77	0.80	0.83	1.00	0.90	0.87
$Fe^{3+}/(Fe^{3+}+[6]Al)$	0.92	1.00	0.71	0.56	0.40	0.95	1.00	0.95	1.00	0.94	1.00	0.88	1.00
Si	6.78	7.73	6.91	6.01	7.26	7.66	6.92	7.36	7.26	6.84	6.79	6.94	6.99
Al(iv)	1.22	0.23	1.09	1.99	0.74	0.34	0.58	0.64	0.59	1.16	1.19	1.06	1.00
Al(vi)	0.06	0.00	0.22	0.37	0.32	0.02	0.00	0.02	0.00	0.04	0.00	0.11	0.00
Fe(iii)	0.70	0.33	0.53	0.48	0.22	0.36	0.83	0.45	0.71	0.67	1.41	0.84	0.86
Ti	0.13	0.01	0.03	0.04	0.06	0.02	0.46	0.03	0.09	0.14	0.05	0.06	0.09
Cr	0.02	0.00	0.00	0.00	0.02	0.00	0.01	0.03	0.01	0.02	0.01	0.02	0.00
Fe(ii)	0.99	0.85	1.26	1.74	1.58	0.87	1.00	1.03	0.86	0.71	0.00	0.40	0.53
Mn	0.03	0.02	0.03	0.02	0.04	0.02	0.03	0.02	0.02	0.02	0.02	0.02	0.02
Mg	3.07	3.82	2.93	2.34	2.77	3.71	3.17	3.42	3.46	3.40	3.74	3.56	3.51
Ca	1.90	1.95	1.97	2.09	1.93	1.92	1.84	1.98	1.94	1.87	1.70	1.83	1.86
Na	0.26	0.05	0.27	0.58	0.19	0.07	0.13	0.12	0.11	0.30	0.26	0.28	0.22
K	0.11	0.01	0.06	0.29	0.02	0.02	0.01	0.01	0.00	0.11	0.04	0.05	0.02
TOTAL	**15.28**	**15.01**	**15.31**	**15.96**	**15.14**	**15.00**	**14.98**	**15.10**	**15.05**	**15.28**	**15.22**	**15.15**	**15.11**

SAMPLE NAME	Tz-28 c4	Tz-28 c4 amph2	Tz-28 c5	Tz-28 c6	Tz-29 c1	Tz-29 c1 amph2	Tz-29 c3	Tz-29 c7 amph1	TZ29 C4 b2	TZ29 C4 d	TZ41-1 1	TZ41-1 2	TZ41-1 3
Rock Type	peg gabnor	peg gabnor	peg gabnor	peg gabnor	peg leuco-gabnor	peg leuco-gabnor	peg leuco-gabnor	peg leuco-gabnor	peg leuco-gabnor	peg leuco-gabnor	mat gabnor	mat gabnor	mat gabnor
Mineral Type	M-H	M-H	M-H	Act	Act	Acti	Act	M-H		Act	M-H	M-H	M-H
SiO_2	50.25	49.16	53.54	54.24	53.14	53.42	53.65	46.47	50.72	51.85	50.03	50.24	49.28
TiO_2	0.63	0.21	1.34	0.12	0.09	0.05		1.54	0.09	0.09	0.39	0.68	0.47
Al_2O_3	3.83	5.36	2.30	1.61	2.38	2.14	1.85	7.58	2.86	1.72	5.45	5.84	5.78
Cr_2O_3	0.04	0.04	0.07	0.00	0.10	0.08	0.00	0.00	0.00	0.00	0.17	0.26	0.04
MgO	13.52	12.44	18.48	17.90	16.78	16.44	15.60	13.53	9.93	10.59	17.37	17.27	17.08
CaO	12.61	11.59	11.61	11.64	12.00	11.92	12.85	12.13	12.03	12.05	11.86	11.93	12.35
MnO	0.24	0.29	0.35	0.36	0.27	0.24	0.20	0.19	0.30	0.37	0.11	0.08	0.12
FeO	14.42	17.01	10.03	10.54	11.57	11.30	12.69	13.26	21.03	19.69	9.29	9.49	9.08
Na_2O	0.38	0.69	0.24	0.20	0.25	0.31	0.13	0.79	0.26	0.19	0.50	0.61	0.50
K_2O	0.07	0.11	0.03	0.03	0.02	0.04	0.03	0.77	0.05	0.05	0.34	0.44	0.43
H_2O	1.97	1.97	2.11	2.02	2.06	1.94	2.03	1.98	1.96	1.98	2.03	2.08	2.03
F	0.04	0.00	0.00	0.11	0.01	0.16	0.04	0.02	0.00	0.00	0.05	0.00	0.02
Cl	0.12	0.17	0.02	0.05	0.03	0.18	0.06	0.07	0.13	0.07	0.02	0.02	0.01
Total	**98.11**	**99.04**	**100.12**	**98.80**	**98.67**	**98.21**	**99.12**	**98.34**	**99.51**	**98.91**	**97.60**	**98.92**	**97.18**
Mg#	0.65	0.67	0.94	0.89	0.83	0.79	0.71	0.71	0.49	0.50	0.92	0.90	0.87
$Fe^{3+}/(Fe^{3+}+[6]Al)$	0.57	0.85	1.00	1.00	1.00	0.88	0.65	0.68	0.77	0.60	0.89	0.87	0.80
Si	7.45	7.21	7.44	7.66	7.59	7.70	7.76	6.87	7.60	7.79	7.18	7.13	7.15
Al(iv)	0.55	0.79	0.38	0.27	0.40	0.30	0.24	1.13	0.40	0.21	0.82	0.87	0.85
Al(vi)	0.12	0.13	0.00	0.00	0.00	0.06	0.08	0.19	0.10	0.10	0.10	0.11	0.14
Fe(iii)	0.16	0.76	0.93	0.80	0.64	0.44	0.14	0.39	0.34	0.15	0.78	0.71	0.55
Ti	0.07	0.02	0.14	0.01	0.01	0.01	0.00	0.17	0.01	0.01	0.04	0.07	0.05
Cr	0.00	0.00	0.01	0.00	0.01	0.01	0.00	0.00	0.00	0.00	0.02	0.03	0.00
Fe(ii)	1.63	1.33	0.24	0.45	0.74	0.92	1.40	1.25	2.30	2.33	0.34	0.42	0.55
Mn	0.03	0.04	0.04	0.04	0.03	0.03	0.02	0.02	0.04	0.05	0.01	0.01	0.01
Mg	2.99	2.72	3.83	3.77	3.57	3.53	3.37	2.98	2.22	2.37	3.71	3.65	3.69
Ca	2.00	1.82	1.73	1.76	1.84	1.84	1.99	1.92	1.93	1.94	1.82	1.81	1.92
Na	0.11	0.19	0.07	0.06	0.07	0.09	0.04	0.23	0.08	0.05	0.14	0.17	0.14
K	0.01	0.02	0.00	0.01	0.00	0.01	0.00	0.15	0.01	0.01	0.06	0.08	0.08
TOTAL	**15.12**	**15.04**	**14.80**	**14.82**	**14.91**	**14.93**	**15.03**	**15.29**	**15.02**	**15.02**	**15.00**	**15.02**	**15.06**

SAMPLE NAME Rock Type Mineral Type	TZ41-5 1 mat gabnor M-H	TZ41-5 2 mat gabnor M-H	TZ41-5 3 mat gabnor M-H	TZ41-7 1 mat gabnor M-H
SiO_2	50.57	50.35	47.14	46.94
TiO_2	0.86	1.07	1.67	1.65
Al_2O_3	5.89	6.31	8.16	7.79
Cr_2O_3	0.13	0.18	0.32	0.32
MgO	16.54	16.28	15.29	15.99
CaO	11.82	11.85	11.77	11.88
MnO	0.13	0.11	0.10	0.10
FeO	9.97	10.32	10.18	10.10
Na_2O	0.60	0.61	1.06	0.83
K_2O	0.36	0.42	0.72	0.70
H_2O	2.00	2.09	1.98	2.02
F	0.17	0.00	0.12	0.03
Cl	0.01	0.01	0.03	0.04
Total	**99.05**	**99.60**	**98.53**	**98.37**
Mg#	0.85	0.84	0.81	0.86
$Fe^{3+}/(Fe^{3++}[6]Al)$	0.76	0.76	0.66	0.86
Si	7.20	7.14	6.84	6.78
Al(iv)	0.80	0.86	1.16	1.22
Al(vi)	0.18	0.19	0.23	0.11
Fe(iii)	0.59	0.58	0.45	0.67
Ti	0.09	0.11	0.18	0.18
Cr	0.01	0.02	0.04	0.04
Fe(ii)	0.60	0.64	0.79	0.55
Mn	0.02	0.01	0.01	0.01
Mg	3.51	3.44	3.30	3.44
Ca	1.80	1.80	1.83	1.84
Na	0.17	0.17	0.30	0.23
K	0.06	0.08	0.13	0.13
TOTAL	15.03	15.04	15.26	15.20

SAMPLE NAME	RZ1-1 1	RZ1-1 2	RZ1-2 1	RZ1-2 2	RZ1-2 3	RZ1-4 1	RZ1-4 2	RZ1-5 1	RZ1-5 2	RZ1 C2 a 2	RZ1 C2 b	RZ1 C2 c2
Rock Type	**meta-gabnor**	**meta-gabnor**	**meta-gabnor**	**meta-gabnor**	**meta-gabnor**	**meta-gabnor**	**meta-gabnor**	**meta-gabnor**	**meta-gabnor**	**meta-gabnor**	**meta-gabnor**	**meta-gabnor**
Mineral Type	**M-H**	**M-H**	**M-H**	**M-H**	**M-H**	**M-H**	**Trem**	**M-H**	**Act**	**Act**	**M-H**	**M-H**
SiO_2	47.32	45.90	49.77	49.67	48.63	50.35	53.39	52.31	52.87	53.03	46.61	52.90
TiO_2	0.86	1.43	0.63	0.26	0.34	0.45	0.23	0.26	0.50	0.36	0.90	0.17
Al_2O_3	8.08	8.50	5.26	7.01	8.56	6.08	2.51	5.81	4.60	3.34	8.93	4.95
Cr_2O_3	0.00	0.00	0.04	0.10	0.05	0.00	0.00	0.07	0.00	0.01	0.00	0.08
MgO	13.11	13.14	15.16	15.92	15.26	15.53	17.09	16.91	14.90	16.38	12.50	17.61
CaO	11.56	11.53	11.72	11.90	11.92	11.90	12.16	11.91	12.38	11.50	11.63	11.79
MnO	0.16	0.14	0.14	0.10	0.14	0.18	0.16	0.14	0.27	0.12	0.15	0.14
FeO	13.81	13.23	12.46	9.86	10.19	11.67	10.81	9.11	12.38	12.13	15.06	9.24
Na_2O	0.91	0.74	0.67	0.75	0.97	0.69	0.24	0.55	0.23	0.35	1.03	0.54
K_2O	0.36	0.61	0.17	0.07	0.08	0.15	0.06	0.04	0.08	0.07	0.43	0.03
H_2O	1.99	1.98	1.99	2.02	2.05	2.01	2.06	2.07	2.08	2.08	1.97	2.12
F	0.00	0.00	0.06	0.06	0.00	0.12	0.03	0.06	0.00	0.00	0.06	0.00
Cl	0.12	0.07	0.07	0.03	0.05	0.04	0.04	0.02	0.06	0.04	0.12	0.02
Total	**98.27**	**97.28**	**98.12**	**97.76**	**98.25**	**99.15**	**98.78**	**99.26**	**100.37**	**99.64**	**99.52**	**100.14**
Mg#	0.72	0.74	0.79	0.84	0.82	0.81	0.82	0.86	0.72	0.84	0.70	0.90
$Fe^{3+}/(Fe^{3+}+[6]Al)$	0.64	0.68	0.85	0.61	0.54	0.73	0.94	0.60	0.46	0.93	0.67	0.76
Si	6.93	6.80	7.22	7.15	6.99	7.20	7.61	7.36	7.51	7.50	6.80	7.39
Al(iv)	1.07	1.20	0.78	0.85	1.01	0.80	0.39	0.64	0.49	0.50	1.20	0.61
Al(vi)	0.33	0.28	0.12	0.34	0.44	0.22	0.03	0.33	0.28	0.06	0.33	0.21
Fe(iii)	0.59	0.61	0.66	0.55	0.52	0.62	0.51	0.50	0.24	0.77	0.68	0.67
Ti	0.09	0.16	0.07	0.03	0.04	0.05	0.02	0.03	0.05	0.04	0.10	0.02
Cr	0.00	0.00	0.00	0.01	0.01	0.00	0.00	0.01	0.00	0.00	0.00	0.01
Fe(ii)	1.10	1.03	0.86	0.64	0.70	0.78	0.78	0.57	1.23	0.67	1.16	0.41
Mn	0.02	0.02	0.02	0.01	0.02	0.02	0.02	0.02	0.03	0.01	0.02	0.02
Mg	2.86	2.90	3.28	3.42	3.27	3.31	3.63	3.55	3.16	3.45	2.72	3.67
Ca	1.82	1.83	1.82	1.84	1.84	1.82	1.86	1.80	1.89	1.74	1.82	1.77
Na	0.26	0.21	0.19	0.21	0.27	0.19	0.07	0.15	0.06	0.10	0.29	0.15
K	0.07	0.12	0.03	0.01	0.02	0.03	0.01	0.01	0.01	0.01	0.08	0.01
TOTAL	**15.14**	**15.16**	**15.04**	**15.06**	**15.12**	**15.04**	**14.94**	**14.95**	**14.96**	**14.85**	**15.18**	**14.92**

SAMPLE NAME	RZ1 C4 a	RZ1 C4 b	RZ1 C4 c	RZ1 C5 a	RZ1 C5 b	RZ1 C5 c	RZ2 C1 a	RZ2 C1 b	RZ2 C1 c	RZ2 C2 a	RZ2 C2 b	RZ2 C2 c
Rock Type	meta-gabnor	meta-gabnor	meta-gabnor	meta-gabnor	meta-gabnor	meta-gabnor	micro-breccia	micro-breccia	micro-breccia	micro-breccia	micro-breccia	micro-breccia
Mineral Type	M-H	Act	M-H	M-H	M-H	M-H	M-H	M-H	M-H	Act	M-H	M-H
SiO_2	45.12	53.54	50.74	47.99	53.03	47.20	45.62	48.95	48.33	46.89	43.02	43.20
TiO_2	0.56	0.20	0.46	0.41	0.08	0.97	1.37	0.25	0.18	0.10	0.11	0.77
Al_2O_3	10.09	2.45	5.49	7.82	3.83	8.39	8.38	5.19	6.51	2.95	4.35	6.79
Cr_2O_3	0.03	0.00	0.05	0.00	0.10	0.00	0.03	0.00	0.05	0.03	0.00	0.05
MgO	11.91	16.36	15.33	14.11	17.93	13.05	13.57	14.58	14.66	14.33	13.25	12.73
CaO	11.53	12.64	11.77	11.51	11.69	11.50	10.97	11.19	11.09	9.02	8.40	9.35
MnO	0.14	0.11	0.12	0.13	0.14	0.08	0.14	0.15	0.19	0.15	0.09	0.06
FeO	15.94	11.62	11.91	13.34	9.18	14.76	12.34	13.15	11.77	6.77	8.32	9.65
Na_2O	1.19	0.19	0.66	0.81	0.44	0.94	0.92	0.66	0.92	0.43	0.44	0.77
K_2O	0.16	0.01	0.15	0.15	0.02	0.36	0.69	0.08	0.25	0.03	0.11	0.57
H_2O	1.97	2.08	2.04	1.96	2.02	1.95	1.97	1.96	1.97	1.77	1.68	1.80
F	0.02	0.00	0.04	0.13	0.16	0.13	0.00	0.05	0.06	0.00	0.01	0.00
Cl	0.10	0.03	0.04	0.07	0.02	0.11	0.03	0.04	0.01	0.03	0.03	0.02
Total	**98.91**	**99.61**	**99.16**	**99.00**	**99.42**	**99.83**	**96.12**	**96.24**	**96.26**	**82.52**	**79.82**	**86.24**
Mg#	0.71	0.76	0.79	0.80	0.91	0.73	0.79	0.81	0.82	0.85	0.91	0.81
$Fe^{3+}/(Fe^{3+}+[6]Al)$	0.72	0.77	0.72	0.75	0.86	0.74	0.73	0.87	0.73	0.40	0.72	0.57
Si	6.62	7.67	7.29	6.95	7.48	6.84	6.80	7.22	7.14	7.85	7.46	7.12
Al(iv)	1.38	0.33	0.71	1.05	0.52	1.16	1.20	0.78	0.86	0.15	0.54	0.88
Al(vi)	0.36	0.08	0.22	0.28	0.11	0.28	0.27	0.12	0.27	0.44	0.34	0.43
Fe(iii)	0.91	0.27	0.56	0.86	0.73	0.77	0.72	0.86	0.73	0.30	0.89	0.59
Ti	0.06	0.02	0.05	0.04	0.01	0.11	0.15	0.03	0.02	0.01	0.01	0.10
Cr	0.00	0.00	0.01	0.00	0.01	0.00	0.00	0.00	0.01	0.00	0.00	0.01
Fe(ii)	1.05	1.12	0.87	0.76	0.36	1.02	0.82	0.77	0.72	0.65	0.32	0.74
Mn	0.02	0.01	0.01	0.02	0.02	0.01	0.02	0.02	0.02	0.02	0.01	0.01
Mg	2.60	3.49	3.28	3.04	3.77	2.82	3.02	3.21	3.23	3.58	3.42	3.13
Ca	1.81	1.94	1.81	1.78	1.77	1.79	1.75	1.77	1.75	1.62	1.56	1.65
Na	0.34	0.05	0.18	0.23	0.12	0.26	0.26	0.19	0.26	0.14	0.15	0.25
K	0.03	0.00	0.03	0.03	0.00	0.07	0.13	0.01	0.05	0.01	0.02	0.12
TOTAL	**15.18**	**14.99**	**15.02**	**15.04**	**14.89**	**15.12**	**15.15**	**14.97**	**15.06**	**14.77**	**14.73**	**15.01**

SAMPLE NAME	RZ2 C2 d	RZ2 C2 f	RZ2 C2 e	RZ2-1 1	RZ2-2 1	RZ2-2 2	RZ2-2 3	RZ2-2 4	RZ2-3 1	RZ2-3 2	RZ2-4 1	RZ2-4 2
Rock Type	Micro-breccia	Micro-breccia	Micro-breccia	Micro-breccia	Micro-breccia	Micro-breccia	Micro-breccia	Micro-breccia	Micro-breccia	Micro-breccia	Micro-breccia	Micro-breccia
Mineral Type	M-H	M-H	M-H	M-H	M-H	M-H	Act	M-H	M-H	Act	M-H	M-H
SiO_2	44.93	43.78	42.25	47.63	47.94	48.28	56.17	46.97	49.51	53.36	46.16	46.58
TiO_2	0.19	0.95	1.24	1.40	0.22	0.24	0.11	0.22	0.34	0.13	1.55	1.64
Al_2O_3	5.79	7.72	7.68	7.98	9.46	8.56	1.67	10.13	6.72	3.08	7.69	8.61
Cr_2O_3	0.00	0.08	0.05	0.11	0.01	0.00	0.05	0.03	0.01	0.00	0.06	0.00
MgO	13.90	12.90	13.05	13.99	13.06	13.02	17.63	12.95	14.80	16.36	14.46	13.43
CaO	9.37	10.15	9.43	11.50	11.28	11.51	12.13	11.17	11.50	12.52	11.45	11.82
MnO	0.16	0.06	0.06	0.15	0.18	0.26	0.14	0.23	0.18	0.24	0.16	0.19
FeO	9.03	11.88	9.67	12.80	13.79	14.20	10.68	14.03	13.12	10.97	12.65	13.28
Na_2O	0.82	0.88	0.98	0.95	1.36	0.90	0.26	1.41	0.73	0.27	1.13	0.82
K_2O	0.10	0.70	0.69	0.78	0.18	0.17	0.02	0.20	0.43	0.02	0.76	0.87
H_2O	1.82	1.86	1.85	2.01	1.97	2.03	2.13	2.00	2.04	2.06	1.97	1.95
F	0.00	0.03	0.02	0.07	0.15	0.00	0.02	0.05	0.04	0.05	0.07	0.15
Cl	0.03	0.04	0.04	0.03	0.05	0.05	0.01	0.07	0.00	0.01	0.03	0.07
Total	**86.32**	**91.09**	**89.90**	**99.39**	**99.65**	**99.22**	**101.03**	**99.46**	**99.42**	**99.08**	**98.13**	**99.41**
Mg#	0.88	0.80	0.82	0.75	0.74	0.74	0.81	0.77	0.81	0.77	0.79	0.73
$Fe^{3+}/(Fe^{3++}$[6]												
Al)	0.67	0.73	0.71	0.69	0.58	0.63	0.84	0.64	0.79	0.63	0.89	0.66
Si	7.27	6.87	6.97	6.89	6.89	6.97	7.80	6.76	7.08	7.63	6.77	6.78
Al(iv)	0.73	1.13	1.03	1.11	1.11	1.03	0.20	1.24	0.92	0.37	1.23	1.22
Al(vi)	0.38	0.29	0.32	0.25	0.50	0.42	0.08	0.48	0.22	0.15	0.09	0.26
Fe(iii)	0.78	0.78	0.78	0.57	0.68	0.71	0.41	0.84	0.82	0.27	0.73	0.51
Ti	0.02	0.11	0.09	0.15	0.02	0.03	0.01	0.02	0.04	0.01	0.17	0.18
Cr	0.00	0.01	0.01	0.01	0.00	0.00	0.01	0.00	0.00	0.00	0.01	0.00
Fe(ii)	0.44	0.77	0.69	0.98	0.98	1.01	0.83	0.85	0.75	1.05	0.82	1.11
Mn	0.02	0.01	0.01	0.02	0.02	0.03	0.02	0.03	0.02	0.03	0.02	0.02
Mg	3.36	3.02	3.10	3.02	2.80	2.80	3.65	2.78	3.16	3.49	3.16	2.92
Ca	1.62	1.71	1.69	1.78	1.74	1.78	1.80	1.72	1.76	1.92	1.80	1.84
Na	0.26	0.27	0.27	0.27	0.38	0.25	0.07	0.39	0.20	0.08	0.32	0.23
K	0.02	0.14	0.11	0.14	0.03	0.03	0.00	0.04	0.08	0.00	0.14	0.16
TOTAL	**14.90**	**15.11**	**15.06**	**15.19**	**15.15**	**15.06**	**14.88**	**15.15**	**15.04**	**15.00**	**15.26**	**15.24**

SAMPLE NAME	RZ8-1 1	RZ8-2 1	RZ8-2 2	RZ8-2 3	RZ8-3 1	RZ8-3 2	RZ8-3 3	RZ8-3 4	RZ9-3 1	RZ9-4 1	RZ9-4 2	RZ9-4 3	RZ9-4 4
Rock Type	Chlor-act	Chlor-act	Chlor-act	Chlor-act	Chlor-act	Chlor-act	Chlor-act	Chlor-act	micro-breccia	micro-breccia	micro-breccia	micro-breccia	micro-breccia
Mineral Type	M-H	M-H	M-H	M-H	Act	Act	M-H	M-H	Act	Act	Trem	Trem	Trem
SiO_2	47.77	49.69	47.65	49.15	54.26	56.63	51.39	47.84	54.24	53.24	52.90	51.00	51.85
TiO_2	1.58	1.12	1.62	1.16	0.14	0.06	0.76	1.30	0.14	0.03	0.01	0.02	0.07
Al_2O_3	8.55	7.44	8.56	7.70	2.56	1.21	5.99	8.47	1.91	1.71	0.95	2.99	3.95
Cr_2O_3	0.14	0.12	0.10	0.08	0.09	0.13	0.09	0.05	0.01	0.00	0.00	0.00	0.03
MgO	15.30	15.72	14.39	15.49	16.75	18.35	15.83	14.98	15.88	14.57	14.26	13.49	13.41
CaO	11.73	11.47	11.82	11.50	11.65	12.13	12.05	11.96	12.84	12.62	12.47	12.39	12.43
MnO	0.10	0.14	0.14	0.16	0.41	0.30	0.18	0.12	0.24	0.31	0.39	0.36	0.34
FeO	10.76	11.13	11.31	10.99	11.08	9.27	10.60	10.69	12.19	14.41	14.85	15.75	15.11
Na_2O	0.96	0.77	1.10	0.89	0.39	0.16	0.72	1.01	0.14	0.06	0.08	0.17	0.21
K_2O	0.39	0.22	0.35	0.24	0.04	0.04	0.08	0.11	0.03	0.03	0.03	0.05	0.07
H_2O	2.07	2.07	2.06	2.07	2.08	2.14	2.09	2.00	2.05	2.05	2.00	2.01	2.04
F	0.00	0.04	0.00	0.02	0.03	0.00	0.01	0.13	0.03	0.00	0.03	0.00	0.01
Cl	0.01	0.00	0.02	0.00	0.01	0.00	0.00	0.00	0.08	0.01	0.02	0.03	0.03
Total	**99.37**	**99.92**	**99.09**	**99.43**	**99.47**	**100.42**	**99.79**	**98.66**	**99.77**	**99.05**	**98.00**	**98.25**	**99.54**
Mg#	0.83	0.87	0.76	0.85	0.83	0.84	0.79	0.80	0.71	0.68	0.66	0.67	0.65
$Fe^{3+}/(Fe^{3+}+[6]Al)$	0.71	0.77	0.54	0.73	0.86	0.85	0.57	0.60	0.51	0.85	1.00	0.91	0.59
Si	6.82	7.00	6.88	6.98	7.66	7.87	7.28	6.89	7.78	7.75	7.81	7.52	7.53
Al(iv)	1.18	1.00	1.12	1.02	0.34	0.13	0.72	1.11	0.22	0.25	0.17	0.48	0.47
Al(vi)	0.26	0.24	0.33	0.27	0.09	0.07	0.29	0.33	0.10	0.04	0.00	0.04	0.21
Fe(iii)	0.64	0.80	0.40	0.71	0.57	0.38	0.39	0.49	0.10	0.24	0.23	0.46	0.30
Ti	0.17	0.12	0.18	0.12	0.01	0.01	0.08	0.14	0.01	0.00	0.00	0.00	0.01
Cr	0.02	0.01	0.01	0.01	0.01	0.01	0.01	0.01	0.00	0.00	0.00	0.00	0.00
Fe(ii)	0.65	0.51	0.97	0.59	0.74	0.70	0.87	0.80	1.36	1.51	1.60	1.49	1.53
Mn	0.01	0.02	0.02	0.02	0.05	0.03	0.02	0.02	0.03	0.04	0.05	0.04	0.04
Mg	3.26	3.30	3.10	3.28	3.53	3.80	3.34	3.22	3.39	3.16	3.14	2.97	2.90
Ca	1.79	1.73	1.83	1.75	1.76	1.80	1.83	1.85	1.97	1.97	1.97	1.96	1.93
Na	0.27	0.21	0.31	0.24	0.11	0.04	0.20	0.28	0.04	0.02	0.02	0.05	0.06
K	0.07	0.04	0.06	0.04	0.01	0.01	0.01	0.02	0.01	0.01	0.00	0.01	0.01
TOTAL	**15.13**	**14.98**	**15.20**	**15.04**	**14.88**	**14.86**	**15.04**	**15.15**	**15.02**	**14.99**	**15.00**	**15.02**	**15.01**

SAMPLE NAME	RZ9-4 5	RZ9-4 6	RZ10-1 1	RZ10-1 2	RZ10-2 1	RZ10-2 2	RZ10-3 1	RZ10-4 1	RZ10-4 2	RZ10-4 3	RZ10-5 1	RZ10-5 2	RZ10-6 1
Rock Type	micro-breccia	micro-breccia	micro-breccia	micro-breccia	micro-breccia	micro-breccia	micro-breccia	micro-breccia	micro-breccia	micro-breccia	micro-breccia	micro-breccia	micro-breccia
Mineral Type	Trem	Trem	M-H	M-H	M-H	M-H	M-H	M-H	M-H	M-H	M-H	M-H	Act
SiO_2	52.49	52.57	48.95	49.47	51.13	49.66	49.02	50.93	50.13	45.29	47.94	45.39	54.09
TiO_2	0.00	0.03	0.72	0.40	0.31	0.28	0.40	0.24	0.28	0.29	1.15	0.26	0.05
Al_2O_3	0.42	1.94	8.02	6.75	5.29	6.58	6.76	3.26	6.07	9.13	7.92	11.96	2.74
Cr_2O_3	0.03	0.00	0.02	0.05	0.05	0.04	0.05	0.05	0.01	0.06	0.16	0.02	0.01
MgO	14.11	14.23	14.99	15.96	15.93	16.12	15.98	16.75	15.99	16.48	14.44	14.15	18.55
CaO	12.58	12.56	11.20	11.69	12.45	11.77	11.72	12.76	11.74	9.47	11.64	11.20	12.22
MnO	0.40	0.37	0.24	0.15	0.23	0.15	0.12	0.11	0.14	0.19	0.20	0.17	0.10
FeO	15.09	14.63	11.92	11.06	11.30	11.28	11.05	11.63	11.12	13.41	12.28	12.05	8.49
Na_2O	0.06	0.12	0.85	0.78	0.58	0.85	0.80	0.25	0.72	0.63	0.72	1.73	0.32
K_2O	0.01	0.04	0.43	0.43	0.01	0.29	0.40	0.03	0.38	0.32	0.59	0.20	0.02
H_2O	1.96	2.00	2.05	2.04	2.04	2.06	1.98	2.04	1.98	1.96	2.01	1.97	2.10
F	0.08	0.06	0.01	0.02	0.07	0.02	0.13	0.00	0.17	0.10	0.03	0.15	0.00
Cl	0.02	0.03	0.05	0.05	0.00	0.01	0.05	0.01	0.02	0.02	0.09	0.04	0.02
Total	**97.23**	**98.58**	**99.44**	**98.84**	**99.40**	**99.11**	**98.45**	**98.07**	**98.75**	**97.34**	**99.16**	**99.27**	**98.70**
Mg#	0.65	0.67	0.85	0.86	0.79	0.86	0.86	0.82	0.84	1.00	0.79	0.88	0.89
$Fe^{3+}/(Fe^{3+}+[6]Al)$	1.00	0.85	0.74	0.78	0.71	0.82	0.81	1.00	0.77	1.00	0.73	0.67	0.86
Si	7.84	7.71	6.96	7.07	7.30	7.08	7.04	7.37	7.18	6.38	6.91	6.48	7.63
Al(iv)	0.07	0.29	1.04	0.93	0.70	0.92	0.96	0.56	0.82	1.52	1.09	1.52	0.37
Al(vi)	0.00	0.04	0.30	0.21	0.19	0.18	0.19	0.00	0.21	0.00	0.25	0.50	0.08
Fe(iii)	0.19	0.25	0.87	0.75	0.46	0.80	0.77	0.60	0.68	2.56	0.67	1.02	0.50
Ti	0.00	0.00	0.08	0.04	0.03	0.03	0.04	0.03	0.03	0.03	0.12	0.03	0.01
Cr	0.00	0.00	0.00	0.01	0.01	0.00	0.01	0.01	0.00	0.01	0.02	0.00	0.00
Fe(ii)	1.69	1.54	0.55	0.57	0.89	0.54	0.55	0.81	0.65	0.00	0.81	0.42	0.50
Mn	0.05	0.05	0.03	0.02	0.03	0.02	0.01	0.01	0.02	0.02	0.02	0.02	0.01
Mg	3.14	3.11	3.18	3.40	3.39	3.42	3.42	3.62	3.41	3.46	3.10	3.01	3.90
Ca	2.01	1.97	1.71	1.79	1.91	1.80	1.80	1.98	1.80	1.43	1.80	1.71	1.85
Na	0.02	0.03	0.23	0.22	0.16	0.24	0.22	0.07	0.20	0.17	0.20	0.48	0.09
K	0.00	0.01	0.08	0.08	0.00	0.05	0.07	0.01	0.07	0.06	0.11	0.04	0.00
TOTAL	**15.03**	**15.02**	**15.02**	**15.08**	**15.07**	**15.08**	**15.10**	**15.06**	**15.07**	**15.64**	**15.11**	**15.23**	**14.94**

SAMPLE NAME	**RZ10-6 2**	**RZ10-6 3**	**RZ10-7 1**	**RZ10-7 2**	**RZ10-7 3**
Rock Type	**micro-breccia**	**micro-breccia**	**micro-breccia**	**micro-breccia**	**micro-breccia**
Mineral Type	**M-H**	**Tremolite**	**M-H**	**M-H**	**M-H**
SiO_2	49.22	55.06	53.43	48.44	48.11
TiO_2	0.56	0.03	0.33	0.30	0.49
Al_2O_3	6.95	0.92	3.70	7.59	7.38
Cr_2O_3	0.09	0.08	0.09	0.06	0.01
MgO	16.49	17.75	18.12	15.92	15.83
CaO	11.76	12.50	11.87	11.76	11.52
MnO	0.13	0.29	0.11	0.12	0.10
FeO	9.81	10.29	8.97	11.27	11.49
Na_2O	0.85	0.12	0.51	0.91	0.89
K_2O	0.45	0.01	0.10	0.29	0.48
H_2O	2.06	2.09	2.09	2.00	2.01
F	0.01	0.01	0.03	0.09	0.05
Cl	0.02	0.01	0.02	0.04	0.05
Total	**98.40**	**99.15**	**99.37**	**98.78**	**98.38**
Mg#	0.88	0.81	0.89	0.88	0.88
$Fe^{3+}/(Fe^{3++}[6]Al)$	0.76	1.00	0.86	0.81	0.85
Si	7.05	7.82	7.49	6.93	6.91
Al(iv)	0.95	0.15	0.51	1.07	1.09
Al(vi)	0.22	0.00	0.10	0.21	0.16
Fe(iii)	0.68	0.35	0.61	0.89	0.94
Ti	0.06	0.00	0.03	0.03	0.05
Cr	0.01	0.01	0.01	0.01	0.00
Fe(ii)	0.50	0.87	0.45	0.46	0.44
Mn	0.02	0.03	0.01	0.01	0.01
Mg	3.52	3.76	3.79	3.39	3.39
Ca	1.80	1.90	1.78	1.80	1.77
Na	0.24	0.03	0.14	0.25	0.25
K	0.08	0.00	0.02	0.05	0.09
TOTAL	**15.12**	**14.93**	**14.94**	**15.11**	**15.11**

SAMPLE NAME	RZ20-1 1	RZ20-1 2	RZ20-2 1	RZ20-2 2	RZ20-2 3	RZ20-3 1	RZ20-3 2	RZ28 C2 a	RZ28 C2 a	RZ28 C2 b	RZ28 C4 a	RZ28 C4 b	RZ28 C4 c
Rock Type			**frag metagabronorite**							**frag-vari metagabronorite**			
Mineral Type	**M-H**	**M-H**	**M-H**	**M-H**	**M-H**	**Act**	**Act**	**M-H**	**M-H**	**M-H**	**M-H**	**M-H**	**M-H**
SiO_2	50.80	51.64	50.04	48.74	51.70	54.62	54.06	52.42	52.42	49.11	50.61	49.56	51.85
TiO_2	0.81	0.25	0.65	0.43	0.20	0.04	0.04	0.09	0.09	0.25	0.21	0.22	0.09
Al_2O_3	6.58	4.89	6.79	6.56	3.96	1.89	1.62	4.32	4.32	7.06	5.10	6.41	3.07
Cr_2O_3	0.07	0.02	0.03	0.01	0.04	0.12	0.07	0.00	0.00	0.05	0.04	0.00	0.09
MgO	16.42	17.52	16.28	16.64	18.38	16.89	16.87	17.10	17.10	14.92	16.15	15.37	17.60
CaO	11.69	11.74	11.68	11.79	11.81	12.09	12.08	12.60	12.60	12.41	12.54	12.52	12.62
MnO	0.12	0.15	0.18	0.16	0.17	0.26	0.26	0.14	0.14	0.18	0.13	0.18	0.24
FeO	10.20	10.15	10.74	10.52	9.19	11.18	11.82	11.11	11.11	12.98	11.56	12.88	10.74
Na_2O	0.77	0.59	0.75	0.76	0.44	0.25	0.16	0.46	0.46	0.87	0.64	0.73	0.40
K_2O	0.49	0.25	0.43	0.42	0.20	0.02	0.02	0.13	0.13	0.34	0.21	0.28	0.10
H_2O	2.10	2.08	2.08	2.04	2.05	2.07	2.08	2.10	2.10	2.05	2.05	2.06	1.98
F	0.00	0.00	0.00	0.00	0.04	0.05	0.00	0.00	0.00	0.00	0.01	0.00	0.18
Cl	0.02	0.03	0.03	0.02	0.02	0.02	0.00	0.04	0.04	0.10	0.04	0.05	0.03
Total	**100.07**	**99.29**	**99.67**	**98.08**	**98.19**	**99.49**	**99.07**	**100.62**	**100.62**	**100.57**	**99.49**	**100.37**	**99.14**
Mg#	0.85	0.91	0.87	0.90	0.95	0.80	0.81	0.83	0.83	0.77	0.80	0.79	0.86
$Fe^{3+}/(Fe^{3+}+[6]Al)$	0.71	0.91	0.79	0.89	1.00	0.88	1.00	0.87	0.87	0.74	0.81	0.81	1.00
Si	7.15	7.27	7.07	7.00	7.32	7.74	7.70	7.37	7.37	7.02	7.26	7.07	7.40
Al(iv)	0.85	0.73	0.93	1.00	0.66	0.26	0.27	0.63	0.63	0.98	0.74	0.93	0.52
Al(vi)	0.24	0.08	0.21	0.11	0.00	0.06	0.00	0.08	0.08	0.21	0.12	0.15	0.00
Fe(iii)	0.60	0.84	0.76	0.88	0.90	0.44	0.59	0.59	0.59	0.60	0.51	0.65	0.66
Ti	0.09	0.03	0.07	0.05	0.02	0.00	0.00	0.01	0.01	0.03	0.02	0.02	0.01
Cr	0.01	0.00	0.00	0.00	0.00	0.01	0.01	0.00	0.00	0.01	0.00	0.00	0.01
Fe(ii)	0.60	0.35	0.51	0.38	0.19	0.89	0.82	0.72	0.72	0.95	0.88	0.88	0.63
Mn	0.01	0.02	0.02	0.02	0.02	0.03	0.03	0.02	0.02	0.02	0.02	0.02	0.03
Mg	3.45	3.68	3.43	3.56	3.88	3.57	3.58	3.58	3.58	3.18	3.45	3.27	3.75
Ca	1.76	1.77	1.77	1.81	1.79	1.84	1.84	1.90	1.90	1.90	1.93	1.91	1.93
Na	0.21	0.16	0.21	0.21	0.12	0.07	0.04	0.13	0.13	0.24	0.18	0.20	0.11
K	0.09	0.04	0.08	0.08	0.04	0.00	0.00	0.02	0.02	0.06	0.04	0.05	0.02
TOTAL	**15.06**	**14.98**	**15.05**	**15.10**	**14.95**	**14.91**	**14.89**	**15.05**	**15.05**	**15.20**	**15.14**	**15.17**	**15.06**

SAMPLE NAME	RZ28 C4 d	RZ28 C4 e	RZ28 C4 f	RZ28 C4 g	RZ28 C4 h	RZ28-1 1	RZ28-2 1	RZ28-2 2	RZ28-3 1	RZ28-4 1	RZ28-4 4	RZ28-4 2	RZ28-4 3
Rock Type	Vari-textured fragment metagabbronorite												
Mineral Type	M-H	M-H	M-H	M-H	M-H	M-H	Act	M-H	M-H	Act	Act	M-H	M-H
SiO_2	48.95	52.13	52.76	50.13	51.91	48.32	52.66	49.16	48.48	53.45	52.08	48.56	49.75
TiO_2	0.23	0.13	0.16	0.35	0.28	0.33	0.16	0.19	0.21	0.14	0.32	0.43	0.48
Al_2O_3	6.02	3.95	3.36	5.49	3.59	7.07	3.06	6.32	7.54	2.66	4.33	7.08	5.98
Cr_2O_3	0.00	0.00	0.00	0.00	0.03	0.00	0.04	0.04	0.02	0.07	0.05	0.12	0.03
MgO	15.52	17.01	17.26	15.67	16.78	14.79	17.21	15.41	14.70	17.41	16.10	14.35	14.66
CaO	12.59	12.57	12.88	12.76	12.86	12.11	12.50	12.39	12.05	12.48	12.59	12.13	12.32
MnO	0.19	0.19	0.14	0.21	0.18	0.20	0.21	0.22	0.18	0.21	0.15	0.18	0.18
FeO	12.60	11.15	10.97	12.26	11.16	12.27	9.65	11.44	12.19	10.16	10.84	13.03	12.53
Na_2O	0.71	0.46	0.36	0.64	0.46	0.87	0.31	0.70	0.97	0.32	0.49	0.72	0.77
K_2O	0.29	0.12	0.11	0.22	0.15	0.35	0.10	0.26	0.41	0.10	0.18	0.37	0.31
H_2O	2.04	2.04	2.09	2.04	2.07	2.02	2.05	2.02	1.91	2.09	2.07	1.96	2.03
F	0.00	0.08	0.00	0.04	0.00	0.00	0.02	0.02	0.25	0.00	0.00	0.14	0.00
Cl	0.05	0.03	0.03	0.04	0.03	0.08	0.03	0.06	0.09	0.01	0.03	0.08	0.07
Total	**99.24**	**99.89**	**100.21**	**99.92**	**99.79**	**98.39**	**98.00**	**98.23**	**98.97**	**99.10**	**99.21**	**99.14**	**99.11**
Mg#	0.79	0.83	0.81	0.77	0.79	0.78	0.82	0.79	0.77	0.82	0.76	0.76	0.73
$Fe^{3+}/(Fe^{3+}$[6]Al)	0.88	0.92	0.94	0.81	0.93	0.71	0.77	0.69	0.64	0.89	0.53	0.71	0.59
Si	7.07	7.39	7.47	7.19	7.43	7.03	7.58	7.14	7.02	7.60	7.47	7.03	7.21
Al(iv)	0.93	0.61	0.53	0.81	0.57	0.97	0.42	0.86	0.98	0.40	0.53	0.97	0.79
Al(vi)	0.09	0.05	0.03	0.12	0.03	0.24	0.10	0.22	0.31	0.05	0.20	0.24	0.24
Fe(iii)	0.65	0.57	0.45	0.48	0.38	0.58	0.32	0.49	0.54	0.39	0.22	0.58	0.34
Ti	0.02	0.01	0.02	0.04	0.03	0.04	0.02	0.02	0.02	0.02	0.03	0.05	0.05
Cr	0.00	0.00	0.00	0.00	0.00	0.00	0.01	0.01	0.00	0.01	0.01	0.01	0.00
Fe(ii)	0.87	0.75	0.85	0.99	0.95	0.91	0.84	0.90	0.93	0.81	1.08	0.99	1.18
Mn	0.02	0.02	0.02	0.03	0.02	0.03	0.03	0.03	0.02	0.02	0.02	0.02	0.02
Mg	3.34	3.59	3.64	3.35	3.58	3.21	3.69	3.34	3.17	3.69	3.44	3.10	3.17
Ca	1.95	1.91	1.95	1.96	1.97	1.89	1.93	1.93	1.87	1.90	1.93	1.88	1.91
Na	0.20	0.13	0.10	0.18	0.13	0.25	0.09	0.20	0.27	0.09	0.13	0.20	0.22
K	0.05	0.02	0.02	0.04	0.03	0.06	0.02	0.05	0.08	0.02	0.03	0.07	0.06
TOTAL	**15.20**	**15.06**	**15.07**	**15.18**	**15.13**	**15.20**	**15.03**	**15.17**	**15.22**	**15.01**	**15.10**	**15.15**	**15.19**

SAMPLE NAME	RZ33 -7 1	RZ33-7 2	RZ33- 7 3	RZ48- 1 1	RZ48- 1 2	RZ48- 1 3	RZ48-2 1	RZ48-2 2	RZ48-2 3	RZ48-3 1	RZ48-3 2	RZ48-3 3??	RZ48-3 4
Rock Type	**frag metagabbronorite**							**matrix metagabbronorite**					
Mineral Type	**M-H**	**M-H**	**M-H**	**M-H**	**M-H**	**M-H**	**M-H**	**M-H**	**M-H**	**M-H**	**Actinolite**	**Barroisite**	**Actinolite**
SiO_2	48.42	48.51	49.59	49.22	50.00	51.37	45.91	46.95	47.19	52.83	53.48	53.24	53.54
TiO_2	1.01	1.02	0.52	0.50	0.52	0.44	0.44	0.41	0.45	0.05	0.07	0.07	0.06
Al_2O_3	5.89	6.61	5.04	7.67	6.15	6.33	10.51	9.27	9.24	1.79	1.33	1.46	2.42
Cr_2O_3	0.03	0.18	0.06	0.00	0.00	0.08	0.02	0.05	0.07	0.01	0.00	0.04	0.04
MgO	17.11	16.63	18.07	16.41	17.26	17.56	15.76	15.82	16.24	18.63	18.73	19.58	17.77
CaO	12.05	11.89	11.90	11.61	11.59	11.38	11.49	11.47	11.61	11.06	12.70	5.95	12.10
MnO	0.13	0.09	0.09	0.14	0.13	0.15	0.14	0.17	0.14	0.26	0.21	0.64	0.24
FeO	9.41	9.59	8.97	10.15	9.64	8.66	9.61	10.23	9.78	10.36	8.42	14.85	10.06
Na_2O	0.69	0.82	0.64	1.03	0.68	0.78	0.98	1.24	1.19	0.10	0.11	0.09	0.23
K_2O	0.35	0.50	0.28	0.16	0.33	0.12	0.13	0.19	0.12	0.02	0.01	0.01	0.03
H_2O	2.00	2.04	2.05	2.06	2.03	2.09	2.00	1.99	2.04	2.05	2.04	2.03	2.08
F	0.06	0.00	0.00	0.00	0.07	0.00	0.05	0.05	0.02	0.00	0.04	0.05	0.01
Cl	0.01	0.02	0.01	0.07	0.02	0.04	0.05	0.10	0.04	0.01	0.01	0.00	0.00
Total	**97.17**	**97.90**	**97.19**	**99.01**	**98.42**	**99.01**	**97.08**	**97.95**	**98.11**	**97.16**	**97.15**	**97.99**	**98.57**
Mg#	0.90	0.87	0.95	0.90	0.93	0.95	0.97	0.92	0.94	1.00	0.87	1.00	0.87
$Fe^{3+}/(Fe^{3++}$[6]Al)	0.96	0.84	1.00	0.76	0.87	0.77	0.73	0.75	0.76	1.00	1.00	1.00	0.99
Si	7.02	7.00	7.13	6.98	7.10	7.20	6.61	6.74	6.74	7.49	7.70	7.12	7.60
Al(iv)	0.98	1.00	0.85	1.02	0.90	0.80	1.39	1.26	1.26	0.30	0.23	0.23	0.40
Al(vi)	0.03	0.12	0.00	0.26	0.13	0.24	0.39	0.31	0.30	0.00	0.00	0.00	0.01
Fe(iii)	0.72	0.64	0.89	0.82	0.89	0.81	1.06	0.94	0.95	1.31	0.40	3.78	0.63
Ti	0.11	0.11	0.06	0.05	0.06	0.05	0.05	0.04	0.05	0.00	0.01	0.01	0.01
Cr	0.00	0.02	0.01	0.00	0.00	0.01	0.00	0.01	0.01	0.00	0.00	0.00	0.00
Fe(ii)	0.42	0.52	0.19	0.38	0.26	0.21	0.10	0.29	0.22	0.00	0.62	0.00	0.57
Mn	0.02	0.01	0.01	0.02	0.02	0.02	0.02	0.02	0.02	0.03	0.03	0.07	0.03
Mg	3.70	3.58	3.87	3.47	3.65	3.67	3.38	3.39	3.46	3.94	4.02	3.90	3.76
Ca	1.87	1.84	1.83	1.76	1.76	1.71	1.77	1.77	1.78	1.68	1.96	0.85	1.84
Na	0.19	0.23	0.18	0.28	0.19	0.21	0.27	0.35	0.33	0.03	0.03	0.02	0.06
K	0.07	0.09	0.05	0.03	0.06	0.02	0.02	0.03	0.02	0.00	0.00	0.00	0.01
TOTAL	**$**	**15.16**	**15.06**	**15.07**	**15.01**	**14.94**	**15.07**	**15.15**	**15.13**	**14.79**	**14.99**	**16.00**	**14.91**

SAMPLE NAME	RZ48-41	RZ48-42	RZ48-51	RZ48-52	RZ48-53	RZ48-54	RZ48-55	RZ48-56	RZ48-61	RZ48-62	RZ48-63	RZ48-64	RZ48-65
Rock Type	Matrix metagabbronorite												
Mineral Type	M-H	M-H	Barr	M-H	M-H	M-H	M-H	Act	M-H	M-H	M-H	M-H	Act
SiO_2	49.59	47.64	53.30	49.84	52.95	47.81	53.98	53.44	49.95	47.78	50.18	49.79	55.39
TiO_2	0.28	0.28	0.09	0.50	0.15	0.31	0.12	0.06	0.17	0.69	0.22	0.55	0.02
Al_2O_3	7.06	9.04	3.44	7.47	5.04	10.17	3.70	2.13	6.18	6.88	6.81	7.17	1.20
Cr_2O_3	0.07	0.00	0.04	0.15	0.07	0.03	0.00	0.01	0.00	0.10	0.01	0.09	0.05
MgO	17.61	16.09	18.63	17.32	18.48	15.55	19.54	18.08	17.90	17.44	17.73	17.18	18.72
CaO	11.12	11.55	4.23	11.22	11.94	11.15	10.64	12.38	10.79	11.42	12.00	11.67	12.44
MnO	0.14	0.13	0.79	0.15	0.17	0.15	0.16	0.21	0.17	0.15	0.11	0.12	0.24
FeO	9.23	9.82	16.37	9.02	8.28	10.37	8.17	9.20	9.84	9.11	8.60	9.10	9.04
Na_2O	0.84	1.13	0.29	0.95	0.56	1.30	0.46	0.18	0.75	0.77	0.77	0.95	0.14
K_2O	0.26	0.20	0.04	0.19	0.24	0.25	0.10	0.04	0.20	0.36	0.05	0.23	0.02
H_2O	2.06	2.01	2.08	2.08	2.08	2.04	2.12	2.07	2.04	2.02	2.02	2.04	2.06
F	0.00	0.06	0.00	0.00	0.08	0.05	0.00	0.00	0.04	0.00	0.12	0.07	0.12
Cl	0.06	0.07	0.02	0.05	0.03	0.05	0.02	0.01	0.03	0.05	0.03	0.05	0.00
Total	**98.32**	**98.01**	**99.33**	**98.93**	**100.08**	**99.24**	**99.01**	**97.81**	**98.05**	**96.77**	**98.66**	**99.01**	**99.42**
Mg#	1.00	0.92	1.00	0.98	0.94	0.92	1.00	0.86	1.00	1.00	0.95	0.92	0.86
$Fe^{3+}/(Fe^{3++}$[6] Al)	0.88	0.72	1.00	0.81	0.80	0.68	0.98	0.98	0.96	0.96	0.79	0.78	1.00
Si	6.99	6.82	6.96	6.99	7.35	6.75	7.42	7.65	7.03	6.88	7.08	7.03	7.78
Al(iv)	1.01	1.18	0.53	1.01	0.65	1.25	0.58	0.35	0.97	1.12	0.92	0.97	0.20
Al(vi)	0.16	0.35	0.00	0.23	0.17	0.45	0.02	0.01	0.05	0.05	0.22	0.23	0.00
Fe(iii)	1.15	0.88	4.27	0.99	0.70	0.96	1.26	0.47	1.39	1.10	0.80	0.78	0.44
Ti	0.03	0.03	0.01	0.05	0.02	0.03	0.01	0.01	0.02	0.07	0.02	0.06	0.00
Cr	0.01	0.00	0.00	0.02	0.01	0.00	0.00	0.00	0.00	0.01	0.00	0.01	0.01
Fe(ii)	0.00	0.29	0.00	0.07	0.26	0.27	0.00	0.63	0.00	0.00	0.21	0.29	0.62
Mn	0.02	0.02	0.09	0.02	0.02	0.02	0.02	0.03	0.02	0.02	0.01	0.01	0.03
Mg	3.70	3.43	3.63	3.62	3.82	3.28	4.01	3.86	3.75	3.75	3.73	3.62	3.92
Ca	1.68	1.77	0.59	1.69	1.77	1.69	1.57	1.90	1.63	1.76	1.81	1.77	1.87
Na	0.23	0.31	0.07	0.26	0.15	0.36	0.12	0.05	0.20	0.22	0.21	0.26	0.04
K	0.05	0.04	0.01	0.03	0.04	0.04	0.02	0.01	0.04	0.07	0.01	0.04	0.00
TOTAL	**15.02**	**15.12**	**16.15**	**14.98**	**14.97**	**15.09**	**15.02**	**14.96**	**15.10**	**15.04**	**15.04**	**15.07**	**14.91**

SAMPLE NAME	RZ48-6 6	RZ48-6 7	RZ48-6 8
Rock Type	matrix metagabbronorite		
Mineral Type	M-H	Act	M-H
SiO_2	50.49	53.36	49.56
TiO_2	0.25	0.04	0.84
Al_2O_3	6.22	2.07	5.34
Cr_2O_3	0.03	0.03	0.02
MgO	17.68	18.54	18.25
CaO	11.99	12.48	11.54
MnO	0.13	0.16	0.14
FeO	8.56	8.90	8.76
Na_2O	0.68	0.19	0.60
K_2O	0.25	0.02	0.31
H_2O	2.03	2.02	2.04
F	0.09	0.11	0.00
Cl	0.03	0.01	0.05
Total	**98.43**	**97.93**	**97.45**
Mg#	0.92	0.88	1.00
$Fe^{3+}/(Fe^{3+}+[6]Al)$	0.78	1.00	1.00
Si	7.16	7.62	7.07
Al(iv)	0.84	0.35	0.90
Al(vi)	0.20	0.00	0.00
Fe(iii)	0.70	0.53	1.04
Ti	0.03	0.00	0.09
Cr	0.00	0.00	0.00
Fe(ii)	0.31	0.53	0.01
Mn	0.02	0.02	0.02
Mg	3.74	3.95	3.88
Ca	1.82	1.91	1.76
Na	0.19	0.05	0.17
K	0.05	0.00	0.06
TOTAL	**15.06**	**14.97**	**14.99**

SAMPLE NAME	rz-1 c1-1	rz-1 c1-2	rz-1 c2-1	rz-1 c2-2	rz-1 c2-3	rz-1 c2-4	rz-1 c2-5	rz-1 c3-1a	rz-1 c3-1b	rz-1 c3-2	rz-1 c3-3	rz-1 c3-4
Mineral Type						**Magnesio-Hornblende**						
CaO (wt%)	11.5	11.5	11.7	11.9	11.7	11.7	11.9	11.5	11.5	11.7	11.9	11.7
^{137}Ba (ppm)	16.6	22.8	2.27	2.5	29.5	12.8	1.81	189	331	350	99.6	272
^{140}Ce	21.5	14.7	3.07	4.01	15.8	11.9	1.30	7.20	3.75	4.28	1.52	4.77
^{59}Co	58.9	55.7	46.9	55.2	61.5	64.9	35.2	7.16	1.79	2.24	5.50	5.92
^{52}Cr	21.6	57.2	217	376	19.6	19.8	112	168	71.7	72.0	210	120
^{65}Cu	3.70	403	3.30	2.16	2.80	2.07	8540	149	48.9	46.9	96.36	80.3
^{133}Cs	0.11	0.11	0.11	0.07	0.10	0.08	0.11	1.72	1.36	1.35	2.55	1.55
^{163}Dy	5.34	3.91	1.14	1.37	7.60	6.02	0.96	0.42	0.49	0.59	0.28	0.43
^{166}Er	2.96	2.23	0.75	0.90	4.13	3.20	0.80	0.24	0.29	0.36	0.39	0.32
^{153}Eu	0.77	0.55	0.45	0.44	0.77	0.56	0.11	0.22	0.25	0.29	0.11	0.29
^{157}Gd	0.08	0.08	0.08	0.08	0.08	0.08	0.54	0.78	0.67	0.55	0.56	0.70
^{178}Hf	1.38	1.24	0.22	0.29	2.58	1.88	0.44	1.63	3.19	2.91	1.04	2.39
^{165}Ho	1.09	0.78	0.24	0.29	1.56	1.22	0.24	0.09	0.09	0.08	0.11	0.10
^{139}La	7.02	5.42	1.04	1.30	5.45	4.10	0.70	6.06	2.98	3.23	1.16	3.89
^{175}Lu	0.37	0.31	0.15	0.15	0.43	0.34	0.20	0.06	0.06	0.07	0.08	0.07
^{93}Nb	1.47	1.30	0.06	0.27	1.61	0.74	0.20	0.80	0.79	0.83	0.81	0.75
^{146}Nd	17.7	12.7	3.82	4.56	17.5	13.8	0.99	2.42	1.97	2.16	1.00	2.28
^{60}Ni	434	428	396	445	467	471	394	169	60.6	64.8	220	157
^{208}Pb	1.34	2.61	0.24	0.30	0.44	0.44	89.1	44.0	23.7	22.1	11.5	20.7
^{141}Pr	3.62	2.53	0.63	0.82	3.07	2.37	0.19	0.76	0.49	0.57	0.17	0.60
^{85}Rb	0.46	0.71	0.29	0.17	1.12	0.87	0.21	23.0	39.4	45.1	12.64	31.9
^{121}Sb	N/A	N/A	N/A	N/A	N/A	N/A	N/A	N/A	N/A	N/A	N/A	N/A
^{45}Sc	88.5	84.0	34.4	31.7	168	147	43.1	269	113	114	395	195
^{147}Sm	4.68	3.27	1.10	1.22	5.54	4.47	0.37	0.47	0.46	0.37	0.28	0.51
^{88}Sr	10.3	9.03	3.33	3.95	9.65	7.37	4.27	42.8	64.4	73.4	50.04	115
^{181}Ta	0.058	0.057	0.003	0.016	0.12	0.04	0.009	0.045	0.070	0.057	0.028	0.075
^{159}Tb	0.79	0.58	0.18	0.19	1.09	0.91	0.11	0.09	0.07	0.06	0.06	0.07
^{169}Tm	0.43	0.31	0.13	0.12	0.53	0.41	0.14	0.05	0.06	0.07	0.07	0.06
^{51}V	291	702	798	736	284	305	542	165	60.1	66.7	206	100
^{172}Yb	2.76	2.12	0.91	0.98	3.30	2.55	1.18	0.24	0.45	0.40	0.43	0.34
^{89}Y	28.8	21.06	6.60	7.75	40.1	31.3	6.87	3.19	3.31	3.16	3.33	3.12
^{91}Zr	18.7	17.72	8.19	7.24	28.5	21.6	6.95	109	129	130	100	115

B-4 TRACE ELEMENT COMPOSITION

SAMPLE NAME	rz2 c1-1b	rz2 c1-1c	rz2 c1-1d	rz2 c1-1e	rz2 c1-1f	rz2 c2-1a	rz2 c2-1b	rz2 c2-1c	rz2 c2-2	rz2 c1-1a	rz2 c4-1	rz2 c4-2	rz2 c4-3
Mineral Type	Magnesio-Hornblende												
CaO (wt%)	11.50	11.50	11.50	11.50	11.50	11.28	11.28	11.28	11.51		11.82	11.82	11.812
^{137}Ba (ppm)	25.87	47.19	57.04	57.14	40.77	1.68	3.96	2.31	7.82	24.47	50.81	4.50	26.40
^{140}Ce	11.13	12.94	9.39	7.87	11.70	2.81	3.61	2.36	4.44	10.67	10.74	2.56	7.81
^{59}Co	73.84	73.25	71.69	66.74	66.82	74.94	68.10	69.99	71.85	63.75	64.27	69.69	52.75
^{52}Cr	181.20	235.40	178.40	214.30	247.70	232.60	253.80	193.30	152.40	188.40	152.10	41.20	136.40
^{65}Cu	0.58	0.54	0.61	0.70	0.47	0.22	0.39	0.30	1.07	0.42	0.16	ND	ND
^{133}Cs	0.05	0.02	0.03	0.11	0.05	0.07	0.08	0.05	0.21	0.07	0.03	0.11	0.03
^{163}Dy	2.80	3.75	2.17	2.02	2.91	1.65	2.84	1.58	0.39	2.78	3.22	0.38	3.06
^{166}Er	1.76	2.25	1.33	1.28	1.85	0.82	1.64	0.90	0.30	1.74	1.95	0.35	1.80
^{153}Eu	0.73	0.84	0.62	0.55	0.75	0.17	0.38	0.15	0.41	0.73	0.71	0.23	0.52
^{157}Gd	0.08	0.08	0.08	0.08	0.08	0.08	0.08	0.08	0.08	0.08	0.08	0.31	0.08
^{178}Hf	1.50	1.70	1.10	1.06	1.38	0.78	0.65	0.67	0.10	1.33	1.15	0.11	1.10
^{165}Ho	0.57	0.75	0.45	0.41	0.63	0.30	0.59	0.30	0.10	0.58	0.68	0.10	0.62
^{139}La	3.21	3.91	3.04	2.62	3.72	0.61	0.83	0.54	1.56	3.31	3.63	1.15	2.46
^{175}Lu	0.28	0.32	0.21	0.19	0.25	0.09	0.22	0.10	0.09	0.26	0.29	0.09	0.21
^{93}Nb	0.31	1.23	3.57	2.92	1.75	0.21	0.55	0.10	0.12	0.27	4.35	0.16	2.21
^{146}Nd	8.58	10.52	6.62	5.78	9.03	3.31	3.99	2.86	1.85	8.24	9.06	1.56	8.11
^{60}Ni	297.80	298	292	247.40	270.40	189.30	203.90	180.90	251.20	262.60	254.30	248.40	182.60
^{208}Pb	0.274	0.356	0.333	0.264	0.255	0.193	0.178	0.274	0.237	0.243	0.175	0.113	0.115
^{141}Pr	1.81	2.14	1.40	1.22	1.86	0.57	0.70	0.46	0.51	1.74	1.87	0.36	1.50
^{85}Rb	3.05	5.74	7.30	6.92	5.20	0.07	0.16	0.88	0.36	2.79	5.78	0.13	2.57
^{121}Sb	N/A	N/A	N/A	N/A	N/A	N/A	N/A	N/A	N/A	N/A	N/A	N/A	N/A
^{45}Sc	81.46	89.30	73.15	71.14	82.71	82.72	73.87	85.11	37.11	79.15	79.16	23.36	88.36
^{147}Sm	2.32	2.88	1.68	1.60	2.35	1.23	1.52	1.07	0.31	2.16	2.56	0.31	2.33
^{88}Sr	13.87	21.00	24.54	21.38	20.14	4.33	5.81	3.73	11.89	13.78	24.83	8.62	12.94
^{181}Ta	0.016	0.085	0.274	0.199	0.098	0.019	0.041	0.010	0.005	0.018	0.292	0.010	0.126
^{159}Tb	0.40	0.54	0.32	0.29	0.43	0.25	0.36	0.21	0.06	0.41	0.46	0.05	0.45
^{169}Tm	0.28	0.32	0.21	0.20	0.25	0.12	0.25	0.12	0.05	0.26	0.28	0.06	0.25
^{51}V	369	348	283	303	312	252	266	266	157	283	333	189	259
^{172}Yb	1.99	2.29	1.51	1.37	1.81	0.61	1.71	0.80	0.53	1.74	1.97	0.55	1.59
^{89}Y	15.51	20.00	12.05	11.24	16.53	7.81	14.58	7.65	2.51	15.66	17.75	2.64	16.79
^{91}Zr	41.48	46.65	31.58	31.08	39.93	13.20	13.68	10.30	6.01	36.87	33.76	5.98	25.04

SAMPLE NAME	Rz33 c7-1	Rz33 c7-2	Rz33 c7-3	Rz33 c7-4	Rz33 c7-5	Rz33 c7-6
Mineral Type			Magnesio-Hornblende			
CaO (wt%)	11.89	11.90	11.90	12.05	12.05	12.05
^{137}Ba (ppm)	15.01	21.18	16.20	14.49	23.35	29.47
^{140}Ce	7.09	6.25	6.93	6.38	8.68	12.39
^{59}Co	55.46	49.38	51.99	53.19	60.77	55.57
^{52}Cr	374.5	392.5	466.1	401.0	522.7	743.1
^{65}Cu	563.2	38.98	200.2	2592.0	57.4	10.5
^{133}Cs	0.18	0.12	0.11	0.11	0.18	0.27
^{163}Dy	2.06	2.31	2.70	2.14	2.51	3.81
^{166}Er	1.34	1.43	1.69	1.43	1.74	2.68
^{153}Eu	0.44	0.37	0.43	0.40	0.51	0.71
^{157}Gd	0.08	0.08	0.08	0.08	0.08	0.08
^{178}Hf	0.77	1.07	1.03	0.92	1.06	1.38
^{165}Ho	0.43	0.48	0.57	0.48	0.55	0.87
^{139}La	2.77	2.47	2.61	2.48	3.26	4.55
^{175}Lu	0.22	0.21	0.25	0.24	0.28	0.43
^{93}Nb	1.24	1.10	0.94	0.81	1.89	3.51
^{146}Nd	5.23	5.07	5.94	4.85	6.08	9.13
^{60}Ni	590.5	461.3	473.9	463.7	514.4	460.4
^{208}Pb	1.08	0.77	0.82	5.67	0.99	1.10
^{141}Pr	1.08	1.01	1.14	0.98	1.31	1.94
^{85}Rb	1.00	1.12	0.97	0.78	1.56	1.32
^{121}Sb	0.08	0.04	0.03	0.03	0.07	0.08
^{45}Sc	89.4	98.1	96.1	96.8	100	136
^{147}Sm	1.34	1.51	1.73	1.31	1.66	2.45
^{88}Sr	12.01	14.92	13.98	12.03	16.33	18.49
^{181}Ta	0.07	0.11	0.08	0.07	0.13	0.20
^{159}Tb	0.28	0.32	0.37	0.29	0.34	0.52
^{169}Tm	0.21	0.21	0.26	0.23	0.25	0.41
^{51}V	341	282	310	301	381.	489
^{172}Yb	1.47	1.42	1.71	1.58	1.92	2.93
^{89}Y	11.73	12.99	15.25	12.36	14.57	23.67
^{91}Zr	19.21	27.50	25.67	21.69	29.51	40.96

SAMPLE NAME	Rz1 c4-1a	Rz1 c4-1b	Rz1 c4-1c	Rz1 c4-1d	Rz1 c4-1e	Rz1 c4-2	Rz1 c4-3a	Rz1 c4-3b	Rz1 c4-4	Rz1 c5-1a	Rz1 c5-1b	Rz1 c5-2	Rz1 c5-3	Rz1 c5-4	Rz1 c5-5
Mineral Type								Actinolite							
CaO (wt%)	11.56	11.56	11.56	11.56	11.56	11.56	11.56	11.56	11.56	11.56	11.56	11.56	11.56	11.56	11.56
^{137}Ba (ppm)	9.32	8.60	7.61	34.23	13.80	13.18	14.36	7.90	12.05	6.76	4.89	20.78	4.42	4.93	13.02
^{140}Ce	9.99	12.12	7.04	24.49	16.27	15.91	17.02	15.57	19.55	1.94	5.05	10.49	0.77	1.85	11.76
^{59}Co	56.87	58.56	53.34	60.26	62.00	57.17	56.04	59.43	51.27	40.81	39.68	53.75	66.56	43.13	54.38
^{52}Cr	26.98	19.67	29.93	34.29	17.43	11.05	16.04	19.34	19.72	295.90	275.00	11.93	14.50	217.60	26.31
^{65}Cu	1.93	0.62	4.90	1.46	1641	1.23	30.94	14.67	36.92	1344	6.41	3.14	16.61	2770	501.8
^{133}Cs	0.09	0.05	0.17	0.07	0.05	0.10	0.08	0.09	0.05	0.05	0.05	0.06	0.05	0.07	0.04
^{163}Dy	4.78	4.76	4.27	7.17	6.65	5.07	4.80	3.72	4.34	2.23	3.18	4.95	1.96	1.77	5.79
^{166}Er	2.76	2.49	2.30	3.87	3.75	2.87	3.11	2.34	2.57	1.62	1.93	2.53	1.76	1.21	3.13
^{153}Eu	0.41	0.44	0.36	0.79	0.68	0.53	0.69	0.59	0.68	0.32	0.60	0.49	0.11	0.26	0.60
^{157}Gd	0.08	0.08	0.08	0.08	0.08	0.08	0.08	0.08	0.08	0.08	0.08	0.08	0.83	0.08	0.08
^{178}Hf	1.46	1.19	1.05	2.80	2.83	1.49	1.19	0.85	1.26	0.37	0.78	1.69	0.16	0.29	1.63
^{165}Ho	0.99	0.91	0.84	1.37	1.34	1.01	0.97	0.76	0.88	0.51	0.65	0.98	0.52	0.40	1.14
^{139}La	3.35	3.65	2.10	7.46	4.88	5.50	5.86	5.37	6.35	0.52	1.18	3.21	0.19	0.53	3.34
^{175}Lu	0.32	0.25	0.27	0.41	0.42	0.32	0.46	0.37	0.33	0.29	0.32	0.27	0.32	0.14	0.33
^{93}Nb	0.68	0.86	0.53	3.74	0.99	0.94	1.18	1.07	1.61	0.48	0.57	0.69	0.18	0.17	0.72
^{146}Nd	11.02	11.14	7.92	21.14	16.90	14.12	15.25	13.38	16.96	2.70	7.20	12.27	1.08	2.18	13.17
^{60}Ni	593.2	568.8	501.7	641.8	600.8	590	578.8	640.9	631.3	317.3	338.4	576.7	638.8	425.2	538.6
^{208}Pb	0.583	0.247	0.332	0.588	0.368	0.901	24.31	8.173	20.34	0.682	0.474	0.5	8.552	875.2	2.995
^{141}Pr	1.96	2.15	1.36	4.14	3.04	2.76	3.07	2.69	3.39	0.46	1.18	2.20	0.15	0.37	2.38
^{85}Rb	0.37	0.33	0.45	1.51	0.74	0.45	0.51	0.35	0.42	0.23	0.22	0.41	0.16	0.17	0.30
^{121}Sb	N/A	N/A	N/A	N/A	N/A	N/A	N/A	N/A	N/A	N/A	N/A	N/A	N/A	N/A	N/A
^{45}Sc	156.5	131.3	148.7	161.7	133	131.2	83.4	76.7	87.4	70.1	107.2	144	32.2	53.3	140.6
^{147}Sm	3.52	3.68	2.83	6.06	5.27	4.11	4.07	3.34	4.44	0.90	2.34	3.82	0.56	0.74	4.27
^{88}Sr	5.25	5.10	4.46	10.22	7.23	7.75	9.02	7.66	8.38	3.81	5.08	6.55	2.17	2.83	5.60
^{181}Ta	0.047	0.045	0.032	0.194	0.048	0.052	0.087	0.061	0.096	0.037	0.022	0.056	0.010	0.015	0.047
^{159}Tb	0.73	0.69	0.62	1.05	0.98	0.74	0.69	0.55	0.68	0.28	0.43	0.75	0.24	0.23	0.85
^{169}Tm	0.34	0.34	0.31	0.51	0.47	0.38	0.43	0.35	0.35	0.26	0.30	0.32	0.28	0.17	0.40
^{51}V	256.5	228	285.5	397	250.4	178.8	191.1	193.6	276.2	1157	882.1	182.5	257.5	920.1	276.8
^{172}Yb	2.27	1.98	2.01	3.42	3.19	2.39	3.15	2.59	2.61	1.87	2.08	2.04	2.04	1.18	2.56
^{89}Y	24.82	24.12	21.45	36.36	34.45	26.65	26.01	20.69	23.67	14.78	17.22	24.85	15.46	11.20	29.69
^{91}Zr	14.88	13.26	15.79	35.04	57.64	17.47	19.05	16.23	16.89	3.75	6.86	16.19	2.15	3.16	14.12

SAMPLE NAME	Rz 9 point 4-1	Rz 9 point 4-2	Rz 9 ponit 4-3	Rz 9 point 4-4	Rz 9 point 4-5	Rz9 c1-2
Mineral Type			**Actinolite**			
CaO (wt%)	12.62	12.47	12.39	12.43	12.58	12.62
^{137}Ba (ppm)	9.32	8.60	7.61	34.23	13.80	13.18
^{140}Ce	9.99	12.12	7.04	24.49	16.27	15.91
^{59}Co	56.87	58.56	53.34	60.26	62.00	57.17
^{52}Cr	26.98	19.67	29.93	34.29	17.43	11.05
^{65}Cu	1.93	0.62	4.90	1.46	1641	1.23
^{133}Cs	0.09	0.05	0.17	0.07	0.05	0.10
^{163}Dy	4.78	4.76	4.27	7.17	6.65	5.07
^{166}Er	2.76	2.49	2.30	3.87	3.75	2.87
^{153}Eu	0.41	0.44	0.36	0.79	0.68	0.53
^{157}Gd	0.08	0.08	0.08	0.08	0.08	0.08
^{178}Hf	1.46	1.19	1.05	2.80	2.83	1.49
^{165}Ho	0.99	0.91	0.84	1.37	1.34	1.01
^{139}La	3.35	3.65	2.10	7.46	4.88	5.50
^{175}Lu	0.32	0.25	0.27	0.41	0.42	0.32
^{93}Nb	0.68	0.86	0.53	3.74	0.99	0.94
^{146}Nd	11.02	11.14	7.92	21.14	16.90	14.12
^{60}Ni	593.2	568.8	501.7	641.8	600.8	590
^{208}Pb	0.583	0.247	0.332	0.588	0.368	0.901
^{141}Pr	1.96	2.15	1.36	4.14	3.04	2.76
^{85}Rb	0.37	0.33	0.45	1.51	0.74	0.45
^{121}Sb	N/A	N/A	N/A	N/A	N/A	N/A
^{45}Sc	156.5	131.3	148.7	161.7	133	131.2
^{147}Sm	3.52	3.68	2.83	6.06	5.27	4.11
^{88}Sr	5.25	5.10	4.46	10.22	7.23	7.75
^{181}Ta	0.047	0.045	0.032	0.194	0.048	0.052
^{159}Tb	0.73	0.69	0.62	1.05	0.98	0.74
^{169}Tm	0.34	0.34	0.31	0.51	0.47	0.38
^{51}V	256.5	228	285.5	397	250.4	178.8
^{172}Yb	2.27	1.98	2.01	3.42	3.19	2.39
^{89}Y	24.82	24.12	21.45	36.36	34.45	26.65
^{91}Zr	14.88	13.26	15.79	35.04	57.64	17.47

APPENDIX

III

Chalcophile and Siderophile Element Data Recalculated to 100%

Abbreviations used:

Rz	= Roby Zone (High-grade Zone samples are from Rz-01 to Rz17, inclusive)
Tz	= Twilight Zone
po	= pyrrhotite
pn	= pentlandite
ccp	= chalcopyrite
Chlor-act	= chlorite-actinolite schist
Meta-gabnor	= metagabbronorite
Leuco-gabnor	= leucogabbronorite
Gabnor	= gabbronorite
ND	= not detected
Frag	= fragment
Mat	= matrix
Peg	= pegmatite
Frag-vari-	= varitextured fragment

C-1 ROBY ZONE

SAMPLE	Rz-01	Rz-05	Rz-12	Rz-16	Rz-17	Rz-19	Rz-20	Rz-22 frag	Rz-25 frag	Rz-26	Rz-27 frag
Rock Type	Chlor-act schist	Chlor-act schist	Chlor-act schist	Chlor-act schist	Chlor-act schist	frag meta-gabnor	frag meta-gabnor	leuco-gabnor	meta-gabnor	frag meta-gabnor	meta-gabnor
Cu (wt%)	1.11	0.53	0.35	1.00	0.80	0.76	0.48	0.60	0.54	0.53	0.17
Fe	43.7	52.4	57.1	41.4	46.2	49.3	53.7	51.8	54.3	54.8	56.9
Ni	0.40	0.42	0.89	0.74	1.00	0.71	0.57	0.72	0.43	0.57	0.14
S	37.2	38.1	40.7	37.8	37.2	38.7	39.6	39.2	38.7	39.7	39.9
Au (ppm)	340	103	296	349	4154	219	193	342	105	212	97
Ir	0.002	0.01	0.08	0.01	0.03	0.02	0.01	0.002	0.004	0.01	0.09
Os	0.02	0.01	0.92	0.08	0.01	0.05	0.07	0.07	0.03	0.99	0.11
Pd	4.36	169	2053	239	2183	132	88	ND	93	95	17
Pt	1.14	15.1	161	28	128	18.4	158	0.25	ND	14.2	3.99
Re	0.01	0.09	0.03	0.13	0.10	0.08	0.06	ND	0.06	0.13	0.06
Rh	ND	ND	ND	ND	0.38	0.18	0.22	0.45	0.16	0.13	0.92
Ru	0.24	0.12	2.07	0.54	1.38	ND	ND	ND	0.17	0.66	0.77

ROBY ZONE

SAMPLE Rock Type	Rz-30 Mat gabnor	Rz-32 frag meta-gabnor	Rz-36 mat meta-gabnor	Rz-41 mat gabnor	Rz-42 mat meta-gabnor	Rz-43 mat meta-gabnor	Rz-44 mat meta-gabnor	Rz-45 mat meta-gabnor	Rz-50 mat meta-gabnor	Rz-54 mat meta-gabnor	Rz-55 mat meta-gabnor
Cu (wt%)	0.79	0.54	0.78	0.65	0.82	0.80	1.06	0.86	1.16	0.71	1.35
Fe	47.6	55.0	54.2	48.4	49.6	53.5	44.2	47.5	48.0	46.5	43.1
Ni	0.69	0.13	0.82	0.63	0.68	0.83	1.16	0.74	0.47	0.54	0.87
S	37.0	40.8	39.6	37.8	38.4	40.2	37.4	37.2	37.7	37.6	37.1
Au (ppm)	175	234	344	352	159	361	240	297	196	272	499
Ir	0.02	0.007	0.02	0.016	0.07	0.06	0.12	0.03	0.005	0.011	0.03
Os	0.08	0.04	0.10	0.02	0.25	0.30	0.35	0.11	0.02	0.02	0.02
Pd	105	53.4	270	101	203	229	484	313	51.9	170	296
Pt	16.8	15.3	32	15.4	34.3	14.1	54.6	42.0	7.54	24.9	38.0
Re	0.07	0.05	0.03	0.05	0.13	0.10	0.05	0.08	0.04	0.05	0.04
Rh	0.20	0.13	0.13	0.17	0.21	0.45	0.96	0.30	0.13	0.17	0.39
Ru	0.08	0.44	0.66	0.45	0.62	1.34	0.65	0.18	ND	0.13	ND

C-2 TWILIGHT ZONE

SAMPLE	Tz-1	Tz-3	Tz-4	Tz-6	Tz-7	Tz-10	Tz-12	Tz-13	Tz-€15	Tz-16	Tz-19	Tz-20
Rock Type	frag gabnor	frag gabnor	frag gabnor	mat gabnor	frag gabnor	frag gabnor	frag leuco-gabnor	frag meta-gabnor	Mat meta-gabnor	mat meta-gabnor	mat meta-gabnor	peg leuco-gabnor
Cu (wt%)	1.30	1.15	1.42	1.09	0.90	1.47	1.23	1.45	1.10	1.03	1.34	0.14
Fe	44.3	45.7	40.3	46.3	48.5	41.8	44.1	36.9	45.8	44.0	42.6	51.6
Ni	0.58	0.59	0.96	0.57	0.50	0.72	0.69	1.02	0.56	0.71	0.75	0.57
S	36.7	36.9	35.8	37.0	37.4	36.2	36.6	34.0	36.6	35.7	36.3	37.6
Au (ppm)	21	23	22	20	23	22	20	26	23	30	24	4
Ir	0.03	0.01	0.03	0.03	0.02	0.01	0.02	0.04	0.02	0.07	0.03	0.07
Os	0.01	0.03	0.03	0.15	0.02	0.02	0.06	0.08	0.01	0.05	0.01	0.07
Pd	259	26	210	187	153	101	11.7	245	177	430	228	391
Pt	30.1	8.78	30.7	25.5	26.2	13.3	14.2	34.8	24.6	86.3	27.7	40.2
Re	0.11	0.01	0.06	0.07	0.04	0.02	0.06	0.02	0.06	0.16	0.09	0.02
Rh	0.004	0.29	0.31	0.09	0.28	0.05	0.75	1.27	0.39	0.26	0.20	ND
Ru	0.09	0.25	1.11	0.10	0.16	0.16	0.40	6.23	0.12	0.37	0.09	0.47

TWILIGHT ZONE

SAMPLE Rock Type	**Tz-21 mat meta-gabnor**	**Tz-22 frag meta-gabnor**	**Tz-25 mat meta gabnor**	**Tz-26 mat meta-gabnor**	**Tz-27 peg leuco-gabnor**	**Tz-28 peg gabnor**	**Tz-29 peg leuco-gabnor**	**Tz-30 Mat leuco-gabnor**	**Tz-39 mat meta-gabnor**	**Tz-40 mat meta-gabnor**	**Tz-42 mat leuco-gabnor**
Cu (wt%)	1.23	1.42	0.74	0.87	1.19	1.32	0.95	0.78	0.28	0.27	0.92
Fe	45.2	42.1	53.5	45.1	46.5	40.1	43.5	46.7	56.7	59.7	47.1
Ni	0.81	0.73	0.55	0.95	1.45	1.08	0.58	0.58	0.27	0.30	0.72
S	34.3	36.2	37.6	36.6	37.1	35.7	36.5	37.6	38.9	40.1	37.1
Au (ppm)	23.5	19.6	16.3	21.9	32.7	14.4	21.1	1523	55.0	46.2	2.00
Ir	0.03	0.02	0.19	0.02	0.02	0.03	0.00	0.03	0.01	0.01	0.001
Os	0.19	0.02	0.06	0.06	2.76	0.17	0.08	0.02	0.06	0.04	0.01
Pd	216	192	196	180	283	169	197	259	59.1	20.8	2.43
Pt	36.1	23.4	30.1	23.3	38.8	218	235	329	107	4.01	0.14
Re	0.06	0.03	0.05	0.05	0.08	0.07	0.007	0.07	0.10	0.09	0.002
Rh	0.01	ND	ND	ND	ND	ND	ND	0.36	0.10	0.11	0.02
Ru	0.08	0.19	ND	0.45	0.67	0.57	0.21	0.16	0.08	0.32	0.16

C-3 MINERAL DATA

SAMPLE	rz-45 p1	rz-45 p2	rz-45 p2 inclu Cu	rz-45 p2	rz-45 p3	rz-45 p4	rz-45 p5	rz-45 p5	rz-45 p6	rz-45 p6	rz-45 p6	rz-45 p7	rz-45 p7	rz-45 p8 pn
	po	po		po	pn	po	pn	po	po	po	po	po	pn	po
Rock Type	mat meta-gabnor	mat meta-gabnor	mat meta-gabnor	mat meta-gabnor	mat meta-gabnor	mat meta-gabnor	mat meta-gabnor	mat meta-gabnor	mat meta-gabnor	mat meta-gabnor	mat meta-gabnor	mat meta-gabnor	mat meta-gabnor	mat meta-gabnor
^{61}Ni (wt%)	0.49	0.44	0.84	4.67	29.6	0.51	19.6	10.1	2.34	12.1	10.9	2.06	14.3	0.81
^{107}Ag (ppm)	1.07	1.86	3.34	4.68	4.25	1.21	6.54	6.47	2.91	20.2	47.5	18.5	9.70	6.20
^{197}Au	0.003	0.005	0.013	0.05	0.01	0.01	0.05	0.06	0.007	0.02	0.14	0.15	0.08	0.14
^{111}Cd	0.87	1.79	0.58	0.33	2.41	1.07	1.06	0.76	1.49	4.48	8.88	0.05	2.15	0.02
^{59}Co	121	110	3865	5757	11120	164	13040	17930	1247	6001	5131	10670	11610	3308
^{65}Cu	0.79	368	10700	701	21.2	0.79	32.9	623	0.79	25860	54150	3371	1317	6.64
^{67}Zn	6.87	25.7	2822	854	6.87	6.87	599	4316	143	1877	12400	2793	6174	68.8
^{193}Ir (ppm)	<0.0025	0.004	<0.0025	0.01	<0.0025	0.008	0.004	0.006	0.004	0.01	0.14	<0.0025	0.01	<0.0025
^{192}Os	<0.018	<0.018	<0.018	<0.018	<0.018	0.03	0.04	<0.018	<0.018	0.02	0.08	<0.018	0.03	<0.018
^{185}Re	0.13	0.11	0.07	0.08	0.09	0.12	0.09	0.06	0.08	0.05	0.05	0.09	0.10	0.08
^{103}Rh	0.48	0.75	0.14	0.25	0.65	0.48	0.34	0.27	0.41	0.54	1.04	0.03	0.43	<0.012
^{101}Ru	1.24	1.45	1.01	0.93	1.97	1.27	1.21	0.74	1.65	3.11	5.60	0.69	1.63	0.07
^{108}Pd	4.25	2.05	23.3	102	618	8.12	697	316	44.7	303	277	93.5	253	1.35
^{195}Pt	<0.01	0.04	0.18	0.24	0.07	<0.01	0.19	0.18	0.03	0.37	1.13	0.15	0.13	<0.01

SAMPLE	Rz-45 p8 Pd	rz-45 p8 pt	rz-45 p9 pn	rz-45 p9	rz-45 p9 ccp	rz-45 p10 po1	rz-45 p10 po2	rz-45 p11 pn	rz-45 p11 po	rz-45 p12 po1	rz-45 p12	rz-45 p12	rz-45 p13	rz-45 p14
Mineral	inclusion	inculsion	po	po	po	po	pn	pn	pn	po	pn	pn	po	pn
Rock Type	mat meta-gabnor	mat meta-gabnor	mat meta-gabnor	Mat meta-gabnor	mat meta-gabnor	mat meta-gabnor	mat meta-gabnor	mat meta-gabnor	mat meta-gabnor	mat meta-gabnor	mat meta-gabnor	mat meta-gabnor	mat meta-gabnor	mat meta-gabnor
^{61}Ni (wt%)	4.74	5.50	0.87	0.97	0.83	0.43	27.0	28.0	9.62	0.42	16.4	9.34	0.60	0.61
^{107}Ag (ppm)	52.6	42.7	5.68	6.07	14.1	1.90	6.66	10.0	9.30	6.85	10.6	11.5	1.27	0.98
^{197}Au	0.83	0.71	0.15	0.13	0.34	0.009	0.015	0.014	0.02	0.007	0.47	0.05	0.004	0.007
^{111}Cd	67.1	58.6	0.02	0.02	0.02	1.76	5.26	3.74	3.84	2.07	3.88	8.55	1.52	1.99
^{59}Co	1233	1196	15100	11790	12680	89.86	9298	10530	3257	81.6	4896	2574	124	229
^{65}Cu	1042	607	0.79	0.79	117	2.72	45.7	1321	84.6	14030	64060	72920	2.82	3.94
^{67}Zn	8661	9475	6.87	113	570	22.8	365	313	229	2337	4129	5411	28.1	20.5
^{193}Ir (ppm)	1.40	0.84	<0.0025	<0.0025	<0.0025	0.004	0.003	<0.0025	<0.0025	<0.0025	0.004	0.06	0.01	0.02
^{192}Os	0.38	1.97	<0.018	<0.018	0.04	<0.018	0.06	0.04	0.08	0.04	0.06	0.13	0.11	0.11
^{185}Re	0.13	0.09	0.08	0.06	0.07	0.10	0.10	0.09	0.09	<0.002	0.01	0.02	0.12	0.12
^{103}Rh	9.81	9.25	<0.012	0.025	0.22	0.49	1.35	0.73	1.0	0.11	<0.012	0.21	0.88	0.86
^{101}Ru	21.0	34.63	0.09	0.06	0.27	1.33	2.95	2.45	2.25	1.90	3.72	5.05	1.64	1.58
^{108}Pd	10470	3554	0.73	10.9	17.9	2.87	870	873	312	1.99	221	137	2.54	2.76
^{195}Pt	7.27	133	<0.01	<0.01	0.02	0.02	0.05	0.02	0.04	<0.01	<0.01	0.18	0.54	0.03

SAMPLE	rz-6 spot1	rz-6 spot2	rz-6 spot3	rz-6 spot4	rz-6 spot5	rz-6 spot6	rz-6 spot7	rz-6 spot8	rz-6 spot9	rz-6 spot10	rz-6 spot11	rz-6 spot12	rz-6 spot13	rz-6 spot14	rz-6 spot15
Mineral	po	po	po	po	po	po	po	po	po	po	po	po	po	po	po
Rock Type	micro-breccia	micro-breccia	micro-breccia	micro-breccia	micro-breccia	micro-breccia	micro-breccia	micro-breccia	micro-breccia	micro-breccia	micro-breccia	micro-breccia	micro-breccia	micro-breccia	micro-breccia
^{61}Ni (wt%)	0.11	0.05	0.04	0.07	0.05	0.08	0.08	0.06	0.04	0.05	0.05	0.08	0.10	0.04	0.06
^{107}Ag (ppm)	0.83	55.2	0.32	DL	DL	0.85	0.01	0.22	DL	DL	0.10	0.01	0.18	0.09	0.79
^{197}Au	0.02	76.5	0.01	0.006	0.015	0.15	0.01	0.009	0.007	0.007	0.007	0.007	0.02	0.02	0.04
^{111}Cd	0.02	0.05	0.02	0.02	0.02	0.04	0.02	0.02	0.02	0.02	0.02	0.02	0.02	0.02	0.14
^{59}Co	3213	969	5377	4754	5448	4702	2462	3206	3746	1929	5393	9090	6119	9643	3545
^{65}Cu	480	13820	10.0	0.79	1.48	291	DL	3.56	DL	DL	DL	DL	DL	DL	437
^{67}Zn	32.6	118	24.1	24.6	23.4	270	60.9	13.9	18.9	15.2	17.3	21.4	16.0	42.8	223
^{193}Ir (ppm)	<0.0025	<0.0025	<0.0025	<0.0025	<0.0025	<0.0025	<0.0025	<0.0025	<0.0025	<0.0025	<0.0025	<0.0025	<0.0025	<0.0025	<0.0025
^{192}Os	0.02	<0.018	<0.018	<0.018	<0.018	<0.018	<0.018	<0.018	<0.018	<0.018	<0.018	<0.018	<0.018	<0.018	<0.018
^{185}Re	0.01	<0.002	0.02	0.02	0.01	0.01	0.02	0.01	0.01	0.01	0.02	0.02	0.02	0.02	0.02
^{103}Rh	0.01	0.38	<0.012	<0.012	<0.012	<0.012	<0.012	<0.012	<0.012	<0.012	<0.012	<0.012	<0.012	<0.012	0.01
^{101}Ru	<0.03	<0.03	<0.03	<0.03	<0.03	<0.03	<0.03	<0.03	<0.03	<0.03	<0.03	<0.03	<0.03	<0.03	<0.03
^{108}Pd	124	2.4	0.5	0.6	0.32	2.70	2.47	0.53	0.09	0.16	0.83	1.36	0.66	0.42	0.87
^{195}Pt	0.29	1.32	0.17	0.02	0.06	0.29	<0.01	0.04	0.13	0.08	<0.01	0.02	<0.01	<0.01	0.03

SAMPLE	rz-6 spot16	rz-6 spot17	rz-6 spot18	rz-6 spot 19	rz-6 spot20	rz-6 spot21	rz-6 spot22
Mineral	po	po	po	po	po	po	po
Rock Type	micro-breccia	micro-breccia	micro-breccia	micro-breccia	micro-breccia	micro-breccia	micro-breccia
^{61}Ni (wt%)	0.06	0.06	0.08	0.04	0.07	0.04	0.06
^{107}Ag (ppm)	0.04	0.05	0.02	0.23	0.01	0.07	0.51
^{197}Au	0.03	0.02	0.007	0.011	0.019	0.01	0.02
^{111}Cd	0.02	0.02	0.03	0.02	0.02	0.02	0.02
^{59}Co	9530	6966	4115	12220	11820	8596	17340
^{65}Cu	3.46	1.941	DL	3.87	6.192	DL	11.6
^{67}Zn	30.1	36.2	9.70	48.5	10.7	87.9	167
^{193}Ir (ppm)	<0.0025	<0.0025	<0.0025	<0.0025	<0.0025	<0.0025	<0.0025
^{192}Os	<0.018	<0.018	<0.018	<0.018	<0.018	<0.018	<0.018
^{185}Re	0.05	0.04	0.01	0.02	0.01	0.01	0.03
^{103}Rh	<0.012	<0.012	<0.012	<0.012	<0.012	<0.012	<0.012
^{101}Ru	<0.03	<0.03	<0.03	<0.03	<0.03	<0.03	<0.03
^{108}Pd	0.73	0.25	0.56	0.25	0.12	0.12	0.49
^{195}Pt	<0.01	<0.01	<0.01	0.04	0.19	1.31	0.09

SAMPLE	rz-45 spot1	rz-45 spot2	rz-45 spot3	rz-45 spot4	r-45 spot5	rz-45 spot6	rz-45 spot6	rz-45 spot7	rz-45 spot7	rz-45 spot8	rz-45 spot9	rz-45 spot10	rz-45 spot11	rz-45 spot12	rz-45 spot13
Mineral	po	po	po	po	pn	po	po	py	pn	po	po	po	po	pn	pn
Rock Type	mat meta-gabnor	mat meta-gabnor	mat meta-gabnor	mat meta-gabnor	mat meta-gabnor	mat meta-gabnor	mat meta-gabnor	mat meta-gabnor	mat meta-gabnor	mat meta-gabnor	mat meta-gabnor	mat meta-gabnor	mat meta-gabnor	mat meta-gabnor	mat meta-gabnor
^{61}Ni (wt%)	1.09	1.08	1.13	0.95	68.2	1.12	2.01	5.85	53.1	1.12	1.75	0.94	2.91	65.7	50.9
^{107}Ag (ppm)	0.31	0.91	0.46	2.15	3.35	2.95	4.41	20.74	25.77	0.20	2.44	0.55	6.26	3.95	5.64
^{197}Au	0.006	0.007	0.006	0.007	0.008	0.01	0.02	0.007	0.31	0.007	0.007	0.007	0.15	0.01	0.03
^{111}Cd	0.03	0.03	0.02	0.02	0.03	0.14	0.08	0.23	0.49	0.03	0.02	0.02	0.02	0.04	0.06
^{59}Co	179	197	178	162	17710	1133	2102	1342	12450	206	218	80.1	4293	10330	8541
^{65}Cu	2.55	4.52	3.78	48.6	6.00	7323	3134	21240	3980	0.79	0.79	0.79	15.6	2.42	29.4
^{67}Zn	196	40.3	64.5	118	73.7	3605	2395	3183	11970	87.4	35.6	87.0	86.8	623	228
^{193}Ir (ppm)	<0.0025	<0.0025	<0.0025	<0.0025	<0.0025	<0.0025	<0.0025	0.005	0.003	0.01	0.01	<0.0025	<0.0025	<0.0025	<0.0025
^{192}Os	<0.018	<0.018	<0.018	<0.018	<0.018	<0.018	<0.018	0.05	0.03	0.06	0.08	<0.018	<0.018	<0.018	<0.018
^{185}Re	0.15	0.12	0.16	0.13	0.10	0.12	0.10	0.03	0.01	0.13	0.14	0.13	0.12	0.14	0.16
^{103}Rh	0.12	0.24	0.21	0.11	0.23	0.35	0.17	1.15	0.50	0.4	0.43	0.26	0.22	0.28	0.31
^{101}Ru	<0.03	<0.03	<0.03	<0.03	0.16	<0.03	<0.03	0.10	0.16	0.13	0.14	<0.03	<0.03	0.19	0.14
^{108}Pd	1.94	0.07	3.70	0.28	825	1.46	17.46	46.88	425	0.69	0.26	0.07	5.36	948	687
^{195}Pt	0.02	<0.01	<0.01	0.02	0.05	0.26	0.31	0.05	0.18	0.10	1.52	0.11	<0.01	0.18	0.02

SAMPLE	rz-45 spot13	rz-45 spot14	rz-45 spot14	rz-45 spot15
Mineral	pn (inclusion)	pn	pn	po
Rock Type	mat meta-gabnor	mat meta-gabnor	mat meta-gabnor	mat meta-gabnor
^{61}Ni (wt%)	12.4	49.7	64.3	1.14
^{107}Ag (ppm)	10.8	18.1	4.80	0.35
^{197}Au	0.08	0.23	0.03	0.009
^{111}Cd	0.13	0.11	0.06	0.02
^{59}Co	12530	12720	12420	166
^{65}Cu	3572	501	3.99	1.07
^{67}Zn	5025	164	65.9	48.4
^{193}Ir (ppm)	<0.0025	0.01	0.005	0.01
^{192}Os	0.02	0.05	0.03	0.03
^{185}Re	0.15	0.14	0.14	0.14
^{103}Rh	0.39	0.29	0.31	0.28
^{101}Ru	0.06	0.21	0.20	0.05
^{108}Pd	189	1078	11187	8.09
^{195}Pt	0.03	1.73	0.36	<0.01

SAMPLE	rz-45 ccp1	rz-45 ccp2	rz-45 ccp3	rz-45 ccp4	rz-45 ccp5	rz-45 ccp5	rz-45 ccp6	rz-45 ccp7	rz-45 ccp8	rz-45 ccp8	rz-45 ccp9	rz-45 ccp10
Mineral	ccp	ccp	ccp	ccp	ccp	ccp	ccp	ccp	ccp	ccp	ccp	ccp
Rock Type	mat meta-gabnor	mat meta-gabnor	mat meta-gabnor	mat meta-gabnor	Mat meta-gabnor	mat meta-gabnor	mat meta-gabnor	mat meta-gabnor	mat meta-gabnor	mat meta-gabnor	mat meta-gabnor	mat meta-gabnor
^{61}Ni (wt%)	0.01	0.56	0.04	1.89	0.01	0.02	0.01	0.14	0.08	0.44	0.05	0.14
^{107}Ag (ppm)	3.96	7.42	23.3	33.9	4.76	94.0	4.79	7.99	5.77	9.97	6.45	6.89
^{197}Au	0.007	0.007	0.06	0.05	0.007	0.007	0.007	0.04	0.03	0.02	0.02	0.01
^{111}Cd	3.80	6.59	2.10	5.12	4.82	5.65	4.93	5.00	5.80	13.9	5.20	8.13
^{59}Co	4.57	120	9.96	376	3.57	6.23	6.83	14.8	9.23	47.4	5.73	12.8
^{65}Cu	127100	120300	125400	146000	159100	141400	153700	160300	181000	153100	168600	185400
^{67}Zn	346700	665300	190400	187900	550600	778600	195800	109300	152900	1269000	155400	74470
^{193}Ir (ppm)	0.003	0.005	0.06	0.007	<0.0025	<0.0025	<0.0025	0.005	<0.0025	0.009	<0.0025	0.004
^{192}Os	0.04	0.05	0.11	<0.018	0.05	0.07	<0.018	<0.018	<0.018	0.08	0.04	0.05
^{185}Re	<0.002	<0.002	0.01	0.005	0.004	<0.002	<0.002	0.01	0.003	0.10	0.003	0.005
^{103}Rh	<0.012	<0.012	<0.012	<0.012	<0.012	<0.012	<0.012	<0.012	<0.012	<0.012	<0.012	<0.012
^{101}Ru	4.60	0.03	3.88	<0.03	5.59	4.56	4.94	4.07	5.34	1.25	4.79	4.03
^{108}Pd	1.50	9.18	7.74	27.9	2.14	1.70	1.75	3.00	2.72	5.19	53.6	2.52
^{195}Pt	<0.01	<0.01	0.23	0.02	<0.01	<0.01	0.02	<0.01	0.04	0.03	0.02	0.04

SAMPLE	rz-30 spot1	rz-30 spot2	rz-30 spot3	rz-30 spot4	rz-30 spot5	rz-30 spot6	rz-30 spot7	rz-30 spot8	rz-30 spot9	rz-30 spot10	rz-30 spot11	rz-30 spot12
Mineral	**po**	**po**	**pn**	**po**	**po**	**po**	**po**	**pn**	**po**	**po**	**po**	**pn**
Rock Type	**mat gabnor**	**mat gabnor**	**mat gabnor**	**mat gabnor**	**mat gabnor**	**mat gabnor**	**mat gabnor**	**mat gabnor**	**mat gabnor**	**mat gabnor**	**mat gabnor**	**mat gabnor**
^{61}Ni (wt%)	0.70	0.62	39.1	0.74	0.68	0.80	0.80	21.4	0.59	1.17	0.82	59.3
^{107}Ag (ppm)	0.33	0.32	2.48	0.93	0.27	0.50	0.41	1.34	1.28	0.56	0.29	5.35
^{197}Au	0.007	0.007	0.04	0.05	0.007	0.03	0.007	0.007	0.007	0.01	0.007	0.01
^{111}Cd	0.02	0.02	0.02	0.02	0.02	0.02	0.03	0.07	0.02	0.02	0.03	0.13
^{59}Co	201	169	16160	228	208	275	240	10010	158	438	260	25720
^{65}Cu	1.39	1.88	11.1	1.16	0.79	2.80	0.31	1424	7.73	0.79	0.94	5403
^{67}Zn	85.4	191	158	64.8	45.4	124	51.1	4104	22.8	30.6	45.8	1110
^{193}Ir (ppm)	0.01	0.01	0.007	0.01	0.02	0.02	0.01	0.01	0.02	0.01	0.01	0.01
^{192}Os	0.05	0.03	0.04	0.04	0.05	0.06	0.05	0.05	0.06	0.05	0.06	0.04
^{185}Re	0.13	0.14	0.11	0.15	0.16	0.17	0.18	0.17	0.18	0.18	0.18	0.12
^{103}Rh	0.22	0.21	0.17	0.24	0.28	0.30	0.28	0.31	0.18	0.28	0.28	0.42
^{101}Ru	0.07	0.07	0.10	0.07	0.10	0.13	0.08	0.15	0.06	0.06	0.11	0.19
^{108}Pd	0.12	0.49	220	5.59	0.65	3.97	0.24	205	0.07	0.33	0.52	423
^{195}Pt	0.42	0.06	0.19	0.10	0.02	0.05	0.17	0.15	0.58	8.99	0.25	0.04

SAMPLE	rz-30 spot12	rz-30 spot 13	rz-30 spot14	rz-30 spot14	rz-30 spot 14
Mineral	pn	pn	po	po	po
Rock Type	mat gabnor	mat gabnor	mat gabnor	mat gabnor	mat gabnor
^{61}Ni (wt%)	53.1	50.5	0.94	7.33	5.08
^{107}Ag (ppm)	4.70	8.63	0.98	3.77	5.54
^{197}Au	0.007	0.01	0.008	0.007	0.03
^{111}Cd	0.16	0.72	0.02	0.02	0.24
^{59}Co	22850	20640	370.5	3794	2607
^{65}Cu	16250	26820	0.79	5020	27020
^{67}Zn	1612	21420	72.6	375	1106
^{193}Ir (ppm)	0.01	0.004	0.02	0.01	0.01
^{192}Os	0.03	<0.018	0.05	0.02	0.03
^{185}Re	0.11	0.058	0.20	0.13	0.09
^{103}Rh	0.73	1.08	0.32	0.55	1.16
^{101}Ru	0.17	0.17	0.12	0.12	0.12
^{108}Pd	363	380	2.08	46.5	37.9
^{195}Pt	0.03	0.03	0.02	0.02	0.06

SAMPLE	Rz-19 spot1	Rz19 spot2	Rz19 spot2	Rz19 spot3	Rz19 spot 4	Rz19 spot4	Rz 19 spot 5	Rz19 spot 6	Rz19 spot 6	Rz19 spot 7	Rz19 spot 8	Rz19 spot 9	Rz19 spot 9	Rz19 spot 10	Rz19 spot 10
Mineral	po	po	po	po	po	po	po	po	po	po	po	pn	pn	po	po
Rock Type	frag meta-gabnor	frag meta-gabnor	frag meta-gabnor	frag meta-gabnor	frag meta-gabnor	frag meta-gabnor	frag meta-gabnor	frag meta-gabnor	frag meta-gabnor	frag meta-gabnor	frag meta-gabnor	frag meta-gabnor	frag meta-gabnor	frag meta-gabnor	frag meta-gabnor
^{61}Ni (wt%)	0.04	0.76	0.81	3.58	0.93	2.88	0.04	0.09	1.28	2.60	0.12	92.6	83.2	3.48	1.61
^{107}Ag (ppm)	DL	0.39	0.57	181	1.30	2.33	DL	0.02	2.44	5.67	0.45	5.04	23.7	2.32	10.9
^{197}Au	0.007	0.009	0.007	0.12	0.01	0.02	0.006	0.007	0.25	0.05	0.05	0.006	0.007	0.01	0.05
^{111}Cd	0.02	0.02	0.02	0.02	0.02	0.02	0.02	0.02	0.02	0.04	0.02	0.05	0.05	0.02	0.02
^{59}Co	29920	1545	136	8305	3071	4699	35540	37740	14170	11080	40400	318	195	9.79	398
^{65}Cu	2.07	3.92	20.4	458	49.4	5.29	4.10	0.79	3.14	740	5.93	6.77	2138	480	94880
^{67}Zn	70.6	222	44.5	522	54.0	180	32.4	35.2	50.9	1340	161	38.6	34.1	59.2	447
^{193}Ir (ppm)	0.01	0.01	0.01	0.01	0.007	0.01	0.008	0.006	0.01	0.03	0.004	0.01	0.009	0.01	0.01
^{192}Os	0.04	0.03	0.03	0.02	0.04	0.03	0.05	0.04	0.07	0.10	0.02	0.04	0.03	0.05	0.04
^{185}Re	0.10	0.09	0.07	0.09	0.08	0.07	0.08	0.06	0.06	0.07	0.04	0.11	0.09	0.11	0.10
^{103}Rh	0.20	0.16	0.15	0.18	0.21	0.18	0.21	0.14	0.28	0.29	0.12	0.32	0.26	0.34	0.90
^{101}Ru	0.08	0.05	0.04	0.04	0.06	0.04	0.11	0.09	0.17	0.19	0.08	<0.03	<0.03	0.12	0.15
^{108}Pd	0.72	0.17	1.70	0.66	0.29	13.7	7.92	0.19	122	17.4	1.94	851	784	13.5	13.9
^{195}Pt	5.33	<0.01	<0.01	<0.01	<0.01	<0.01	29.2	4.12	2.40	0.84	11.3	<0.01	<0.01	<0.01	<0.01

SAMPLE	Rz19 spot 10 inclusion	Rz19 spot 11	Rz19 spot 11	Rz19 spot 12	Rz19 spot 13	rz-19 spot 14	rz-19 spot 14	rz-19 spot 15	rz-19 spot16	rz-19 spot17	rz-19 spot18	rz-19 spot18	rz-19 spot18	rz-19 spot19	rz-19 spot19
Mineral	ccp	po	po	pn	pn	po	po	po	po	po	pn	po	po	pn	po
Rock Type	frag meta-gabnor	frag meta-gabnor	frag meta-gabnor	frag meta-gabnor	frag meta-gabnor	frag meta-gabnor	frag meta-gabnor	frag meta-gabnor	frag meta-gabnor	frag meta-gabnor	frag meta-gabnor	frag meta-gabnor	frag meta-gabnor	frag meta-gabnor	frag meta-gabnor
^{61}Ni (wt%)	0.49	3.04	1.79	76.2	88.4	0.17	0.29	0.03	0.07	48.4	1.27	0.57	0.79	27.6	8.35
^{107}Ag (ppm)	27.3	2.26	1.49	6.31	7.59	0.65	0.41	0.11	0.45	28.6	0.94	0.29	2.89	33.6	14.2
^{197}Au	0.11	0.01	0.006	0.01	0.009	0.007	0.007	0.007	0.16	0.06	0.01	0.01	0.01	0.06	0.07
^{111}Cd	0.09	0.05	0.02	0.05	0.38	0.02	0.02	0.02	0.02	0.04	0.02	0.04	0.05	1.26	0.26
^{59}Co	24.4	13.9	8.83	382	213	23610	14090	30100	34260	487	5694	1436	346	6.51	5.41
^{65}Cu	391300	179	109	15170	20.2	0.79	4.58	0.79	629	13630	42.2	5.98	2276	91280	307500
^{67}Zn	1316	25.9	30.7	130	11370	20.5	33.7	27.3	60.6	90.1	24.6	27.5	331	12860	2191
^{193}Ir (ppm)	0.01	0.01	0.01	0.01	0.004	0.008	0.007	0.01	0.01	0.02	0.009	0.01	0.007	0.02	0.02
^{192}Os	0.05	0.04	0.04	0.04	0.02	0.07	0.05	0.05	0.06	0.10	0.04	0.05	0.04	0.09	0.07
^{185}Re	0.13	0.11	0.13	0.11	0.05	0.09	0.07	0.11	0.12	0.14	0.06	0.08	0.06	0.17	0.13
^{103}Rh	2.95	0.32	0.37	0.39	0.18	0.13	0.12	0.22	0.23	0.49	0.14	0.18	0.17	1.73	5.38
^{101}Ru	0.24	0.16	0.15	<0.03	<0.03	0.09	0.09	0.10	0.11	<0.03	0.06	0.09	0.07	0.08	0.19
^{108}Pd	10.8	14.5	2.61	728	121	0.69	0.38	3.21	2.51	1764	11.9	2.91	29.3	279	75.2
^{195}Pt	<0.01	<0.01	<0.01	<0.01	<0.01	9.45	4.92	5.93	5.92	0.05	<0.01	<0.01	<0.01	<0.01	<0.01

SAMPLE	rz-19 spot2	rz-19 spot2	rz-19 spot21	rz-19 spot21	rz-19 spot22	rz-19 spot22	rz-19 spot22	rz-19 spot22	rz-19 spot22	rz-19 spot23	rz-19 spot24 inclusion	rz-19 spot24
Mineral	pn	pn	po	po	pn	pn	pn	pn	pn	po	pn	pn
Rock Type	frag meta-gabnor	frag meta-gabnor	frag meta-gabnor	frag meta-gabnor	frag meta-gabnor	frag meta-gabnor	frag meta-gabnor	frag meta-gabnor	frag meta-gabnor	frag meta-gabnor	frag meta-gabnor	frag meta-gabnor
^{61}Ni (wt%)	52.5	47.9	0.15	0.05	53.8	55.4	57.3	56.9	58.5	0.73	22.7	26.8
^{107}Ag (ppm)	8.60	6.86	0.06	0.01	8.40	12.47	8.84	44.93	4.17	2.57	39.49	27.2
^{197}Au	0.007	0.007	0.005	0.007	0.006	0.007	0.007	0.013	0.007	0.007	0.07	0.04
^{111}Cd	0.19	0.05	0.02	0.02	0.03	0.04	0.05	0.08	0.06	0.02	0.05	0.11
^{59}Co	11.4	34.9	28190	37910	327	340	349	340	362	231	428	361
^{65}Cu	3764	343	3.78	0.79	10180	11670	6782	15970	1012	18.0	9066	969
^{67}Zn	1729	139	36.9	25.9	29.0	44.5	32.4	52.4	34.3	25.5	136	176
^{193}Ir (ppm)	0.02	0.02	0.002	0.02	0.01	0.01	0.01	0.01	0.01	0.01	0.01	0.01
^{192}Os	0.07	0.11	0.04	0.09	0.05	0.06	0.05	0.05	0.04	0.05	0.07	0.07
^{185}Re	0.12	0.18	0.06	0.10	0.12	0.11	0.12	0.15	0.13	0.11	0.13	0.09
^{103}Rh	0.32	0.40	0.02	0.24	0.41	0.44	0.41	0.54	0.33	0.24	0.63	0.37
^{101}Ru	<0.03	<0.03	<0.03	0.14	<0.03	<0.03	<0.03	<0.03	<0.03	0.08	<0.03	<0.03
^{108}Pd	713	654	2.02	0.31	117	119	126	146	114	1.29	72.9	67.5
^{195}Pt	<0.01	<0.01	11.8	18.7	0.02	0.02	0.02	0.02	<0.01	<0.01	<0.01	<0.01